INAUGURAL-DISSERTATION

zur Erlangung der Doktorwürde

der

Naturwissenschaftlich-Mathematischen Gesamtfakultät

der

Ruprecht-Karls-Universität Heidelberg

vorgelegt von

Master of Science Annika Eisenschmidt

aus Spielmes

Tag der mündlichen Prüfung: 20.01.2017

Dinuclear copper(II) patellamide complexes: Studies on their potential hydrolase-like activities and *in vivo* stabilities

Gutachter:

Prof. Dr. Peter Comba

Prof. Dr. Roland Krämer

This thesis has been accomplished at the Institute of Inorganic Chemistry at Heidelberg University from December 2013 until November 2016 and was supervised by Prof. Dr. Peter Comba. Experimental work was also performed under supervision of Prof. Dr. Dirk-Peter Herten at the CellNetworks Cluster and the Physical Chemistry Institute at Heidelberg University during August and September 2015 as well as under supervision of Prof. Dr. Lawrence R. Gahan at the School of Chemistry and Molecular Biosciences (SCMB), and at the Centre of Advanced Imaging (CAI) under the supervision of Dr. Jeffrey Harmer at the University of Queensland, Brisbane, Australia, between May and June 2016. Computational research was carried out additionally at the Indian Institute of Chemical Technology Hyderabad, India under the supervision of Prof. Dr. Sastry between September and November 2015.

Parts of the presented thesis have been published in or submitted to scientific journals:

- P. Comba, A. Eisenschmidt, N. Kipper, J. Schießl, *J. Inorg. Biochem.*, **2016**, *159*, 70-75.
- P. Comba, A. Eisenschmidt, L. R. Gahan, G. R. Hanson, N. Mehrkens, M. Westphal, *Dalton Trans.*, **2016**.
- P. Comba, A. Eisenschmidt, L. R. Gahan, D.-P. Herten, G. Nette, G. Schenk, M. Seefeld, manuscript in preparation.

Oral presentations:

- MD study on the dinuclear copper(II) complexes of cyclic *pseudo*-peptides, *MCBR meeting,* 07.11.2015, IIT New Delhi, India.
- Potential biological importance of *pseudo*-octapeptides for *L. patellum* and *Prochloron,* 19.01.2016, Heidelberg Chemical Society, Heidelberg.
- What we know about cyclic peptides from *Prochloron*, 30.08.2016, *MACB meeting,* Invited lecture, NFMC Tiruchirappalli, Tamil Nadu, India.

Research Symposium Poster Publications

- P. Comba, A. Eisenschmidt, L. R. Gahan, G. R. Hanson, N. Mehrkens, M. Westphal, *European Bioinorganic Conference*, 24.-28.08.2014, Binding site preference of Zn^{II} and Cu^{II} in cyclic *pseudo*-peptides promotes phosphoester hydrolysis activity.
- P. Comba, A. Eisenschmidt, J. Schießl, *German coordination chemistry meeting*, 22.-24.03.2015, Glycosidase activity of dinuclear Cu^{II} patellamide complexes.

- P. Comba, A. Eisenschmidt, N. Kipper, J. Schießl, *Heidelberg Forum for Molecular Catalysis*, 12.06.2015, Towards an understanding of the metabolic role of cyclic *pseudo*-peptides in *L. patella*.
- P. Comba, A. Eisenschmidt, Dirk-Peter Herten, Martin Seefeld, *German coordination chemistry meeting*, 28.2.-01.03.2015, Investigation of the copper(II) binding of patellamides in blue-green algae.

Für meine Familie

JEDES LEBEN IST EIN EXPERIMENT, JE MEHR DU EXPERIMENTIERST, DESTO MEHR LEBST DU.

Ralph Waldo Emerson

Table of Molecules

1) Cyclic *pseudo*-octapeptides referred to and their corresponding abbreviations:

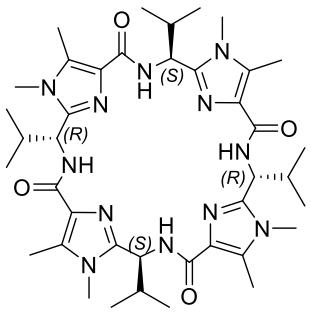

H_4pat^1

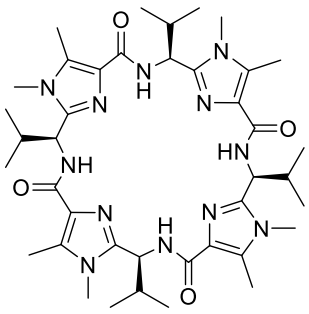

H_4pat^2

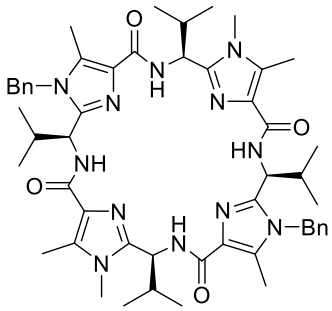

H_4pat^3

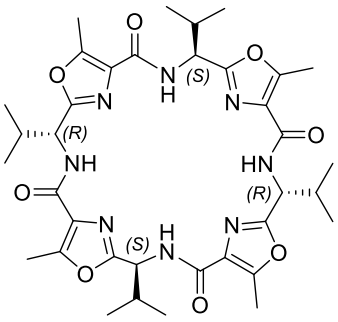

H_4pat^4

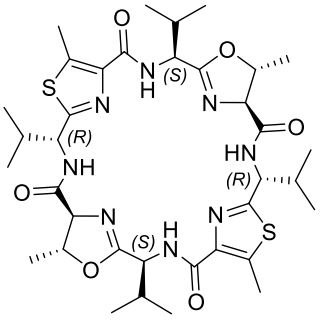

H_4pat^5

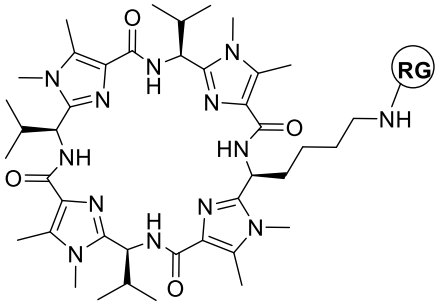

H_4pat-reporter group

RG=Proxyl, Atto550

2) Substrates for the investigation of hydrolysis activities referred to and their corresponding abbreviations:

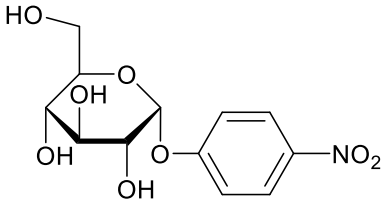

4-Nitrophenyl-α-D-glucopyranoside

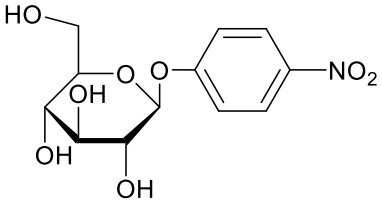

4-Nitrophenyl-β-D-glucopyranoside

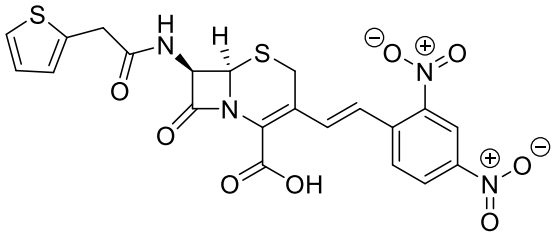

Nitrocefin

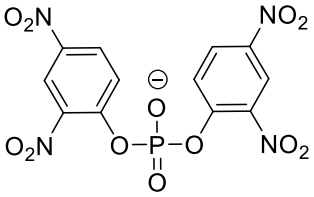

Bis-(2,4-dinitrophenyl)phosphate (BDNPP)

List of abbreviations

A	atm	physical atmosphere
	Å	Ångström
	Ala	Alanine
	APCI	atmospheric pressure chemical ionisation
	APD	avalanche photodiode
	aq	aqueous solution
	ATP	adenosine triphosphate
B	BDNPP	bis(2,4-dinitrophenyl)phosphate
	Bn	benzyl
	Boc	*tert*-butylcarboxycarbonyl
	Bu	butyl
	BS-DFT	broken symmetry density functional theory
C	c	concentration
	calcd.	calculated
	CAPS	*N*-cyclohexyl-3-aminopropanesulfonic acid
	Cbz	carboxybenzyl
	CHES	2-(*N*-cyclohexylamino)ethanesulfonic acid
	Chl	chlorophyll
	COMU®	(1-cyano-2-ethoxy-2-oxoethylidenaminooxy)dimethyl-aminomorpholino-carbenium hexafluorophosphate
	COSY	correlated spectroscopy
	CW	continuous wave
	Cys	cysteine
D	d	day(s)
	DCM	dichloromethane
	DEER	double electron-electron resonance
	DEPT	distortionless enhancement by polarization transfer
	DFT	density functional theory
	DMF	dimethylformamide

	DMSO	dimethylsulfoxide
E	EC	Enzyme Commission
	E. coli	*Escherichia coli*
	EDIPA	*N,N*-diisopropylethylamine (HÜNIG's base)
	EPR	electron paramagnetic resonance
	e.g.	*exempli gratia* (for example)
	eq.	equivalents
	Eq.	equation
	ESI	electrospray ionisation
	Et	ethyl
	Et_2O	diethylether
	EtOAc	ethyl acetate
	EtOH	ethanol
	ε	extinction coefficient
F	FAB	fast atom bombardment
	FDPP	pentafluorophenyl diphenylphosphinate
	FCM	flow cytometry
	FRET	FÖRSTER resonance electron transfer
	FSC	forward scattered light
	FT	fluorescent tag
G	G	Gauss
	GGA	generalised gradient approximation
	GH	glycoside hydrolase
	GTP	guanosine-5'-triphosphate
H	h	hour(s)
	H	hydrogen
	HEPES	4-(2-hydroxyethyl)-1-piperazineethanesulfonic acid
	HEWL	hen egg white lysozyme
	HF	HARTREE FOCK
	His	histidine
	HMBC	heteronuclear multiple bond correlation

	HPLC	high performance liquid chromatography
	HR	high resolution
	HSQC	heteronuclear single quantum coherence
	Hz	Hertz
I	IC	Internal Conversion
	i.e.	*id est* (that is)
	Ind	indicator
	Int.	intensity
	IR	Infrared (spectroscopy)
	ISC	Intersystem Crossing
	ITC	Isothermal Titration Calorimetry
	IUGS	International Union of Geological Sciences
J	*J*	coupling constant
K	k_{cat}	first order rate constant
	K_M	MICHAELIS constant
L	λ	wavelength
	LDA	local density approximation
	LMCT	ligand metal charge transfer
M	m	multiplet
	M	molar [mol/L]
	MD	molecular dynamics
	Me	methyl
	MeCN	acetonitrile
	MeOH	methanol
	MES	2-(*N*-morpholino)ethanesulfonic acid
	Met	methionine
	min	minute
	MM	molecular mechanics
	mol	number of moles of compound
	MS	mass spectrometry
N	neg.	negative

	NMM	*N*-methylmorpholine
	NMR	nuclear magnetic resonance (spectroscopy)
	NRP	non-ribosomal pathway
O	OTf^-	trifluoromethane sulfonate
P	*p.a*.	*pro analysis*
	PAGE	polyacrylamide gel electrophoresis
	PAM	pulse amplitude modulated photosynthesis measurement
	PAP	purple acid phosphatase
	PELDOR	pulsed electron-electron double resonance
	Ph	phenyl
	Phe	phenylalanine
	PKS	polyketide synthase
	PMT	photomultiplier tubes
	pos.	positive
	ppm	parts per million
	PS	photosystem
R	RIPP	ribosomal production and post-translational modification
	RMS	root mean square
	rt	room temperature
	ROS	reactive oxygen species
S	SAG	Sammlung von Algenkulturen der Universität Göttingen
	SEM	standard error of means
	SD	standard deviation
	SQUID	superconducting quantum interference device
	SSC	side scattered light
T	t	time
	TMEDA	*N*,*N*,*N*',*N*'-Tetramethylethane-1,2-diamine
	TFA	trifluoroacetic acid
	THF	tetrahydrofuran
	TON	turnover number
	TRIS	(tris-hydroxymethyl)-aminomethane

U	UV	ultraviolet light
	UPLC	ultra performance liquid chromatography
V	vis	visible light
	Val	valine
	vs.	*versus*

Abstract

The blue-green alga *Prochloron* produces and exports cyclic octapeptides (patellamides) to its obligate host, the ascidian *Lissoclinum patella,* in large quantities. Since the Cu^{II} concentration in the ascidians is a factor of 10^4 greater when compared to the surrounding sea water, previous studies on model Cu^{II} complexes with synthetic cyclic octapeptide derivatives were performed and revealed these complexes to be efficient phosphatase- and carboanhydrase-mimics. Their biological role, however, is so far unknown.

With the work presented in this thesis, the dependence of the phosphatase activity of dinuclear patellamide complexes on the side chain configuration as well as on the catalytic metal centre is explored. The results show that the complexes based on ligands with the natural *R* and *S* configuration of the patellamide-ligand backbone exhibit 3-5 times higher hydrolysis efficiencies as compared to complexes with ligands that exhibit 4*S* side chain configuration. Beyond that, the effect on phosphatase efficiency induced by the substitution of the catalytic metal centre Cu^{II} for Zn^{II} was investigated. Since only one of the three Zn^{II} patellamide complexes showed catalytic activity, a structural investigation was carried out. In addition to hydrolysis measurements this was accomplished by means of NMR, MS, ITC and a combined MM and QM study. The results indicate a similar binding behaviour of patellamides towards Zn^{II} as shown for Cu^{II}, *i.e*. a coordination site spanned by two nitrogen atoms that are part of a heterocycle and a deprotonated amide nitrogen. Therefore, the lack of phosphatase activity might be caused by the small stability of these complexes under aqueous conditions, as used for the hydrolysis assay.

In addition, α- and β-glycosidase- as well as β-lactamase-like activity of the Cu^{II} patellamide complexes was examined. It was shown that the imidazole-based complexes act as hydrolases not only for phosphate ester cleavage at pH 7-8 but also for the hydrolysis of glycosidic bonds at alkaline conditions (pH 10). Moreover, β-lactamase-like activity was observed at pH 11.5 for one of the patellamide based complexes. Consequently, these results indicate the ability of the Cu^{II} complexes to act as very efficient, pH-dependent catalysts. Recent findings from BEHRENDT *et al*. pointed to a rapid fluctuation of the pH in close proximity to *Prochloron* depending on the irradiance. Therefore, the glycosidase and lactamase results could indicate the dinuclear Cu^{II} complexes to adopt different functions during day- and night-time, respectively.

As a contribution towards the elucidation of the metabolic significance of the patellamide complexes, the formation of the complexes was investigated *in vitro* in buffer at pH 8.2 as well as *in vivo.* Therefore, a patellamide ligands with an appended reporter groups (RG) were prepared (see Figure 1).

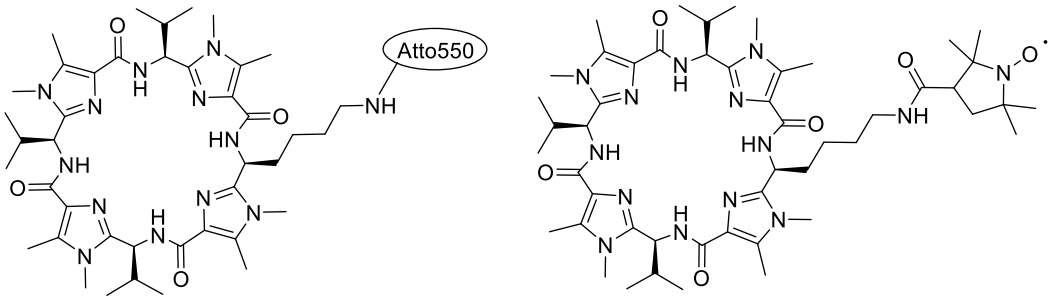

Figure 1. Model ligands with reporter groups Atto550 and Proxyl.

The fluorescent tag Atto550 as well as the spin label Proxyl were chosen as the reporter groups. *In vitro* studies with H_4pat-Atto550 indicate the formation of a Cu^{II} complex in buffer, however, results from EPR studies with the ligand H_4pat-Proxyl and Cu^{II} could so far not verify this finding. In addition, a protocol for the uptake of patellamides by *Prochloron* was developed allowing the introduction of the ligand H_4pat-RG into the cells. Results from flow cytometry as well as confocal microscopy support the formation of a Cu^{II} patellamide complex *in vivo*. In addition, preliminary *in vivo* hydrolysis measurements are presented.

In conclusion, the work presented contributes to an improved understanding of the hydrolase-like activities of the patellamide-based copper(II) complexes and gives a first insight on the stabilities of the complexes in *Prochloron* cells.

Kurzfassung

Die Blau-Grün Alge *Prochloron* produziert und exportiert in großen Mengen zyklische Oktapeptide (Patellamide) an ihren obligaten Wirt, *Lissoclinum patella* (Ascidie). Da die Kupfer(II)-Ionenkonzentration in den Ascidien im Vergleich zum umgebenden Meerwasser um den Faktor 10^4 erhöht ist, wurden Studien über vermeintliche Kupfer(II)-patellamid Komplexe durchgeführt. Mit Hilfe dieser Untersuchungen konnte gezeigt werden, dass es sich bei den dinuklearen Kupfer(II)-Komplexen der Peptide um effiziente Katalysatoren für biologisch relevante Hydrolysereaktionen handelt, wie z.B. Phosphatase und Carboanhydrase. Ihre Rolle im Stoffwechsel der Ascidien und der Blau-Grün Algen ist jedoch bisher noch unbekannt.

In der vorliegenden Arbeit wurden Studien zur Abhängigkeit der Phosphataseaktivität der dinuklearen Kupfer(II)-Komplexe von der Seitenkettenkonfiguration der Liganden sowie vom katalytischen Metallzentrum durchgeführt. Die Ergebnisse zeigen, dass die Komplexe mit Liganden natürlicher *RS* Stereokonfiguration drei- bis fünffach erhöhte Hydrolyseeffizienz aufweisen im Vergleich zu Komplexen mit Liganden nicht-natürlicher Stereokonfiguration. Darüber hinaus wurde der Einfluss des Metallzentrums auf die Phosphataseeffizienz der Komplexe durch den Austausch von Kupfer(II) durch Zink(II) untersucht. Da nur einer der drei untersuchten Zink(II)-patellamid Komplexe katalytische Aktivität zeigte, wurde eine strukturelle Untersuchung der Komplexe durchgeführt. Dazu wurden neben den Hydrolysemessungen auch NMR-, MS- und ITC-Titrationen, sowie eine vergleichende MM- und QM-Studie unternommen. Die Ergebnisse der Untersuchung deuten auf ein ähnliches Bindungsverhalten von Zink(II) in Patellamiden wie bereits für Kupfer(II) gezeigt. Dabei bindet das Metallion in einer Bindungstasche, die von zwei Stickstoffen in einem Heterozyklus und einem deprotonierten Amidstickstoff aufgespannt wird. Die ausbleibende Phosphataseaktivität ist daher vermutlich auf eine mangelnde Stabilität der Zink(II)-Komplexe unter wässrigen Bedingungen zurückzuführen.

Darüber hinaus wurden die α- und β-Glykosidase- sowie β-Lactamase-artige Aktivität der Kupfer(II)-patellamid Komplexe untersucht. Es konnte gezeigt werden, dass die Imidazol-basierten Komplexe nicht nur Phosphatester bei pH 7-8 spalten können, sondern auch dazu in der Lage sind unter basischen Bedingungen (pH 10) glykosidische Bindungen zu hydrolysieren. Außerdem konnte β-Lactamase-artige Aktivität bei pH 11.5 für einen der Patellamid-basierten Komplexe beobachtet werden. Diese Ergebnisse deuten darauf hin, dass die Kupfer(II)-Komplexe pH-abhängige, schaltbare

Katalysatoren sind. BEHRENDT *et al.* berichteten kürzlich, dass der pH Wert in unmittelbarer Nähe zu *Prochloron* in Abhängigkeit der Beleuchtungsstärke fluktuiert. Vor dem Hintergrund dieser Ergebnisse könnten die Hydrolyseergebnisse bedeuten, dass die dinuklearen Kupfer(II)-Komplexe verschiedene Funktionen im Laufe des Tages, in Abhängigkeit der Sonneneinstrahlung, erfüllen.
Um einen Beitrag zur Aufklärung der metabolischen Bedeutung der Patellamid-Komplexe zu leisten, wurde die Bildung der Kupfer(II)-Komplexe *in vitro* (pH 8.2) sowie *in vivo* untersucht. Dazu wurden Patellamid-Liganden mit verschiedenen Reportergruppen dargestellt (siehe Abbildung 1).

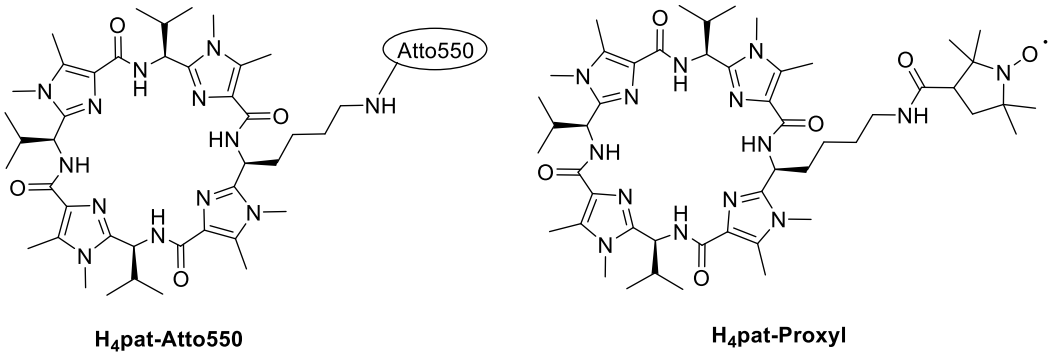

Abbildung 1. Modell-Liganden mit Reportergruppen Atto550 und Proxyl.

Als Reportergruppen wurden zum einen der Fluoreszenzfarbstoff Atto550 gewählt, sowie zum anderen das Spin-Label Proxyl. *In vitro* Untersuchungen mit dem Liganden H_4pat-Atto550 weisen auf die Bildung eines Kupfer(II)-Komplexes in gepufferter Lösung hin, allerdings konnten ESR-Experimente mit dem Liganden H_4pat-Proxyl dieses Resultat bisher nicht eindeutig verifizieren. Im nächsten Schritt wurde ein Protokoll für die Aufnahme der Modell-Liganden in die Zellen etabliert. Die Ergebnisse von Durchflusszytometrie und Konfokalmikroskopie deuten auf die Bildung eines Kupfer(II)-patellamid Komplexes *in vivo* hin. Abschließend werden erste *in vivo* Hydrolysemessungen präsentiert.
Folglich trägt die hier vorgelegte Arbeit zu einem besseren Verständnis der Hydrolase-artigen Aktivität der Patellamid-basierten Kupfer(II)-Komplexe bei und gibt einen ersten Einblick in die Stabilität der Komplexe in *Prochloron* Zellen.

Table of Contents

1 State of the Art

1.1 *Prochloron* - a special cyanobacterium

The International Union of Geological Sciences (IUGS) is the body responsible for the official geological periodisation. To IUGS, the atmospheric scientists PAUL CRUTZEN and EUGENE STOERMER put forward the suggestion to call the era from the 1960s onwards 'Anthropocene'.[1] If the commission decides in favour of granting this title, it would mean that humans consider themselves as predominantly responsible for the sedimentation observed on earth since then.

Without the emergence of oxytrophic organisms, namely cyanobacteria, more than 2.5 billion years ago, there would neither be an Anthropocene nor anyone claiming that title to be suitable, simply because of the lack of air to breathe – there would not be sufficient dioxygen. The first organisms to produce dioxygen, as a very toxic waste product from the metabolic conversion of CO_2, were cyanobacteria. This development was driven by the need of reduced carbon species for the growth of organisms, consequently the resulting amount of oxidation equivalents could not be buffered any longer by auxiliary substrates like reduced Fe^{II} or sulfur species (S^{-II}) and therefore dioxygen was directly released to the atmosphere.[2] Cyanobacteria are to date the only reported examples of oxyphototrophs among prokaryotes and are mainly responsible for the present composition of the biosphere and oxic atmosphere. This is the case due to their photosynthetic dioxygen production. Beyond that, scientists nowadays also agree, that all higher plants acquired their efficient machineries, chloroplasts and mitochondria amongst them, by the incorporation of prokaryotes as symbionts, emphasising their importance for the development of higher plants. This is commonly referred to as theory of symbiogenesis.[3]

The hypothesis was first proposed by KONSTANTIN MERESCHKOWSKY in 1910 and did not gain much attention until almost seventy years later, when accumulating discoveries were made supporting endosymbiotic origins of mitochondria and chloroplasts. [4-6] Models for the prokaryotic ancestor of red

algal chloroplasts, the unicellular cyanobacteria, were found; only the potential model ancestor for the green algal chloroplast was missing – until the discovery of *Prochloron*.[6-8] This photosynthetic symbiont of ascidians exhibits not only chlorophyll *a*, but also chlorophyll *b*, allowing a more efficient collection of sun light, like eukaryotes, *i.e.* higher plants and algae. However, it did not have blue or red protein pigments (phycobilins), which is in contrast to findings for other oxygenic photosynthetic prokaryotes, often exploiting the green pigment chlorophyll *a* and adjunctive phycobilins. These findings fostered further in-depth research on the biochemical features of *Prochloron*, its cytology, physiology, ecology and phylogeny, even though all of these studies were limited by the fact that *Prochloron* has to date not been brought into laboratory culture[9,10] (there is a paper claiming the contrary[11] but the report could not be confirmed). It was initially named *Prochloron didemni*[7], nowadays however numerous clades have been found, and since it could not be associated with the blue-green algae (cyanobacteria), therefore it was grouped into a new sub-class, the prochlorophyta. During the course of research more prochlorophytes were found, resembling the particular membrane-bound chlorophyll *a*/*b* light harvesting complexes (LHC), which are not related to the chlorophyll *a*/*b* antenna in the LHC of eukaryotic oxyphototophs,[12,13] namely *Prochlorothrix* and *Prochlorococcus.*[14,15] They both lack phycobilin, but are in contrast to *Prochloron* free-floating and can be kept in culture (non-axenic). Since the genes coding for chlorophyll *b* synthesis in prochlorophytes are similar to the respective genes found in chlorophytes it is believed that they share an evolutionary ancestry[16] or must have undergone a significant gene transfer. Contrastingly, the chlorophyll *a*/*b* LHC proteins evidently evolved independently in the algal classes.[12] Accumulating information from nucleotide sequences indicate that the prochlorophytes are, despite their special pigment composition, related closely phylogenetically to the blue-green algae,[17] and are therefore probably not the one missing link in chloroplast evolution but certainly belong to one of the lineages in the cyanobacteria in which chlorophyll *b* evolved.[12,18] It is consequently believed that prochlorophyta can be subsumed into cyanobacteria or cyanophyta.[19]

Prochloron is an extremely large prokaryote, with a diameter of 7-25 µm (see Figure 1.1). It is a spherical cell with thylakoid membranes stacked to the periphery. *Prochloron* is always found as an obligate symbiont of subtropical and tropical ascidians, like *Diplosoma virens, Tridemnum cyclops*, *Didemnum molle* and the genus *Lissoclinum* – *Lissoclinum punctatum, Lissoclinum bistratum* and *Lissoclinum patella* amongst them. *Prochloron* is the only reported obligate photosymbiont in the phylum chordata.[20] This is particularly interesting, because a *Prochloron* draft genome was published[21]

that did not show any lack of relevant metabolic genes, which could explain why it can neither sustain photosynthesis nor reproduce *ex hospite* (outside the host). Currently research is being undertaken by KÜHL and BEHRENDT to unravel the secrets of *Prochloron*'s precise microenvironment and consequently understand the requirements to transfer it to laboratory culture.[9]

Figure 1.1. Left: Microscopy picture of *Prochloron,* showing the stacked thylakoid membranes inside (taken with a confocal microscope λ_{exc}=665 nm); middle: *Lissoclinum patella* colony ~200 cm^2 on a coral; right: ~10 cm^2 on a stone.

For carbon assimilation, *Prochloron*, like other blue-green algae, uses carboxysomes,[22] in which carbonic anhydrase is abundant, as well as Rubisco[23] fixing it from CO_2 to phosphoglyceric acid. It could be shown that there an active supply of organic products to its host is likely and these organic products seem to be early metabolites of the CALVIN cycle.[24] Approximately 12-56% of the reduced carbon species are contributed from this translocation for host respiration and that is primarily host-dependent.[25,26]

With an oxygen evolving complex and electron transport observed *via* photosystem (PS) I and II, *Prochloron*'s photosynthetic apparatus appears related to that of other cyanobacteria. Moreover, distinct light harvesting supercomplexes associated with the chlorophyll *a*/*b* proteins are existent in PSI and PSII[27,28] allowing an efficient photosynthetic electron transport system. This leads to maximum quantum yields of PSII up to 0.82, which is significantly higher than for most cyanobacteria, but of the same order of magnitude as observed for higher plants.[29,30]

The putative fixation of N_2 by *Prochloron* is subject of ongoing discussion.[21,31] Results indicating additional nitrogen fixation in the symbioses were provided by KOIKE *et al.* in 1993.[32] Moreover, it could be shown that the major nitrogenous waste of the host is ammonium,[33] which is taken up by *Prochloron*.[34] PEARL raised the idea, that N_2 fixation assists to meet the prokaryotic nitrogen requirements.[35] This is supported by nitrogen isotope ratios measured in the *L. patella* and in *Prochloron* cells, which point to a nitrogenase activity.[36]

More recent studies focussed on the *Prochloron* genome, the microbiome as well as on the micro-environment and added significantly to the understanding of the ecology of *Prochloron*.[21,37,38]
Thereby it was demonstrated that *Prochloron* is subject to rapid and dynamic chemical changes in its direct environment.[9] Upon irradiation, the pH as well as the O_2 saturation levels are altered drastically within 15-30 min – changing the interior zone of the ascidians from an anoxic and neutral/slightly acidic environment (pH ~7.0) to a dioxygen super saturation level and strongly alkaline pH values (10.5) compared to the surrounding sea water (pH 8.2).[9] Surprisingly, no photo inhibition was observed, even upon irradiance levels comparable to direct sunlight, and the photosynthesis recovered quickly after periods of extremely low dioxygen saturation levels.[9] Since CO_2 is absent at these alkaline conditions and photosynthesis consequently is solely dependent on HCO_3^-, this points to an HCO_3^- dependent carbon transport mechanism.[39] These findings are in line with genome studies[21] that prove the existence of low affinity carbon transport pumps and the lack of many carbon transporters that were found in other cyanobacteria.[40] Apparently, these low affinity pumps are capable of transporting sufficient HCO_3^- into the cells even under high irradiance.
To what extent the biochemical and photosynthetic activity of *Prochloron* is influenced by the host is uncertain to date and subject of ongoing research.[22,41] Implications on possible communication mechanisms across the cell membrane arose from secondary metabolites found inside *Prochloron* as well as in close proximity to it, in the ascidians. These secondary metabolites are small cyclic peptides, that are ribosomally expressed and are commonly referred to as cyanobactins.[21,42,43]

1.2 Ribosomal expression of cyclic peptides

Prochloron exhibits a rich variety in metabolites that are apparently expressed depending on which host it is living in symbiosis with. So far it could not be determined whether an epigenetic expression regulation governs the metabolite synthesis.
The cyclic peptides were first discovered during the 1980s by researchers screening marine metabolites for potential pharmaceutical applications.[44] Medicinal applications of the natural cyclic peptides and a series of synthetic derivatives have been studied thoroughly and it was shown that these peptides exhibit cytotoxic,[44] antibacterial, antineoplastic and antiviral activities.[45,46]. Some of the metabolites found in host organisms of *Prochloron* are summarised in Figure 1.2.

Three different expression pathways are known for prokaryotes: the ribosomal production and post-translational modification (RIPP), the production of a non-ribosomal pathway (NRP) and the mixed process, where polyketide synthases (PKS) and the non-ribosomal pathway intervene.[47,48]

Typically, one would expect the NRP mechanism for the expression of small cyclic peptides with *R*-amino acids in the scaffold, however, the cyanobactins found in *L. patella*, ascidiacylclamide, patellamides A-G and ulicyclamide, are all expressed *via* the RIPP mechanism, shown by NAISMITH and JASPARS in 2012.[46,49,50] As this mechanism is usually only observed for peptides of metabolical importance, it gives rise to the hypothesis that the cyclic peptides might act as key metabolites. [51-53] At the same time the patellamides show a similar size but increased flexibility as compared to the prosthetic group porphyrin in haem or chlorophyll.[54] Thus, one might also encounter an involvement of the patellamides as multifunctional prosthetic groups in proteins to be their biological function.

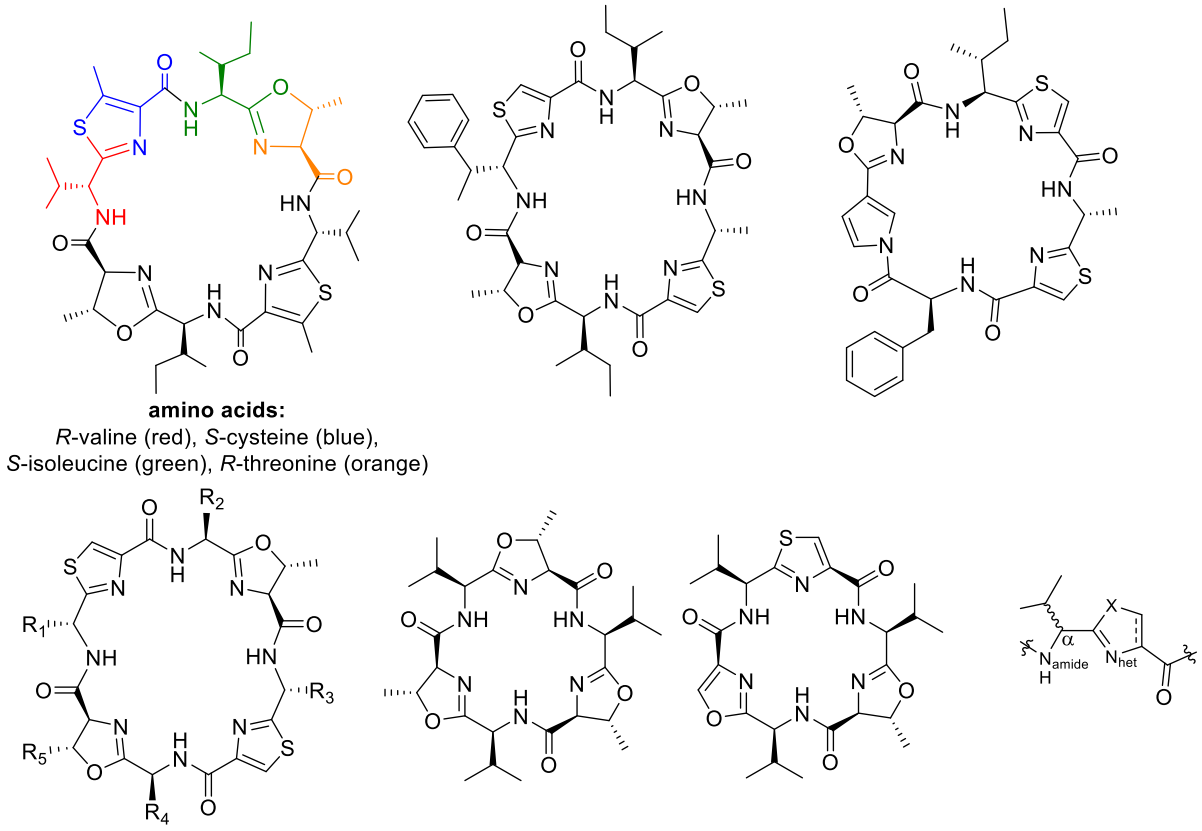

Figure 1.2. Ascidiacyclamide,[55] Patellamide A,[56] Ulicyclamide,[57] Patellamide skeleton (see also Table 1.1), Westiellamide,[58] Bistratamide D,[59] schematic representation of one cyanobactine building block (left to right, top to bottom). The colour code in ascidiacyclamide shows the amino acid building blocks of one half of the molecule.[60-62]

Common chemical features of the cyanobactins are the heterocycles, *i.e*. thiazole, oxazole, as well as oxazoline, which are connected *via* peptide bonds. The amino acid residues are hydrophobic, and often originate from valine or *iso*-leucine. *N*-heterocycles result from the condensation of threonine, cysteine and serine side chains with carbonyl groups in the peptide sequence.[62] Condensation of six or eight amino acids results in hexa- or octapeptides, and since the peptide functionalities are hidden in the heterocycle, the macrocycles are called *pseudo*-peptides (see Figure 1.2 for highlighted constituents and the corresponding amino acids and Table 1.1 for the side chains of patellamide A-G).

Table 1.1. Amino acids contributing to the side chains of Patellamide A-G.[56]

Patellamide	R_1	R_2	R_3	R_4	R_5
A	*R*-Val	*S*-Ile	*R*-Val	*S*-Ile	H
B	*R*-Phe	*S*-Ile	*R*-Ala	*S*-Leu	CH_3
C	*R*-Phe	*S*-Ile	*R*-Ala	*S*-Val	CH_3
D	*R*-Phe	*S*-Ile	*R*-Ala	*S*-Ile	CH_3
E	*R*-Phe	*S*-Ile	*R*-Val	*S*-Val	CH_3
F	*R*-Val	*S*-Val	*R*-Phe	*S*-Val	H
G	*R*-Ala	*S*-Leu	*R*-Phe	*S*-Ile	CH_3

The *pseudo*-octapeptides isolated from *L. patella* show a strong preorganisation for the coordination of metal ions with their 21-azacrown-7 and 24-azacrown-8 structures. Interestingly, none of the natural peptides exhibit imidazole heterocycles that are commonly conserved in metal ion binding sites of metabolic importance.[2] The imidazole heterocycle could originate from the incorporation of 2,3-diaminopropionic acid, a closely related analogue of serine, which would result in the formation of imidazole upon cyclisation. However, 2,3-diaminopropionic acid is of low natural abundance, which might be the reason why it is not part of the heterocycles.[62-64] Another common feature in the cyclic octapeptides is the alternate *R,S,R,S* stereoconfiguration of the side chains, leading to a limited flexibility of the macrocycles.

The rigidity of the systems was investigated by density functional theory (DFT), showing that it is primarily governed by the incorporated heterocycle.[65,66] Thiazole is expected to be the most flexible moiety, exhibiting comparably small energy barriers (max. ~5 kJ/mol) for twisting along the dihedral N_{amide}-C_{α}-C_{azole}-X (see Figure 1.2) as well as three minima at 30°, 80° and 160°.[65,66] Oxazole shows higher energy barriers (~8 kJ/mol) and minima at 60° and 170°. The investigation of the imidazole heterocycle

gave energy barriers of approximately 30 kJ/mol and minima at 90° and 150° respectively, indicating imidazole-containing octapeptides to be the least flexible.[65]

Analyses of the octapeptides by means of DFT calculations, in addition to X-ray crystallography and ^{1}H-NMR spectroscopy imply two different conformations: the saddle-shaped structure and the twisted structure, called 'figure-of-eight' conformation (see Figure 1.3).[67]

In the saddle-shaped conformation all nitrogen atoms point towards the inside of the macrocycle, allowing the peptide to adopt C_2 symmetry. The twisted figure of eight conformer on the other hand is characterised by intramolecular NH···O=C and NH···O_{het} hydrogen bonds resulting in a less symmetrical conformation with the oxazoline ring rotated in a way, such that the nitrogen atoms of the oxazoline moieties are forced to face the outside of the macrocycle.[68]

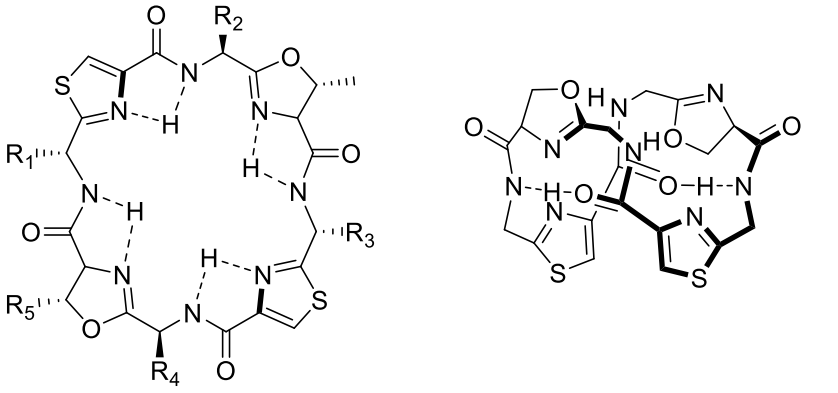

Figure 1.3. Preferred conformations of cyclic *pseudo*-peptides.[67,69]

Less is known about the cyclic hexapeptides, like the bistratamides (see Figure 1.2), which could be extracted from *Lissoclinum bistratum*, first described by HAWKINS *et al.* in 1989.[70] Although the exact expression mechanism was not elucidated, it is believed that *Prochloron*, the symbiont of *L. bistratum*, expresses the cyclic peptides as observed in the *L. patella* symbiosis. This is especially indicated by the fact that the bistratamides are mainly found in close proximity to the *Prochloron* cells, which suggests at least an involvement in the biosynthesis.[70] Very closely related hexapeptides were found from the extraction of the terrestrial blue-green alga *Westiellopsis prolifica* ("The blue-green alga was collected from a mud sample"[58]), called westiellamides (see Figure 1.2).[58] The structural difference between westiellamides and bistratamides is mainly the incorporation of a thiazole instead of an oxazoline. Both classes of cyclic hexapeptides were shown to be moderately cytotoxic.[58,70] Interestingly

Westiellopsis prolifica, being a cyanophyte, could be grown in laboratory culture in BG 11 medium under axenic conditions – unlike all prochlorophytes.[9] This however indicates that the cyclic peptides are not necessarily related by communication between the host ascidian and *Prochloron*, since *Westiellopsis* is a free-floating prokaryote. Nevertheless, given their high bioactivity, the cyclic peptides might play an important role in anti-predator mechanisms. However this is equally disputable, because of the sheer quantity of cyanobactins found in *Lissoclinum patella* and *Lissoclinum bistratum* – up to several percent of the dry weight.[51,52] Consequently, the current focus of research is on the putative metabolic role of the cyclic peptides. The significantly increased metal ion concentration, in particular of Cu^{II} and Zn^{II} to about 10^4-fold in comparison to the surrounding sea water implied a metal-coordination related metabolic role.[71] Different functions have been discussed, the involvement in metal ion transport and storage as well as their role as potential prosthetic groups amongst them. Therefore, the coordination chemistry of natural cyclic hexa- and octapeptides was studied and is presented in the next paragraph.[67,71]

1.3 Metal complexes of cyclic hexa- and octapeptides

The metal ion concentrations (Cu^{II} and Zn^{II}) found in ascidians are comparably high, which is surprising if compared to the cytotoxic effects known at these concentrations for other microorganisms.[71] Given the constitution of the patellamides with four heterocyclic-nitrogen atoms and four amide-nitrogen atoms, pointing towards the inside of the cyclic peptide, potentially acting as donor atoms, the coordination chemistry of these macrocycles has been studied extensively *in vitro*.[72]

ITC measurements, as well as data from CD, UV-vis and NMR spectroscopy indicate a metal ion binding of both Cu^{II} as well as Zn^{II} with stability constants in the range of $\log K(Zn^{II}) \approx 2\text{-}4$ / $\log K(Cu^{II}) \approx 4\text{-}5$.[67] The X-ray structure of the dinuclear Cu^{II} complex of ascidiaycylamide with carbonate as a bridging coligand was the first natural metal complex that could be investigated in the solid state (and is shown in Figure 1.4).[71] In this complex, two metal ions are binding to the ligand, the Cu^{II} is coordinated by two heterocyclic nitrogens as well as a deprotonated amide nitrogen, providing a N_{het}-N_{amide}-N_{het} binding motif. This is accompanied by acidification of the solution, since protons are released from the ligand upon complexation. Consequently, two equivalents of base have to be added in order to achieve the formation of a dinuclear complex.[73] As the pH in sea water is approximately 8.2, which is slightly

alkaline, it is not unlikely, that the dinuclear copper(II) patellamide complexes are associated with the metabolic role of the cyclic octapeptides.

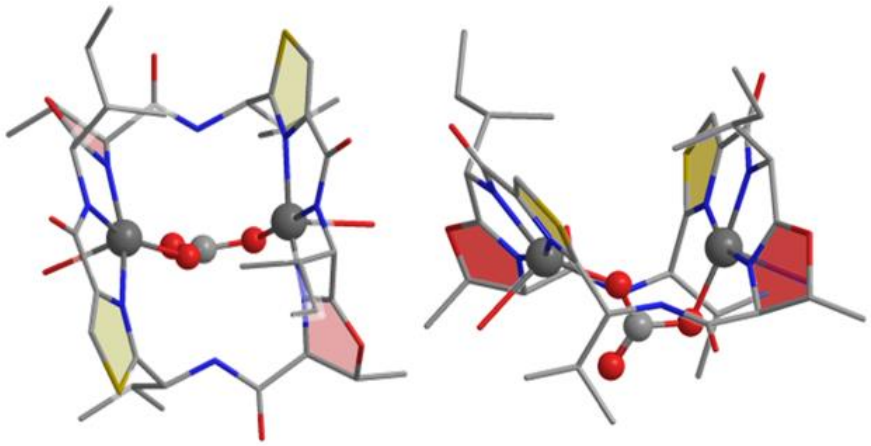

Figure 1.4. Top and side view of the carbonato-bridged dinuclear Cu^{II} complex of ascidiacyclamide determined by X-ray crystallography (grey: C, yellow: S, blue: N, red: O).[71] Reprinted with permission from [74] Copyright 2012 Wiley-VCH.

An investigation of the metal-binding capability of patellamide D by means of EPR, CD and UV-vis titrations indicated the following complexation scenario:[71]

$$(Cu^{2+})_{solv.} + \mathbf{H_4patD} + NEt_3 \longrightarrow [Cu(\mathbf{H_3patD})]^{+} + NEt_3H^{+}$$

$$[Cu(\mathbf{H_3patD})]^{+} + (Cu^{2+})_{solv.} + NEt_3 \longrightarrow [Cu_2(\mathbf{H_2patD})]^{2+} + NEt_3H^{+}$$

$$[Cu_2(\mathbf{H_2patD})]^{2+} + NEt_3 + H_2O \longrightarrow [Cu_2(\mathbf{H_2patD})(OH)]^{+} + NEt_3H^{+}$$

$$[Cu_2(\mathbf{H_2patD})(OH)]^{+} + CO_2 \longrightarrow [Cu_2(\mathbf{H_2patD})(CO_3)] + H_2O$$

The addition of one equivalent of base leads to the deprotonation of the ligand, which alters the complex formation equilibrium in a way that allows the formation of a mononuclear copper(II) complex. Upon the addition of one more equivalent of base and copper, a dinuclear complex is observed. As soon as more equivalents of base are added, one of the copper(II) ions in the complexes is observed to be coordinated by a hydroxido coligand. Interestingly, the dinuclear patellamide complex with OH^- as the coligand is observed to form a carbonato-bridged complex upon exposure to air, as shown for the respective ascidiacyclamide complex (see Figure 1.4).

1.4 Model peptides and their metal complexes

Obtaining patellamides from natural sources is not only invasive, but also time-consuming and delivers comparably small amounts of the peptides, similar to recombinant expression. Therefore, a more efficient route was developed by HABERHAUER *et al.* to synthetically produce patellamides in a larger scale.[62] An additional benefit of this technique is that variations in terms of ligand structure, *i.e.* preorganisation of the metal ion sites, as well as the donor sets and consequently the tuning of the electronics of the metal sites, became accessible.

1.4.1 Synthesis of model patellamides

The synthesis of the most accessible model patellamide H_4pat^2 is summarised in Scheme 1.1.
By the choice of the amino acid, various side chains can be selected. With the technique shown in Scheme 1.1, imidazole moieties are obtained upon azeotropic removal of water in xylene. The natural peptide ascidiacyclamide as well as three model ligands that can be prepared analogously to the method described in the Scheme below are depicted in Figure 1.5 and 1.6.

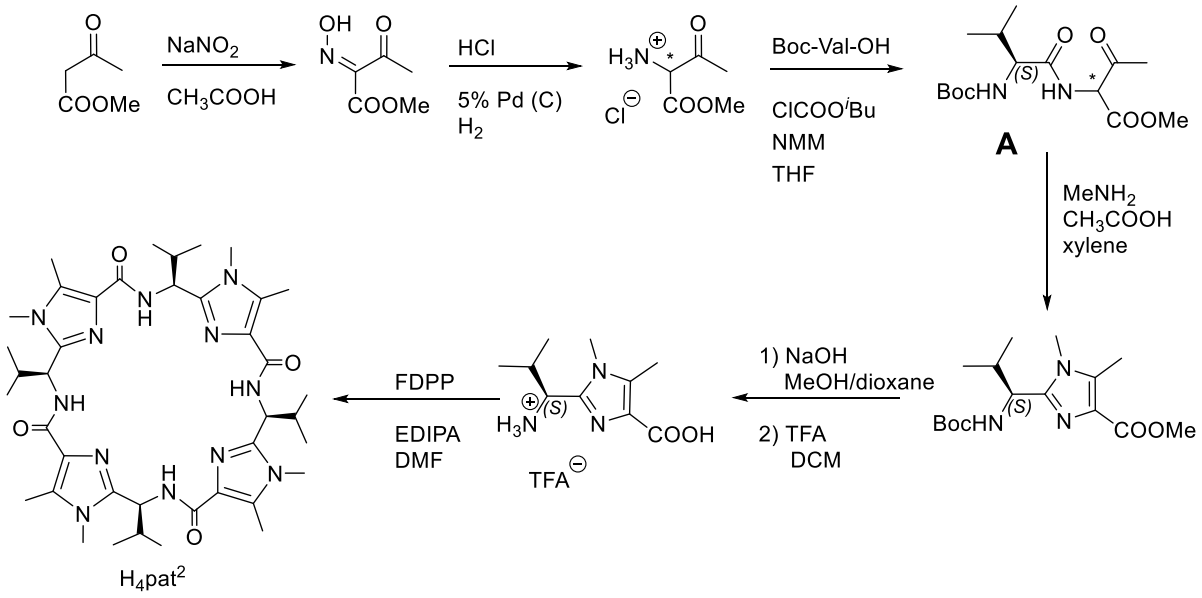

Scheme 1.1. Synthesis of H_4pat^2 as reported by HABERHAUER *et al.*[62]

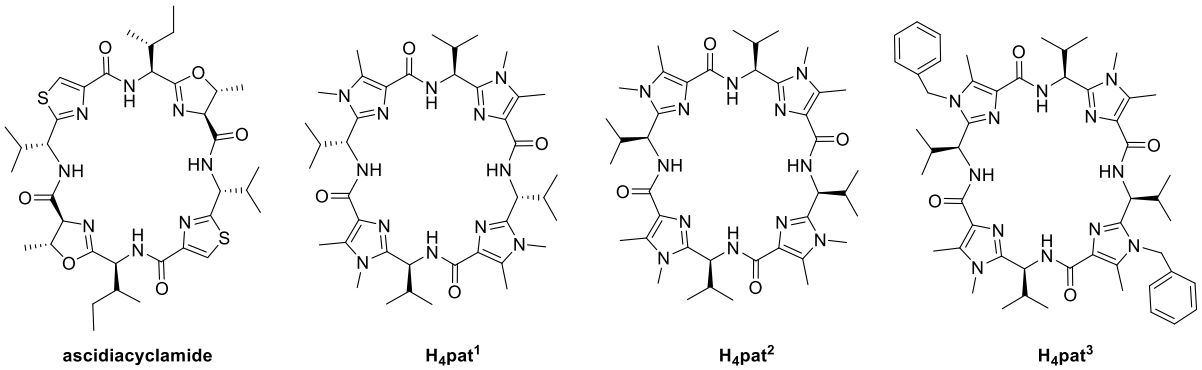

Figure 1.5. Ascidiacyclamide (left) and synthetic *pseudo*-octapeptides H_4pat^1, H_4pat^2 and H_4pat^3.

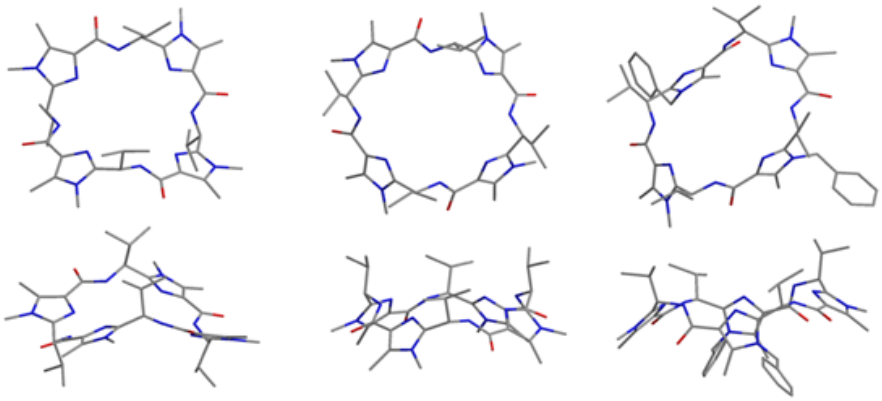

Figure 1.6. Top and side views of the crystal structures of H_4pat^1,[75] H_4pat^2,[76] and H_4pat^3 (grey: C, blue: N, red: O, hydrogen atoms are omitted for clarity).[73] Adapted with permission from [77].

HABERHAUER moreover developed an efficient route to oxazole-based ligands (see Scheme 1.2) and to a very close analogue of the natural ascidiacyclamide, H_4pat^5 (Scheme 1.3) with missing methyl groups in two of the side chains.[61,72]

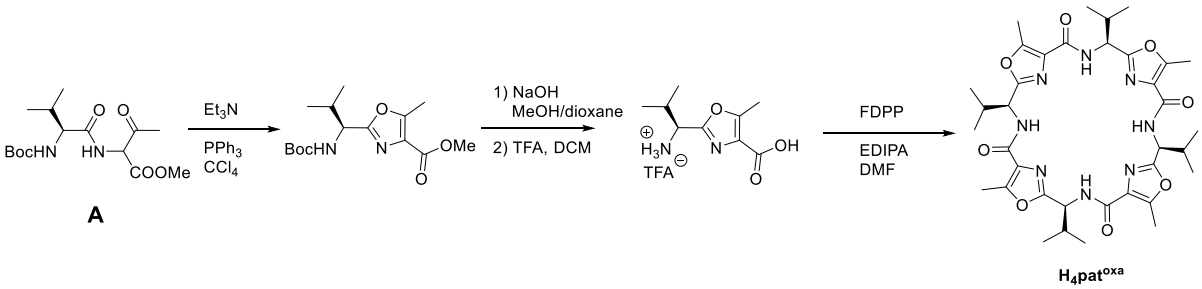

Scheme 1.2. Synthesis of H_4pat^{oxa} as reported by HABERHAUER *et al.*[62]

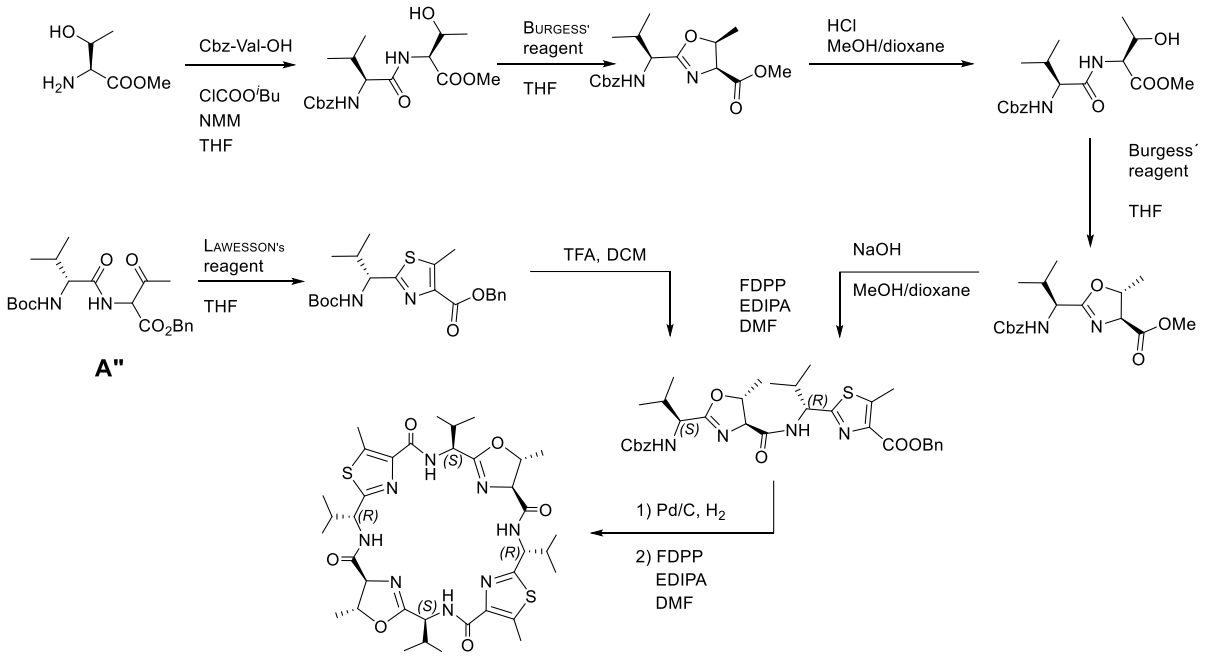

Scheme 1.3. Synthesis of H_4pat^5 as reported by HABERHAUER *et al.*[62]

The synthetic approach is very elegant, as all routes start from the same reactant, namely methyl 2-((*S*)-2-((*tert*-butoxycarbonyl)amino)-3-methylbutanamido)-3-oxobutanoate (highlighted as **A** in Scheme 1.2) or the respective (*R*) configured equivalent (highlighted as **A"** in Scheme 1.3). In the subsequent step **A**/**A"** is reacted to the heterocycle of choice, *i.e.* either an imidazole, a thiazole, an oxazole or the respective oxazoline. These building blocks are *N*- as well as *C*- protected and upon deprotection that can be carried out giving quantitative yields, the building blocks are coupled by the coupling reagent FDPP (Pentafluorophenyl Diphenylphosphinate) with yields between 20-30%.[47] However, recently a cheaper and more efficient coupling reagent was developed, COMU ((1-cyano-2-ethoxy-2-oxoethylidenaminooxy)dimethylamino-morpholino-carbenium-hexafluorophosphate); thus, in recent reports usually COMU was used as coupling agent.[78,79]

Two components of the peptides are of crucial importance for the stereochemistry of the ligands: the heterocyclic moiety and the stereo-configuration of the side chains. The model patellamides H_4pat^1 and H_4pat^5 show an alternate *R,S,R,S* configuration as observed in the natural products, resulting in a saddle-shaped preorganised geometry of the ligand (see Figure 1.6).[67] H_4pat^2, H_4pat^{oxa} and H_4pat^4, on the contrary, have an all-*S* configuration of the side chains and are therefore easier to prepare. On the other hand, they lack, as does H_4pat^1, two partially saturated heterocycles compared to the natural peptides. Only H_4pat^5 comprises both features, exhibiting oxazolines and thiazoles as

heterocyclic moieties. This is however not unimportant, since the oxazoline is not planar and is therefore influencing the potential metal ion binding behaviour, as also expected from the different pK_a values of the heterocycles: *N*-methyl imidazole≈7.0, oxazole 0.8, oxazoline 4.8, thiazoline 2.5.[80]

1.4.2 Metal complexes

So far, the patellamide coordination chemistry has primarily concentrated on Cu^{II}. An important reason, apart from the putative relevance of Cu^{II} for the ascidians,[72] is that UV-vis-, CD- and EPR spectroscopy in combination with force field and/or DFT calculations has allowed a thorough analysis of the solution structures, equilibria and hydrolase-type reaction pathways of these complexes.[61,75,79-84] These investigations showed that the model ligands are complementary for the binding of Cu^{II} and Zn^{II}, like reported for the natural patellamides. Isothermal calorimetric studies indicate a higher stability constant for the dinuclear Cu^{II} complex with ligand H_4pat^1, a ligand composed of building blocks with alternating *R* and *S* side chains, mimicking the side chain arrangement of the natural patellamides (log*K*=6.2).[67] The Cu^{II} complexes of ligands H_4pat^2, H_4pat^3 and H_4pat^{oxa} show lower stabilities: log*K*=4.6; 5.2; 5.5; which is in the range of the stability constants observed for the Cu^{II} binding of natural octapeptides.[79] From the collective data on the Cu^{II} binding behaviour of the model ligands, a cooperative binding is implicated.[67]

UV-vis-, CD-, EPR-spectroscopy and mass spectrometry studies of the copper(II) complexes with various model patellamides[77] revealed the solution equilibria shown in Scheme 1.4 (*n.b.* that the outside coordination does only occur for oxazole-based model patellamides). All investigations presented here were carried out in methanol with MeO^- as the base for solubility reasons. Therefore, the pH of the solutions under investigation is not known and the results must hence be interpreted carefully, when speaking about the function and structure of the complexes at aqueous conditions. The Scheme 1.4 shows two different arrangements of the dinuclear copper(II) patellamide complex with one hydroxido-coligand: (a) the terminal binding mode and (b) the bridging mode, the latter of which has been confirmed with X-ray crystal structure determination (see Figure 1.7).[67]

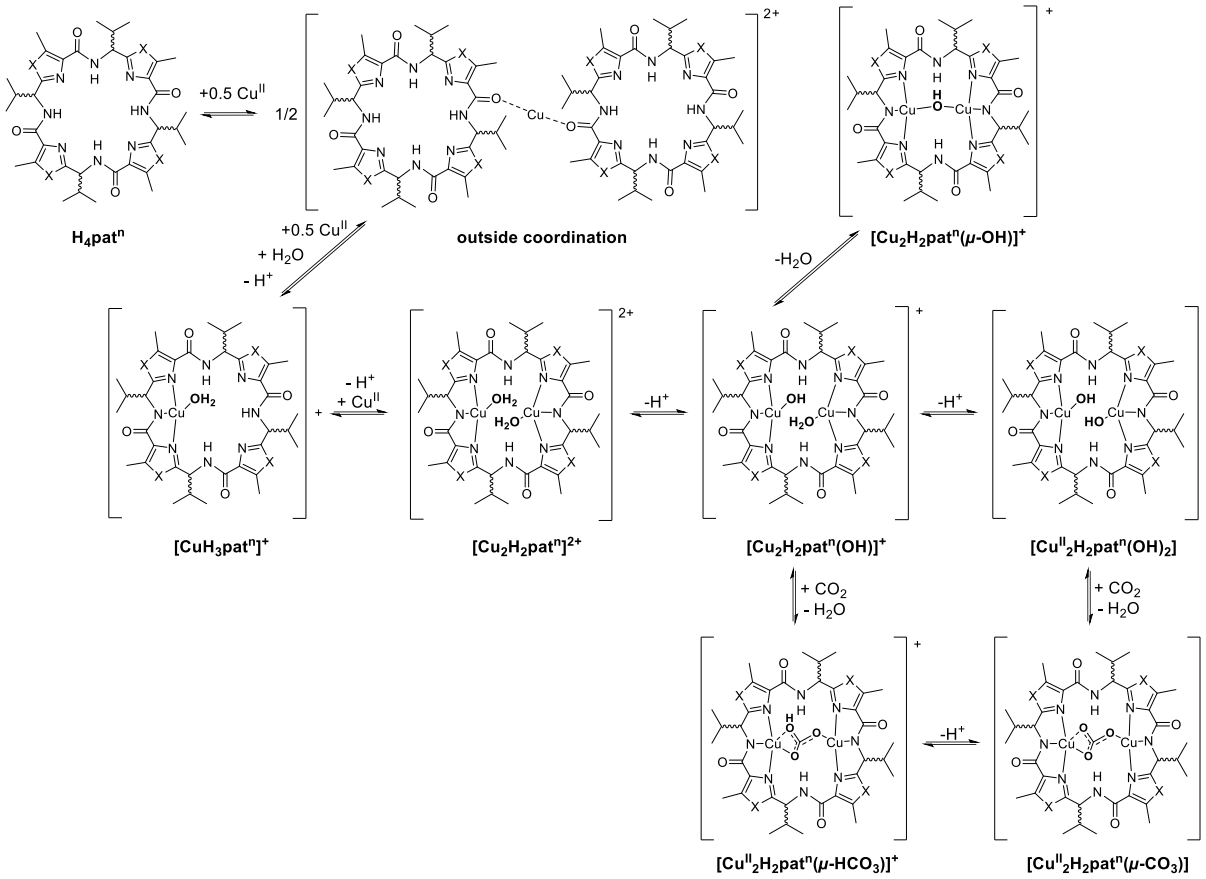

Scheme 1.4. Cu^{II} complexation equilibria of model patellamides H_4pat^n.[77]

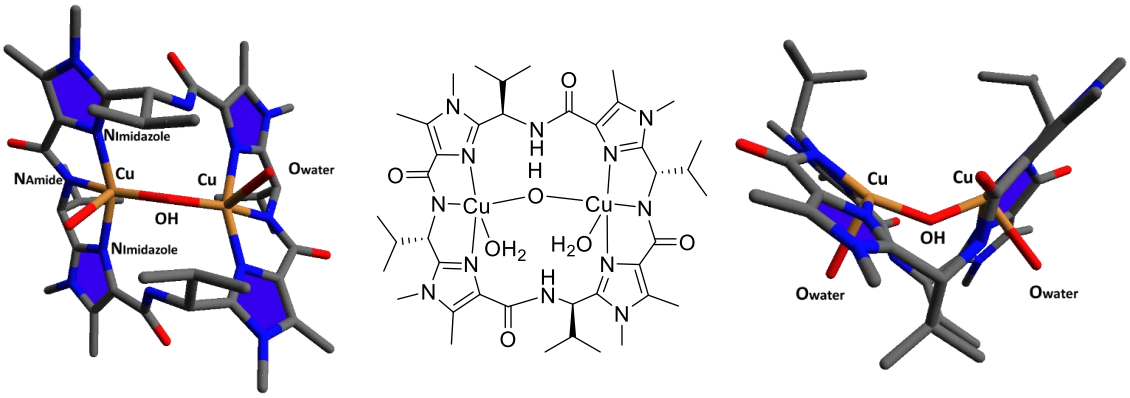

Figure 1.7. Top and side view of $[Cu_2(H_2pat^1)(\mu\text{-}OH)(H_2O)_2]^+$ (orange: Cu, grey: C, blue: N, red: O, hydrogen atoms are omitted for clarity).[67]

The binding motif of Cu^{II} in $[Cu_2(H_2pat^1)(\mu\text{-}OH)(H_2O)_2]^+$ is in agreement with expectations from the crystal structure of the dinuclear Cu^{II} complex of ascidiacyclamide – the copper(II) cations are

coordinated by two heterocyclic nitrogens (imidazole in this case), and a deprotonated amide nitrogen. Additionally, each of the copper(II) ions is coordinated by a water molecule and a bridging hydroxido-coligand. This results in a square-pyramidal coordination environment for the Cu^{II} ions, which is also expected from EPR spectroscopy as well as DFT calculations.[85]

Studies on putative zinc(II) complexes with model patellamides have been recently carried out, indicating an overall similar coordination behaviour as observed for the respective copper(II) species.[47] Isothermal calorimetric measurements give an ambiguous number of binding events, *i.e.* 1.51±0.16 (H_4pat^1) and 1.69±0.78 (H_4pat^2), however results from MS investigations indicate the complexes to be dinuclear. The stability constants determined for these species are $\log K_1K_2$=5.0; 4.5 for H_4pat^1 and H_4pat^2 respectively, which are in accordance with studies on natural peptides (*vide supra*).

1.5 Observed catalytic activity observed for dinuclear patellamide complexes

The driving force of patellamide complex investigations was always the urge to understand their potential biological role. As pointed out above, the slightly basic pH of seawater supports the assumption that the copper(II) patellamide complexes are formed in *L. patella* and *Prochloron*. Since the determined binding constants with Cu^{II} and Zn^{II} are rather small, the function of the patellamides as chelators performing metal ion storage and transport is not very likely. Consequently, the potential role of the dinuclear complexes as catalysts was the focus of research. Dinuclear metal ion sites have various advantages compared to just one metal ion in the active site, *i.e.* a lower thermodynamic driving force for redox reactions due to charge-delocalisation, a decreased activation barrier for solvent and enzyme reorganisation, the preorientation and electrostatic activation of substrates as well as the easier formation of nucleophiles, which could in turn initiate hydrolysis.[86] Moreover, the dinuclear sites are capable to stabilise transition states that are involved in the hydrolysis.[86] Since dinuclear metal ion complexes are abundant as effective catalysts in nature, several studies on the putative catalytic reactivity of the model patellamide complexes were carried out and are summarised briefly in this section after a short excursion about copper cation based enzymes.

1.5.1 Cu^{II} in natural catalysts

In nature, copper cations are predominantly found as the metal centres for catalysis of redox reactions, similar to Fe^{II} based enzyme sites.[87] For example Cu^{II} is present in cytochrome c oxidase and in the $Cu^{II}Zn^{II}$ superoxide dismutase. Moreover, it is relevant for oxygen transport (hemocyanin) as well as electron transport, as observed in plastocyanin during photosynthesis.[2] All these functions are enabled by the capability of copper ions to exist in two oxidation states, *i.e*. the oxidised (hard) +2 and the reduced (soft) +1 state. Similarly, as known for iron, the reduced form Cu^{I} can undergo FENTON chemistry with hydrogen peroxide.[2] It is important to note, that prokaryotes (like *Prochloron*) have developed under anoxic conditions. This also means that copper was not soluble and consequently only available in small quantities.[88,89] Therefore, some cyanobacteria, like *Synechocystis* sp. show an adapted metabolism depending on the relative metal ion availabilities.[87] It can use plastocyanine (Cu^{II}) and cytochrom c (Fe^{II}) interchangeably as an electron carrier and thereby sustain its metabolism during times of iron(II) or copper(II) deficiency.[87,90,91]

From a spectroscopic point of view three different 'classical' copper cation binding sites exist – type 1, 2 and 3, as presented in Table 1.2.[2] Often, combinations of multiple sites of one type are found in enzyme, *e.g*. 8 type 2 sites were reported for dopamine-β-monooxygenase.[2] Equally, combinations of the three sites are found in natural enzymes, as for example trimers consisting of type 2 and type 3 have been reported.[2,92] For copper ion storage proteins, usually copper cations are found to adopt the +1 oxidation state and are bound to cysteinate residues.[93]

Enzymes containing binding site 3 were found to serve for functions ranging from oxygen transport (haemocyanin) to monooxygenase activity (tyrosinase). Inspired by this, and as the patellamides were shown to bind two Cu^{II} ions similar observed for the type 3 sites, it was proposed by JASPARS and DE VISSER[94] that the Cu^{II} complexes might be involved in oxygen activation. They implied by DFT calculations that the dinuclear Cu^{II} complex with a bridging carbonato ligand (see Figure 1.4) might be a precursor complex for the subsequent binding of oxygen, as the coligand forces the Cu^{II} complex to adopt a certain geometry, that is in turn preparing the complex for subsequent oxygen binding. These studies were supported by IR investigations revealing a Cu_2O_2 cluster formation (ligand: natural ascidiacyclamide).

Table 1.2. Typical copper centres and examples of their observed function, adapted from [2].

Structure / Name / Characteristics	Coordination geometry	Typical Function
Type 1 'blue' copper centres Distorted polyeder (3+2 coordination)	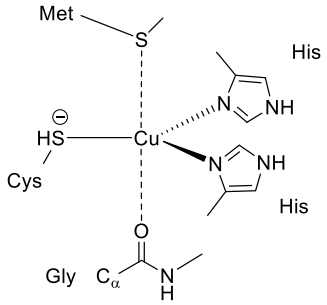	**Electron Transport** (Plastocyanin, Azurin) Blue Oxidases (Laccase, Ascorbate Oxidase)
Type 2 non – blue copper centre Nearly planar coordination sphere Coordination number: 4	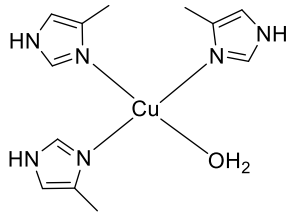	**Non – blue Oxidases** (Galactose Oxidase, Amine Oxidase) **Dioxygenases, terminal Oxidases**
Type 3 copper dimers Distance Cu-Cu: ≥360 pm Coordination number: 4	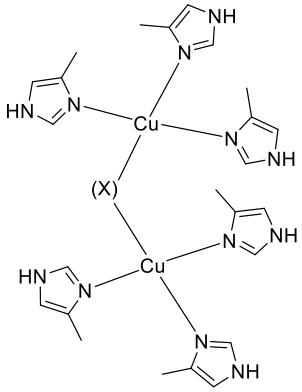	**Oxygen transport** (Hemocyanine) **Monooxygenases** (Tyrosinase)

The activation of dioxygen would imply that the copper(II) ions must undergo at some stage a change of oxidation state from +2 to +1, which is possible, if patellamides were to act as cofactors in hydrophobic environments or if the cells provided a sufficiently reductive milieu. The change in distance between the copper(II) centres, that one expects from a bridged coordination to a non-bridged coordination (3.5 Å to 4.5 Å), would furthermore be in line with expectations for respective tyrosinase and catecholase systems.[95,96]

In addition to the investigation of the dinuclear copper(II) patellamide complexes as potential oxygen activating enzymes, the crystal structure of the carbonato-bridged complex also stimulated research

on the potential role of dinuclear copper(II) patellamide complexes as carbonic anhydrases, which was consequently studied in detail.

1.5.2 Carbonic anhydrase-like activity

Experiments were carried out with labelled $^{13}CO_2$ and $^{18}OH_2$, which could prove the generation of labelled bicarbonate as well as labelled dinuclear patellamide complexes with carbonate as a coligand (observed by mass spectrometry).[74] It is proposed, that one copper(II) centre coordinates the CO_2 molecule, and the second Cu^{II} coordinates water. The latter acts as a LEWIS acid and consequently causes a lower pK_a value of the coordinated water, which is in turn deprotonated at physiological pH value (see Scheme 1.5).

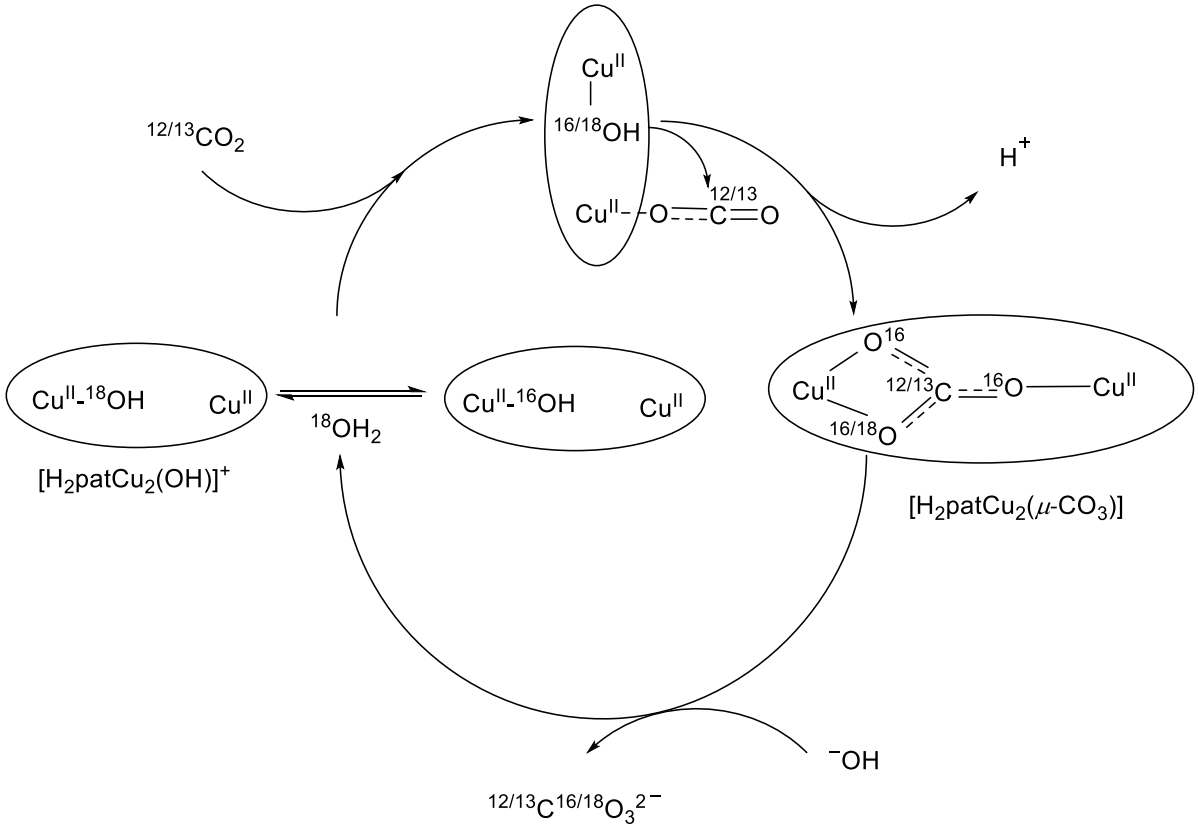

Scheme 1.5. Schematic representation of expected carbonic anhydrase-like activity of the dinuclear Cu^{II} patellamide complexes, adapted with permission from [77].

This resulting hydroxido-ligand could then be activated to attack the carbon of CO_2 nucleophilically.[97] Subsequent kinetic measurements at varying pH values proved the finding and showed that the

dinuclear Cu^{II} complex of H_4pat[1] is the fastest carbonic anhydrase model reported to date at pH 8.07 (k_{cat}=7.3x10^3 s^{-1}).[97] This finding is particularly interesting, since all known natural carbonic anhydrases are mononuclear enzymes with zinc(II) in the active site instead of copper(II).[2] The respective dinuclear copper(II) complex of H_4pat[5] also showed a high activity (k_{cat}=4.7x10^3 s^{-1}), whereas for the complexes of the ligands exhibiting all-*S* conformation k_{cat} values of ~1.8x10^3 s^{-1} were found. This means that the efficiency of the catalysis is more dependent on the conformation of the side chains than on the type of incorporated heterocycle. In the light of pH fluctuation upon altered levels of irradiation,[9] these findings could imply that in darkness (acidic pH, low O_2 saturation) respiration, *i.e*. carbohydrate catabolism, is triggered and produced CO_2 is released efficiently. Upon exposure to sunlight (basic pH, O_2 super saturation) on the other hand, the hydration of CO_2 is catalysed, making it readily available for photosynthesis.

1.5.3 Phosphatase-like activity

As the carbonic anhydrase-like activity is related to a metal-ion assisted deprotonation of water, hydrolase activities were investigated. Initially phosphatase-like activity was studied, since alkaline phosphatase in *E. coli*, another prokaryote, was shown to be active at pH 8, the pH of sea water.[98] Consequently it was considered likely that the potential phosphatase like activity of dinuclear copper(II) patellamide complexes is taking place at physiological pH values as well. Bis(2,4-dinitrophenyl)phosphate (BDNPP) was used as the phosphoester model substrate, due to the strong colour change upon hydrolysis, leading to simple and accurate spectrophotometric kinetic measurements.[99] Similarly, as observed for the kinetic carbonic anhydrase investigations, the dinuclear Cu^{II} complex with the model ligand H_4pat[1] (*RS*) showed maximum activity and efficiency,[100] supporting the hypothesis that the natural conformation of the ligands adds to their catalytic efficiency (see Table 1.3).[100]

The mechanism of the phosphatase activity is expected to be similar to the carbonic anhydrase activity with one copper(II) ion lowering the pK_a value of the coordinated water to an extent that allows nucleophilic attack of the phosphoester, held in place by the second copper(II) ion.

Table 1.3. Hydrolysis data and kinetic properties of $[M^{II}_2(H_2pat^{\gamma})(OH)]^+$ for BDNPP hydrolysis.[a)]

catalyst	pH_{max}	$v_{0.max}$ [Ms^{-1}]	pK_a(I)	pK_a(II)	γ
$[Cu^{II}_2(H_2pat^1)(OH)]^+$ [b)]	7.21	$1.58x10^{-7} \pm 3.00x10^{-9}$	6.91 ± 0.21	7.31 ± 0.20	0.079 ± 0.016
$[Zn^{II}_2(H_2pat^1)(OH)]^+$	no complexation				
$[Cu^{II}_2(H_2pat^2)(OH)]^+$ [c)]	6.69	$1.40x10^{-8} \pm 0.48x10^{-8}$	6.28 ± 0.28	7.04 ± 0.46	0.065 ± 0.033
$[Zn^{II}_2(H_2pat^2)(OH)]^+$	no complexation				
$[Cu_2^{II}(H_2pat^3)(OH)]^+$ [b)]	6.50	$3.45x10^{-8} \pm 6.28x10^{-8}$	6.32 ± 0.57	6.58 ± 0.52	0.077 ± 0.132
$[Zn^{II}_2(H_2pat^3)(OH)]^+$ [b)]	6.02	$1.78x10^{-8} \pm 2.24x10^{-9}$	5.32 ± 0.69	6.68 ± 0.71	0.080 ± 0.011

[a)] The $v_{0.max}$ values depend on the BDNPP concentration, and this varies in some of the experiments,

[b)] Data from the dissertation of MEHRKENS, 2015 [47]

[c)] Data from reference [100]

Results of dinuclear Zn^{II} complexes of H_4pat^1 and H_4pat^2 indicate a lower stability of the complexes under the conditions of the assay (buffer/MeCN/MeOH mixtures - MeCN and MeOH were required for solubility) compared to the stability constants determined with ITC in MeOH with MeO^- as the base. However, $[Zn^{II}_2(H_2pat^3)(OH)]^+$ shows phosphatase-like activity and exhibits a slightly more acidic optimum pH value. Although this is in contrast to the pK_a values for the first deprotonation of the respective aqua complexes: Zn^{II}, pK_a=9.5 [101], Cu^{II}, pK_a=8.0.[102,103] This is not an uncommon observation and is primarily related to the coordination geometries around the two metal ions.

Overall, the results from model patellamide Cu^{II} complex investigations indicate a hydrolase-like activity to be their metabolic role.

2 Aim

Previous work has focused on the structural features of copper(II) patellamide complexes as well as on their putative phosphatase and carbonic anhydrase activity. For these catalyses, maximum activity was observed for the dinuclear copper(II) complexes of the naturally configured H_4pat^1 ligand.[97,100] Building on this result, in the thesis presented here, a new ligand was developed with *R and S* stereochemistry and oxazole heterocycles, H_4pat^4 (see Figure 2.1). The aim was to investigate the ligand regarding its copper(II) complex formation and to study the conformation of the complexes, especially compared to complexes with H_4pat^1. In addition, it was envisaged to probe the potential phosphatase-like activity of the dinuclear copper(II) complexes with H_4pat^4 as well as with the closest analogue of the patellamides, H_4pat^5 (see Figure 2.1). The results of this study could consequently allow a conclusion about the influence of the side chain orientation for catalytic activity of the respective copper(II) complexes.

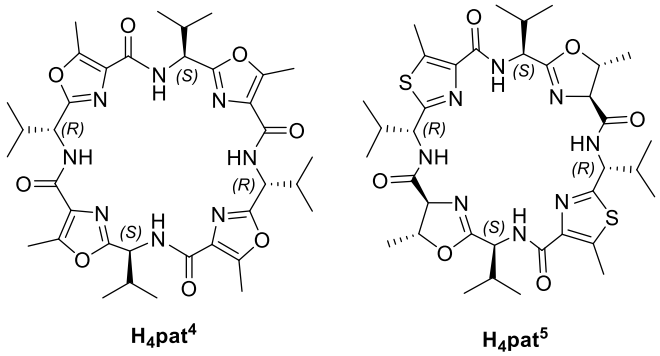

Figure 2.1. Model patellamides H_4pat^4 and H_4pat^5.

Spectroscopic evidence from the investigations concerning Zn^{II} coordination chemistry and phosphatase-like activity delivered ambiguous results. Therefore, a detailed theoretical investigation of the binding sites of putative dinuclear Zn^{II} complexes was carried out and is presented as the second part of Chapter 3.

The focus of Chapter 4 is on the application of dinuclear copper(II) patellamide complexes as catalysts for further hydrolase reactions at non-physiological pH values. For that, α-/β-glycosidase- and β-lactamase-like activity were tested, all typically active at alkaline pH values, *i.e.* 9-11. The results of this study could assist in answering the questions as to whether the dinuclear copper(II) complexes are specific for carboanhydrase and phosphatase activity at pH 7-8, or if the complexes could act as multifunctional pH-dependent catalysts.

So far, the hydrolase activities measured *in vitro* have given hints towards the metabolic relevance of patellamides being related with hydrolase activities of dinuclear Cu^{II} complexes. However, previously no *in vivo* measurements were carried out to test the hypothesis that the hydrolysis reactions are the metabolic role of the peptide complexes. Therefore, an investigation of the Cu^{II} binding behaviour of patellamides in *Prochloron* cells was carried out, together with preliminary *in vivo* hydrolase studies. For these studies, presented in Chapter 5, a patellamide-analogue was prepared and labelled with reporter groups (see Figure 2.2). Both a photosensitive group Atto550 and the spin label Proxyl were employed.

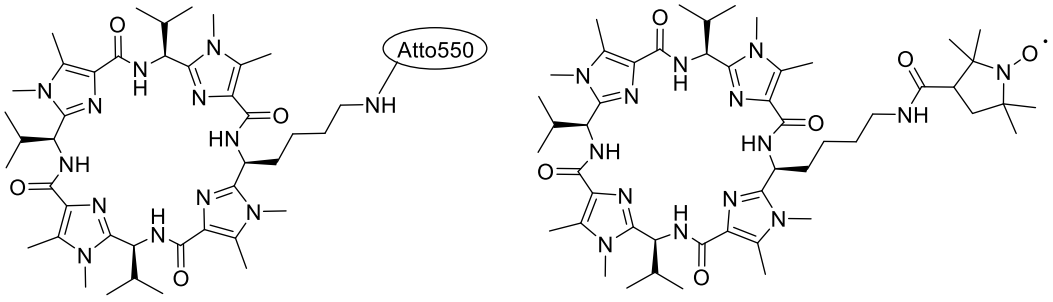

H_4pat-Atto550 **H_4pat-Proxyl**

Figure 2.2. Model ligands with reporter groups.

Insight on the copper(II) binding behaviour of patellamides in *Prochloron* cells would be an important foundation for the investigation of the catalytic activity *in vivo* and consequently contribute to the understanding of the metabolic role of patellamides.

3 Phosphatase-like activity*

Phosphatases, as well as phosphoryl group transfer kinases, are abundant and important enzymes in nature, participating *e.g.* in the regulation of phosphate levels in eukaryote cells, or in signal transduction.[104] For phosphoryl transfer reactions often Mg^{II} is incorporated in the active site, coordinating the phosphoester and thus allowing the nucleophilic attack of the respective alcohol.[104] The hydrolytic enzymes alkaline phosphatase (AP) and serine/threonine phosphatases seem to be predominantly dependent on dinuclear Fe^{II} and Zn^{II} cores.[105] In other phosphatase enzymes like purple acid phosphatase (PAP), active sites composed of Fe^{III}-Fe^{II} (mammals), Fe^{III}-Zn^{II} and Fe^{III}-Mn^{II} (plants) were found.[106,107] This is surprising, since Fe^{II} and Mn^{II} ions introduce the risk of free radical reactions, so called FENTON-type reactions, which are neither necessary for the function as phosphatase enzymes, nor beneficial for the organism. However, it has been suggested that mammalian PAPs might also be key regulators in the immune defence system by the generation of the afore-mentioned reactive oxygen species (ROS), like hydroxyl and superoxide radicals.[108,109]

For a thorough understanding of the mechanism of this class of enzymes, as well as for the potential application as bioremediators and the development of anti-osteoporotic drugs, model catalysts were developed.[105,110,111]

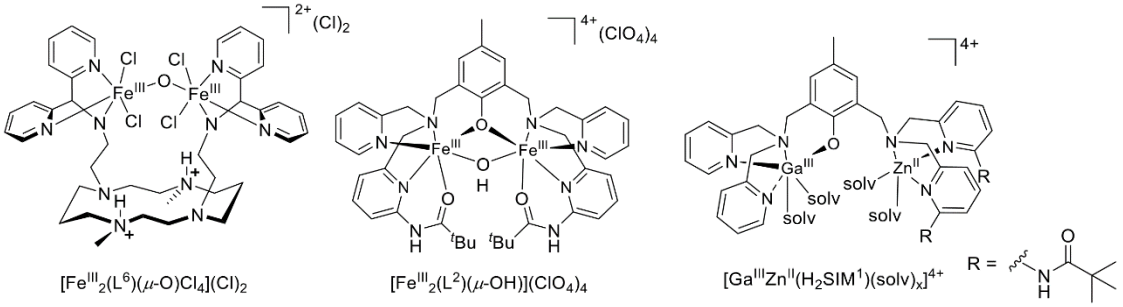

Figure 3.1. Model phosphatase complexes. Reprinted with permission from [105].

* Main parts of this Chapter are published in: 'Dinuclear Zinc(II) and Copper(II)/Zinc(II) complexes of artificial Patellamides as Phosphatase models', Peter Comba, Annika Eisenschmidt, Lawrence R. Gahan, Graeme R. Hanson, Nina Mehrkens, Michael Westphal, *Dalton Trans*. 2016, accepted manuscript.

In Figure 3.1 examples for model phosphatase complexes recently developed in the COMBA group are depicted. The respective ligands were designed with special emphasis on the second coordination sphere, allowing hydrogen bond formation.[105] In addition to that, it could be shown that the asymmetry of the ligand allows modelling of the natural enzyme more accurately and contributes to a higher hydrolase activity.[112-114] These two features are implemented in the complex $[Ga^{III}Zn^{II}(H_2SIM^1)(solv)_x]^{4+}$, which shows high catalytic efficiency (k_{cat}/K_M=1.07 $M^{-1}s^{-1}$) and moderate substrate affinity (7±1 mM).[105]

3.1 Phosphatase-like activity of Cu^{II} patellamide complexes with natural side chain configuration

The efficient phosphatase activity might play an important metabolic role of the dinuclear Cu^{II} complexes as shown in previous studies.[79,100] As implicated from these investigations on the phosphatase and carbonic anhydrase-like activity, the configuration of the side chains of the *pseudo*-octapeptides seems to be more important than the heterocyclic moieties for the catalytic rate and efficiency of the respective dinuclear copper(II) complexes. To support this finding, additional phosphatase investigations on dinuclear Cu^{II} complexes of the ligands H_4pat^4 and H_4pat^5 were carried out and are discussed here.[115]

The model patellamide H_4pat^4 is an oxazole-based ligand that exhibits natural *RS* side-chain configuration. The synthesis was carried out analogously to the reported synthesis for an all-*S* oxazole ligand and is described in detail in the Experimental Section B.[62] H_4pat^5, on the other hand, is the closest analogue to the natural ascidiacyclamide. It was already shown to form dinuclear Cu^{II} complexes[85] which exhibit carbonic anhydrase activity.[97] In this Chapter the properties and phosphatase-like activity of the respective dinuclear Cu^{II} complexes of H_4pat^4 and H_4pat^5 will be presented and compared with the imidazole based H_4pat^1 species.

To gain insight in the conformation of the dinuclear copper(II) complexes, DFT calculations (DFT, UB3LYP, def2-TZVP; for a detailed explanation of the method see Experimental Section A2) have been carried out for two possible arrangements: a bridging hydroxido-coligand: **A**, $[Cu_2(H_2pat^n)(\mu\text{-}OH)(H_2O)_2]^+$ and an isomer that exhibits a terminally bound hydroxido-coligand: **B**, $[Cu_2(H_2pat^n)(OH)(H_2O)_3]^+$ (see Figure 3.2 and Table 3.1).

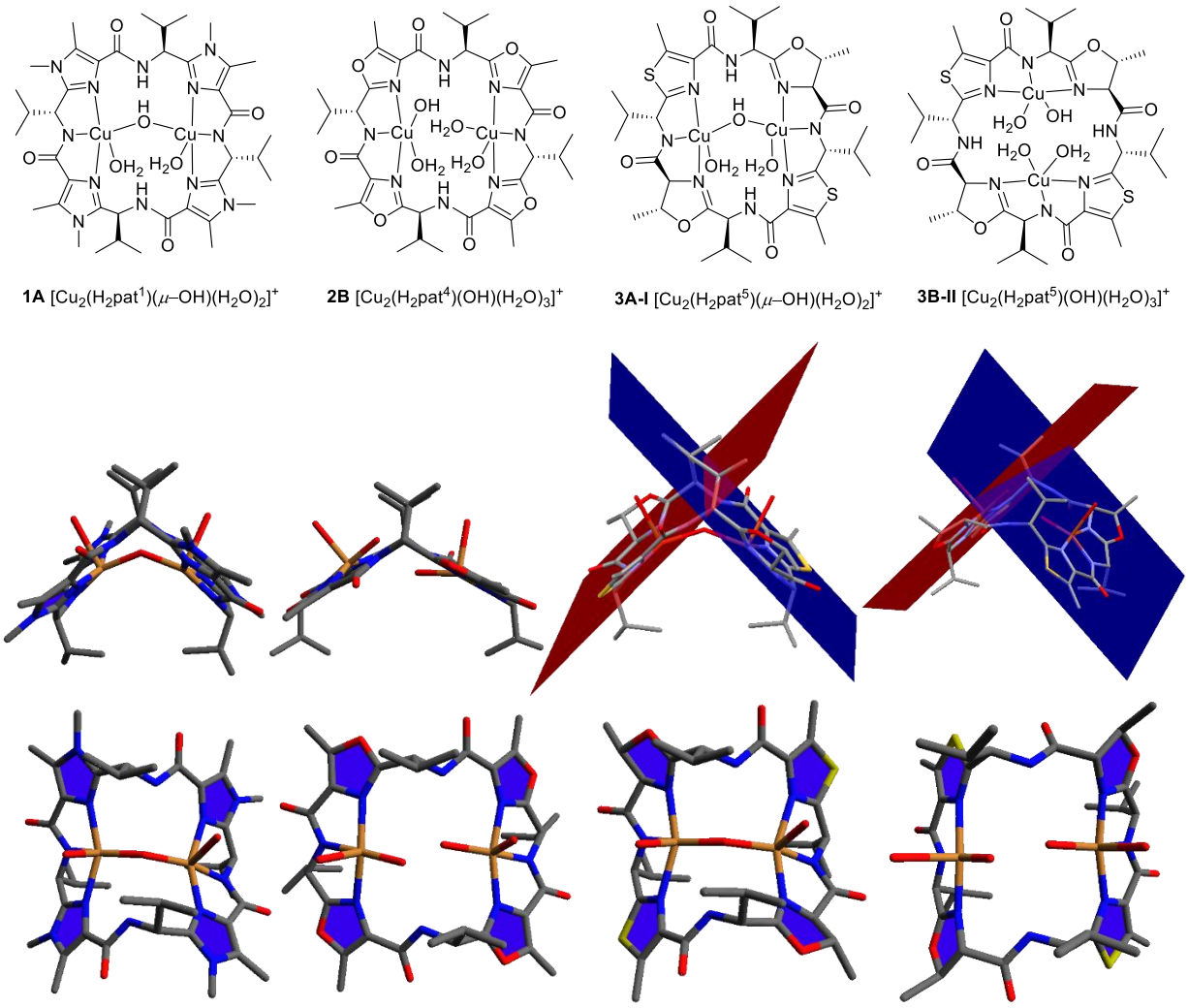

Figure 3.2. Possible structures of dinuclear Cu^{II} species of H_4pat^1, H_4pat^4 and H_4pat^5. Top: schematic representation of the example complexes; Bottom: Structures from DFT optimisation for $[Cu_2(H_2pat^1)(\mu\text{-}OH)(H_2O)_2]^+$**1A**, $[Cu_2(H_2pat^4)(OH)(H_2O)_3]^+$ **2B** and $[Cu_2(H_2pat^5)(\mu\text{-}OH)(H_2O)_2]^+$ **3A-I** as well as $[Cu_2(H_2pat^5)(OH)(H_2O)_3]^+$ **3A-II**. **I** and **II** refer to different coordination modes in H_4pat^5. (orange: Cu, grey: C, blue: N, red: O, yellow: S, hydrogen atoms are omitted for clarity).

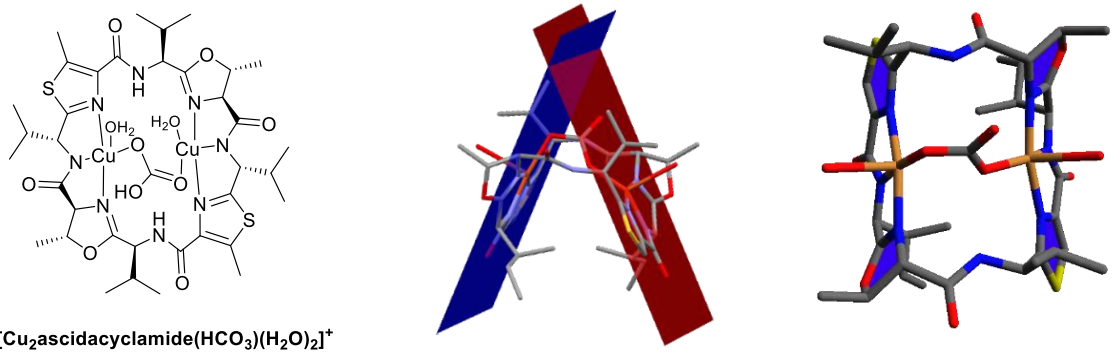

Figure 3.3. Crystal structure of $[Cu_2ascid(HCO_3)(H_2O)_3]^+$ [71] (orange: Cu, grey: C, blue: N, red: O, yellow: S, hydrogen atoms are omitted for clarity).[71]

The results of the structure optimisations for the dinuclear Cu^{II} complexes of H_4pat^1, H_4pat^4 and H_4pat^5 are additionally compared to the carbonate-bridged dinuclear Cu^{II} complex of ascidiacyclamide (see Figure 3.3). Moreover, experimental structural parameters for complex **1A** that were elucidated by X-ray crystal structure determination by DOVALIL and are provided in Table 3.1.[85,116]

Table 3.1. DFT computed and experimental structural parameters of the dinuclear Cu^{II} complexes of H_4pat^1, H_4pat^4, H_4pat^5 and ascidiacyclamide as shown in Figure 3.2 and Figure 3.3. a) from X-ray crystal structure determination.[85,116]

Species	$Cu^{II}\cdots Cu^{II}$ [Å]	Angle between coordination planes [°]
1A $[Cu_2(H_2pat^1)(\mu\text{-}OH)(H_2O)_2]^+$	3.79	84
1B $[Cu_2(H_2pat^1)(OH)(H_2O)_3]^+$	5.23	112
1A $[Cu_2(H_2pat^1)(\mu\text{-}OH)(H_2O)_2]^{+\ a)}$	3.63	77
2A $[Cu_2(H_2pat^4)(\mu\text{-}OH)(H_2O)_2]^+$	3.72	91
2B $[Cu_2(H_2pat^4)((OH)(H_2O)_3]^+$	5.25	120
3A-I $[Cu_2(H_2pat^5)(\mu\text{-}OH)(H_2O)_2]^+$	3.81	86
3B-I $[Cu_2(H_2pat^5)(OH)(H_2O)_3]^+$	5.31	106
3A-II $[Cu_2(H_2pat^5)(\mu\text{-}OH)(H_2O)_2]^+$	3.56	52
3B-II $[Cu_2(H_2pat^5)(OH)(H_2O)_3]^+$	5.14	79
$[Cu_2ascid(\mu\text{-}HCO_3)(H_2O)_3]^+$ [71]	4.30	46

As a result of the computations, similar $Cu^{II}\cdots Cu^{II}$ distances in the complexes are expected, with approximately 3.8 Å for the μ-OH^- (**A**) bridged species, and 5.2 Å for the non-bridged ones (**B**) for all investigated model patellamide complexes. The respective $Cu^{II}\cdots Cu^{II}$ distance is approximately 0.2 Å shorter in the X-ray crystal structure of **1A** as compared to the computed structure. A conformational change between the bridged and the terminally bound hydroxide coordination mode is also represented by the variation of the angle between the Cu^{II} coordination sites. In Figures 3.2 and 3.3 the coordination planes are additionally highlighted as red and blue planes and are spanned by N_{het}-N_{amide}-N_{het}-Cu^{II}. An angle of 84-91° for the bridged and 106-120° for the non-bridged complexes is expected. In the structure obtained by X-ray crystallography, the planes exhibit an angle of 77°, which is slightly smaller than the predictions from DFT optimisation (84°).

For the copper(II) complexes of the ligand H_4pat^5 two different coordination sites must be considered: **I** with the saturated part of the oxazoline heterocycle inside the coordination site of Cu^{II} and **II** with

the saturated carbon pointing away from the coordination site. The difference between the coordination mode is best represented in Figure 3.2, top right. The dinuclear Cu^{II} ascidiacyclamide complex with HCO_3^- as a bridging coligand has been shown to exhibit coordination site **II**.[71] Comparing the dinuclear copper(II) complex of the natural ascidiacyclamide and the copper(II) complexes of H_4pat^5 (**3-II**), it becomes obvious, that the $Cu^{II}\cdots Cu^{II}$ distance in the natural ligand complex, with HCO_3^- as a bridging coligand (4.30 Å), is just in between the distances observed for the OH^- bridged (3.6 Å) and the non-bridged conformation (5.1 Å). Moreover, as expected, coordination site **II** allows the complexes to adopt a smaller angle between the Cu^{II} sites.[71] This difference in distances is most likely caused by the different coligands OH^- and CO_3^{2-}, respectively. Interestingly, all Cu^{II} centres discussed above show a square pyramidal geometry of the donor atoms around the metal centre. Consequently, the following energy splitting of the 3d-orbitals due to the coordination of ligands is expected, as shown in Scheme 3.1.

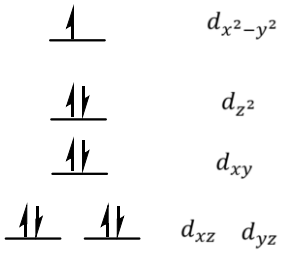

Scheme 3.1. Expected 3d-orbital splitting of Cu^{II} in the model patellamide complexes shown in Figures 3.2/3.3.

To prove that H_4pat^4 does, as described for its all-*S* analogue,[85] also form dinuclear Cu^{II} complexes, HR FAB (-) mass spectrometry was carried out. The expected mass signal for the dinuclear copper(II) complex with one hydroxide ion (see Table 3.2) is observed. As explained initially, in the further discussion the phosphatase activity of dinuclear copper(II) complexes of H_4pat^5, first described by DOVALIL,[85] will be investigated alongside the H_4pat^4 species. Therefore, HR FAB (-) mass spectrometry was used to ensure the formation of the species reported in a previous thesis (see Table 3.2).[85]

Table 3.2. Molecular formulae, experimental and calculated masses of the observed and dinuclear copper(II) complexes of H_4pat^4 and H_4pat^5 (HR FAB (-) MS).

Species	Molecular formula	Experimental	Calculated
$[Cu_2(pat^4)(OH)]^-$	$C_{36}H_{45}Cu_2N_8O_9^-$	859.1903	859.1902
$[Cu_2(pat^5)(OH)]^-$	$C_{36}H_{49}Cu_2N_8O_7S_2^-$	895.1764	895.1758
$[Cu_2(pat^5)(OMe)]^-$	$C_{37}H_{51}Cu_2N_8O_7S_2^-$	909.1921	909.1914

It is more likely that the non-bridged species of the complexes shown in Figure 3.2 $[Cu_2(H_2pat^n)(OH)(H_2O)_3]^+$ (**B**) is the active one, with the terminally coordinated hydroxide ion acting as the nucleophile, as substrate coordination may be preferred to such an active site. This is thought to be the case since the terminally bound hydroxide ions usually show higher activity as compared to bridging hydroxide ions.[117,118] However, since it cannot be ascertained which of the two arrangements is the catalytically active one, in the following discussion it is referred to the dinuclear complexes of H_4pat^1 as **1**, H_4pat^4 as **2**, of H_4pat^5 as **3.** For clarity, in the following discussion the aqua-ligands will be omitted in the molecular formulae.

With the reported $[Cu_2(H_2pat^4)(OH)]^+$ and $[Cu_2(H_2pat^5)(OH)]^+$ species, prepared *in situ*, in the study presented here phosphatase-like activity was investigated. For that, the dependence of catalysis on pH was determined in the range between pH 5 and 11 in steps of 0.5 pH units or smaller using the activated model substrate BDNPP, as described previously.[99,119,120] The method involves measuring spectrophotometrically the change in absorbance of the hydrolysis product of BDNPP, 2,4-dinitrophenolate, which displays a strong absorption at 400 nm (ε = 12,100 $M^{-1}cm^{-1}$, 25°C)[121,122]; a multicomponent buffer is used for pH control (see Scheme 3.2).

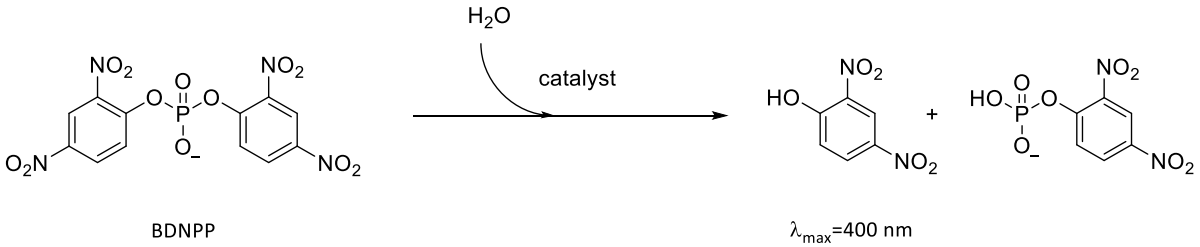

Scheme 3.2. Phosphate ester hydrolysis of model substrate BDNPP by catalyst.

Based on experiments without copper(II), one and two equivalents of copper(II), only the dinuclear complex is assumed to be catalytically active. Consequently the data from the measured pH profiles were fitted by a non-linear regression to a MICHAELIS-MENTEN model, equation 3.1, which is based on a model for a diprotic system (see Scheme 3.3).[99]

$$v_0 = \frac{v_{\max}\left(1 + \frac{\gamma K_{a_2}}{[H^+]}\right)}{\left(1 + \frac{[H^+]}{K_{a_1}} + \frac{K_{a_2}}{[H^+]}\right)} \qquad (3.1)$$

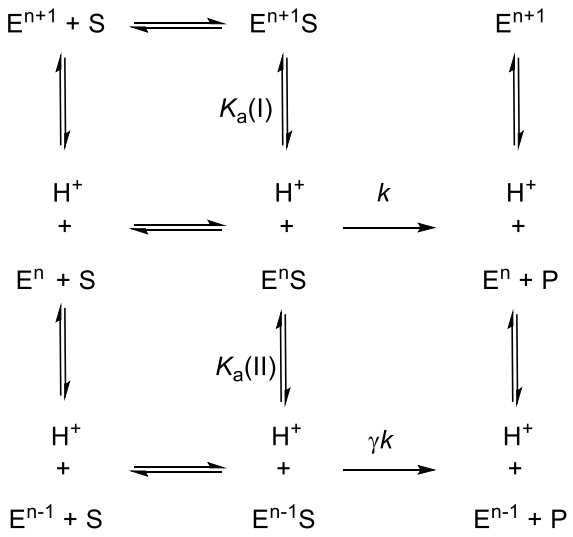

Scheme 3.3. Representation of the diprotic system with two active species[99] (adapted from reference [105]).

Here, v_0 is the initial and $v_{0,max}$ the maximum reaction rate, reached under given conditions and optimum pH. The factor *γ* is related to the relative activity of the two active species in equilibrium (E^nS and $E^{n-1}S$); a value of *γ* below one corresponds to a more active E^nS adduct and a value higher than one considers the deprotonated adduct $E^{n-1}S$ as more active. The equilibrium constants for the two deprotonation steps pK_a(I) and pK_a(II) are given in Table 3.3.

All measurements were carried out with a constant catalyst (40 µM) and substrate concentration (5 mM) in a 5 : 45 : 50 MeOH : MeCN : aqueous buffer mixture as solvent. The initial rates at each pH value were corrected for the corresponding autohydrolysis (blank) rates. The pH profiles are shown in Figure 3.4. The parameters obtained from fitting the pH profiles to equation 3.1 are summarised in Table 3.3.

The pH optimum with maximum initial velocity, v_{max}, is almost identical for the complexes, with 7.73 for **2** and 7.57 for **3**. However, the pH range in which they are active, estimated by pK_a(II)–pK_a(I), varies significantly. Whereas pK_a(I) for **2** is at 6.99, *i.e.* the first water, coordinated to the metal centre is deprotonated and could thus in turn undergo nucleophilic attack at the phosphoester, pK_a(II) is at 8.47, almost 1.5 pH units shifted. This is similar to other phosphatase model complexes,[105] but different from the activity window observed for imidazole based cyclic peptides, that are usually observed to be active in a range of ca. 0.4-0.8 pH units (see Chapter 1.5.3).

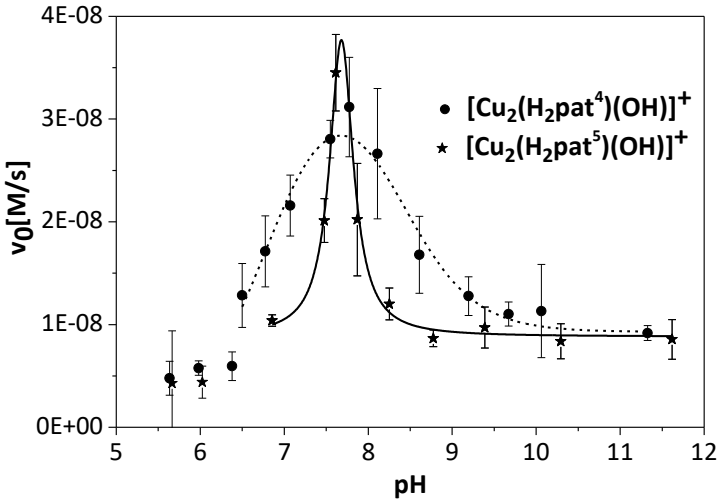

Figure 3.4. pH profile of the BDNPP hydrolysis with **2** $[Cu_2(H_2pat^4)(OH)]^+$ (dashed) and **3** $[Cu_2(H_2pat^5)(OH)]^+$ (solid) [BDNPP] = 5 mM; [cat] = 40 µM, 25°C. Adapted from reference [115] with permission from The Royal Society of Chemistry.

Table 3.3. Hydrolysis data and kinetic properties of **1** $[Cu_2(H_2pat^4)(OH)]^+$ and **2** $[Cu_2(H_2pat^5)(OH)]^+$ for BDNPP hydrolysis.[115]

catalyst	pH_{max}	$v_{0,max}$ [Ms^{-1}]	pK_a(I)	pK_a(II)	γ
1 $[Cu_2(H_2pat^1)(OH)]^+$ [47]	7.21	$1.58x10^{-7} \pm 3.00x10^{-9}$	6.91 ± 0.21	7.31 ± 0.20	0.079 ± 0.016
2 $[Cu_2(H_2pat^4)(OH)]^+$	7.73	$3.64x10^{-8} \pm 2.19x10^{-9}$	6.99 ± 0.35	8.47 ± 0.04	0.255 ± 0.016
3 $[Cu_2(H_2pat^5)(OH)]^+$	7.57	$3.00x10^{-8} \pm 1.50x10^{-9}$	7.41 ± 0.37	7.71 ± 0.39	0.171 ±0.008

The dinuclear complex **3** on the other hand shows a relatively narrow pH range of activity with pK_a(II)–pK_a(I) = 0.3, similar to $[Cu^{II}_2(H_2pat^1)(OH)]^+$. Compared to the Cu^{II} ion with its first pK_a=8.0 [102,103], the naturally configured ligands (*RS*) do not seem to alter the acidity of the metal centre significantly. For the more rigid[66] ligand H_4pat^1, with imidazole as a heterocycle the pK_a of the water coordinated to one Cu^{II} centre is lowered to 7.2, compared to 6.5 for the 4*S* configured ligands H_4pat^2 and H_4pat^4 (pK_a of not coordinated water: 15.7). Apart from the similarities in the pH optimum and pH range, the maximum velocity v_0 observed at 5 mM BDNPP for **2** and **3** is found to be a third of that reported for the H_4pat^1 based systems. Subsequent measurements at the optimum pH in dependence of the substrate concentration were also fitted according to a MICHAELIS-MENTEN model (see Figure 3.5 and Table 3.4). Here, the concentration of BDNPP was varied between 1 and 10 mM. The data were fitted to equation 3.2, providing the MICHAELIS constant K_M, which was used to determine k_{cat} (equation 3.3).

The results are summarised and compared with the data obtained for the phosphatase-like activity of **1**, $[Cu^{II}_2(H_2pat^1)(OH)]^+$ in Table 3.4.

$$v = v_{max} \cdot \frac{[S]_0}{(K_M + [S]_0)} \tag{3.2}$$

$$k_{cat} = \frac{v_{max}}{[K]_0} \tag{3.3}$$

Table 3.4. MICHAELIS-MENTEN parameters for the phosphatase activities. Adapted from reference [115] with permission from The Royal Society of Chemistry.

catalyst	k_{cat} x 10^{-3} [s^{-1}]	K_M [mM]	k_{cat}/K_M [$M^{-1}s^{-1}$]
1 $[Cu_2(H_2pat^1)(OH)]^+$ [47]	3.95 ± 0.07	26.4 ± 2.20	0.15
2 $[Cu_2(H_2pat^4)(OH)]^+$	6.60 ± 0.32	14.69 ± 10.28	0.45
3 $[Cu_2(H_2pat^5)(OH)]^+$	2.26 ±0.03	4.22 ± 1.56	0.53

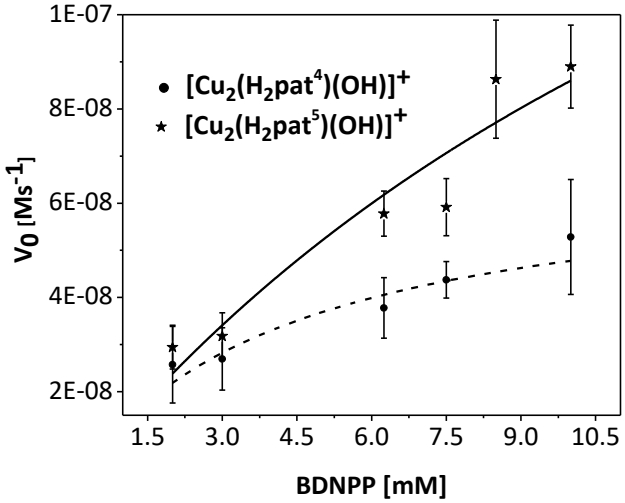

Figure 3.5. Overlay of MICHAELIS-MENTEN measurements of **2** (dashed), and **3** (solid) catalysed BDNPP hydrolysis; pH for the substrate dependence: 7.73 $[Cu_2(H_2pat^4)(OH)]^+$, 7.57 $[Cu_2(H_2pat^5)(OH)]^+$; [cat] = 30 µM; 25°C.[115]

Compared to previously investigated dinuclear copper(II) patellamide based phosphatase models, $[Cu^{II}_2(H_2pat^4)(OH)]^+$, **2,** exhibits the highest hydrolysis rate reported to date. The catalytic efficiency however is the second largest known, with the natural ligand system $[Cu^{II}_2(H_2pat^5)(OH)]^+$, **3**, being superior. This is the case despite its lower hydrolysis rate, but due to the very low substrate affinity (as compared to other model phosphatases).[105] The hydrolysis rates reported for all three model

complexes presented are in the same range, while the substrate affinity varies greatly leading to significantly different efficiencies. Interestingly, the dinuclear copper(II) complex of H_4pat^1 shows the highest substrate affinity. The substrate affinity reported for the dinuclear copper(II) complex of H_4pat^4 however, is significantly smaller, which might be due to much lower pK_a value of the oxazole system. The lowest substrate affinity is observed for the dinuclear complex of the ascidiacyclamide-like ligand H_4pat^5. So, summing up the results for the dinuclear copper(II) complexes of ligands with natural side chain configuration but different donor sets, one can conclude, that the imidazole-based system **1** shows the lowest efficiency (0.15 $M^{-1}s^{-1}$), the oxazole based system **2** shows an efficiency that is increased by a factor of 3 as compared to the imidazole system (0.45 $M^{-1}s^{-1}$) and the system with thiazole and oxazoline heterocycles **3** shows maximum efficiency (0.53 $M^{-1}s^{-1}$).[123]

Compared to the phosphatase activity of copper(II) complexes with 4*S* configured ligands and imidazole heterocycles H_4pat^2 and H_4pat^3 (with subtle changes in the residues attached to the imidazoles, see Figure 3.6), the catalytic efficiency of the complexes **2** and **3** with naturally configured ligands, is increased by a factor of approximately 3-5. This is predominantly caused by the comparably high hydrolysis rate of **2** and **3**. The results from the study of dinuclear Cu^{II} complexes with naturally configured ligands, H_4pat^4 and H_4pat^5, support the hypothesis that the natural side chain orientation is crucial for a high efficiency. Additionally, it could be shown that the Cu^{II} complex of the oxazole based ligand H_4pat^4 shows a very large pH range of activity of ~1.5 pH units, whereas the H_4pat^1 and H_4pat^5 based complex show a narrow pH activity range of ~0.3 pH units.

However, the patellamides might not be individually floating in the cytosol of *Prochloron* and *L. patella.* Instead it is not unlikely that they act as cofactors/prosthetic groups (like haem) in enzyme pockets, where an additional hydrogen bond network might stabilise the substrate as well as the attacking hydroxide group, which could lead to a significantly broader pH activity range. This would not be an uncommon observation, since catalytic metal ion sites in biology are all incorporated in a larger peptide environment (as discussed for the copper sites in the introduction 1.5.1).[2]

3.2 Phosphatase-like activity of Zn^{II} patellamide complexes*

3.2.1 Dinuclear Zn^{II} patellamide complexes in solution

In the previous section the peptide ligands were systematically changed and the effect of this on the hydrolase activity was investigated, indicating a strong importance of the choice of the natural stereoconfiguration. However, after changing the configuration of the side chains and the donor sites, a third approach to alter the phosphatase performance of the catalyst might be the exchange of the metal centre. Since Zn^{II} often is the metal centre of choice for many reported enzymatic hydrolyses,[124-126] and as it is present at elevated quantities in ascidians with concentrations close to that of Cu^{II},[127] the zinc(II) patellamide coordination chemistry has been investigated. The study comprises solution equilibria involving the imidazole based ligands H_4pat^1-H_4pat^3 (see Figure 3.6) with Zn^{II}, complex stabilities and phosphatase activities.

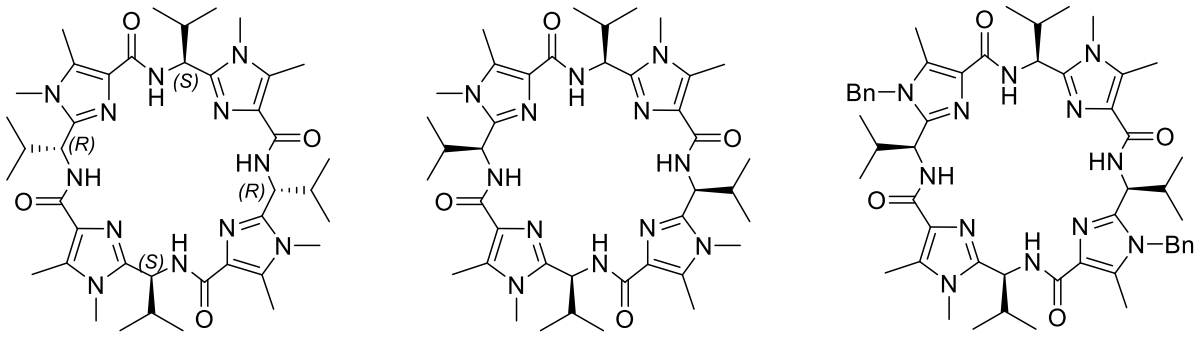

Figure 3.6. Chemical structure of H_4pat^1, H_4pat^2 and H_4pat^3.

As discussed earlier, the complex stability constants were determined in MeOH with MeO^- as a base for the model ligands H_4pat^1 and H_4pat^2 with Cu^{II} and Zn^{II}. It could be shown that the Zn^{II} complexes are one order of magnitude less stable than the respective Cu^{II} complexes. Since the results from Cu^{II} experiments indicate cooperative binding, a similar complexation behaviour is expected for the binding of Zn^{II} ions, and this is supported by mass spectrometry. While the complexation of Cu^{II} is

* NMR titrations, MS and EPR experiments as well as phosphatase measurements mentioned in this Chapter were carried out by Dr. Nina Mehrkens.

driven by enthalpy, the binding of Zn^{II} is mainly encompassed by a change in entropy (see Table 3.5). From published data on the crystal structures as well as NMR investigations it became obvious that the free ligands adopt the saddle-shaped conformation.[72] It seems that the angle between both planes defined by the three donors (Heterocycle-Amide-Heterocycle) in H_4pat^1 is ideal for the coordination of two metal ions and for Cu^{II} it has been shown that coordination of the first metal centre preorganises the ligand for coordination of the second one, leading to cooperative binding of two metal ions.[72,75] This is supported by the stability data reported in Table 3.5, indicating a higher degree of ligand preorganisation for the ligand with natural configuration of the side chains compared to the 4*S* ligand H_4pat^2.

Table 3.5. Zn^{II} [47]and Cu^{II} [73] stability constants as well as entropies and enthalpies of complexation with the patellamide derivatives H_4pat^1 and H_4pat^2, obtained from calorimetry (ITC) in MeOH with MeO^- as added base. [a] computed M^{II} : L ratio; [b] overall stability constant for L + 2M = M_2L. [115]

	$[Cu_2(H_2pat^1)]^{2+}$	$[Zn_2(H_2pat^1)]^{2+}$	$[Cu_2(H_2pat^2)]^{2+}$	$[Zn_2(H_2pat^2)]^{2+}$
N [a]	1.90±0.09	1.51±0.16	1.84±0.08	1.69±0.78
K [b]	$1.71\cdot10^6$±0.71	$1.03\cdot10^5$±0.30	$4.03\cdot10^4$±0.55	$3.34\cdot10^4$±0.57
Δ*H* [kJ/mol]	46.8±4.6	-40.86±0.77	84.52 ±7.7	-7.69±3.64
Δ*S* [J/(mol K)]	278.56	-41.04	371.53	60.67

The formation of the dinuclear zinc(II) complexes was additionally studied by NMR spectroscopy*, i.e.* ^{13}C, ^1H and 2D techniques (HMBC and HSQC). These data imply that $[Zn^{II}_2(H_2pat^1)(OH)]^+$ is a C_2-symmetric complex with two chemically different imidazole donor groups (see Figures 3.7, 3.8 and 3.9).

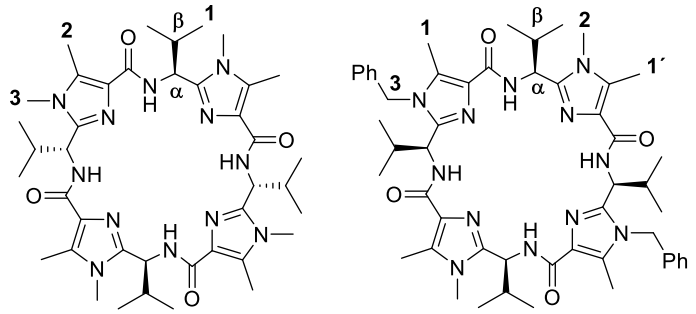

Figure 3.7. Nomenclature of H_4pat^1 and H_4pat^3 as used in the NMR spectra shown in Figures 3.8 and 3.9. Adapted from reference [115] with permission from The Royal Society of Chemistry.

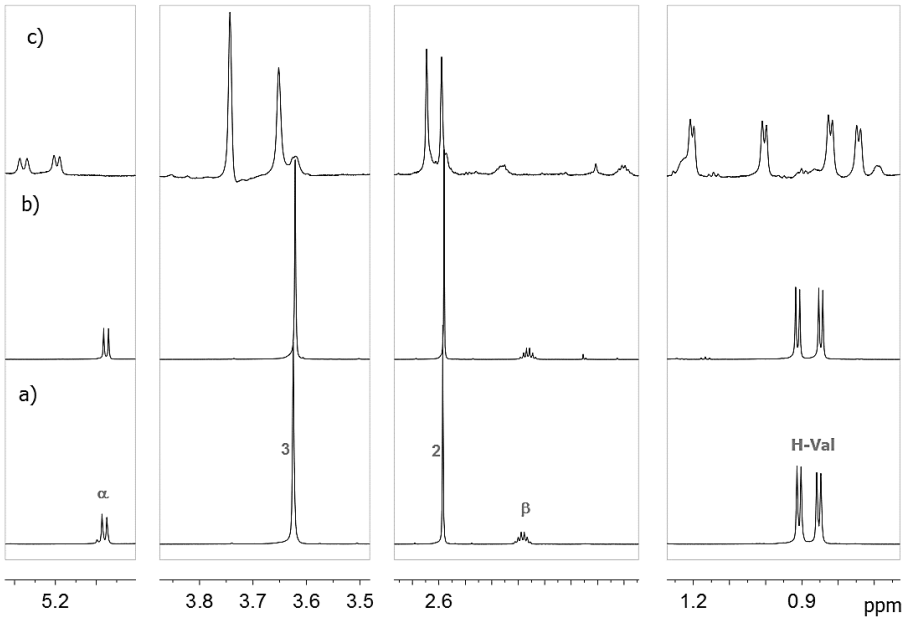

Figure 3.8. ^{1}H-NMR spectra of a) H_4pat^1, b) H_4pat^1+7.5 equivalents of MeO^-, and c) $[Zn_2(H_2pat^1)(OH)]^+$ in CD_3OD (10 mM), *v* = 600 MHz, 25°C. Reprinted from reference [115] with permission from The Royal Society of Chemistry.

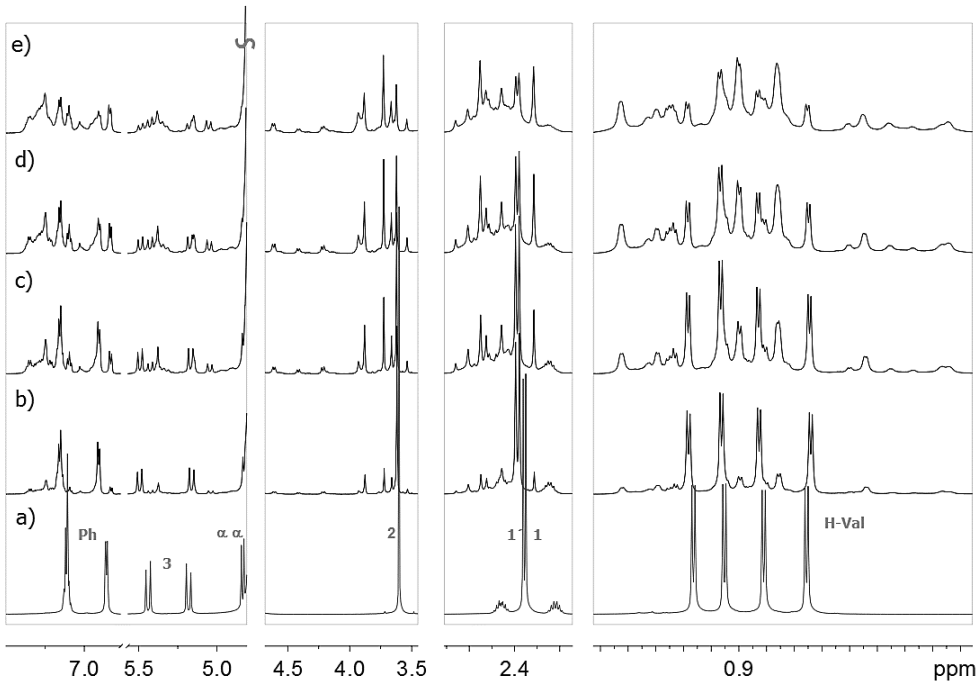

Figure 3.9. ^{1}H-NMR spectra of a) H_4pat^3, b) H_4pat^3 + 2eq. $ZnOTf_2$, c) H_4pat^3 + 2eq. $ZnOTf_2$ + 2eq. MeO^-, d) H_4pat^3 + 2eq. $ZnOTf_2$ + 4eq. MeO^- e) H_4pat^3 + 2eq. $ZnOTf_2$ + 8eq. MeO^-in a CD_3OD : $CDCl_3$ mixture (3 : 1 v/v) (10 mM), *v* = 600 MHz, 25°C. Reprinted from reference [115] with permission from The Royal Society of Chemistry.

Neither for H_4pat^1 nor for H_4pat^2 the formation of a mononuclear Zn^{II} complex as an intermediate species was observed. This gives further support for the theory of cooperative binding, as discussed above.[67,116] H_4pat^1 and H_4pat^2 only show complex formation upon addition of large amounts of base and in the absence of water, which is in contrast to observations for H_4pat^3 (see below). For the all-*S* configured ligand H_4pat^2 however, there is always free ligand in solution, even after the addition of an excess of base. These findings are in line with the observations from mass spectrometry and the slightly lower complex stability determined by ITC (see Table 3.5).

The NMR titration of H_4pat^3 with Zn^{II} and MeO^- is represented in Figure 3.9. From the spectrum of the pure ligand it becomes obvious that the ligand adopts C_2 symmetry. Upon addition of Zn^{II}, the NMR spectrum changes immediately, indicating the binding of the cation without additional base. This is different than observed for H_4pat^1 and H_4pat^2. As soon as base is added to the solution of H_4pat^3 with Zn^{II}, the complex is transformed to a new species, however no clear endpoint can be observed for that titration, analogous to the H_4pat^2 experiments. This is interpreted as an indication for a smaller cooperativity in the Zn^{II} binding of H_4pat^3 and points to an equilibrium between the protonated ligand and the mononuclear complex as well as, upon addition of base, a dinuclear complex.

This observation is similar to the respective Cu^{II} experiments, followed by EPR spectroscopy, validating the hypothesis that both metal cations exhibit similar complex building behaviour with H_4pat^3. The dinuclear Zn^{II} complex is observed at a ligand : Zn^{II} : base ratio of 1 : 2 : 2, and their intensities increase upon addition of base. However, due to the precipitation of $Zn(OH)_2$ with >4 equivalents of added base, it was not possible to drive the equilibrium towards a single species.

3.2.2 Phosphatase activity of dinuclear Zn^{II} patellamide complexes

The phosphatase-like activity of the Zn^{II} patellamide complexes was investigated, following the procedure described in Chapter 3.1. All experiments were carried out in a 5 : 45 : 50 MeOH : MeCN : aqueous buffer as solvent mixture, in contrast to the ITC and NMR experiments discussed above (MeOH and MeO^-). The mixture was chosen for solubility of the complexes and the substrate and the buffer was used to adjust the pH. It could be shown that the dinuclear Zn^{II} complex of H_4pat^3 exhibits substrate affinities similar to the respective Cu^{II} species and about twice the catalytic rate and efficiency, implying that the Zn^{II} ion is coordinated by the ligand in a similar fashion (see Table

3.6). However, neither for the dinuclear $[Zn_2(H_2pat^1)(OH)]^+$ nor for the $[Zn_2(H_2pat^2)(OH)]^+$ complex catalytic activity was observed.

Table 3.6. MICHAELIS-MENTEN parameters for the phosphatase activities. Adapted from reference [115] with permission from The Royal Society of Chemistry.

catalyst	k_{cat} x 10^{-3} [s^{-1}]	K_M [mM]	k_{cat}/K_M[$M^{-1}s^{-1}$]
$[Cu^{II}_2(H_2pat^1)(OH)]^{+}$ a)	3.95 ± 0.07	26.4 ± 2.20	0.15 ± 0.03
$[Zn^{II}_2(H_2pat^1)(OH)]^{+}$	No complexation		
$[Cu^{II}_2(H_2pat^2)(OH)]^{+}$ b)	0.39 ± 0.03	5.5 ± 0.64	0.07 ± 0.05
$[Zn^{II}_2(H_2pat^2)(OH)]^{+}$	No complexation		
$[Cu_2^{II}(H_2pat^3)(OH)]^{+}$ a)	2.34 ± 0.07	16.56 ± 1.61	0.14 ± 0.04
$[Zn^{II}_2(H_2pat^3)(OH)]^{+}$ a)	4.89 ± 0.00	16.98 ± 0.05	0.29 ± 0.02

a) Data from the dissertation of MEHRKENS, 2015.[47] b) Data from reference [100].

However, since mass spectrometry, ^{1}H NMR spectroscopy and ITC measurements point to a complex formation, the question is raised whether or not the Zn^{II} ions in H_4pat^1 and H_4pat^2 might be coordinated to a different binding site, *i.e*. the N_{amide}-N_{het}-N_{amide} site, as opposed to the results for copper(II) complex of $[Cu_2H_2pat^1(\mu\text{-}OH)(H_2O)_2]^+$ (Figure 1.4) and the carbonato-bridged dinuclear Cu^{II} complex of ascidiacyclamide (Figure 1.7).[71]

3.2.3 Computational conformation prediction of dinuclear Zn^{II} patellamide complexes in solution

Whereas in all mono- and dinuclear Cu^{II} complexes of cyclic *pseudo*-octapeptides the metal centre is coordinated by two heterocycles and a deprotonated amide (H-site, see Figure 3.10), the dinuclear Cu^{II} complexes of westiellamide-type *pseudo*-hexapeptides exhibit Cu^{II} binding to two amides and one heterocyclic nitrogen (A-site).[80,84]

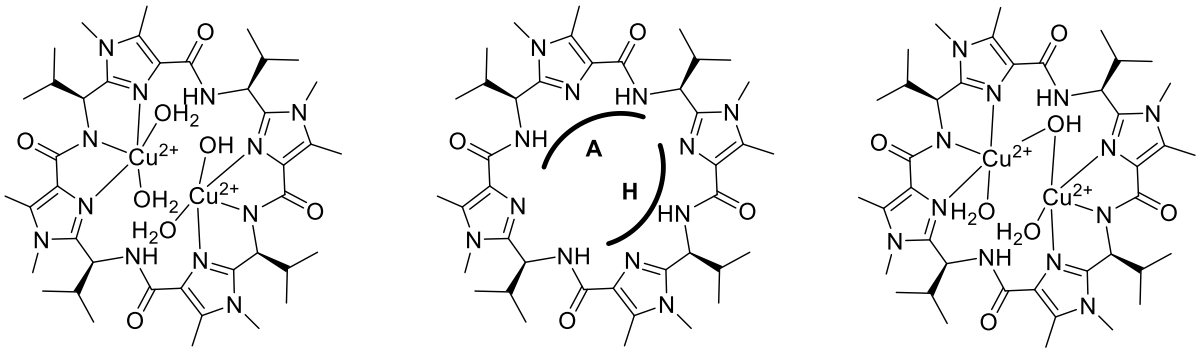

A = amide site, H = heterocycle site

Figure 3.10. Possible coordination sites for patellamide complexes (ligand H_4pat^2; A: amide site, H: heterocycle site) and structural models of the observed dinuclear Cu^{II} complexes (A site) with a terminal (left) or a bridging (right) OH^- group. Adapted from reference [115] with permission from The Royal Society of Chemistry.

Since no phosphatase activity could be observed for the patellamide-type Zn^{II} complexes of H_4pat^1 and H_4pat^2 (*vide supra*), one might expect a coordination mode that is different from the respective Cu^{II} complexes. Since ^{1}H-NMR studies could only show the formation of a C_2-symmetric species, it was difficult to find experimental evidence for either of the two possibilities (H or A sites, see Figure 3.10). Therefore, a molecular-mechanics-based structural and steric energy analysis was performed with the MOMEC programme and force field, since it is developed and suited for the description of transition metal complexes (for a detailed description of the method see Experimental Section A2).[128-131]

The chemical environment of an atom in a molecule is presented in atom types in molecular mechanics force fields. For example, an sp^3-hybridised carbon atom is assigned to the atom type CT. In MOMEC the atom type nomenclature was designed similarly to the AMBER force field.[132]

For the patellamides and the copper(II) ion atom types were assigned as depicted in Figure 3.11 on the basis of published data.[129,131,133-141] As a basis the established MOMEC97 force field was used [130] and supplemented with parameters for stretches, bends and torsions between different atom types not present in the original force field (see Table 3.7). A detailed description of atom type parameterisation is given elsewhere.[130] For the additional parameter optimisation an automatic procedure in the development version of MOMEC was used.[142]

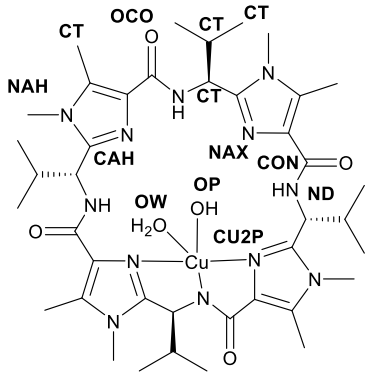

H_4pat^1

Figure 3.11. Depiction of the different atom types in the ligand H_4pat^1.

Table 3.7. Examples of introduced bond stretch parameters (STR), Angle bending parameters (BEN), periodicity and offset angle value for the torsional functions (TOR). FC = force constant, Ref.= Ideal value. The complete force field is given in the ESI of reference [115].

Interaction	Atom type			FC [mdyn/Å]	Ref. bond distance [Å]
STR	CU2P	NAX		0.340	1.935
STR	CU2P	ND		0.708	1.912
STR	CU2P	OP		0.100	2.150
				FC [mdyn/rad]	Ref. angle [rad]
BEN	NAX	ZN2	ND	0.050	1.571
BEN	ND	ZN2	ND	0.013	1.571
BEN	NAX·	ZN2	ND	0.015	1.571
			FC [mdyn/rad]	periodicity	offset angle [rad]
TOR	**CAH	CAH**	0.010	2.000	1.551
TOR	**CAH	CT**	0.002	6.000	0.843
TOR	**CAH	NAH**	0.017	2.000	1.570

All possible dinuclear structures (H- and A-site, with a terminal or a bridging OH^-, see Figure 3.10) for Zn^{II} and Cu^{II} coordinated to H_4pat^1, H_4pat^2 or H_4pat^3 (with ligands di- or tetra-deprotonated for the H- and A-type structures, respectively) were optimised and then subjected to a conformational search *via* a Monte-Carlo/random kick algorithm.[143,144] For the different structures, only one low energy conformation each was found, and these are given in Table 3.8; Figure 3.12 shows an overlay plot of the optimised lowest energy and the experimental structure of $[Cu_2(H_2pat^1)(OH)(H_2O)_2]^+$ (H-site, bridging OH^-) for a visual validation that the force field can reproduce the structures.

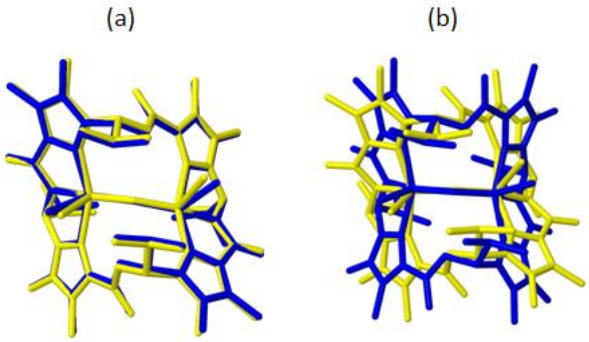

Figure 3.12. a) Overlay plot of the crystal structure (yellow)[75]and the strain energy minimised structure (blue) of $[Cu^{II}_2H_2pat^1(\mu\text{-}OH)(H_2O)_2]^+$, and b) overlay plot of the corresponding crystal structure (yellow) and DFT-optimised structure (bridging OH^-, H-site). Quatfit was used for the overlay plots. Reprinted from reference [115] with permission from The Royal Society of Chemistry.

Table 3.8. Strain energies [kJ/mol] for the different coordination geometries of the dinuclear Cu^{II} and Zn^{II} complexes (coligands and charges of the complexes omitted in the formulae) of H_4pat^n.[115]

		$[M_2(H_2pat^1)]^+$			$[M_2(H_2pat^2)]^+$			$[M_2(H_2pat^3)]^+$		
		A	H	Δ(H-A)	A	H	Δ(H-A)	A	H	Δ(H-A)
Cu^{2+}	μ-OH	70.1	15.8	-54.3	42	30	-12	19.7	31.9	12.2
	OH	61.9	0	-61.9	33.6	0	-34	0	7.7	7.7
Zn^{2+}	μ-OH	39.1	0	-39.1	27.6	12.4	-15	25.8	45	19.2
	OH	39.4	10	-28.4	0	5	5	0	30.8	30.8

The molecular mechanics based conformational analysis implies for the dinuclear Cu^{II} and Zn^{II} complexes of H_4pat^1 and H_4pat^2 that the imidazole binding site (H) is favoured. This is in agreement with the available crystal structure of the hydroxide-bridged Cu^{II} complex of H_4pat^1.[75] However, the force field calculations also suggest that, for the Cu^{II} complexes of H_4pat^3, the amide motif is preferred by 7.7 kJ/mol. Since the force field used for the Zn^{II} complexes was based on a rather small set of experimental structural data, and because a structural force field does not necessarily allow the accurate prediction of relative stabilities,[145,146] in addition to the fact that the number and mode of coordination of OH_2 and OH^- (terminal or bridging) is both unknown and difficult to predict with force field calculations, the molecular mechanics conformational search was supplemented by a DFT analysis of the low energy conformations of the dinuclear complexes of H_4pat^1, H_4pat^2 and H_4pat^3 (see Table 3.9; for computational details see Experimental Section A2). It emerges that there is only a small energy difference between structures with bridging and terminal OH^-. Importantly, the energies of

the complexes with metal ions coordinated in the amide binding sites are, independent of the metal ion, the ligand or the type of structure (terminal or bridging OH^-), exceedingly large. The strain induced to the ligands by dinuclear metal coordination to the amide sites is also reflected in the geometries of the optimised structures (DFT). While all structures with metal ions in the H-sites are saddle-shaped, *i.e*. similar to all structurally characterised Cu^{II} complexes,[67] all optimised structures with metal ions in the A-sites are asymmetric and distorted (see Figure 3.13 and 3.14).

In conclusion from the molecular mechanics and DFT-based computational analysis, it becomes obvious that, for all three ligands considered here, the site confirmed experimentally for the corresponding Cu^{II} complexes is also preferred by Zn^{II}. Thus, it is expected that the Zn^{II} complexes are structurally very similar to the well characterised Cu^{II} analogues, *i.e*. the two metal ions are both located in heterocycle pockets with two heterocycles and one amide each coordinated to the metal ions (H-site).

Table 3.9. Energy differences [kJ/mol] for the different coordination modes (ORCA 3.0.1, B3LYP/def2-TZVP).[115]

		$[M_2(H_2pat^1)]^+$ Heterocycle (H)	$[M_2(H_2pat^2)]^+$ Heterocycle (H)	$[M_2(H_2pat^3)]^+$ Heterocycle (H)
Cu^{2+}	μ-OH	0	0	0
	OH	26.0	39.4	38.1
Zn^{2+}	μ-OH	0	48.6	38.5
	OH	8.0	0	0

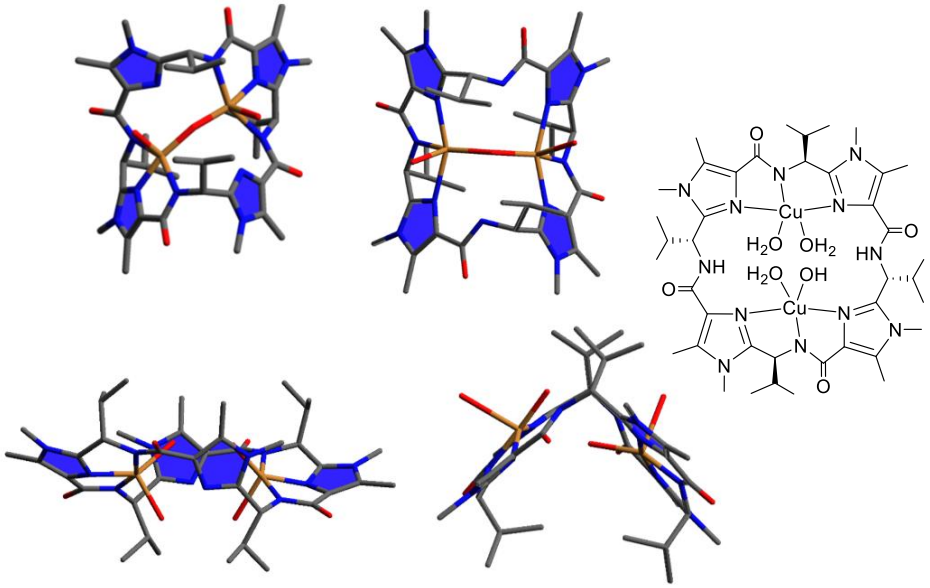

Figure 3.13. Calculated structures of dinuclear Cu^{II} H_4pat^1 complexes, right: Amide binding pocket, left: Heterocycle site, top: bridged coordination, bottom: non-bridged (orange: Cu, grey: C, blue: N, red: O, hydrogen atoms are omitted for clarity). Adapted from reference [115] with permission from The Royal Society of Chemistry.

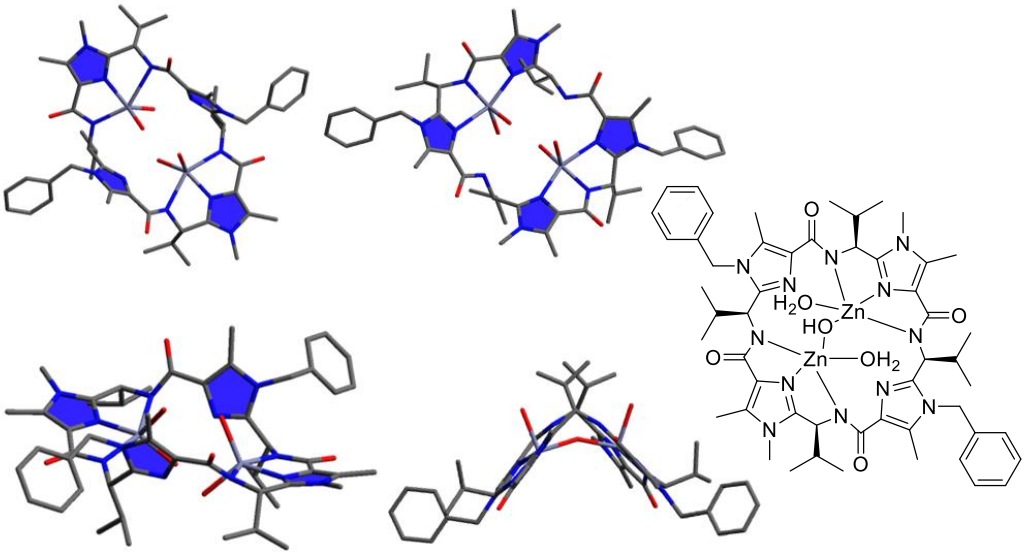

Figure 3.14. Calculated structures of dinuclear Zn^{II} H_4pat^4 complexes, right: Amide binding pocket, left: Heterocycle site, top: bridged coordination, bottom: non-bridged (violet: Zn, grey: C, blue: N, red: O, hydrogen atoms are omitted for clarity). Adapted from reference [115] with permission from The Royal Society of Chemistry.

3.3 Summary and Conclusion

In this Chapter it could be shown that the efficiency of phosphatase activity for dinuclear Cu^{II} complexes is maximum for ligands exhibiting the natural *RS* stereoconfiguration. Moreover, the dicopper(II) complexes of H_4pat^5 exhibit minimum substrate affinity and maximum catalytic efficiency (k_{cat}/K_M=0.53 $M^{-1}s^{-1}$) of all patellamide based phosphatase models reported to date. Firstly, this indicates that the natural steroconfiguration is crucial for high catalytic efficiencies. Secondly, it could be shown, that the catalytic efficiency is governed by the flexibility of the ligand, that is predominantly dependent on the heterocycles incorporated. The more flexible the ligand backbone, the higher is the catalytic efficiency that is observed.[115]

From the computational investigations regarding the Zn^{II} binding behaviour, the Zn^{II} complexes are expected to be structurally similar to the Cu^{II} analogues. Consequently, the fact that neither $[Zn_2(H_2pat^1)(OH)]^+$ nor $[Zn_2(H_2pat^2)(OH)]^+$ exhibit phosphatase activity may be caused by the small stability of these complexes at the hydrolysis conditions (5 : 45 : 50 MeOH : MeCN : aqueous buffer).

4 Glycosidase- and β-Lactamase-like activity*

Previous investigations pointed out that dinuclear Cu^{II} complexes show carboanhydrase-like activity at pH 8.1 as well as a phosphatase-like activity at pH 6.5–7.7.[97,100] Whether or not the complexes are capable of catalysing further reactions, since they would be a rather rare example for Cu^{II} based enzymes in these classes, was the central question of subsequent research. For that reason, α- and β-glycosidase as well as β-lactamase were chosen to be studied, as the respective assays are well established and the activities belong to the hydrolase enzyme class (Enzyme Commission Number3-EC 3). In this Chapter the dinuclear Cu^{II} complexes of the cyclic *pseudo*-octapeptides H_4pat^1 (*RS*) and H_4pat^2 (4*S*), the solution structures of which are known from a combination of EPR spectroscopy, spectra simulations and molecular modeling[61,72,81] are investigated.

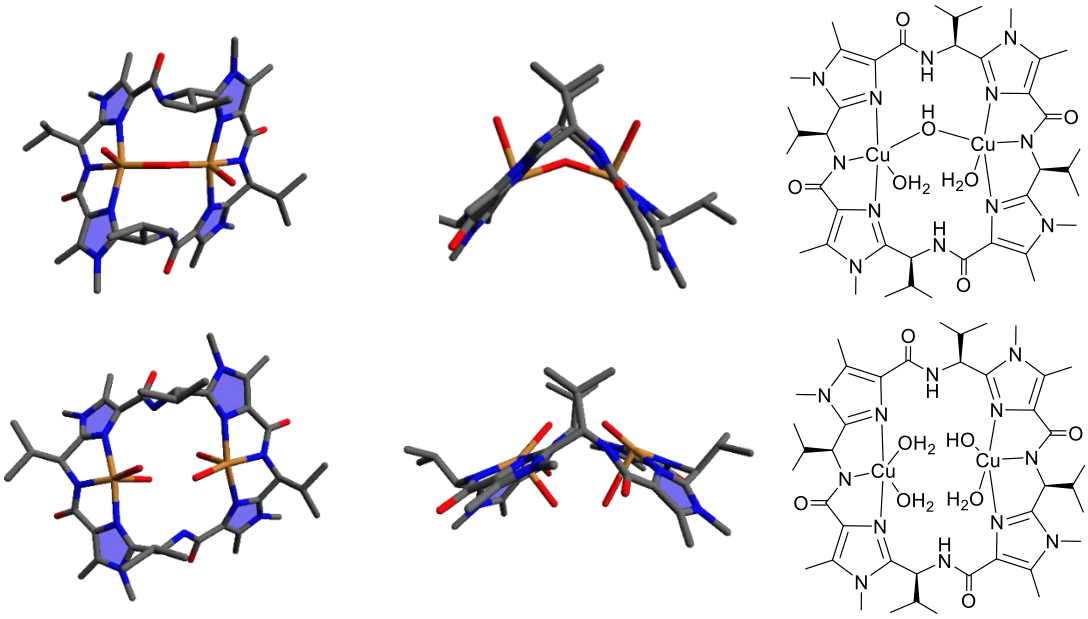

Figure 4.1. Possible structures of dinuclear Cu^{II} species of H_4pat^2: **4A** $[Cu_2(H_2pat^2)(\mu\text{-}OH)(H_2O)_2]^+$ (top) and **4B** $[Cu_2(H_2pat^2)(OH)(H_2O)_3]^+$ (bottom); (orange: Cu^{II}, grey: C, blue: N, red: O, hydrogen atoms are omitted for clarity).

* Main parts of this Chapter are published in 'Glycosidase and β-lactamase-like activity of dinuclear copper(II) patellamide complexes', Peter Comba, Annika Eisenschmidt, Nora Kipper, Jasmin Schießl, *J. Inorg. Biochem.* **2016**, *159*, 70-75.

The synthesis of the ligands was accomplished as described previously.[60-62,76] In addition to the μ-hydroxido-bridged coordination mode, a dicopper(II) complex with a terminal OH^- donor is also possible and both structures have been computed (DFT, UB3LYP, def2-TZVP, see Experimental Section A2) as discussed in the previous Chapter for **1** $[Cu_2(H_2pat^1)(OH)]^+$. Figure 4.1 shows the corresponding structures for **4A** and **4B** and Table 4.1 summarises structural information of the predicted structures.

Table 4.1. DFT computed structural parameters of the dinuclear Cu^{II} complexes structures **1** and **4**.

Species	$Cu^{II}\cdots Cu^{II}$ [Å]	Angle between coordination planes [°]
1A $[Cu_2H_2pat^1(\mu\text{-}OH)(H_2O)_2]^+$	3.79	84
1B $[Cu_2H_2pat^1(OH)(H_2O)_3]^+$	5.23	112
4A $[Cu_2(H_2pat^2)(\mu\text{-}OH)(H_2O)_2]^+$	3.98	107
4B $[Cu_2(H_2pat^2)(OH)(H_2O)_3]^+$	5.23	132

The major difference between the bridged complex **4A** and non-bridged complex **4B** with the same ligand H_4pat^2 is the angle between the two copper(II) coordination planes (spanned by N_{het}-N_{amide}-N_{het} and Cu^{II}). The angle between the two sites in **4A** is 107°, **4B** adopts a different conformation with a 132° angle between the two sites (twist of the imidazole-amide-imidazole-copper planes). This leads to a larger distance between the copper(II) centres (3.98 Å in **4A**, 5.23 Å in **4B**). Compared to the complexes with natural side chain configuration **1A** and **1B** this means that the dinuclear Cu^{II} complexes with H_4pat^2 exhibit larger angles between the copper(II) coordination sites but show similar $Cu^{II}\cdots Cu^{II}$ distances.

4.1 Glycosidase-like activity

Glycosyl transfer as well as hydrolase reactions are essential in biology since these reactions produce polysaccharides, which have storage, as well as structural functions, and show specific signalling roles.[147] This leads their tasks to range from energy uptake to cell wall expansion and degradation. Consequently, a great variety of enzymes that can selectively hydrolyse glycosidic bonds, so called *O*-glycosyl hydrolases, is provided by nature.[147] A prominent example of this class of enzymes is the hen egg white lysozyme (HEWL) which is commonly used in biological laboratories to hydrolyse the cell walls of prokaryotes. In fact, HEWL was the first glycosyl hydrolase to have its 3D structure solved.[148,149] The catalytically active amino acids were shown to be aspartate and glutamate residues,

which is in line with later findings for other hydrolases. However, for the viral neuramidase and bacterial sialidase enzymes, an additional tyrosine residue was found to be present in the active site.[147] Neuramidase hydrolyses the glycosidic bond between sialic acid and other sugars and thus allows viral release. Variant 1 of neuramidase is known to most people, although they are probably not aware of it. It is referred to as 'N1' in the 'H5N1' influenza pandemic, H5 represents variant 5 of haemagglutinin, a carbohydrate binding protein. In version 5, a mutation alters the protein in a way that allows influenza to cross the species divide.[150]

According to their structure, glycosidases are divided into approximately 100 families and subfamilies.[151] Most of these have an organic active site responsible for the catalytic glycoside cleavage depicted in Scheme 4.1. The enzymatic hydrolysis takes place in most glycoside hydrolysis (GH) families *via* an acid catalysis requiring two components, a proton donor and a nucleophile (base).[152,153] Two different mechanisms were first proposed by KOSHLAND:[152]

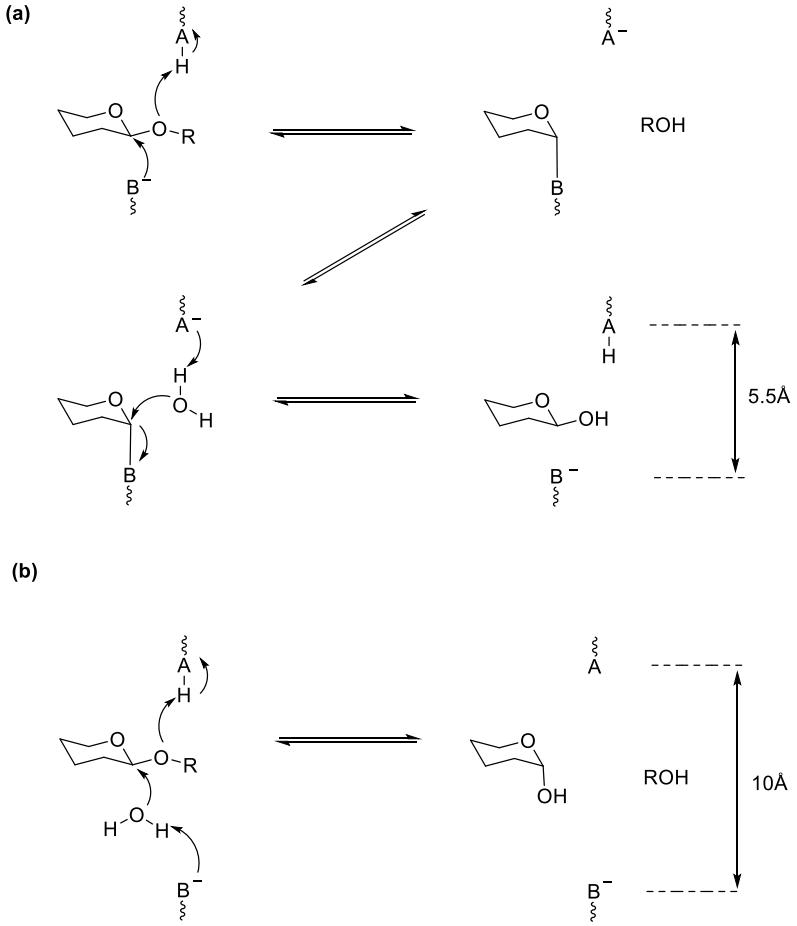

Scheme 4.1. Two possible mechanisms of enzymatic glycosidic bond hydrolysis: (a) retaining mechanism, (b) inverting mechanism. Adapted from [147] Copyright 1995, with permission from Elsevier.

Depending on the distance between residues A and B, path (a) or (b) is favoured and thus, the anomeric configuration is retained (a) or inverted (b). The position of the proton donor A is in both scenarios within hydrogen-bond distance to the glycosidic oxygen. The base on the other hand is ~5.5 Å distant from A, allowing the direct activation of the anomeric carbon in retaining enzymes, as opposed to ~10 Å, facilitating the binding of an additional water molecule between the substrate and B in the inverting scenario (see Scheme 4.1).[154] Natural glycosidase activity is reported to be in the range of K_M=4-14 mM and k_{cat}=0.14-14 s^{-1} for α-glycosidase activity[155] (substrate phenyl-α-glycoside) and K_M=0.07 mM, k_{cat}=169 s^{-1} for *Agrobacterium* β-glucosidase (substrate: 4-nitrophenyl-D-glucoside).[156]

Only family 4 has been reported to be NAD^+ as well as probably Mn^{2+} dependent[155,157] with a proposed active species shown in Figure 4.2.

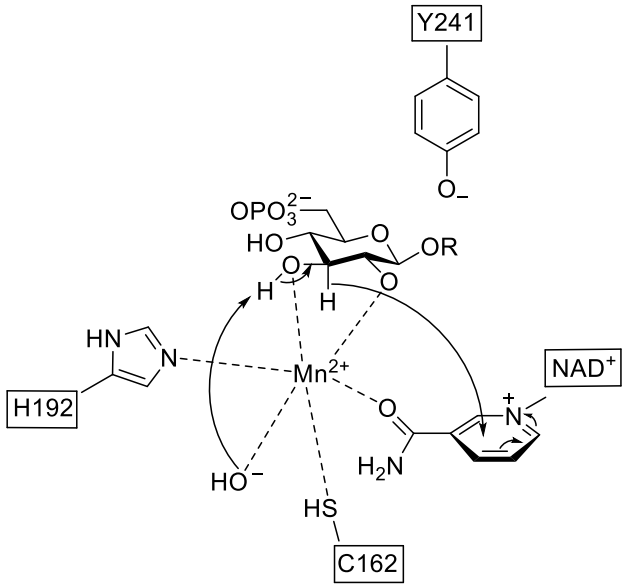

Figure 4.2. Proposed catalytically active species in BglT (6-phospho-β-glucosidase). Adapted from [155] Copyright 2005, with permission from Elsevier.

Here, k_{cat} was found to be 1.9 s^{-1} and K_M=41 µM with *p*-nitrophenol-β-glucopyranoside-6-phosphate as the substrate and the pH optimum at pH 8.0, pK_a(I)=7.08 and pK_a(II)=9.31. Although pK_a(I) would be in the perfect range to correspond to a tyrosine-OH group, there was no conserved tyrosine residue found in the hydrolase family.[155]

Given the importance of glycosidic bonds, artificial enzyme mimics were investigated to model the glycoside hydrolysis reactions. As the use of these enzymes for glycosyl transfer reactions is limited by their low availability,[158] the design and evaluation of new glycosidase mimics with increased

selectivity and reaction yields is desirable. These could prove particularly useful as antiviral agents, food fillers, or as a new class of antibiotics.[159] Apart from the study of metal ions accelerating the glycosidic bond cleavage, amongst them Cu^{II}, Ni^{II}, Co^{II}, Al^{III} and La^{III}, for a long time only substrates with an additional binding site for LEWIS acids like Al^{III}, Zn^{II} and Fe^{III} were investigated.[159] Recently, a few studies on dinuclear copper(II) complexes as enzyme models for glycosidase have appeared.[159-163]
The experimental investigations involved 4-nitrophenyl-α-*D*-glucopyranoside and 4-nitrophenyl-β-*D*-glucopyranoside as glycosidase model substrates, since the hydrolysis product of these highly activated ethers are spectrophotometrically easily detectable (Scheme 4.2).[159]

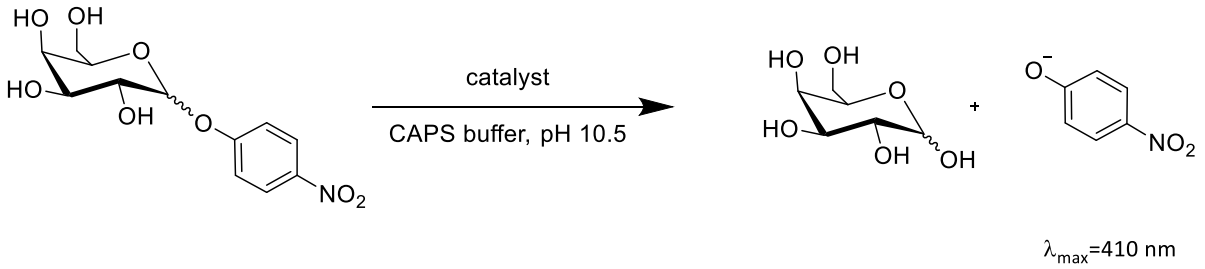

Scheme 4.2. Catalytic hydrolysis of 4-nitrophenyl-*D*-galactopyranoside.[159]

Only few substrates have been reported, often based on 4-nitrophenole as the chromogenic group released upon hydrolysis.[159-162] STRIEGLER *et al*.[164] published model complexes working at an optimum pH of 10.5 with a rather high substrate affinity for 4-nitrophenyl-α-*D*-glucopyranoside of 138 mM (**C**) and 211 mM (**D**), respectively (see Figure 4.3), and k_{cat}/K_M=1.268x10^{-4} M^{-1}s^{-1} and 3.949x10^{-5} M^{-1}s^{-1}.

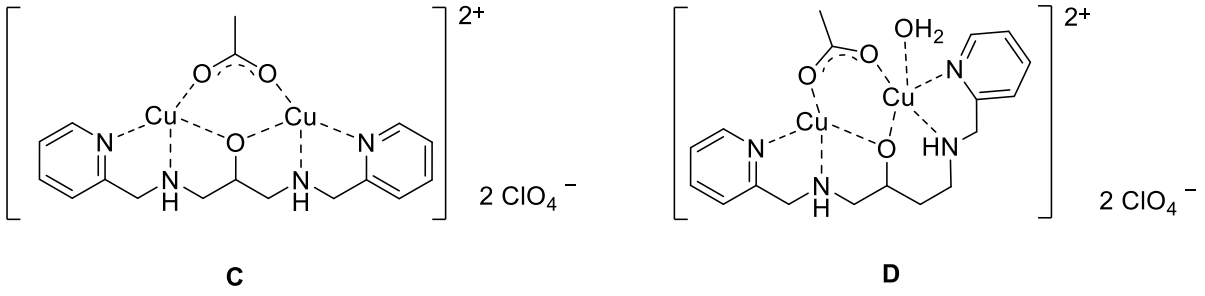

C **D**

Figure 4.3. Dinuclear Cu^{II} complexes applied as model glycoside hydrolases.[159]

For the investigation of the patellamide-based complexes **1** and **4** (see Figure 4.4) concerning their glycosidase-like activity, 4-nitrophenyl-α-*D*-glucopyranoside or 4-nitrophenyl-β-*D*-glucopyranoside

were employed as substrates. Setup and data processing of the assays was performed analogously to the procedure described in detail in Chapter 3.1. The corresponding pH profiles for α- as well as β-glycosidase-like activity are shown in Figure 4.5. The determined pH profiles were fitted to equation 4.1.[99] The catalytic rates as well as the pH values for the two deprotonation steps pK_a(I) and pK_a(II) are given in Table 4.2. Since it cannot be determined with certainty which of the two arrangements is the catalytically active one, in the following it is referred to the dinuclear copper complexes of H_4pat^1 as **1**, H_4pat^4 as **2**, of H_4pat^2 as **4**.

$$v_0 = \frac{v_{\max}\left(1 + \frac{\gamma K_{a_2}}{[H^+]}\right)}{\left(1 + \frac{[H^+]}{K_{a_1}} + \frac{K_{a_2}}{[H^+]}\right)} \tag{4.1}$$

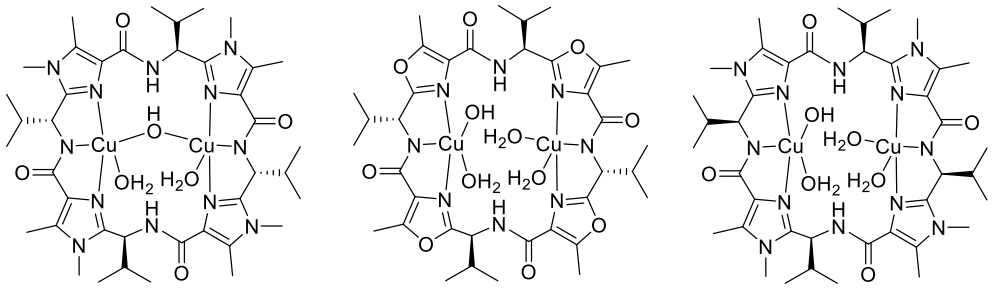

1A $[Cu_2(H_2pat^1)(\mu\text{–}OH)(H_2O)_2]^+$ **2B** $[Cu_2(H_2pat^4)(OH)(H_2O)_3]^+$ **4B** $[Cu_2(H_2pat^2)(OH)(H_2O)_3]^+$

Figure 4.4. Schematic representation of **1A**, **2B** and **4B**. **A** refers to the bridging OH^- mode, **B** to the terminally bound mode.

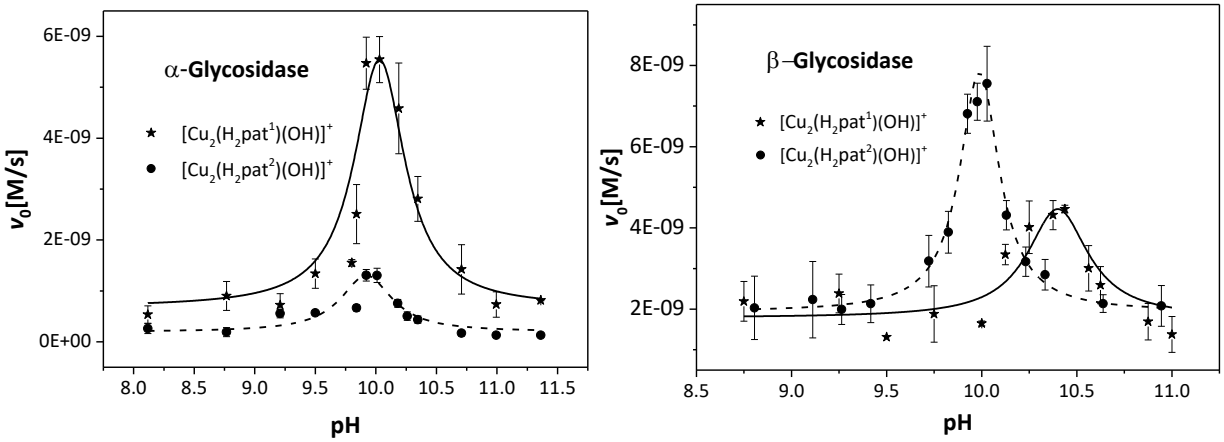

Figure 4.5. pH profiles of the $[Cu^{II}_2(H_4pat^1)(OH)]^+$ (solid) **1**, $[Cu^{II}_2(H_4pat^2)(OH)]^+$ **4** (dashed) catalysed 4-nitrophenyl-α-*D*-glucopyranoside (left) and 4-nitrophenyl-β-*D*-glucopyranoside (right) hydrolysis [substrate] = 10.5 mM; [cat] = 40 µM; 25°C.

Table 4.2. Hydrolysis data and kinetic properties of **1** $[Cu_2(H_2pat^1)(OH)]^+$ and **4** $[Cu_2(H_2pat^2)(OH)]^+$ for glycosidase activity.[165]

Catalyst		pH_{max}	$v_{0,max}$ [Ms^{-1}]	pK_a(I)	pK_a(II)	γ
α-glycosidase	**1**	10.03	6.19 ± 0.53	9.86 ± 0.03	10.20 ± 0.14	0.1954 ± 0.0357
	4	9.92	1.11 ± 0.21	9.73 ± 0.09	10.09 ± 0.04	0.1748 ± 0.0417
β-glycosidase	**1**	10.36	3.36 ± 0.03	10.19±0.04	10.53 ± 0.04	0.2378 ± 0.0521
	4	9.43	5.86 ± 0.02	9.21 ± 0.02	9.64 ± 0.02	0.2435 ± 0.508

The dinuclear Cu^{II} complex **2** (see Figure 4.4) that was shown to exhibit phosphatase activity in Chapter 3 was also studied concerning its potential activity towards glycosidic bond cleavage, but did not show catalytic properties.

Measurements at the optimum pH values in dependence of the substrate concentration of **1** and **4** were fitted according to a MICHAELIS-MENTEN model (see Figure 4.6 and Table 4.3). Here, the concentration of 4-nitrophenyl-α/β-*D*-glucopyranoside was varied between 1 and 10 mM. The data were fitted to equation 4.2, providing the MICHAELIS-MENTEN constant K_M, which was used to determine k_{cat} (equation 4.3).

$$v = v_{max} \cdot \frac{[S]_0}{(K_M + [S]_0)} \tag{4.2}$$

$$k_{cat} = \frac{v_{max}}{[K]_0} \tag{4.3}$$

The difference of the determined pK_a values for α-glycosidase-like activity is approximately 0.4 pH units and the maximum activities are observed at pH=10.03 ($[Cu^{II}_2(H_4pat^1)(OH)]^+$, **1** and 9.92 ($[Cu^{II}_2(H_4pat^2)(OH)]^+$, **4**. For the β-glycosidase-like activity, the difference between the determined pK_a values is similar (0.3 for **1** and 0.4 for **4**). The catalytic rates of **1** and **4** are of the same order of magnitude for α- and β-glycosidase. However, whereas α-glycosidase is catalysed by **1** and **4** at an optimal pH of ca. 10.0, the pH optima observed for β-glycosidase activity are shifted, to 9.4 for **4** and to 10.4 for **1**.

The uncatalysed background rate constants for α- and β-glycosidase are k_{uncat}=0.0135x10^{-4} s^{-1} and k_{uncat}=0.0286x10^{-4} s^{-1}, respectively,[166] and this corresponds to rate enhancements k_{cat}/k_{uncat} for the H_4pat^1 and H_4pat^2 based catalysts of 115 and 21 for α- and of 43 and 37 for β-glycosidase. That is, the catalyst with the configuration of the natural product (H_4pat^1) generally is a more efficient catalyst,

and this observation was also made for the carbonic anhydrase and phosphatase activities, as pointed out in Chapter 3.[97,100] Nevertheless, it seems that the side-chain configuration is less crucial for β-glycosidase-like activity, since the catalytic rate is almost identical and the catalytic efficiency k_{cat}/K_M is even higher for **4** than observed for **1**.

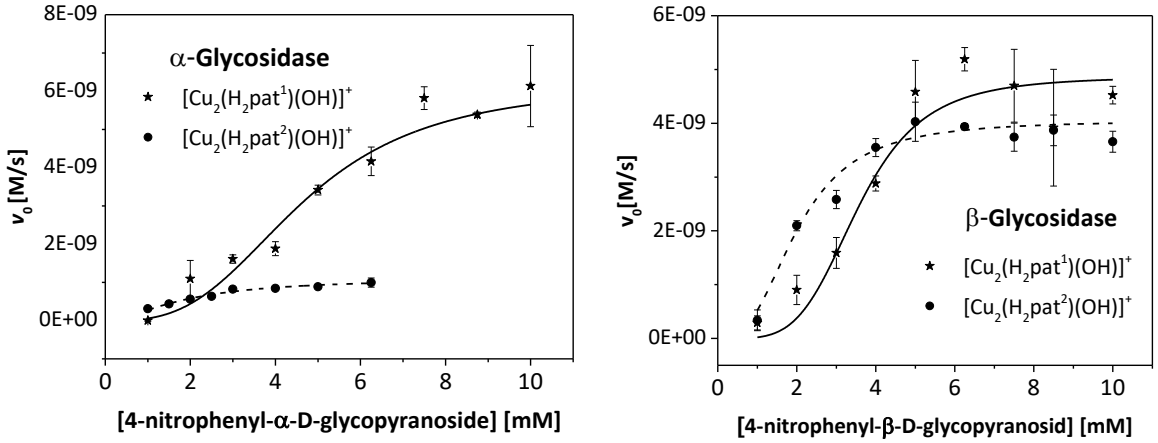

Figure 4.6. Overlay of MICHAELIS-MENTEN measurements of **1** $[Cu_2(H_2pat^1)(OH)]^+$ (solid) and **4** $[Cu_2(H_2pat^2)(OH)]^+$ (dashed). Left: α-glycoside hydrolysis at pH 10.03 (**1**) and 9.92 (**4**). Right: β-glycoside hydrolysis: at pH 10.36 (**1**) and 9.43 (**4**). [cat] = 40 µM; 25°C.

Table 4.3. MICHAELIS-MENTEN parameters for the glycosidase activities.[165]

catalyst		k_{cat} x 10^{-3} [s^{-1}]	K_M [mM]	k_{cat}/K_M [$M^{-1}s^{-1}$]
α-glycosidase	**1**	1.55 ± 0.13	4.64 ± 0.43	3.30
	4	0.28 ± 0.01	1.90 ± 0.47	1.49
β-glycosidase	**1**	1.22 ± 0.09	3.56 ± 0.23	3.43
	4	1.08 ± 0.04	2.12 ± 0.17	5.09

The fact that β-glycosidase shows higher catalytic efficiencies as compared with α-glycosidase-like activity might be caused by a lower activation energy for the formation of the respective catalyst-substrate complex. This is probably rationalised by a smaller steric hindrance caused by the equatorial β-arrangement of the nitrophenol, which could in turn facilitate a more efficient hydrolysis, as opposed to the axial α-position. To demonstrate this, Figure 4.7 depicts the parallel arrangement of the nitrophenol ring to the $Cu^{II}\cdots Cu^{II}$ vector as one example of possible arrangements for the enzyme-model substrate complex. Since the pH optima for β-glycosidase however differ greatly, pH 10.4 for **1** and 9.4 for **4**, it must additionally be considered that the mechanisms might not be identical for the β-glycoside hydrolysis.

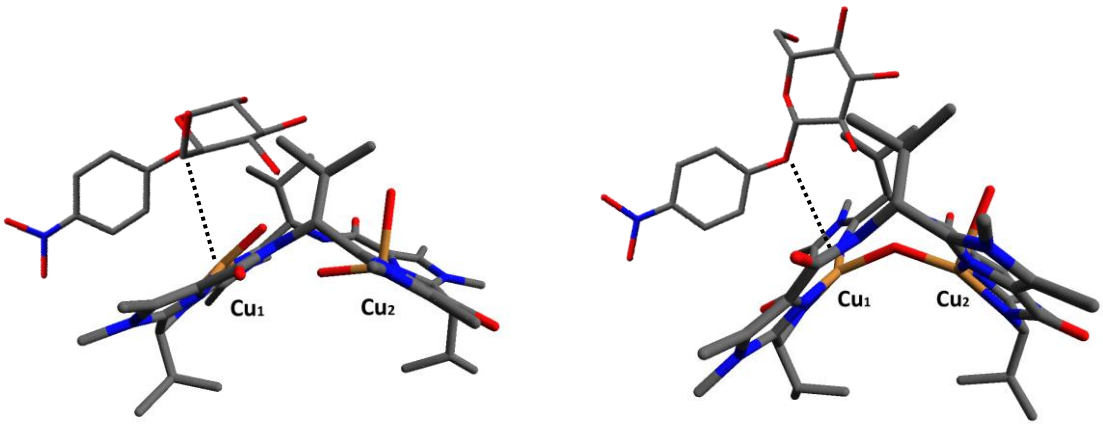

Figure 4.7. Putative structure of the catalyst-substrate complex consisting of **1A** and the α–glycoside (left) as well as **1B** and the β–glycoside (right), (orange: Cu^{II}, grey: C, blue: N, red: O, hydrogen atoms are omitted for clarity).

One potential pathway would be similar to what was described for phosphatase activity: initially the substrate is complexed by one Cu^{II} ion (Cu_1) and the other Cu^{II} (Cu_2) coordinates water that is deprotonated at pH 10 and can thus act as a nucleophile and attack the anomeric carbon atom. Probably for **1**, the bridged complex $[Cu_2(H_2pat^1)(\mu\text{-}OH)(H_2O)_2]^+$ is the catalytically active species, which would be in line with higher pK_a(I) values.

Interestingly, other model glycosides (*vide supra*) also show an optimum performance in the range of pH 9.5-10.5. So far, it has not been studied whether and how this is related to the substrate used. Probably, the indigo based substrate that has been proposed as an alternative glycosidase substrate by BÖTTCHER recently should be prepared (the five step synthesis is reported) and tested to examine the potential substrate dependence of determined catalytic properties of the catalysts.[167]

In addition, it must be considered that the complex prepared *in situ* with Cu^{II} and H_4pat^1 (and equally with H_4pat^2) can exhibit one pair of pK_a values for each structural arrangement. Since **1** and **4** show activity at pH 10 (glycosidase) and pH 7.3 (phosphatase), in contrast to complex **2** that only seems to be active at pH 7, structural changes might be encountered, facilitating the various pH activity ranges. To support this assumption EPR spectra have been recorded at pH 7.3 and 10.0 of the respective Cu^{II} patellamide complexes, results of which will be presented in Chapter 4.3 after the study of the complexes as potential β-lactamase models.

4.2 β-Lactamase-like activity

Six different subtypes of β-lactam antibiotics; penams, cephems, monobactams, clavams, penems and carbapenems are known.[168] Five of them are readily hydrolysed by metallo-β-lactamases (MβLs), only monobactams withstand the hydrolases. This is a development that must be considered with concern, especially since carbapenems represent the group of β-lactams with the broadest spectrum of activity, that are at the same time resistant to other lactamases, namely serine-β-lactamases produced by resistant pathogens. In addition, the horizontal transference of resistance genes is widely observed and so far no therapeutic for metallo-β-lactamases has been reported.[168]

The β-lactamases in general comprise, based on the respective amino acid sequence, the four classes A-D. Metallo-β-lactamases represent class B and require Zn^{II} for activity. MβLs are also grouped in different subclasses B1, B2 and B3 (see Figure 4.8), although all show the same common fold and limited sequence homology.[169] Recently, a further class B4 has been proposed.[170,171]

The active site of B1 was shown to be dimetallic with two different coordination sites, which are depicted in Figure 4.8: the cysteine site (left) and the so called histidine site (right). In the cysteine site Zn^{II} is coordinated in a trigonal bipyramidal fashion by cysteine, aspartate, a histidine and two water/hydroxido ligands, of which one acts as a bridging ligand to the second site.

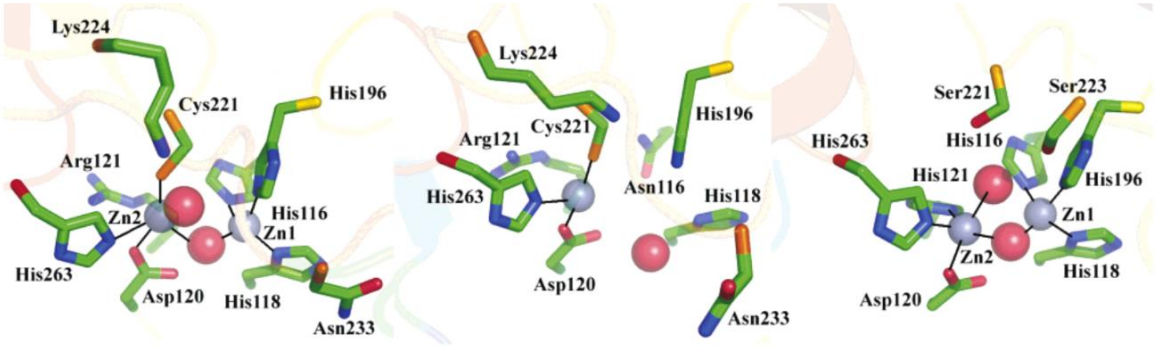

Figure 4.8. Structures of the active sites of MβLs. From left to right: B1 type from *B. cereus*; B2 type CphA from *Aeromonas hydrophila*; B3 type L1 from *Stenotrophomonas maltophilia* (grey spheres: Zn^{II}, red spheres: O (water), solid bonds: coordinative bonds). Reprinted with permission from [169] Copyright American Chemical Society.

The histidine site is constituted by three histidine residues and one water/hydroxido ligand, coordinating the second Zn^{II} in a tetrahedral mode. Some mononuclear B1 sites are reported as well, in which the Zn^{II} ion is coordinated in the histidine site. B2 sites on the other hand are always mononuclear and still exhibit full catalytic efficiency. The Zn^{II} in the B2 site is found to be coordinated

in the cysteine site. The B3 site is very similar to B1 with the cysteine residue being replaced by a serine, which does not contribute to the coordinative bonds. Instead, the Zn^{II} is coordinated by two histidines, aspartate and a water/hydroxido coligand. The replacement of the cysteine by histidine causes the coordination shell of the Zn^{II} to be rotated by 80°.[169]

The Zn^{II} ions are thought to bind water and, due to their LEWIS acidity, decrease its pK_a, resulting in a hydroxido complex. The detailed mechanism is not fully elucidated,[169,171] however a proposed mechanism of the cleavage is shown in Scheme 4.3 for New Delhi Metallo-β-lactamase 1 (NDM-1).[168]

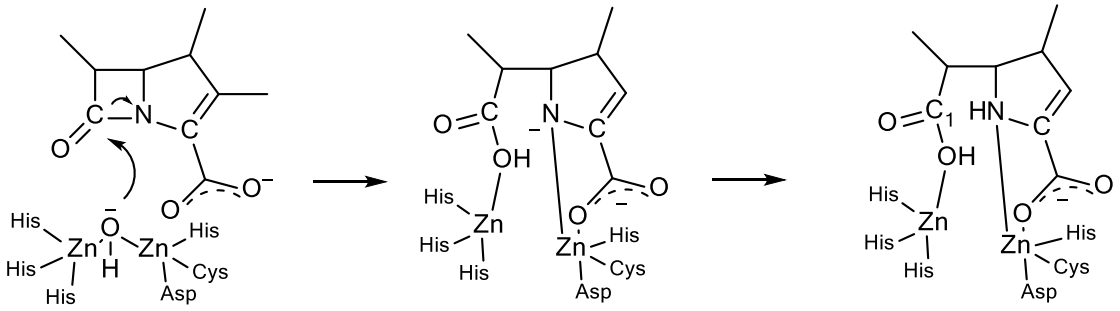

Scheme 4.3. Proposed mechanism of the hydrolysis of β-lactam-antibiotics *via* NDM-1.[168,171]

Upon cleavage of the amide bond, the formerly antibiotic compound cannot bind irreversibly to penicillin binding protein (PBP), which is responsible for the establishment of peptide bonds in murein, a component of the bacterial cell wall. Due to their broad substrate specificity profile and the high activity of class B metallo-β-lactamases, especially towards carbapenems, current research focuses on understanding this class of enzymes. Profound comprehension of the mechanism and the structures of metallo-β-lactamases might be the foundation for a potential application in bioremediation, as well as for sensible drug design.[171]

Thus, model complexes were developed mimicking the natural enzymes. Often dinuclear Zn^{II} complexes were investigated, but also examples of Co^{III} and Cd^{II} based models emerged, exhibiting similar activity.[171,172] A comprehensive overview on model complexes is given in reference [171]. For many Zn^{II} based models, pK_a values at physiological pH, *i.e.* 7-8 are found, with the Co^{III} and Cd^{II} based models shown to be efficient at more basic conditions (pH 8-10). Two examples of β-lactamase model complexes are depicted in Figure 4.9.

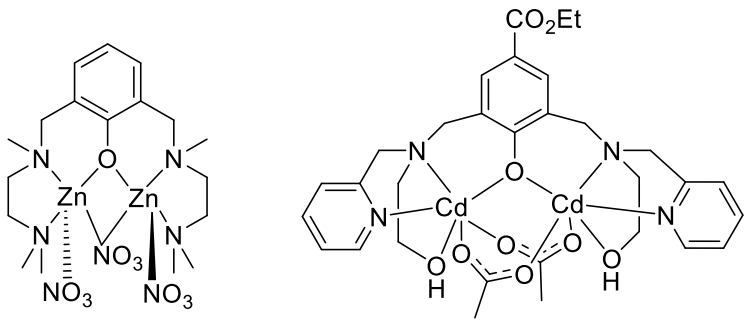

Figure 4.9. Examples of β-lactamase model complexes.[171,172]

Complex **E** is a dinuclear Zn^{II} complex, showing k_{obs} of 0.228×10^{-3} s^{-1} at a catalyst concentration of 500 µM and 37.5 µM nitrocefin.[173] The Cd^{II} complex **F**, shows a pK_a at 10.1 and a catalytic rate k_{cat} of 9.4×10^{-3} s^{-1} ([cat]=5 µM, [nitrocefin]=25 µM).[172]

The uncatalysed background β-lactam hydrolysis rate is reported to be $k_{uncat}=2.5 \times 10^{-6}$ s^{-1}.[174] The kinetic MICHEALIS-MENTEN data reported for natural β-lactamase activity are in the range of K_M =16-100 µM and k_{cat}=0.3-200 s^{-1} for *Bacteroides fragilis* and *Aeromonas hydrophila*, respectively (substrate nitrocefin).[175] Nitrocefin is often used as a model substrate due to its hydrolysis-induced colour change, which can be monitored spectrophotometrically (see Scheme 4.4).

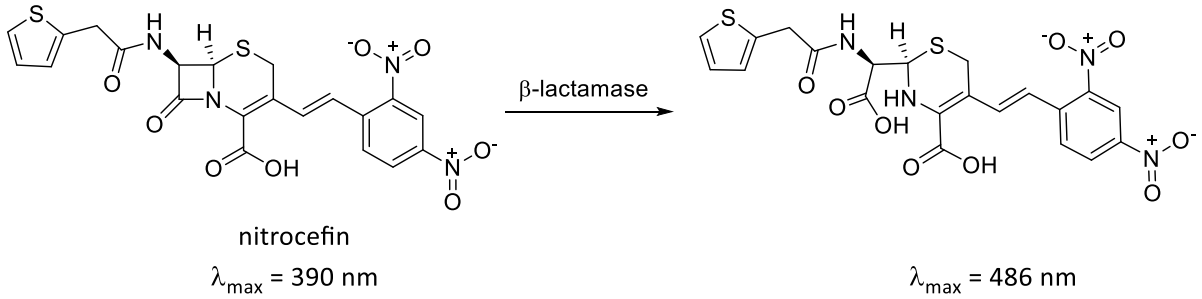

Scheme 4.4. Schematic representation of β-lactam hydrolysis.

Similar to the glycosidase-and phosphatase-like activity measurements, the optimal pH range for maximum lactamase activity of **1** and **4** was determined by pH-dependent measurements with a constant catalyst (5 µM) and substrate concentration (25 µM) in a 1:1 MeCN : buffer mixture as solvent at 37°C. The initial rates at each pH value were corrected for the corresponding auto hydrolysis

rates. For $[Cu_2(H_2pat^2)(OH)]^+$ **4** no activity could be observed. The pH profile for $[Cu_2(H_2pat^1)(OH)]^+$ **1** is shown in Figure 4.10 and the resulting kinetic parameters and pK_a values are summarised in Table 4.4.

Table 4.4. Kinetic data from pH profiles of $[Cu_2(H_2pat^1)(OH)]^+$ (**1**) for the hydrolysis of nitrocefin and the corresponding MICHAELIS-MENTEN parameters determined at pH 11.5.[165]

catalyst	pH_{max}	$v_{0,\,max}$ 10^{-9} [M/s]	pK_a(I)	k_{cat} x 10^{-3}[s^{-1}]	K_M [μM]	k_{cat}/K_M [$M^{-1}s^{-1}$]
1	11.50	3.82 ± 0.03	≈11.3	1.134 ±0.91	22.47	50.47

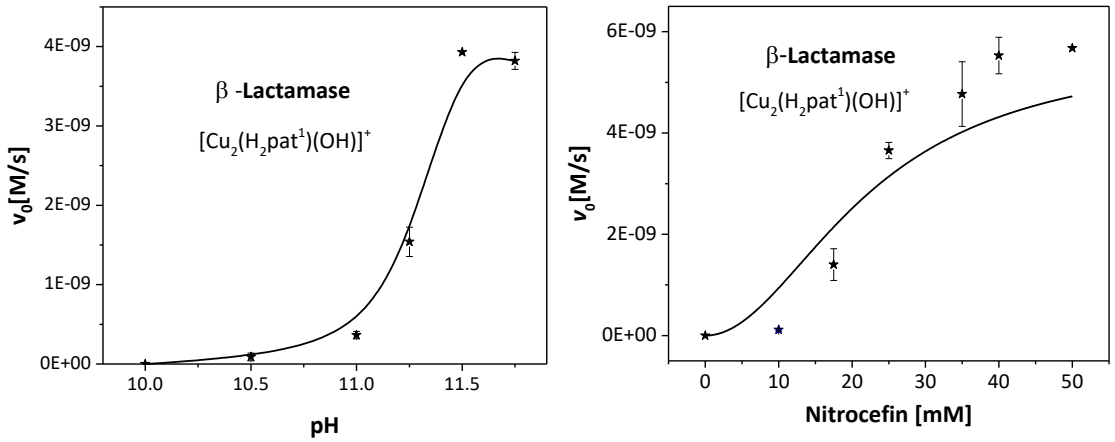

Figure 4.10. Left: pH profile of the $[Cu_2(H_2pat^1)(OH)]^+$ **1** catalysed nitrocefin hydrolysis [nitrocefin] = 25 μM, [cat] = 5 μM, 37°C; the solid line is a basis spline function and not fit to a kinetic model. Right: Substrate dependent MICHAELIS-MENTEN measurement at pH 11.5.

β-lactamase-like activity is observed at pH 11.5 with resulting k_{cat}/K_M=50.5 $M^{-1}s^{-1}$, and this is consistent with similar dinuclear model complexes as discussed above.[172] It corresponds to a rate enhancement of k_{cat}/k_{uncat}=454. The mechanism of the catalytic bond cleavage is most likely similar to the proposed mechanism shown in Scheme 4.3, *i.e.* the catalytically active species might be the μ-OH^- bridged species, **1A**. The hydroxide ion might then act as a nucleophile and attack the carbonyl carbon in the β-lactam ring, resulting in bond cleavage between C and N. This could result in a complex, in which one copper(II) ion is coordinated by OH^- (bound to the carbonyl C) and the other copper(II) ion is coordinated by the nitrogen of the former β-lactam ring. The active catalyst is probably recovered by the exchange of the product with water molecules.

Since neither activity for complex **4** (imidazole-based ligand, 4*S*) nor for complex **2** (oxazole based, *RS*) was observed, the question as to whether this might be associated with a different complex geometry is dealt with in detail in the following.

4.3 EPR study of $[Cu_2(H_2pat^1)(OH)]^+$ and $[Cu_2(H_2pat^4)(OH)]^+$ at pH 7.3 and 10.0

The previous parts of this Chapter showed that **1**, $[Cu_2(H_2pat^1)(OH)]^+$ and **4**, $[Cu_2(H_2pat^2)(OH)]^+$ hydrolyse α- and β-glucosides at pH 10, and **1** is also a potent lactamase model at pH 11.5. However, **2**, $[Cu_2(H_2pat^4)(OH)]^+$ (oxazole-based, *RS*) does not show hydrolysis-like activity under these basic conditions. Thus, the question is raised whether this is primarily due to the stability of the complex at a higher pH or whether the complex formed at pH 10 has a structure different from the species at pH 7-8, when phosphatase activity is observed. In order to establish the stability constants in buffer, ITC measurements are in the focus of ongoing research, but so far no results were obtained. For that reason, EPR experiments have been carried out to characterise the respective species for **1** and **2** at pH 7.3 and pH 10.0, which correspond to the pH optima for **1** for phosphatase and glycosidase-like activity.

EPR is a useful tool to investigate paramagnetic species like radicals and open shell metal ions. For metal ions, depending on the geometry of the complex, the electronic properties of the ions are altered and the concise arrangement of d orbital energy levels is influenced. Thus, EPR delivers for transition metal ions like Cu^{II} (d^9, ^2D) insight in the coordination geometry, possible dynamic processes as well as reaction dynamics. EPR is especially powerful when it comes to the estimation of the ligand field for Cu^{II}, since a view in the spectrum gives a hint on whether one should expect a trigonal bipyramidal (d_{z^2} as the ground state d-orbital with one electron) or an elongated octahedral coordination environment ($d_{x^2-y^2}$).[176]

Five contributions for the ground state of paramagnetic centres are expected and can be summarised in the Spin Hamilton operator as shown in equation 4.4, first described by ABRAGAM and PRYCE:[177-180]

$$\hat{H}_{AP} = \frac{\mu_B}{\hbar} B g \hat{S} + \hat{S} D \hat{S} + \sum_k \hat{S} A_k \hat{I}_k - \sum_k \gamma_k B \hat{I}_k + \sum_{I_k > 1/2} \hat{I}_k P_k \hat{I}_k \qquad (4.4)$$

Here, μ_B is the BOHR's Magneton, B the magnetic flux density, g and A_k are 3 x 3 matrices of the dimensionless magnetic moment g and of the hyperfine coupling constant A_k. P represents the quadrupole tensor and γ_k is the gyromagnetic ratio of the considered atomic nuclei. The first term describes the electron ZEEMAN interaction, the second term characterises the electronic quadrupole interaction (zero field splitting, zero for a system with one unpaired electron like Cu^{II}). The third term

comprises the hyperfine interaction, whereas the fourth term signifies the nuclear ZEEMAN interaction and the last term describes the nuclear quadrupole interaction.

As soon as an external magnetic field is applied, the degenerate arrangements of the electron spin are split into two states. This interaction of the unpaired electron with the magnetic field B is described in the electron ZEEMAN term. A transition from the energetically favoured to the less favoured state of the electron spin can be achieved by supplying enough energy. The amount of energy needed depends on the magnetic field that splits the state. Typically, the employed techniques in the investigation of metal ions use magnetic fields with 0.3 T or 1.25 T; the corresponding energy necessary to populate the unfavoured spin state is in the microwave range of 8-12 GHz / 35 GHz and commonly referred to as X- and Q-band.

$$\Delta E = h\nu = g\beta B \tag{4.5}$$

The g value is often compared to the chemical shift δ observed in NMR spectroscopy and is 2.00232 for a free electron (*n.b*. that in NMR the shift is reported relative to a standard, whereas absolute values are given for g). The deviation of the g-value from the value for the free electron originates from spin-orbit coupling that is unique for every element, and can be altered by its chemical environment.

The hyperfine coupling (third term) refers to the interaction between the magnetic moment of the electron spin and the nuclear spin of the metal ion and the ligand. These nuclear spins are also quantised, induced by the field and can be described as:

$$E_{M_S M_I} = M_S \frac{\mu_B}{\hbar} gB + AM_S \hat{I}_M \tag{4.6}$$

If the symmetry of the investigated metal centre is lower than cubic, anisotropy of g- and A-tensors is expected.[178] In order to extract information from the spectra, simulations are carried out.

In this case, simulations were performed with Molecular Sophe[181] and XSophe,[182] which employ the Spin Hamilton operator as shown in equation 4.4. Recorded spectra with corresponding simulations are given in Figure 4.11 for **1** $[Cu_2(H_2pat^1)(OH)]^+$ and in Figure 4.12 for **2** $[Cu_2(H_2pat^4)(OH)]^+$, respectively.

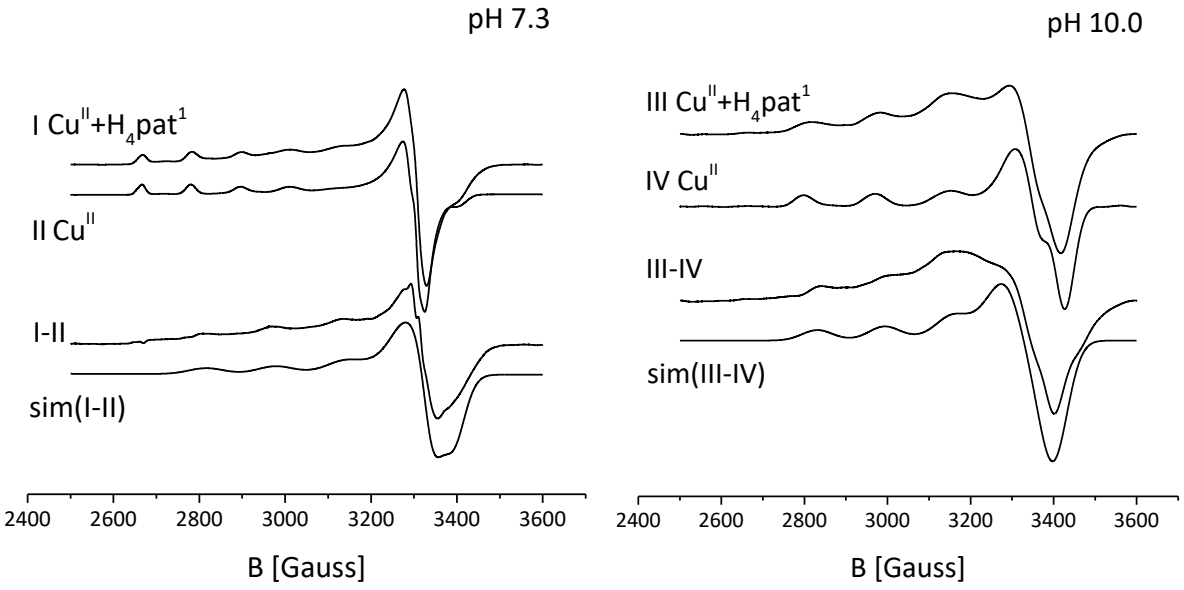

Figure 4.11. Experimental EPR spectra of the complex species **1** $[Cu_2(H_2pat^1)(OH)]^+$ (1 mM, **I** (9.635075 GHz) and **III** (9.636163 GHz)) and a Cu^{II} solution (1 mM, **II** (9.632445 GHz) and **IV** (9.635244 GHz)) at pH 7.3 (left) and pH 10.0 (right) in a 3:1 MeOH : buffer solution.

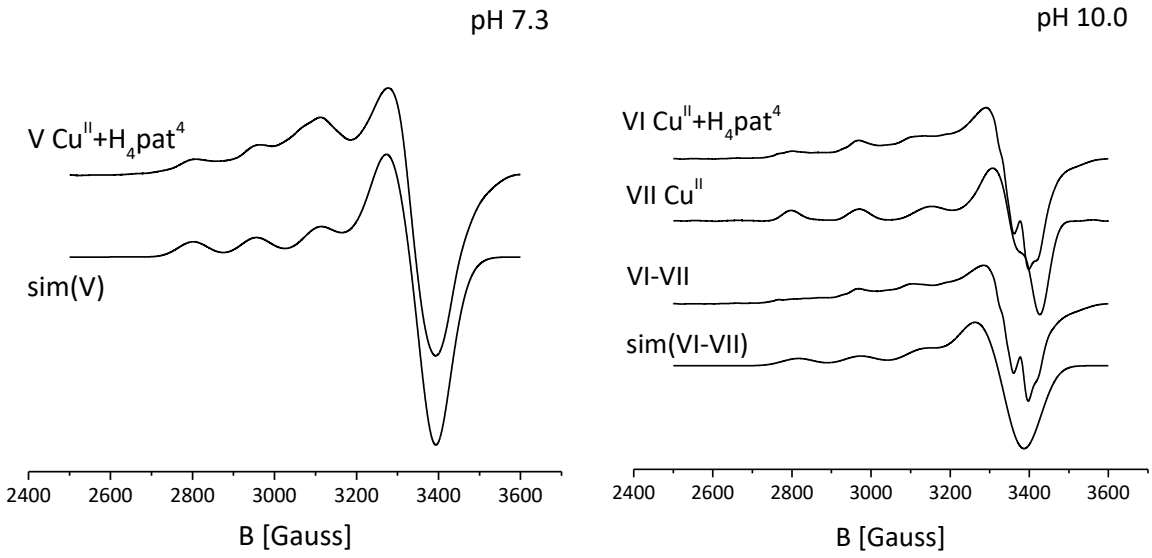

Figure 4.12. Experimental EPR spectra of the complex species **2** $[Cu_2(H_2pat^4)(OH)]^+$ (1 mM, **V** (9.635573 GHz) and **VI** (9.634977 GHz)) and a Cu^{II} solution (1 mM, **VII** (9.635244 GHz)) at pH 7.3 (left) and pH 10.0 (right) in a 3:1 MeOH : buffer solution.

Table 4.5. g- and A- tensors [10^{-4} cm^{-1}] for the species labelled in Figure 4.11 and 4.12 (**1** and **2**) compared with previously characterised species of **1**.[85]

Species	g_x	g_y	g_z	A_x	A_y	A_z
1 2 eq. MeO^- [85]	2.0719	2.0456	2.258	4.019	4.423	166.878
1 3 eq. MeO^- [85]	2.0503	2.0539	2.2600	12.6896	9.2275	161.641
1 pH 7.3 (I-II)	2.0895	2.0655	2.2530	0.8670	4.3750	168.00
1 pH 10.0 (III-IV)	2.0779	2.0456	2.24983	4.99844	4.99687	165.00
2 pH 7.3 (V)	2.0760	2.0615	2.27056	18.6	7.375	162.00
2 pH 10.0 (VI-VII)	2.0950	2.0475	2.2575	17.0	13.7	164.00

All previously published EPR experiments of patellamides with Cu^{II} were carried out in MeOH with MeO^- as a base, without exact knowledge about the pH in solution. However, since the exact pH seems to be crucial for the catalytic activity of the complexes, in the EPR experiments shown here the solvent was chosen to be a mixture of buffer : MeOH 1 : 3, with methanol needed for the solubility of the ligand and for the formation of a proper glass at 30 K. Solubility was a problem, since the final complex concentration (the complexes were prepared *in situ*) in solution had to be 1 mM in order to obtain a reasonable signal/noise ratio from the EPR experiments. However, it would be preferable to carry out these experiments at the same concentrations at which the hydrolyses were investigated, *i.e*. 40 µM (glycosidase) and 5 µM (β-lactamase), respectively.

Figure 4.11 shows the spectra recorded for **1** $[Cu_2(H_2pat^1)(OH)]^+$ at pH 7.3 and pH 10.0 as well as the corresponding spectra of a $Cu(OTf)_2$ solution at the respective pH values. Moreover, a difference spectrum is shown, the result from subtracting the signal of the solvated Cu^{II} ion from the signal of the Cu^{II} complex. A simulation of the species observed in the difference spectrum was attempted, and the respective g- and A- tensors are summarised in Table 4.5. It is important to note that at pH 10 a small amount of precipitate was observed, which most likely corresponds to copper(II) hydroxide. Nevertheless, the spectra of the remaining solution indicated the formation of a copper(II) complex and were consequently interpreted.

First and foremost, the spectra show that there is free Cu^{II} in the mixture at pH 7.3. Judging from the qualitative difference of the spectra it also seems that the amount of non-coordinated Cu^{II} is smaller at pH 10.0, which is expected, since one would expect a higher pH to cause the deprotonation of the ligands and consequently enable complex formation due to equilibria shifting. The EPR spectra indicate a square-pyramidal coordination, as observed previously[85] and as expected by DFT as well as

a crystal structure.[67] Due to the poor resolution of the spectrum, to which buffer as the solvent contributed, no hyperfine couplings were derivable. In addition, the spectra do not seem to show the presence of a dinuclear complex. There are different explanations for this; it could on the one hand mean that the spectrum is *pseudo*-mononuclear.[85] This would be the case if dipole-dipole interactions of the Cu^{II} centres in the complexes are cancelled out, which is known in the literature for the respective dinuclear Cu^{II} complex of the natural ascidiacyclamide.[71] It would be expected for an orientation of the g- and A-tensors of the Cu^{II} ions of α=54.7° and β=37.5° (EULER angles), which is also called the 'magic angle' setup. Another possible explanation for the absence of signals arising from a dinuclear species would be that the dinuclear complex is only formed in small quantities, enough to act as a catalyst, and the main species formed in aqueous solutions is the mononuclear species. Currently ITC measurements in aqueous solution are underway to shed more light on that matter. For the following discussion however, the complexes prepared *in situ* are referred to as dinuclear complexes.

The quality of simulations is hampered by the line width of the experimental spectra, thus all data obtained must be interpreted with caution. If compared to the g- and A-values obtained for the same complex **1**, $[Cu_2(H_2pat^1)(OH)]^+$ in MeOH with two equivalents of MeO^- as a base,[85] it becomes obvious that the ligand field orientation of **1** at pH 7.3 and pH 10.0 seem to be similar, albeit not identical.

From the comparison of the DFT optimised structures of **1** and **2** (see Chapter 3.1), one would expect similar g- and A-tensors. Compared to the spectrum of **1** at pH 7.3 less uncoordinated Cu^{II} is present in the solution of **2** at pH 7.3. Probably this correlates with a higher stability of the complex and/or a lower pK_a of the amide protons of the ligand. Since it was impossible to align the spectra of **2** and Cu^{II} at pH 7.3 in a way that would allow a subtraction giving a sensible spectrum corresponding to an either mono- or dinuclear Cu^{II} complex, no difference spectrum is shown and instead the simulation of the original spectrum is depicted (see Figure 4.12). Moreover, the simulation of the difference spectrum at pH 10.0 is shown. From these approximate simulations, it becomes clear that the ligand field indeed is similar to what is observed for **1**, $[Cu_2(H_2pat^1)(OH)]^+$, but the A-tensors observed vary significantly (10×10^{-4} cm^{-1}). In addition, the simulations of **2**, $[Cu_2(H_2pat^4)(OH)]^+$ at pH 7.3 and pH 10.0 imply a significantly different species at the respective pH values. This would support the hypothesis that the main species present at these pH values do differ. Consequently, the absence of catalytic activity of **2** at pH 10.0 might be caused by the formation of an inactive complex.

4.4 Conclusion

In this Chapter it was shown that **1**, $[Cu_2(H_2pat^1)(OH)]^+$, as well as **4**, $[Cu_2(H_2pat^2)(OH)]^+$, catalyse the hydrolysis of α- as well as of β-glycosides at pH 10 and **1** additionally shows β-lactamase-like activity at pH 11.5. This means, that the patellamide-dicopper(II) complexes are among the few examples of dinuclear metal complexes acting as glycosidase-like model compounds.

Taking into account the reactivity observed at alkaline pH values, the copper(II) complexes are expected to be dinuclear. This assumption was also confirmed by hydrolysis experiments with varying ligand : copper ratios. Concomitant EPR experiments however showed mononuclear species, which might be due to the fact that dinuclear complexes are appearing as *pseudo*-mononuclear due to magic angle setup. However, it can also not be excluded that the dinuclear copper(II) complex does exhibit very small stability constants in aqueous conditions and thus, only a small portion of copper(II) in the solution is complexed, leading to a signal that cannot be determined over the background signal of free copper(II) ions. Another possible explanation of the missing signal for a dinuclear copper(II) complex is the formation of a strongly antiferromagnetically coupled complex, and this theory will be discussed in depth in the next Chapter. Taking into account the broad reactivity pattern of these compounds with respect to hydrolysis reactions, namely phosphatase, carbonic anhydrase, glycosidases as well as β-lactamase, several questions emerge.

First, it is uncertain whether the catalytic activities observed for the dinuclear copper(II) complexes can be associated with the function of the cyclic peptides in *Prochloron* or *L. patella*. Therefore, the next Chapter of this thesis is dedicated to *in vivo* studies towards an understanding of the stability of dinuclear copper(II) complexes with these naturally occurring ligands.

Second, and not less important, is the question, whether all of the catalysed hydrolyses observed are of importance for the symbiosis partners. This question is the focus of ongoing research and is particularly interesting, in the light of the findings from KÜHL *et al*., who showed, that the pH in the host, *Lissoclinum patella* in close proximity to *Prochloron* cells does vary greatly from pH 7 in darkness to 11 upon irradiation of sunlight.[9] Consequently, the dinuclear copper(II) patellamide complexes might act as light-dependent catalysts, provided the stability of the complexes is similar at these pH values in the cell and the oxidation state is identical (this question is addressed in detail in the next Chapter). If glycosidase as well as carbonic anhydrase activity were mediated by the same dinuclear copper(II) patellamide complexes in the cell, this would indicate that the same enzyme is capable of

fixing carbon from CO_2 as well as to catabolise the products from the assimilation (CALVIN-BENSON cycle). *Prochloron* could consequently use glucose as a carbon source to maintain its metabolism under non-photosynthetic conditions, similar as reported for *Synechocystis*.[87]

5 Is copper(II) coordinated to patellamides inside *Prochloron* cells?*

Although synthetic models of the natural patellamides bind Cu^{II} and exhibit catalytic activity *in vitro* as dicopper(II) complexes, their biological role is still not known. In this Chapter the question is addressed as to whether the complexes of the cyclic *pseudo*-octapeptides are also formed inside the *Prochloron* cells. Therefore, a patellamide ligand with an appended reporter group (RG) was designed and studied concerning its binding behaviour towards Cu^{II} *in vivo.*

The concentration of copper cations in living cells and their oxidation state is a topic that is not well studied for cyanobacteria. It is known that mammalian (eukaryotic) cells exhibit a reductive interior atmosphere,[183] and the free copper cations are thus present as Cu^{I} ions.[183] The copper ion homeostasis is regulated by a copper ion importing and exporting system and leads to a Cu cation concentration in the cell in the femtomolar range.[183] Similar systems were also found for the prokaryotes *Enterobacteria*.[184] Here, interior copper(II) concentrations of 10^{-6} M were reported, as compared to 10^{-8} M in the surrounding medium.[184] From a proteomic study on *Synechocystis* sp. (cyanobacterium) it became clear that the export mechanism is the main regulator of the copper cation concentration.[87] However, exact copper cation concentrations for cyanobacterial cells are not published so far. JASPARS *et al.* reported in 2001 that after extraction of the *Prochloron* cells in the DCM phase the copper(II) concentration was found to correspond to a 10^4 times enrichment compared to the surrounding sea water.[185] Typically, the copper(II) and zinc(II) concentrations in sea water are in the range of 1.1-22.9 nM and 3.0-24.0 nM respectively.[186,187] Obviously, the copper(II) concentration is subject to geological, environmental, seasonal as well as agricultural influences, but in the absence of data from the areas where *Prochloron* can be found, the data from reference [186], 4 nM Cu^{II} and 6 nM Zn^{II}, are taken as rough estimates. Thus, speaking of a 10^4 times increased concentration in the cells as compared to the surrounding sea water would correspond to an *in vivo*

* Main parts of this Chapter will be published in:'Is Cu^{II} coordinated to patellamides inside *Prochloron* cells?' Peter Comba, Annika Eisenschmidt, Lawrence R. Gahan, Dirk-Peter Herten, Geoffrey Nette, Gerhard Schenk, Martin Seefeld., manuscript in preparation.

concentration of 40 µM Cu^{II} and 60 µM Zn^{II}. This in turn would be ten times more concentrated as the respective number given for *Enterobacteria* (as mentioned above). The question about the reductive/oxidative milieu in the cells remains. What is known is, as discussed in detail already, that depending on the level of irradiance, the pH is fluctuating and the same is true for the level of oxygen saturation (*n.b.*: the oxygen saturation and pH were not measured inside *Prochloron* cells, but in close proximity to it).[9] As a consequence of this oscillation during day/night time, the oxidative environment might be correlated to the level of oxygen in the cells, but so far there is no proof for this hypothesis. If this was the case, one would expect an alkaline environment (pH 11) as well as dioxygen super saturation upon solar irradiation[9] and consequently copper cations to be present as Cu^{II}. In the darkness, on the other hand, an interior milieu of pH 7.0 is expected together with an anoxic environment,[9] which would favour Cu^{I}. So far, the coordination chemistry of Cu^{I} to patellamides was not studied in detail. Research in this field would certainly improve the understanding of relative stabilities of the putative copper(I) as compared to the copper(II) complexes. This leaves to summarise, that an approximate internal concentration of 40 µM for copper(II) and 60 µM for zinc(II) is expected in *Prochloron* and that copper is possibly divalent during exposure to sunlight and monovalent during darkness.

After evaluating the metal ion concentration, it is important to get an understanding about potential chelators in addition to the patellamides, their concentrations and binding affinities for Cu^{I}/Cu^{II} and Zn^{II} in the cells. Again, no data for *Prochloron* or similar cyanobacteria (prochlorophyta) is available (but this is the focus of ongoing research carried out by BEHRENDT and KÜHL). RABINOWITZ *et al*.[188] published absolute metabolite concentrations for *E. coli* and thus could show that amino acids like glutamate, glutamine, aspartate, valine and alanine, to mention a few, are present in the millimolar scale.[188] Apart from amino acids, other metabolites like ATP, GTP and citrate are also present in similar concentrations.[188] AKGÜL *et al.* presented a study on the amino acid composition of the dried cyanobacteria *Nostoc spongiaeforme* and *Rivularia bullata*. However, for the sample preparation, all peptides in the cell were hydrolysed first, thus the respective amount of amino acids reported does not correspond to the concentration of amino acids in solution. If one would nevertheless use these values and expects the native cyanobacteria to have an approximate water content of 70%,[189] cytosol concentrations of the amino acids glycine, threonine and leucine of 37.9 mM, 25.5 mM and 28.8 mM had to be anticipated (and this resembles the composition of all proteins and metabolites in cyanobacteria). If that concentration was the metabolite concentration of amino acids in cytosol, it

would be about ten times as much as reported for *E. coli*. The binding constants of amino acid copper(II) complexes of the composition 1:1 are in the range of log*K*=7-9 and for the composition 2:1 one expects logβ values between 12 and 16.[190] These stability constants are significantly higher than the ones known for patellamide copper(II) complexes, that are typically in the range between logK_1K_2=4-6, depending on the patellamide backbone.[67] Even despite the exact knowledge of the amino acid concentration in cyanobacteria and *Prochloron* in particular, one can estimate from the stability constants that the formation of copper(II) amino acid complexes should be preferred over the formation of patellamide complexes. But, as mentioned earlier, the stability constants greatly depend on the pH and the oxidation state of the copper cation. In addition, so far no experiments were carried out to elucidate whether or not the copper(II) patellamide complexes might be integrated in a protein as a prosthetic group. That would not be unexpected, since in nature all metal centres in enzymes are embedded in a larger protein.[2,191-193] If that was the case, the stability constants measured previously for patellamides would be challenged.[67] Thus, on the basis of what is known about prokaryotes and cyanobacteria, one would expect that the patellamides are most likely bound to a protein pocket exhibiting higher copper(II) stability constants than what was measured for the 'free' octapeptides. In order to support this hypothesis, native PAGE experiments with a cell lysate of *Prochloron* and added patellamide and a fluorescent tag were performed. Native PAGE was chosen, as the denaturing of proteins should be excluded in order to keep potential patellamide-protein interactions intact (see Experimental Section E). Only two bands were observed, none of which was fluorescent. Hence, as these experiments were not conclusive, they should be repeated/improved in order to evaluate the hypothesis raised with experimental proof.

5.1 Synthesis of H_4pat-RG

The synthesis of the cyclic octapeptide H_4pat-RG was accomplished analogously to the modular approach used for the synthesis of other cyclic peptides prepared for earlier studies (see Scheme 5.1 for the synthesis of the patellamide-dye conjugate). The initial steps towards the formation of the monomer building blocks **5** and **6** were accomplished on the basis of a published approach.[62]

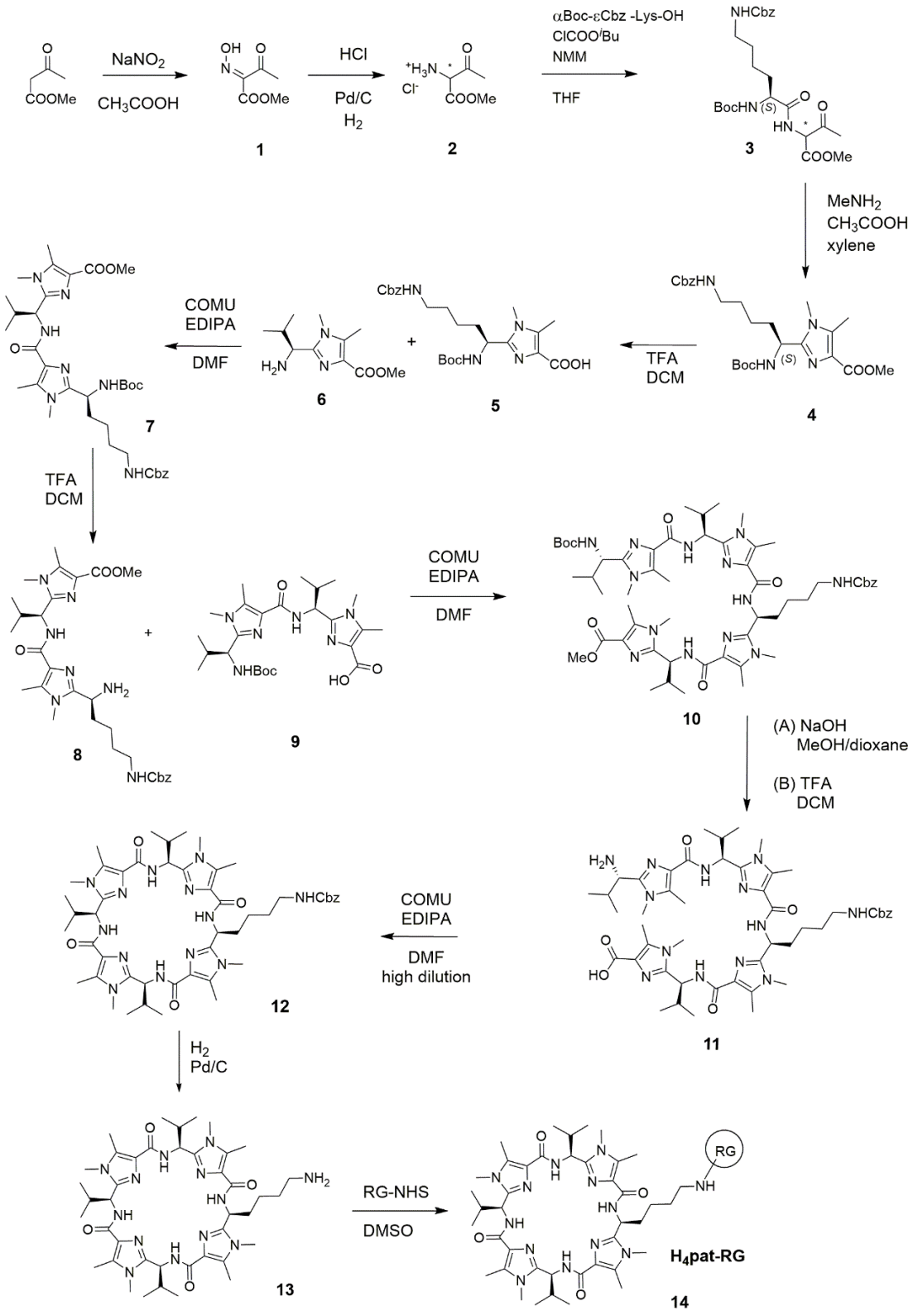

Scheme 5.1. Synthesis of H_4pat-RG (**14**), the syntheses of **6** and **9** are omitted for clarity and were accomplished as described in [62]. RG: Atto550 or Proxyl.

For that the α-Boc ε-Cbz protected lysine was activated by treatment with *iso*-butyl-chloroformate and coupled to the keto ester **2** to give the resulting amidoketone **3**, which was reacted with methylamine in the presence of acetic acid under azeotropic removal of water from refluxing xylene giving building block **4**. The deprotection of the Boc protecting group was accomplished by addition of TFA in DCM, which afforded **5**. Analogously to the strategy reported for **4**, the respective valine-imidazole monomer was produced, which gave compound **6** after hydrolysis with NaOH in dioxane/MeOH. The coupling of **5** and **6** was accomplished through COMU activation and addition of EDIPA in dry DMF and yielded the dimer **7** in 55 % yield. **7** was subsequently deprotected at the N-terminus, and coupled with **9**, which was obtained analogously to the described route to **7**, yielding the linear tetramer **10** in 48 % yield. Deprotection of the N- as well as the C-terminus produced **11**, which was then cyclised in a high-dilution reaction to give 27 % of the Cbz-protected cyclic peptide **12**. This was followed by deprotection of the ε-N-terminus upon treatment with H_2 and 5 % palladium on carbon, producing **13** in 84% yield, which could subsequently be reacted with the NHS activated ester of the respective reporter group in DMSO. Two different reporter groups were chosen: (I) Atto550, a rhodamine-based fluorescent dye (Figure 5.1), which alters the photophysical properties and (II) Proxyl, which alters the EPR signal upon copper(II) binding (Figure 5.2).

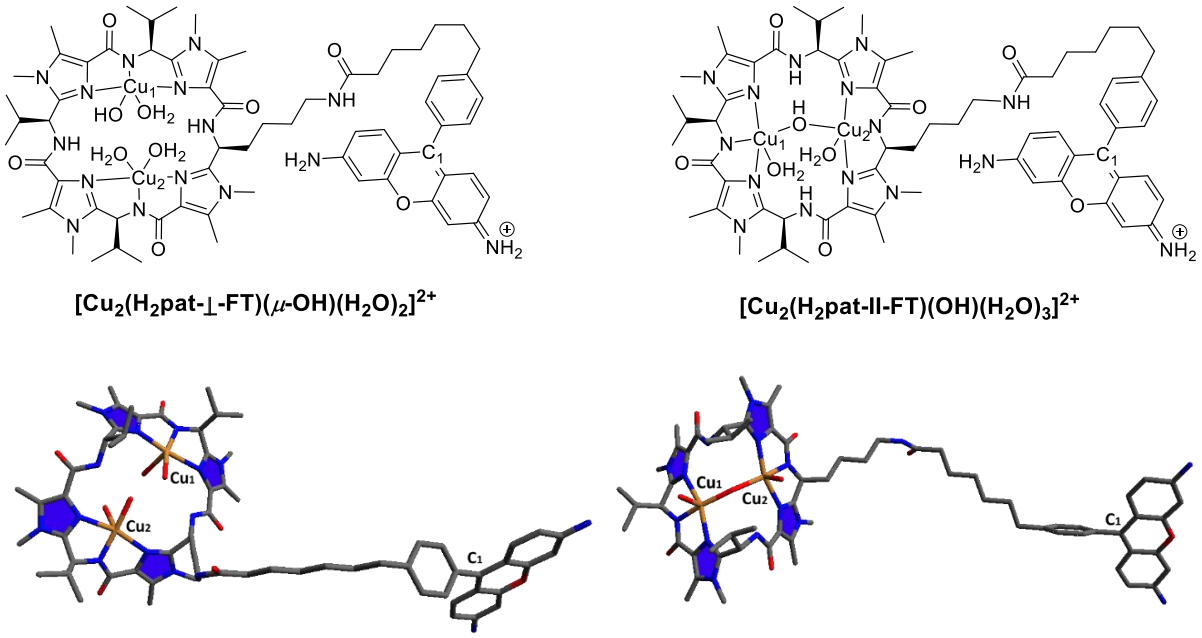

Figure 5.1. Models of dinuclear [$Cu_2(H_2pat\text{-}FT)$] complexes; left: Cu^{II} coordinated by three water molecules and a hydroxido ligand, C_4-chain perpendicular to the $Cu^{II}\cdots Cu^{II}$ vector (⊥); right: Cu^{II} coordinated by two water molecules and a bridging hydroxido coligand, C_4-chain parallel to the $Cu^{II}\cdots Cu^{II}$ vector (‖), FT=fluorescent tag (orange: Cu, grey: C, blue: N, red: O, hydrogen atoms are omitted for clarity).

The adduct H_4pat-Atto550 was purified by HPLC and characterised by UHPLC-MS as well as by UV-vis spectroscopy, whereas the H_4pat-Proxyl ligand was purified by repetitive washing with ice brine solution and characterised by elemental analysis as well as UHPLC-MS.

The choice of the appropriate fluorescent dye was crucial, since *Prochloron* is one of the few known examples of prokaryotic oxygenic autotrophs containing chlorophyll *b* in addition to chlorophyll *a*.[6] This means that the range for observation, often referred to as 'green gap' between 520 nm and 600 nm, is narrow.[194] Therefore, as a photophysically sensitive group Atto550 was chosen with an excitation maximum of λ_{exc}=554 nm and an emission maximum of λ_{em}=574 nm.

Proxyl on the other hand was chosen as a spin-label due to its easy synthetic availability and its small size, as compared to *e.g.* Trityl.[195] It was shown to have a lifetime of several minutes *in vivo* (in rats)[196] and since all EPR experiments envisaged are carried out in frozen solution, reduction inside the cells should be circumvented to an extent that allows use of Proxyl as a reporter *in vivo*.

From structure optimisation of a conjugate with a rhodamine derivative (the structure of Atto550 is not yet available) it became clear that the distance between the Cu^{II} centres and the fluorescent tag (C_1, Figure 5.1) is in the range between 13.5–25.4 Å (Cu_1 and Cu_2), depending on where the side chain is located relative to the Cu^{II} binding sites, *i.e.* parallel or perpendicular to the $Cu^{II}\cdots Cu^{II}$ vector. For the perpendicular arrangement of the side chain to the $Cu^{II}\cdots Cu^{II}$ vector distances between 13.5–21.7 Å are expected, whereas the C_1-Cu_n distance is approx. 18.5–25.4 Å for the parallel orientation. The distances between the Cu^{II} ions and the O_1 of the Proxyl group in H_4pat-Proxyl are expected to be in the range of 11.2 to 17.6 Å (see Figure 5.2).

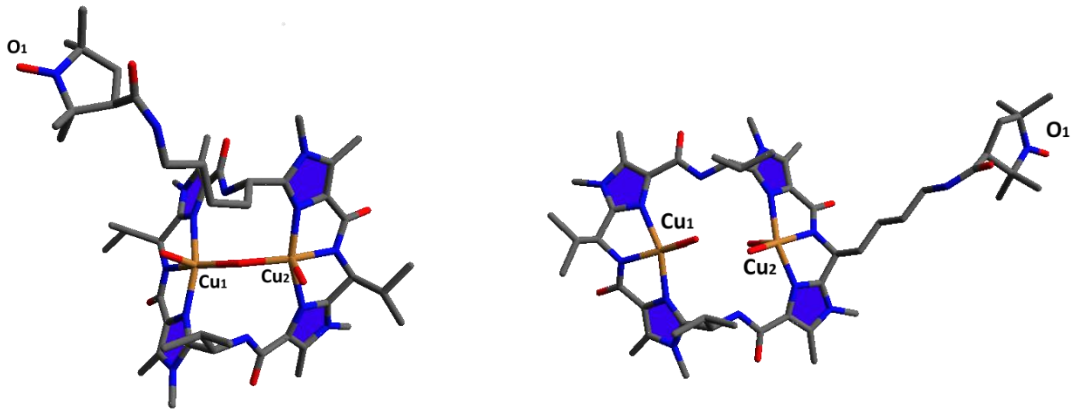

Figure 5.2. Models of dinuclear [Cu_2(H_2pat-Proxyl)] complexes; left: Cu^{II} coordinated by two water molecules and a bridging hydroxido coligand, C_4-chain perpendicular to the $Cu^{II}\cdots Cu^{II}$ vector (⊥); right: Cu^{II} coordinated by three water molecules and a hydroxido ligand, C_4-chain parallel to the $Cu^{II}\cdots Cu^{II}$ vector (∥) (orange: Cu, grey: C, blue: N, red: O, hydrogen atoms are omitted for clarity).

5.2 Fluorescence spectroscopy

Due to its high sensitivity, fluorescence spectroscopy is widely applied for imaging and sensing, especially in biological systems. It exploits the emission of light induced by the decay of an electronically excited singlet state. The term singlet means, that the electron in the excited orbital is oriented antiparallel to the second electron in the ground state orbital and the transition between the excited state S_1 and the ground state S_0 is consequently spin-allowed and happens rapidly. Fluorescence emission rates are typically in the range of 10^8-10^9 s^{-1}. The lifetime τ is thus 10^{-8}-10^{-9} s and describes the average time between excitation of an electron and the return to the ground state. The concise form of the absorption and emission spectra, as well as their position in the electromagnetic spectrum gives insight on the respective vibrational as well as rotational states of the investigated substance. The typical excitation and emission processes involving electronically excited species are visualised in a JABLONSKI diagram, as shown in Scheme 5.2.[197]

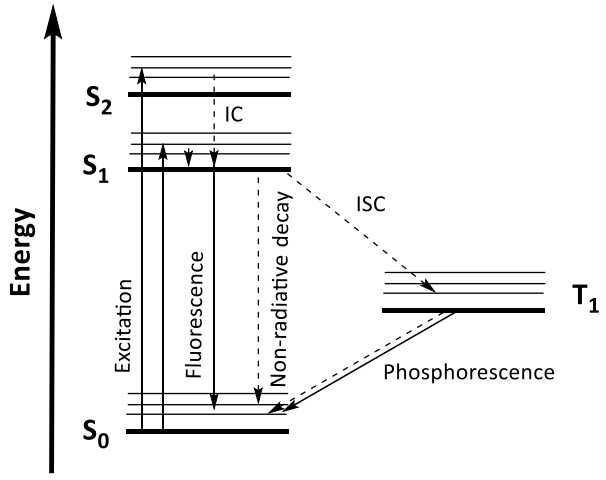

Scheme 5.2. JABLONSKI diagram: depicting the excitation from the S_0 singlet ground state to the S_1, S_2, excited singlet states and relaxation *via* Internal Conversion (IC), fluorescence, non-radiative decay and Intersystem Crossing (ISC) to T_1-excited triplet state, that can relax to S_0 *via* phosphorescence (dashed lines characterise non-radiative transitions).

Absorption transitions occur in 10^{-15} s, which is too short for a significant effect on the position of the nuclei (the BORN-OPPENHEIMER approximation). These excitations are described as vertical transitions and summarised as the FRANCK-CONDON principle. Upon excitation of S_0 due to the absorption of a photon with the respective energy, the excited state reached relaxes rapidly to the lowest

electronically excited singlet state S_1. This is believed to be the case since all excited singlet states are energetically very similar and not resolved in solution due to broadening induced by rotational terms. The relaxation process is described as Internal Conversion (IC) and typically happens within 10^{-12} s by the distribution of excess energy to rotations and vibrations in the molecule. Once the excited singlet state with the lowest vibrational quantum number is reached, light can be emitted and the singlet ground state S_0 is regenerated.[197]

An alternative relaxation path starting from S_1 is called Intersystem Crossing (ISC) and leads to a triplet T_1 state. This transition is spin-forbidden and so is the relaxation from T_1 to S_0, which is called phosphorescence. This leads to significantly smaller transition rates 10^3-1 s^{-1} and longer lifetimes (10 ms to 1 s) as compared to fluorescence.

Since emission always occurs from S_1 or T_1, the emitted energy is smaller than the absorbed, as S_1 and T_1 are populated only after non-radiative conversion, which means a loss of energy. This leads the emitted wavelengths to be red-shifted, which is called STOKES shift that can be observed for example for the fluorescent dye Atto-550, of which the absorption and emission spectra are shown in Figure 5.3. Fluorescent dyes are designed such that they have delocalised electrons in an extended π-system which have strong absorption and emission bands in the UV-vis region.

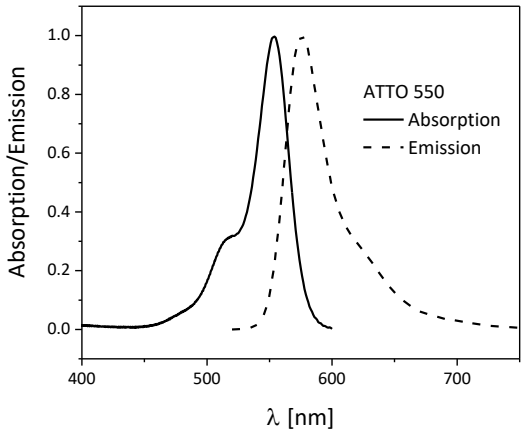

Figure 5.3. Absorption and emission spectrum of Atto-550, λ_{exc}=554 nm, λ_{em}=574 nm.

Since emission for fluorescence is solely observed from S_1 to S_0, the emission spectrum is independent on the excitation wavelength (KASHA's rule).[197] Together with the FRANCK CONDON principle of vertical transitions this leads the absorption and emission spectra to be mirror images (see Figure 5.3), as the absorption spectrum consists of all rotational bands of S_0 and the emission spectrum is composed of the respective rotational bands of the S_1 state.

Fluorescence lifetime and quantum yield are common parameters for the description of fluorophores and can be related as shown in equation 5.1:

$$Q = \frac{\gamma}{\gamma + k_{nr}} \tag{5.1}$$

Here, Q is the quantum yield, γ is the emissive rate of the fluorophore and k_{nr} signifies the rate of all non-radiative decays to S_0 (see Figure 5.4). The quantum yield is typically below 1 and is strongly dependent on the temperature, the polarity of the solvent, the pH and the capacity for hydrogen-bond formation.[197]

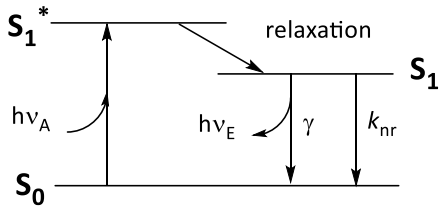

Figure 5.4. Simplified JABLONSKI diagram emphasising on transition rates.

The transition probability also defines the fluorescence lifetime τ:

$$\tau = \frac{1}{\gamma + k_{nr}} \tag{5.2}$$

In the absence of non-radiative decay this leads to the intrinsic life time τ_0:

$$\tau_0 = \frac{1}{\gamma} \tag{5.3}$$

By dividing τ by τ_0, the quantum yield is obtained. Non-radiative decays that lower the emission rate are summarised as fluorescence quenching. One of the possible mechanisms would for example be collisional quenching, where the energy of the excited fluorophore is transmitted to the quenching partner (*n.b.* that Q refers to the quenching partner in the following discussion and not to the quantum yield). This diffusion-controlled quenching mechanism is called dynamic quenching:[123]

$$F^* + Q \rightarrow F + Q^* \tag{5.4}$$

The collision between an excited fluorophore F* and Q leads to an energy transfer, providing F in S_0 and Q*, which releases its energy to its surrounding. This happens *via* a spin flip, since the resulting T_1 states exhibit long lifetimes and are additionally quenched by Q in solution. Typical examples for Q are molecular dioxygen, acrylamide or I^- and Br^-. Since the phosphorescence transition is spin-forbidden and consequently comparably slow, in liquids the transition $T_1 \rightarrow S_0$ happens usually non-radiatively. The formation of a radical ion pair *via* electron transfer, which could recombine after non-radiative decay is another possible relaxation mechanism, and is equally likely as a charge transfer for halogen ions. All these mechanisms affect the excited states of the fluorophore. Static quenching on the other side alters the ground state of the fluorophore, for example by formation of a complex.

$$F + Q \underset{}{\overset{k}{\rightleftharpoons}} FQ \tag{5.5}$$

$$[F] = \frac{[FQ]}{k[Q]} \tag{5.6}$$

$$[F]_0 = [F] + [FQ] = [FQ]\left(1 + \frac{1}{k[Q]}\right) \tag{5.7}$$

For proportionality of the concentration to the measured intensity, the following expression can be deduced as the STERN-VOLMER equation for static quenching:

$$\frac{F_0}{F} = 1 + k[Q] \tag{5.8}$$

The complex formed, FQ, is not fluorescent and consequently, the formation of the complex has no influence on the fluorescence life time, whereas dynamic quenching alters the lifetime of the fluorophore. In addition, static quenching is usually lower at higher temperatures, since the formation of the FQ complexes is temperature dependent and they are less stable at higher temperatures. Dynamic quenching on the contrary, is increased at higher temperatures, since the diffusion velocity is higher and thus more diffusion controlled collisions can happen. Often however, two or more regimes of quenching are observed, resulting in a combined quenching. This leads to several overlaying slopes in STERN-VOLMER plots, *i.e.* F_0/F plotted to the concentration of the quencher [Q].[197]

5.2.1 Cu^{II} binding behaviour of H_4pat-Atto550 *in vitro*

The sensitivity of the fluorophore-labelled patellamide towards Cu^{II} in aqueous solution of H_4pat-Atto550 (1.8 µM in 100 mM TRIS buffer, pH 8.2 as observed for sea water[198], T=298 K) was titrated with Cu^{II} (0.125–10 eq., using a $CuSO_4$ solution in buffer). At each titration step, emission spectra were recorded. Upon addition of Cu^{II} a strong fluorescence quenching was observed (see Figure 5.5). The control experiments, *i.e.* titrations of H_4pat-Atto550 with buffer and the titration of Atto-NHS with Cu^{II} lead to significantly smaller fluorescence intensity decreases (Figure 5.5). The quenching behaviour of the fluorescence-dye-conjugate is biphasic with Cu^{II}, as the quenching starts linearly and is followed by an additional quenching mechanism, observable at excess Cu^{II}. Static quenching should be observed due to Cu^{II} complexation of the patellamide ligand in the starting phase. Fluorescence lifetime measurements confirm this assumption (see Figure 5.6), as no changes are observed. The second phase of quenching might be due to a saturation effect but could also be caused by the formation of a dinuclear species. However, binding of Cu^{II} to patellamide derivatives has been found to show cooperativity in methanolic solutions, *i.e.* it is not likely that formation of dinuclear complexes only occurs after addition of 10 eq. of Cu^{II}.[74] In first approximation the model for static quenching is applied to the initial linear slope in the STERN-VOLMER plot to the equivalent point (Figure 5.5).[199] In this case, I_f is the fluorescence intensity measured at the metal ion concentration of each titration step. A linear fit yields the STERN-VOLMER constant K_S of the respective Cu^{II} patellamide complex.

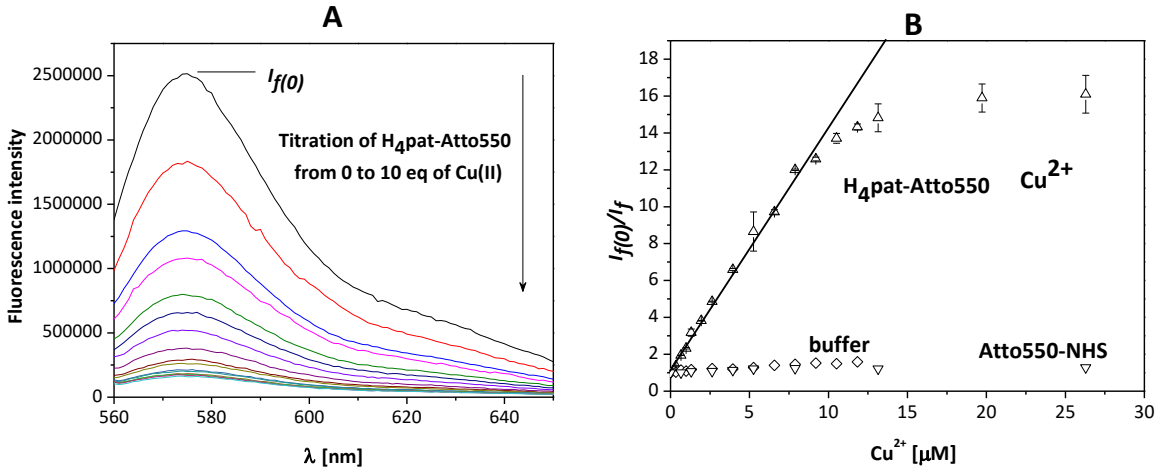

Figure 5.5. Titration of the fluorescing dye-conjugate with Cu^{II}, measured by fluorescence spectroscopy (aqueous solution of H_4pat- Atto550 in 100 mM TRIS buffer, pH 8.2, T=293 K). **A** Full emission spectrum and **B** STERN-VOLMER plot (H_4pat-Atto550 + Cu^{II}, up triangle) compared to titrations of the conjugate H_4pat-Atto550 + buffer (diamond) and Atto550-NHS + Cu^{II} (down triangle).

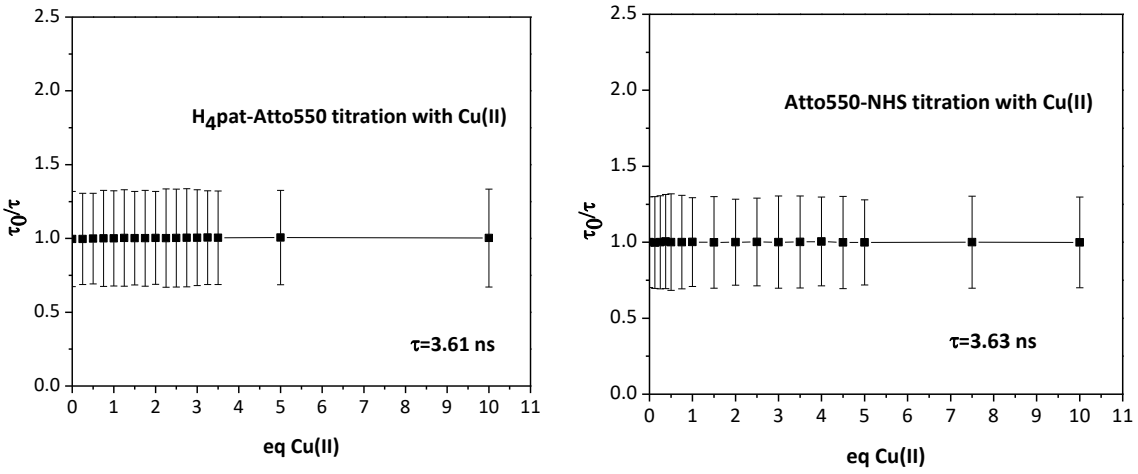

Figure 5.6. Fluorescence lifetime measurements: 100 mM TRIS buffer, pH 8.2, T=298 K. Concentrations: [H_4pat-Atto550]=1.8 µM [Atto550-NHS]=2.3 µM.

The fit estimates K_s to be of the order of 1.35(2)x10^6 M^{-1}. As the stability constant for the dinuclear Cu^{II} complexes of the model patellamides H_4pat^1 1.7x10^6 M^{-1} and H_4pat^2 are 4.03x10^4 M^{-1} respectively, the STERN-VOLMER constant K_s is within the expectations. Again, one must note, that the ITC stability constants were determined in methanolic solutions as opposed to buffered solutions used for the titration of the fluorescent tagged patellamide with Cu^{II}. Moreover, the model used for the determination of the STERN-VOLMER constant, clearly does not describe the whole curve observed and further investigations, *e.g*. by ITC, should be carried out to validate the binding affinity. One should also note that nothing is known about the charge of the fluorescent label, which, if it was negative it might contribute to the stability of the complex.

5.2.2 Uptake of H_4pat-Atto550 by *Prochloron* and its photophysical analysis

For *in vivo* fluorescence imaging two different techniques were applied: single cell confocal microscopy and flow cytometry (FCM). Both techniques allow the determination of optical parameters of single complete cells instead of giving average values for the whole population.

A simplified schematic light path for a confocal microscope is shown in Scheme 5.3. The technique was originally developed by MINSKY,[200] who wanted to circumvent the constraints of wide-field fluorescence microscopes, which excite the complete sample simultaneously. The resolution of the

wide-field approaches is hampered by the fact that this technique gives information of the whole sample at once, leading to a major contribution from the background that is not in focus.[201]

In confocal microscopy a collimated laser beam is coupled into the objective and leaves the objective focussed. At the focal point, the laser beam has a diffraction-limited dimension with an approximate diameter of 300 nm (the focal volume). This means that only a small area of the sample is illuminated and hence, the fluorescence measured corresponds mainly to the focal point due to the proportionality of the excitation to the observable intensity. Fluorescence light is detected through a pinhole to reduce the out-of-focus signal, which however also contributes to a loss of signal. To meet that obstacle, an avalanche photodiode (APD) is used. As a consequence of the setup, the confocal microscope exhibits a better lateral as well as axial resolution compared with wide-field techniques.[202]

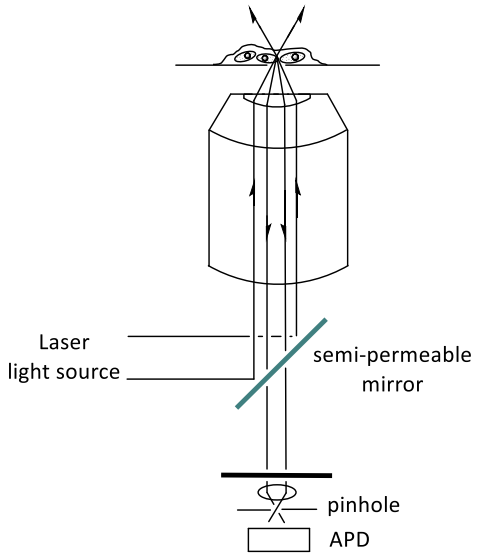

Scheme 5.3. Light path in a confocal microscope. Adapted from reference [202].

Another detection method for the fluorescence of a population is flow cytometry. This technique quantifies various optical parameters of complete cells simultaneously with a high throughput rate.[203] A simplified schematic setup of a flow cytometer is shown in Scheme 5.4. Here, a peristaltic pump generates a fluidic flow that is hydrodynamically focussed using a sheath-air flow design. The resulting isolated particles in a fluid stream are characterised by a beam of light as they flow through the flow cell (see Scheme 5.3). As samples all cells or particles with the size in the range between 0.2 and 150 µm are suitable, with the condition that cells must be disaggregated in order to analyse just one particle/cell at a given measuring interval. The characteristic measured variables are the forward

scattered light (FSC) and the side scattered light (SSC). Mostly diffracted light is measured with FSC and is proportional to the particle size. SSC on the other hand is proportional to internal complexity or cell granularity and depicts the primarily refracted and reflected light (see Scheme 5.4). In addition, the fluorescence at different wavelengths is observed (typically four channels between 400 nm and 700 nm). The correlation of FSC and SSC provides information on subpopulations in the sample, which can be analysed separately.

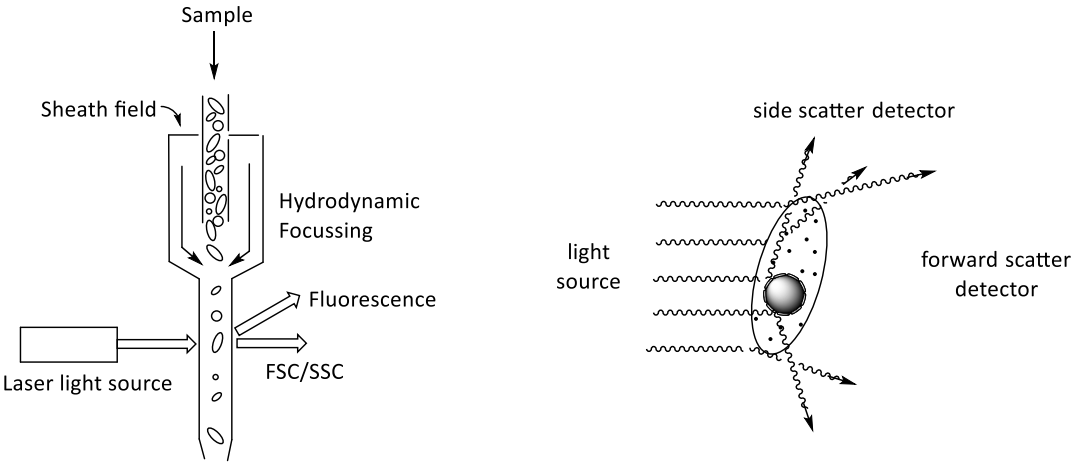

Scheme 5.4. Left: schematic representation of the fluidics in a flow cytometer. Right: representation of side scattered and forward scattered light from diffraction at a cell. Adapted from reference [204].

In order to find the best method to stimulate the uptake of H_4pat-Atto550 by *Prochloron*, different protocols were investigated.

As not many reports have been published on the introduction of peptides into prokaryotes, standard techniques for the stimulation of biomolecule uptake, as established for *Escherichia Coli*, were applied,[205] *i.e.* heat shock treatment at 42°C for up to 40 s and incubation at room temperature for up to 30 min. After the treatment the cells were washed twice and subsequently pulsed amplitude-modulated photosynthesis measurements (PAM) were used to ascertain that the *Prochloron* cells were still photosynthetically active.[206,207] The amount of patellamide taken up by the cells was determined by flow cytometry; here λ_{exc}=535 nm (excitation of H_4pat-Atto550) and λ_{exc}=640 nm (excitation of chlorophyll *b*) were used as excitation wavelengths (Figure 5.7 C and D). It is apparent that the heat shock treatment (40 s at 42°C) leads to the same ratio of FL575/FL675 (*i.e*. the ratio of fluorescence by H_4pat-Atto550 and chlorophyll *b*, respectively) of about 0.016, as observed for incubation for 30 min at room temperature. This indicates that the transport of patellamides into

Prochloron occurs by a passive mechanism. The setup of the experiment leads, after dilution with cyanobacteria and buffer, to the final concentration of 5.8×10^{-8} M for H_4pat-Atto550 in the sample. With the expected passive mechanism, this concentration consequently is the maximum expected concentration inside the cells; however, this cannot be validated with an independent technique. If the mechanism is not passive, but the cell instead uses for example vesicles or the transport is accomplished *via* active transporters in the membrane, which are potentially gradient-driven, the concentration of H_4pat-Atto550 in the cell might be higher or lower than the exterior concentration. Since the emission of chlorophyll *b* is very intense, it was also verified that the observed fluorescence intensity does not solely originate from the fluorescence of chlorophyll *b*. The corresponding experimental data from fluorescence spectroscopy and confocal microscopy are shown in Figure 5.7 A and B.

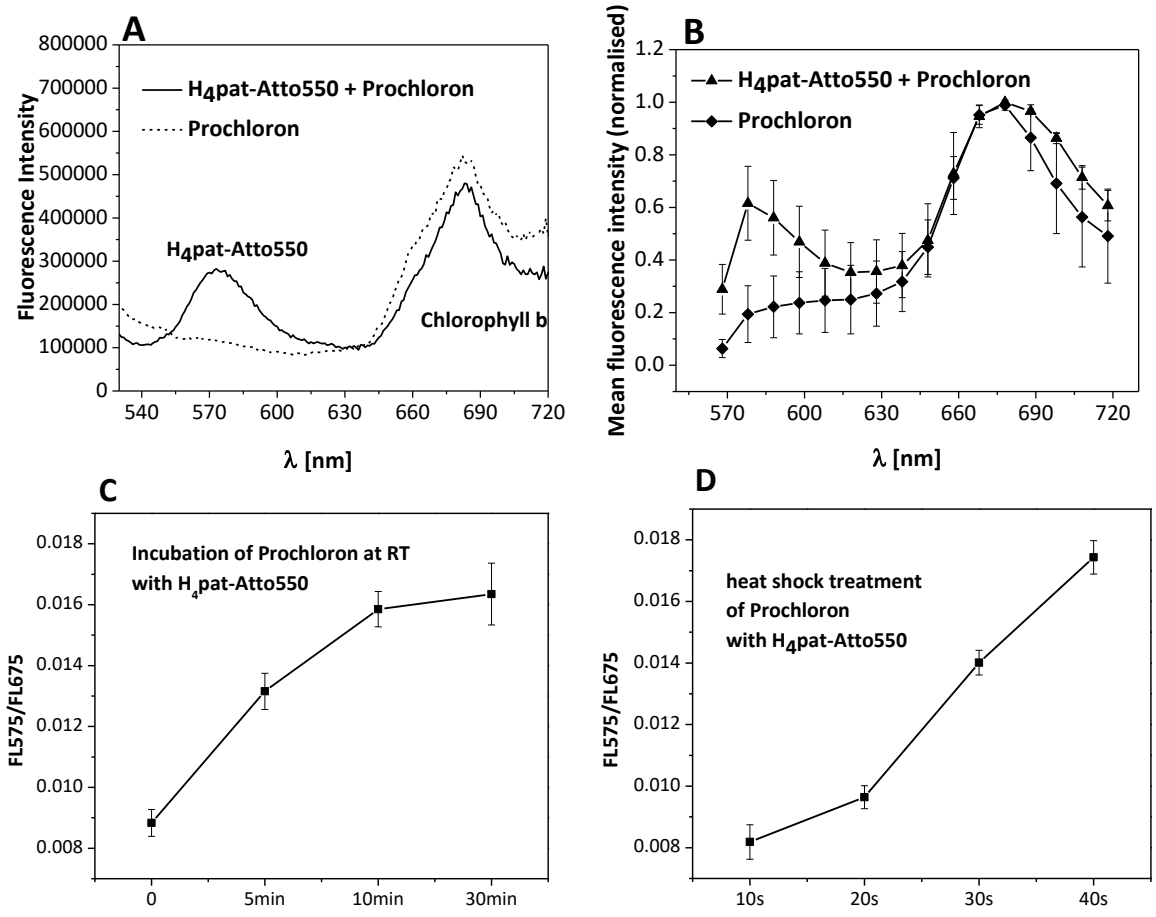

Figure 5.7. A: Fluorescence intensity of a *Prochloron* sample treated with H_4pat-Atto550 for 40 s at 42°C (λ_{exc}=500 nm); **B:** Fluorescence intensity from confocal microscopy; *Prochloron* treated with H_4pat-Atto550 for 40 s at 42°C (for raw data see Experimental Section F3); **C** and **D:** FL575/FL675, *i.e.* ratio of the fluorescence intensity of H_4pat-Atto550 (FL575) *vs*. to the fluorescence intensity from chlorophyll *b* (FL675).

5.2.3 Treatment with Cu^{II}

In order to establish a valid protocol to investigate the Cu^{II} binding behaviour of the fluorescent dye-patellamide conjugate by means of flow cytometry and confocal microscopy, *Synechococcus leopolienses* (*S.L.*) and *Prochlorothrix hollandica* (*P.H.*) were studied. Both cyanobacteria are readily available from a cyanobacteria database, whereas *Prochloron* can only be handled for about 1-2 weeks *in hospite* in a fresh water aquarium after sampling from tropical waters. *S.L.* was chosen as a model, since it is a cyanobacterium that is easy to handle. Consequently, it was used primarily to learn how to treat cyanobacteria in general. *P.H.* on the other hand is the taxonomically closest cyanobacterium to *Prochloron*, available from a database and was therefore used in a second step after establishing working routines with *Synechococcus leopoliensis*. Thus, all experiments with *S.L.* were carried out solely to establish a protocol and are not discussed in the following (see Appendix I). H_4pat-Atto550 was added to the cyanobacteria, which were then heat shocked for 40 s at 42°C and subsequently chilled on ice for 1 min (a). Alternatively, samples (b) and (c) were incubated with H_4pat-Atto550 and 5 eq. of a Cu^{II} salt. After rinsing the cells, sample (c) was additionally treated with an excess of 10 eq. of cyclam (1,4,8,11-tetraazacyclotetradecane) relative to H_4pat-Atto550, applied as a strong competitor for Cu^{II} coordination to reinstall the fluorescence upon removing Cu^{II} from H_4pat-Atto550. All samples were analysed by FCM and the mean ratio (and its SEM) of fluorescence observed at 575 nm, compared to fluorescence at 675 nm, was plotted (Figure 5.8 A).

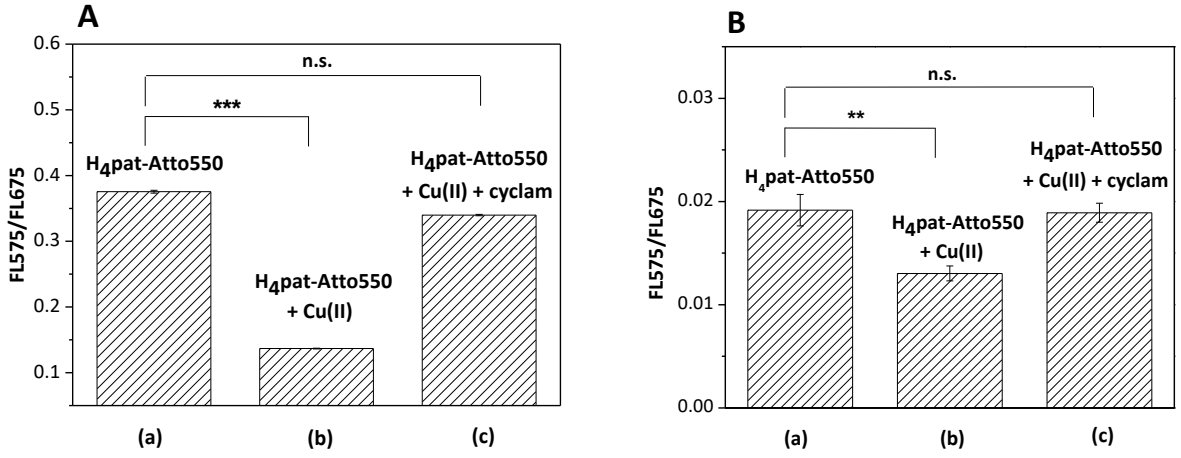

Figure 5.8. Mean and SEM of FL575/FL675 for **A** *Prochlorothrix hollandica* (n=12,000) and **B** *Prochloron* (n=4,000) treated **(a)** with H_4pat-Atto550 **(b)** with H_4pat-Atto550 and Cu^{II} and **(c)** with H_4pat-Atto550 and Cu^{II} and subsequently cyclam (10 eq.). [$p \geq 0.05$ – not significant (n.s.), $p \leq 0.05$ – Significant (*), $p \leq 0.01$ – highly significant (**), $p \leq 0.001$ extremely significant (***)]. n: number of cells per population, p: probability.

For *Prochlorothrix hollandica* samples (a) and (c) are not significantly different, whereas sample (b) shows a very large ($p<0.001$) difference compared to (a) and (c). This lends strong support for the hypothesis that Cu^{II} is binding to H_4pat-Atto550 in *Prochlorothrix hollandica*. In addition, the binding constant of the Cu^{II} patellamide complex seems to be significantly smaller than that of the corresponding Cu^{II}-cyclam complex, which is in accordance with expectations, as the stability constant for $[Cu^{II}(cyclam)]^{2+}$ is log*K*=14.7 (pH 7),[208,209] orders of magnitude higher than what was observed from photophysical measurements for the H_4pat-Atto550 ligand studied here (*vide supra*). Consequently, the established protocol was also applied to *Prochloron* cells. At least ten measurements at random positions within three Lab-Tek chambers were conducted per condition and the experiment was carried out twice. The results are summarised in Figure 5.8 B. It emerges that samples (a) and (c) are not significantly different, but sample (b) is significantly different from (a) and (c), exactly as observed for *Prochlorothrix hollandica*. This implies that the Cu^{II}-patellamide complex is stable in the *Prochloron* cells and, if it is a dinuclear complex, could consequently act as a phosphatase-, glycosidase-, β-lactamase- and carbonic anhydrase-like catalyst, as observed *in vitro*. It should be noted here that in spite of *Prochlorothrix hollandica* being the taxonomically closest cyanobacterium it does contain significantly less chlorophyll *b*, compared to *Prochloron* which leads to larger values for the observed ratios FL575/FL675 in the range of 0.2-0.4 compared to the values observed for *Prochloron* (0.013-0.020).

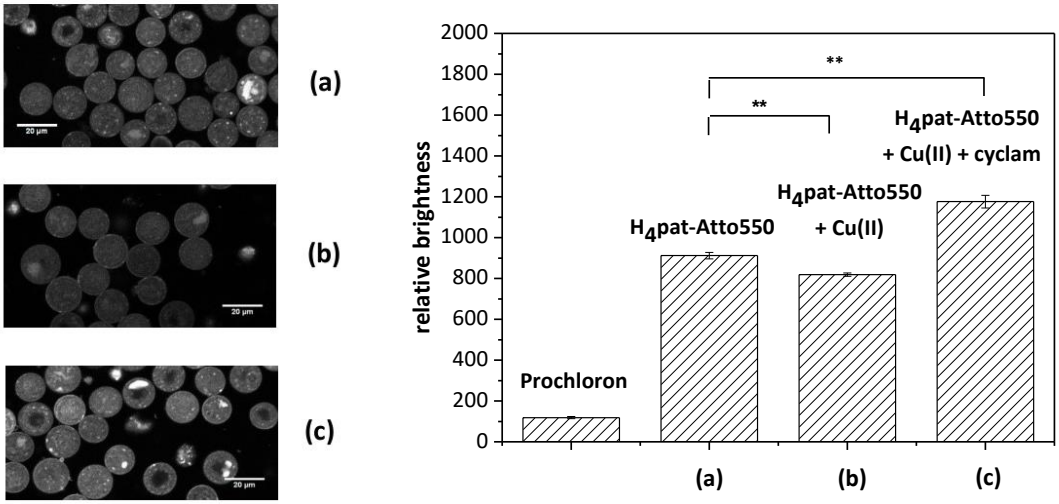

Figure 5.9. Left: confocal microscopy pictures of *Prochloron* cells and right: Mean and SEM of FL574 for *Prochloron* (n=600) treated **(a)** with H_4pat-Atto550, **(b)** with H_4pat-Atto550 and Cu^{II}, and **(c)** with H_4pat-Atto550 and Cu^{II} and subsequently with cyclam.

Samples prepared identically as described for FCM were also investigated concerning their relative brightness at 574 nm by confocal microscopy, and the results are depicted in Figure 5.9 (preliminary experiments with *S.L.* and *P.H* are shown in Appendix I.) In order to validate that the observed brightness originates solely from the fluorescent-dye-patellamide conjugate, the relative brightness of *Prochloron* at λ_{em}=574 nm was plotted as the first bar in Figure 5.9. Sample (b) shows a significantly lower brightness compared to samples (a) and (c) but at the same time sample (c) is significantly brighter than sample (a). This implies that Cu^{II} is binding to the patellamide-fluorescent-dye conjugate. Upon addition of an excess of cyclam, the added Cu^{II} as well as the endogenous Cu^{II} ions are removed by cyclam (the copper(II) concentration in *L. patella* is reported to be enriched 10^4 compared to the surrounding sea water).[71] Although FCM does not show a significant difference for samples (a) and (c) of *Prochloron* (Figure 5.8), it is worth noting that the mean of the ratio FL575/675 of (c) is higher than the mean observed for (a) although the difference is not significant. The sample size for FCM is ~12,000 per population, whereas the populations investigated with confocal microscopy consist of ~600 *Prochloron* cells. Importantly, unlike the FCM data (normalised to background chlorophyll), the data from confocal microscopy are not normalised.

To exclude the occurrence of an 'inner filter effect', additional absorption measurements of a sample of *P.H*. lysate treated identically (same population density and copper(II) concentration) to the samples prepared for FCM and confocal microscopy (see Experimental Section G) were carried out (see Figure5.10).*

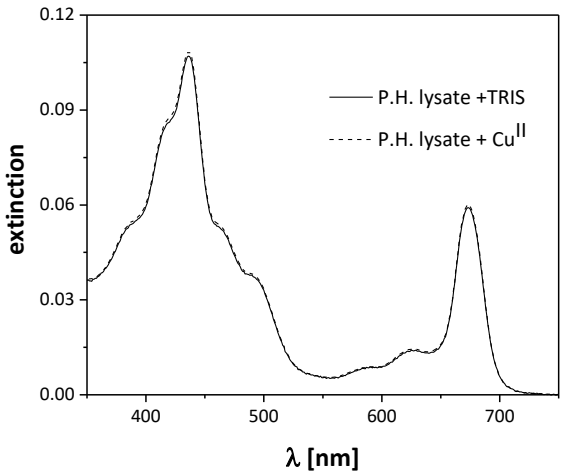

Figure 5.10. Absorption spectrum of a *Prochlorothrix hollandica* (*P.H.*) lysate solution treated with Cu^{II} and a solution of *P.H.* lysate solution treated with the equivalent volume of TRIS buffer. [Cu^{II}]= 2.9×10^{-7} M.

* The absorption experiment shown in Figure 5.10 was carried out by Martin Seefeld.

As a control sample the same volume as used for copper(II) addition was supplemented with TRIS buffer. *P.H.* was used, since no *Prochloron* was available.

The absorption spectra show no difference between the sample treated with Cu^{II} and the control sample. This is interpreted as no significant change in the concentration of Cu^{II} complexes in the cytosol (over background) upon addition of $Cu(SO_4)$ in the concentration used for FCM and confocal microscopy experiments. If this result from the investigation of *P.H.* was transferable to *Prochloron*, for the FCM and confocal microscopy experiments this means that the absorption of copper(II) complexes formed in the cytosol with putative free amino acids/proteins/phosphates and other chelators does not absorb the fluorescence of the fluorescent tag Atto550 significantly over background. Consequently, no 'inner filter effect' is expected. Therefore, the lowered relative brightness of sample (b) compared to (a) and (c) cannot be caused by the absorption of the fluorescence from copper(II) complexes that could potentially form with amino acids or other metabolites. As a result, the collected data indicate that a copper(II) complex is formed with the patellamide H_4pat-Atto550 *in vitro* as well as *in vivo*. However, by means of fluorescence spectroscopy it is impossible to predict whether the copper(II) complex formed is a mononuclear or a dinuclear species.

This finding gives support for the hypothesis raised at the beginning of this Chapter: the patellamides seem to provide higher stability constants in the cells, probably as prosthetic groups in bigger proteins than expected so far,[67] as otherwise no decrease in the fluorescence intensity would be expected.

5.3 EPR investigations

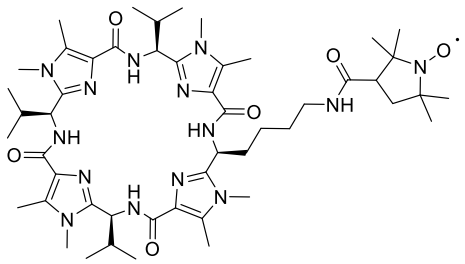

Figure 5.11. Spin-labelled ligand H_4pat-Proxyl discussed in this Chapter.

The spin-labelled ligand H_4pat-Proxyl was investigated concerning its copper(II) binding behaviour. This was accomplished predominantly by means of X-band CW EPR as well as pulsed Q-band EPR and

DEER experiments. For a copper(II) complex of the H_4pat-Proxyl ligand one would expect a coupling between the electron spin of the Cu^{II} ions and the electron of the Proxyl (NO) radical. This should lead to a broadening of both signals arising from the magnetic dipole interaction. The Cu^{II} in the complex moreover is expected to show different g- and A-tensors than those observed for non-coordinated Cu^{II} in solution.[85]

The experiments reported in the previous section and this subsection are all carried out with the ultimate goal to establish whether Cu^{II} is binding to patellamides inside *Prochloron* cells and consequently, were performed in aqueous buffer solution. The experiments were carried out at 125 K (liquid N_2 cooling) or 30 K (He cooling) as a frozen solution, giving a paramagnetic sample diluted in a glassy matrix. In order to prepare a glass from an aqueous solution, 10% glycerol was used. The glassy sample shows a superposition of orientations (also called 'polycrystalline'). Freezing leads the paramagnetic species to be immobile and oriented randomly in the magnetic field. Thus, the anisotropy of the g- and A-tensors can be observed (as opposed to room temperature measurements in which only isotropic g- and A-values are observable due to unconstrained tumbling in solution).

Figure 5.12 shows CW EPR spectra at X band of H_4pat-Proxyl (I), the *in situ* prepared copper(II) complex of H_4pat-Proxyl (II) and Cu^{II} in MeOH with methanolate as the base. On the right, a difference spectrum of I-II is shown as well as a simulated spectrum.

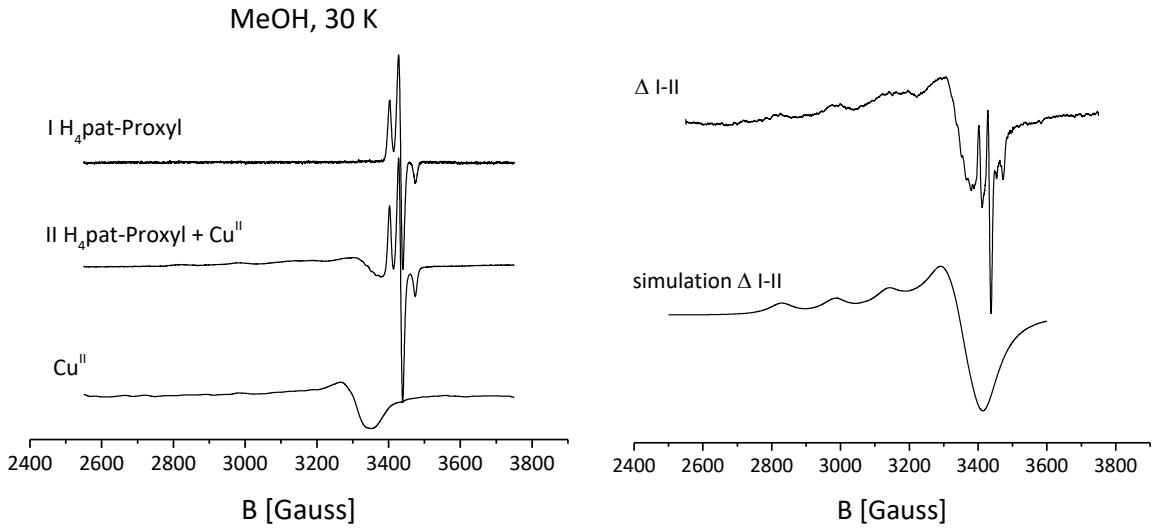

Figure 5.12. Left: experimental EPR spectra of the ligand H_4pat-Proxyl (**I** (9.636287 GHz)), a solution of 1 eq. of H_4pat-Proxyl and 5 eq. of Cu^{II} and 2 eq. of MeO^- in MeOH (**II** (9.636125 GHz)) as well as a measurement of Cu^{II} and 2 eq. of MeO^- in MeOH (9.635768 GHz)(top to bottom). The ligand concentration was chosen to be 500 µM (X-band). Right: difference spectrum of I and II and a simulation of the difference spectrum I-II.

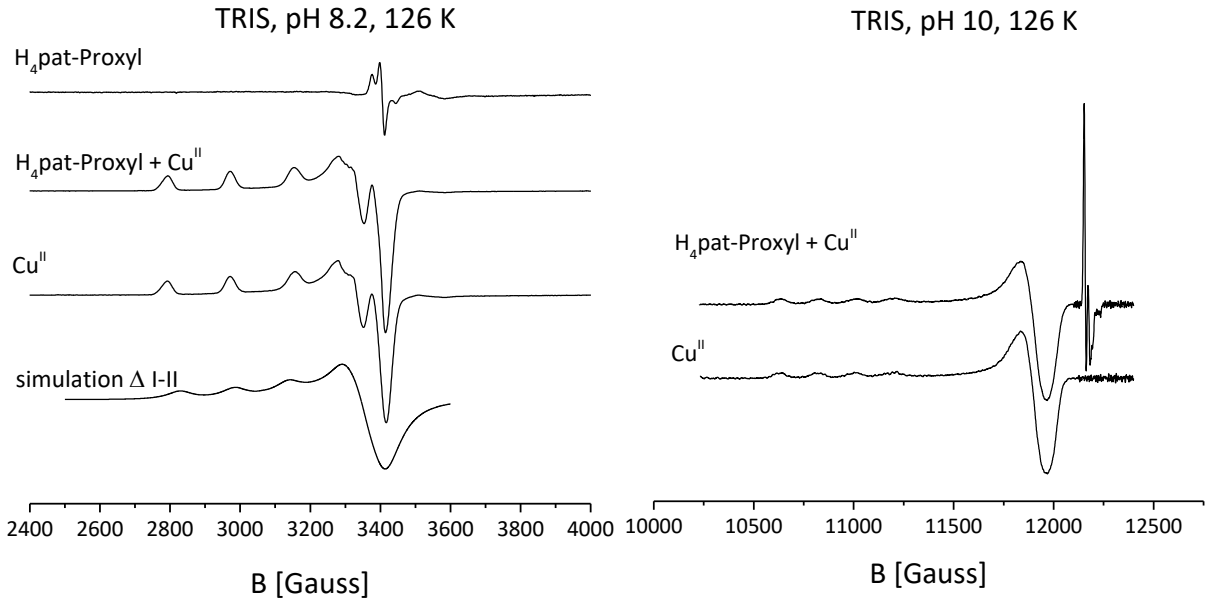

Figure 5.13. Left top to bottom: experimental CW-EPR spectra of the ligand H_4pat-Proxyl (9.45729 GHz), a solution of 1 eq. of H_4pat-Proxyl and 5 eq. of Cu^{II} (9.45485 GHz), a solution of Cu^{II} (9.456059 GHz) and the simulation from Figure 5.12 (X-band). Right: first derivative of experimental spin-echo-detected EPR spectra of the ligand H_4pat-Proxyl and 5 eq. of Cu^{II} (34.114 GHz) and a solution of Cu^{II} (34.17457 GHz). The ligand concentration was chosen to be 500 µM in TRIS buffer.

These spectra given in Figure 5.12 show a copper(II) complex with the g- and A-tensors as listed in Table 5.1. Moreover, it becomes obvious that the species observed in the presence of ligand H_4pat-Proxyl is significantly different to Cu^{II} in solution.

Table 5.1. g- and A- tensors [10^{-4} cm^{-1}] of the difference spectrum shown in Figure 5.12 for H_4pat-Proxyl + Cu^{II}.

	g_x	g_y	g_z	A_x	A_y	A_z
H_4pat-Proxyl + Cu^{II}	2.05	2.05	2.2481	4	4	162

As discussed in detail in Chapter 4.3, the EPR signal is interpreted as *pseudo*-mononuclear. A broadening of the EPR signals, as mentioned earlier, was however not observed, predominantly obvious from the comparison of the NO-signal (see Figure 5.12 left). The absence broadening from magnetic dipole interaction is surprising, since the distance between the Cu^{II} centres and the NO-radical is expected to be in the range of 11-17 Å (as reported from DFT calculations, discussed in 5.1). Although the strength of the interaction is proportional to r^{-3}, usually broadening is observed for distances between 10 and 100 Å.[210]

As a next step the same measurements were carried out in TRIS buffer at pH 8.2, since these are the conditions used for *Prochloron* handling. The respective measured spectra are shown in Figure 5.13. The EPR signal arising from Cu^{II} in the spectrum containing ligand H_4pat-Proxyl and Cu^{II} is not significantly different to the signal observed for Cu^{II} in TRIS buffer. In the light of the previous fluorescence studies, carried out at the same conditions, this indicates that the copper(II) complex probably shows a small stability constant in TRIS at pH 8.2, resulting in small intensities that are overlaid with the much stronger signal from unbound Cu^{II} ions. This suggestion is underpinned by the qualitative comparison of the simulation (from MeOH measurements) with the experimental spectra. Consequently, measurements at smaller proton concentrations were carried out (pH 10) in order to stimulate the deprotonation of the ligand, leading to increased formation of the copper(II) complex. The results are summarised in Figure 5.13 on the right. In addition, these spectra were recorded at Q-band, *i.e.* at a higher magnetic field leading to a larger difference in the split states and thus a better resolved spectrum (whereas it is important to note, that one term of relaxation, the CURIE term is B-dependent and thus leads to line broadening and potentially to a loss of information).[178,211] Again, there is no difference between the copper(II) signals observed in the solution with H_4pat-Proxyl and the spectrum of Cu^{II} in solution. Subsequently spectra with varying ligand : Cu^{II} concentrations ranging from 1 : 5 to 5 : 1 were recorded, none of them showing the formation of a complex to an extent that would be distinguishable from the free copper(II) signal. An additional explanation for the absence of signals arising from a copper(II) complex, could be the formation of an EPR-silent species, a rational example of which is the bridged dinuclear copper(II) complex. This hypothesis was checked by broken-symmetry DFT calculations with ORCA to determine the exchange coupling constant (geometry-optimised structures (ORCA), def2-TZVP, for a detailed review on the method see reference [212]). A HEISENBERG-DIRAC-VAN VLECK Spin Hamilton operator[213-216] is used for the description of the magnetic properties of the complex. *J* describes the spin coupling (see equation 5.9) and S_1/S_2 correspond to the spin operators[217] of the metal centres.

$$\hat{H} = 2J_{Cu-Cu}\hat{S}_1\hat{S}_2 \tag{5.9}$$

For the calculation of *J*, the exchange coupling constant,[218-222] a broken symmetry approach is applied for the DFT calculation (see equation 5.10).

$$J_{Cu-Cu} = \frac{E_{BS} - E_{HS}}{\langle \hat{S} \rangle_{HS}^2 - \langle \hat{S} \rangle_{BS}^2} \tag{5.10}$$

For the OH^- bridged species antiferromagnetic coupling with an exchange coupling constant of $J_{Cu\text{-}Cu}$=–410 Hz ($Cu^{II}\cdots Cu^{II}$ distance: 3.9 Å) was predicted, contrary to the non-bridged species ($J_{Cu\text{-}Cu}$=–6 Hz, $Cu^{II}\cdots Cu^{II}$ distance: 5.3 Å). Thus, at 125 K, according to the BOLTZMANN distribution 0.89% of all molecules would be expected to populate the excited state of the bridged conformation (ratio of molecules in the excited state compared to molecules in the ground state at 30 K: $2.8\text{x}10^{-9}$). Consequently, no EPR signal is observable at that temperature, whereas an EPR signal for the non-bridged conformation would be expected with 93% at 125 K and 75% at 30 K. This hypothesis could further be supported SQUID (superconducting quantum interference device) measurements with an appropriate amount of powder of the complexes.[223] However, so far, the patellamide complex chemistry was always limited by the fact that attempted precipitation (*e.g*. in MeOH upon addition of diethylether) usually delivers a mixture of the ligand as a powder and the respective copper(II) salt as crystals and a small amount of complex as a powder (and this was also the case for the sample that was characterised via X-ray crystal structure determination [116]). For SQUID measurements, however, the exact composition of the powder sample must be known. Therefore, temperature dependent EVANS NMR spectra should be preferred, as they can be carried out in solution which would also allow to use different solvents and compare the results.[224,225] These experiments will be carried out as soon as possible.

A well-established technique to measure distances of ca. 0.5-3 nm is the double electron-electron resonance (DEER),[210,226] which is also known as PELDOR: pulsed electron-electron double resonance, and is the analogue of NMR spin echo double resonance. It measures dipolar coupling between unpaired electrons by pulsed EPR techniques. Since the dipolar coupling is dependent on the radial separation, conclusions can be drawn about the distance between the unpaired electrons (see equation 5.11):[227]

$$\hat{H}_{dd} = -\frac{\mu_0}{4\pi} g_1 g_2 \mu_B^2 \left(\frac{\hat{S}_1 \hat{S}_2}{r^3} - 3 \frac{(\hat{S}_1 r)(\hat{S}_2 r)}{r^5} \right) \tag{5.11}$$

DEER experiments were also carried out in a frozen solution to avoid averaging of the dipolar coupling term introduced from molecular tumbling. Initially a spin-echo-detected field sweep must be

performed to determine the pump and the observer frequency (this means that centre A is excited with the respective pump pulse and centre B is observed). The time-domain signal consists of two components: (a) an exponential decay arising from randomly distributed, non-fixed spins in the frozen solution, and (b) the modulation of the electron spin echo caused by the dipolar coupling between the spins, which can consequently be related to the distance.[210,226,227]

This experiment was performed with a solution of H_4pat-Proxyl and 3 eq. of Cu^{II} in TRIS buffer at pH 8.2 and pH 10 at Q-band, but did not provide a modulation on top of the exponential decay. This indicates, as described above, that the copper(II) complex with H_4pat-Proxyl is probably only present in small quantities that are overlaid by free Cu^{II} signals.

As an alternative approach ESEEM (electron spin echo envelope modulation, two- or three-pulse) measurements could be carried out. Upon increasing the time between the pulses in ESEEM the echo signal decays exponentially primarily due to spin-lattice and spin-spin relaxation. Interactions with nuclei in chemically close proximity to the centre observed lead to a modulation of the exponential decay (quadrupole and hyperfine interactions).[228,229] Consequently, a deuterated patellamide ligand is currently being prepared to apply this technique.

Once the *in vitro* EPR experiments will be brought to a stage that allows the validation of the binding of copper(II) to the patellamides, *in vivo* experiments with *Prochloron* will have to be carried out.

5.4 *In vivo* hydrolase

Ultimately, the purpose of patellamide research is to understand their metabolic relevance or that of their copper(II) complexes. Since *in vitro* studies point to an involvement of the copper(II) complexes in catalytic reactions, in a proof-of principle study, the hydrolase activity was measured in *Prochloron* cells. These experiments are considered as preliminary and must be interpreted carefully, since the concentration of ligand inside the cells cannot be determined accurately, and the medium that *Prochloron* was kept in, BG 11, contains metal salts, specifically also divalent 3d-metal ions like Zn^{II} (772 nM), Cu^{II} (316 nM) and Mn^{II} (3,471 nM) but also alkaline earth metal ions like Ca^{II} (245 µM) and Mg^{II} (304 µM).

The substrate (nitrocefin for β-lactamase and SunRed substrate for phosphatase) was added to the *Prochloron* samples in BG 11 medium. Therefore, it is not entirely certain whether or not the measured kinetic data are related to hydrolase activities taking place outside or inside the cell.

However, no catalysts for β-lactamase or phosphatase activity would be expected to be present in the medium, consequently the hydrolysis observed is attributed to processes inside the cells.
Three different samples were investigated:

(i) *Prochloron,*

(ii) *Prochloron* incubated at room temperature for 15 min with H_4pat^1 ([H_4pat^1] in the cuvette: 1 µM), and

(iii) *Prochloron* incubated at room temperature for 15 min with H_4pat^1 (as per sample ii), with 1:2 ligand : cyclam.

After the incubation, the *Prochloron* cells were washed and subsequently investigated concerning the hydrolysis of model substrates. Detailed descriptions of the experimental setups are given in the Experimental Section. The velocity of the β-lactamase-like activity is shown in Figure 5.14 and was measured at pH 8.2. The difference observed for the lactamase rate for (i) *Prochloron* compared to (ii) *Prochloron*, incubated with the model patellamide H_4pat^1, is not significant. However, upon addition of cyclam (iii), the observed velocity decreases drastically to less than half of what is observed for samples (i) and (ii). This leaves the conclusion that the observed β-lactamase-like activity is probably 3d-metal ion dependent, *i.e.* Cu^{II} could be the active metal centre, but other transition metals are equally likely, since cyclam is not a Cu^{II} selective ligand. Similar to the lactamase measurement, the observations for phosphatase reactivity indicate a metal ion dependence (see Figure 5.14, right), whereas the addition of H_4pat^1 did not lead to an increased hydrolase rate.

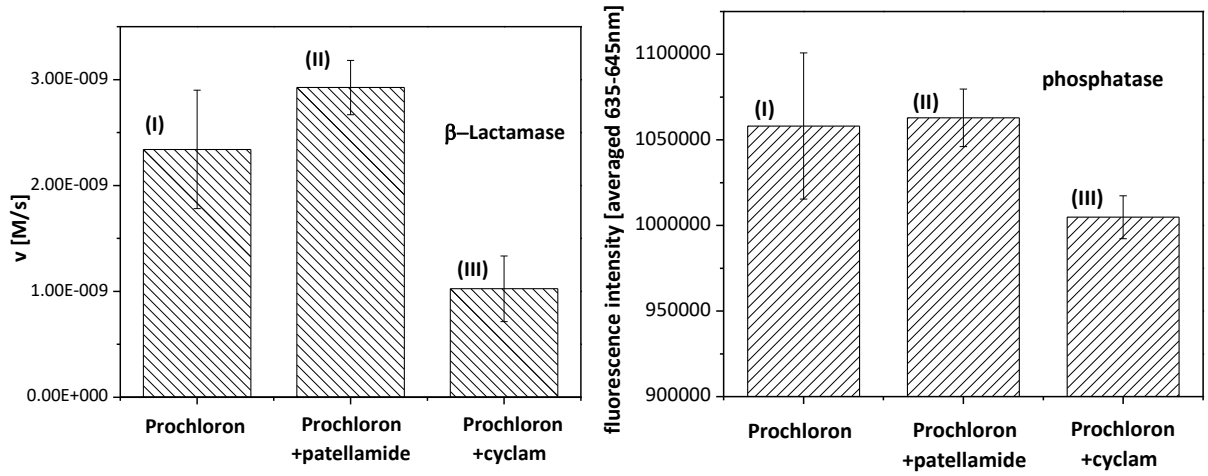

Figure 5.14. Rates of β-lactamase (left) and phosphatase activity (right) in *Prochloron*, *Prochloron* and H_4pat^1 and *Prochloron* with H_4pat^1 and added *cyclam* respectively at pH 8.2.

If the concentration of natural patellamides as well as the concentration of other lactamase/ phosphatase enzymes was significantly higher than that of the model patellamide, no change of the hydrolase rate would be expected upon addition of the *pseudo*-octapeptides, as observed in the experiments. In order to prove this hypothesis, more experiments, *e.g.* including selective phosphatase inhibitors and more selective Cu^{II} ligands instead of cyclam, need to be carried out. In addition, single molecule FRET (FÖRSTER resonance electron transfer) experiments with a substrate that releases a fluorophore could be carried out with a fluorescent tag labelled patellamide copper(II) complex to examine the relative distance between the fluorescent groups.

5.5 Conclusion

In this Chapter the synthesis of a fluorescent-dye-derivatised and a spin-labelled patellamide is reported. The former was studied photophysically and by means of optical spectroscopy concerning its Cu^{II} ion sensing. It could be shown that the fluorescence of the ligand is Cu^{II} dependent with a STERN-VOLMER constant of K_s=1.35(2)x10^6 M^{-1}, which is of the same order of magnitude as the binding constant observed for similar model patellamides.[72] Moreover, it was revealed that the model peptide is taken up by the cell, probably by a passive mechanism. The imaging *via* flow cytometry as well as confocal microscopy studies imply that a Cu^{II} patellamide complex forms in the cells, as observed *in vitro*. From the fluorescence investigations, it is however unfortunately impossible to determine whether or not the complex formed is a mono- or a dinuclear complex.

From the EPR study it became obvious that the binding constant of the copper(II) patellamide complex in buffer is small, leading to a signal which not was observable over the background signal (Cu^{II}). Although spectra recorded in MeOH as a solvent clearly showed the formation of a complex, no proof for a dinuclear complex could be obtained. In conclusion, further investigations by means of pulsed EPR will help to circumvent this obstacle and will shed light on the structure of the Cu^{II} patellamide complexes formed inside the cells.

Preliminary hydrolysis studies indicate a 3d-metal ion dependence of the catalyses. In future experiments, methods will have to be explored in order to control the patellamide and copper(II) concentration as well as the activity of other phosphatase/lactamase enzymes.

Altogether, the formation of Cu^{II} complexes inside *Prochloron* cells could be shown, but so far the existence of a dinuclear complex under aqueous conditions could not be proven. If the copper(II)

complex observed was dinuclear, this would indicate that the catalysis of various hydrolysis reaction observed *in vitro*, carbonic anhydrase, phosphatase, lactamase and glycosidase activities and probably others, not yet explored, might be the metabolic purpose of the patellamides.

6 Conclusion and outlook

The work presented in this thesis focused on the potential metabolic role of patellamides and their dinuclear copper(II) complexes for *Prochloron*.

The studies give further support for the hypothesis that the patellamide-ligand backbone, *i.e.* the stereoconfiguration of the *iso*-propyl side chains has a significant influence on the hydrolysis activity of the respective dinuclear copper(II) complexes. This was exemplified by the study of phosphatase-like activity with two naturally *R* and *S* configured ligands H_4pat^4 and H_4pat^5 (the respective dinuclear copper(II) complexes are depicted in Figure 6.1).

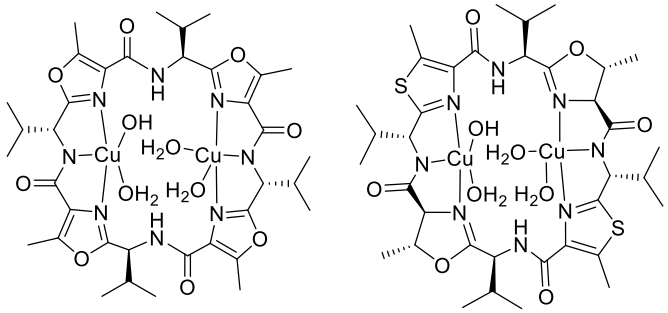

Figure 6.1. Schematic representation of the dinuclear Cu^{II} complexes under investigation concerning their phosphatase-like activity in Chapter 3.

The dinuclear complex $[Cu_2(H_2pat^4)(OH)]^+$ exhibits the highest catalytic rate observed for a model patellamide complex to date as well as a high catalytic efficiency (k_{cat}/K_M=0.45 $M^{-1}s^{-1}$), whereas $[Cu_2(H_2pat^5)(OH)]^+$ showed maximum catalytic efficiency (k_{cat}/K_M=0.53 $M^{-1}s^{-1}$).[123] If compared to the phosphatase activity of copper(II) complexes with 4*S* configured ligands and imidazole heterocycles the catalytic efficiency of the complexes $[Cu_2(H_2pat^4)(OH)]^+$ and $[Cu_2(H_2pat^5)(OH)]^+$ with naturally configured ligands, is increased by a factor of approximately 3-5. Compared to other model

phosphatase complexes, the H_4pat^4 and H_4pat^5 based dinculear copper(II) complexes exhibit efficiencies that are approximately half of the efficiencies reported for the best model compounds.[105] In addition, it could be shown, that the pH range for phosphatase activitiy is rather narrow (0.3 pH units) for the dinuclear copper(II) complexes of H_4pat^5 and all imidazole-based ligands (H_4pat^1-H_4pat^3). This is however not the case for $[Cu_2(H_2pat^4)(OH)(H_2O)_3]^+$ which shows broad activity between pH 7 and 8.5.

Furthermore, the Zn^{II} complexes show a similar coordination motif as expected for Cu^{II} complexes, *i.e.* binding to the heterocycle pocket spanned by N_{het}-N_{amide}-N_{het}. The lack of catalytic activity of the zinc(II)-based complexes is consequently likely to be caused by their small stability under aqueous conditions.

The concise catalytic mechanism is currently investigated by means of DFT, including the formation of the catalyst-substrate complex, the nucleophilic attack of a metal-ion-stabilised hydroxide ion and the subsequent release of the product.

With the study discussed in Chapter 4, the capacity of the patellamide based copper(II) complexes to act as catalyst for further hydrolases was explored. These investigations showed that the imidazole-based complexes are potent hydrolases not only for phosphate ester cleavage but also for the hydrolysis of glycosidic bonds at alkaline conditions (pH 10). Interestingly, the copper(II) complexes show higher catalytic efficiencies for β-glycosidase (k_{cat}/K_M=3.43-5.09 $M^{-1}s^{-1}$) compared to α-glycosidase activity (k_{cat}/K_M=1.49-3.30 $M^{-1}s^{-1}$). Probably, this is correlated with a lower activation energy for the formation of the respective catalyst-substrate complex, due to a smaller steric hindrance caused by the equatorial β-arrangement of the nitrophenol, which could in turn facilitate a more efficient hydrolysis, as opposed to the axial α-position. The dinuclear copper(II) patellamide complexes moreover show an efficiency that is ~10^4 times higher as compared with the model glycosidases reported by STRIEGLER *et al.* (k_{cat}/K_M=3.95x10^{-5}-1.27x10^{-4} $M^{-1}s^{-1}$).

In addition, β-lactamase-like activity was observed at pH 11.5 of $[Cu_2(H_2pat^1)(OH)]^+$ with an efficiency of k_{cat}/K_M=50.5 $M^{-1}s^{-1}$. This is consistent with similar dinuclear model complexes, that show efficiencies in the range of k_{cat}/K_M=100-200 $M^{-1}s^{-1}$.[172]

The results of Chapter 4 point to a putative involvement of the complexes as tuneable pH-dependent catalysts. It is known that the pH in *L. patella* (in close proximity to *Prochloron*) is fluctuating strongly, depending on the irradiation level.[9,38] Therefore, the results presented could mean that the complexes change their target reaction depending on the time of the day.

By introduction of different reporter groups to a patellamide the *in vitro* and *in vivo* stability of the dinuclear Cu^{II} complexes could be investigated. As reporter groups the spin label proxyl and the fluorescent dye Atto550 was chosen. *In vitro* EPR and fluorescence quenching experiments point to the formation of copper(II) complexes. From the titration of the fluorescent dye labelled patellamide with copper(II) the STERN-VOLMER constant could be estimated to be K_s=1.35(2)x10^6 M^{-1}. This finding fits the expectations from isothermal calorimetric measurements, that were carried out previously in methanol.[230]

In order to perform *in vivo* measurements, a protocol for the uptake of patellamides by *Prochloron* was established, which could be used to incubate the cells with the cyclic octapeptides. From *in vivo* fluorescence studies by flow cytometry and confocal microscopy one can conclude that the intensity of the reporter fluorescent tag Atto550 is decreased upon the addition of Cu^{II} compared to the fluorescence of chlorophyll *b* in the cells. This indicates the formation of a copper(II) complex *in vivo* in *Prochloron*. EPR experiments however, could not prove the existence of the complexes in the cells. Therefore, a deuterated ligand is currently prepared, which will subsequently be investigated concerning its Cu^{II} binding behaviour by ESEEM measurements.[228] Moreover, isothermal calorimetric titrations of the model patellamides with Cu^{II} in buffer are in the focus of ongoing research. Results from this technique could support the formation of a dinuclear complex at aqueous conditions.

Preliminary *in vivo* hydrolysis experiments support the involvement of a 3d-metal ion. Further studies will have to be carried out to validate whether or not copper(II) is the metal ion involved as well as to probe the potential role of the patellamides during the hydrolyses.

So far, no experiments were conducted to investigate the stability of the copper(II) complexes in the host, *L. patella*. However, this is not unimportant, since large quantities of patellamides were found in the ascidians. Whether or not the complexes play a role for *Prochloron* and/or *L. patella* should be the focus of future research.

Since patellamides were found in the hosts in close proximity to *Prochloron* and *Prochloro*n could not be brought in laboratory culture to date, experiments on the potential influence of the concentration of patellamides in cell culture media on the viability of single *Prochloron* cells will be tested in future work.

Apart from this approach, the formation and stability of copper(I) patellamide complexes should be investigated in detail, as well as their putative role as a tyrosinase/catecholase-like catalysts. This path

of research should especially be studied, as the oxygen saturation level varies greatly[9] and consequently, a reducing environment in the *Prochloron* cell at darkness might be expected. Moreover, the intracellular environment in mammalian cells is anticipated to be reducing, which could particularly play a role for *L. patella* cells.[231]

Experimental Section

A) General techniques

A1) Materials, methods and analytical techniques

Some of the reactions reported were carried out under an inert atmosphere of argon or nitrogen using standard SCHLENK-techniques. Glassware was heated and dried under vacuum prior to use. All chemicals were purchased from Sigma-Aldrich GmbH, ABCR GmbH & Co. KG and Merck at the highest available purity. Dry solvents were purchased and used as delivered. For optimised comprehensibility, names of compounds synthesised were simplified instead of usage of the exact IUPAC name.

Chromatography

Reactions were monitored by TLC on silica gel 60 F254 thin layer plates (POLYGRAM SIL G/UV, Machery-Nagel). UV light at an excitation wavelength λ=254 nm was applied to accomplish detection. Flash chromatography was performed using dried (overnight, 120°C) silica gel 60 (230-400 mesh) from Sigma Aldrich.

Mass spectrometry

High resolution mass spectra (HR ESI MS) were recorded with a Finnigan MAT8230 and a Joel JMS-700 spectrometer by Dr. Jürgen Gross and co-workers at the mass spectrometry facility in the Organic Chemistry department of Heidelberg University on a ICR Apex-Qe and a JEOL JMS-700. Atmospheric pressure chemical ionization mass spectra (APCI MS) were recorded on a Waters UPLC-SQD2 single quadrupole.

NMR spectroscopy

Nuclear magnetic resonance spectra were recorded with a Bruker Avance I (200 MHz) or a Bruker Avance III (600 MHz) spectrometer equipped with a cryoprobe. Chemical shifts δ are given in ppm and coupling constants *J* in Hz and refer to $^{3}J_{H\text{-}H}$ couplings. All spectra were calibrated using the residual ^{1}H- or ^{13}C-signals of the deuterated solvents. Spectra were recorded at 295 K. The following abbreviations are used to describe the multiplicities of the signals: s (singlet), bs (broad singlet), d (doublet), t (triplet), qn (quintet), m (multiplet). Signals were assigned using DEPT, HSQC and HMBC spectra.

Ligand syntheses

The cyclic *pseudo*-peptides H_4pat[1], H_4pat[2] and H_4pat[5] were prepared according to previously described procedures.[62,85] The synthesis of H_4pat-Atto550, H_4pat-Proxyl and H_4pat[4] were accomplished analogously to the previously reported *pseudo*-peptide syntheses[62] and are described in detail in Part B of the Experimental Section.

The purification of the dye conjugate H_4pat-Atto550 was performed with a HPLC (Agilent, Waldbronn, serial number 1100), equipped with a binary pump G1312A, a degasser G1322A, a diode array detector G1315 A and a fluorescence detector G1321A. The chromatographic separation was performed using a reversed phase column from Knaur, Berlin (250 mm length, 4 mm inner diameter, ODS-Hypersil with pore diameter of 5 µm).

EPR experiments

All X-band (9.462 GHz) continuous wave (CW) EPR spectra at 30 K were recorded with an Elexsyxs E500 spectrometer fitted with an ER 4116 DM dual mode resonator. Temperatures of 30 K at the sample position were delivered by an ER 4112HV-CF58uc In-Cavity Cryogen-Free VT System.

All X-Band CW EPR spectra at 120-140 K were recorded with a Bruker Elex540 spectrometer using a Bruker super-high Q cavity. Frozen solution (110 - 140 K) X-band CW EPR spectra where recorded with a modulation amplitude of 0.5 mT, a modulation frequency of 100 kHz and a non-saturating microwave power of 20 mW (10 dB attenuation of a 200 mW source). Temperatures of 110-140 K at the sample position were delivered by a flow-through LN_2 cryostat in conjunction with a Eurotherm B-VT-2000 variable temperature controller.

Pulse EPR measurement were carried out on a Bruker X-/Q Elex580 spectrometer equipped pulse EPR & ENDOR Resonator (EN 5107D2) and a cryogen - free variable temperature cryostat from Cryogenic Limited (model PT415). The Q-band (34.2 GHz) field sweep FID-detected EPR spectra were recorded at 125 K by integrating over the FID created from a single pulse of length 600 ns (FID, free induction decay). The Q-band (34.2 GHz) field sweep echo-detected EPR spectra were recorded at 35K by integrating over the echo created from a two pulse $\pi/2$ - τ - π - τ - echo, with t = 40 ns, $t_{\pi/2}$ = 80 and t_{π} = 240 ns. The fields at both X-band and Q-band (at 125 K) were calibrated using DPPH with the known g-value of 2.0036.

All Spin Hamilton parameters were provided by computer simulations of the experimental spectra with XSophe[182] or MoSophe[181]. For visualisation Xepr was used.

Elemental analysis

All elemental microanalyses were recorded on a vario MICRO cube spectrometer (Elementar) at the microanalytical laboratory of the Heidelberg University.

A2) Computational methods

DFT calculations

DFT has been chosen as method for structural prediction, since the theoretical method is a reasonable compromise between accuracy and effort for the patellamide systems. It is usually (but not guaranteed) more accurate than the *ab initio* method HARTREE FOCK, since with HF the electron correlation energy can only partially be predicted.[232] At the same time further wave-function based correlated methods, like MØLLER PLESSET perturbation theory[233] or coupled cluster,[234] the HARTREE-FOCK based methods, would be preferable due to their higher accuracy, but are currently only feasible for small systems.

The DFT states that all electronic ground state properties can be described by the electron density of the system.[235] The intrinsic energy of a system in its electronic ground state can therefore be described by a functional that depends on the density. Since the electron density is only dependent on the three spatial vectors, unlike wave function based methods, which depend on the number of electrons in the system, DFT is in principle a much faster computational technique. Since the electronic energy in DFT is described as a functional of the electron density, this density has to be determined. This is accomplished incorporating the kinetic energy of the electrons, the kinetic energy of the cores, the electron-core attraction, the electron-electron repulsion and the core-core repulsion (equation A1).

$$E[\rho] = T_e + T_n + V_{en}[\rho] + V_{ee}[\rho] + V_{nn} \qquad \text{(A1)}$$

Applying the BORN-OPPENHEIMER approximation, stating that the electron movement is independent of the core movement (since from the perspective of the electron the core is not moving) the electron movement can be described as a movement in a field of non-moving cores. This results in a kinetic energy of the cores of T_n=0 and causes the last term to be an additive summand. Moreover, the core-electron interaction is known. Thus, KOHN and SHAM proposed a procedure to deduce the remaining terms.[236] It is based on the assumption, that the electron density of an interacting system can be approximated by a system, consisting of non-interacting quasi particles that can be described by orthogonal one-electron orbitals (which leads to similar computational costs as compared to HF methods but offers the benefit of ideally complete electron correlation). These particles would in turn only interact with the external potential V_{ext}.

The electron density thus would only consist of the sum of square of all one-electron KOHN SHAM orbitals.

$$\rho^{KS} = \sum_{i=1}^{N} \left|\psi_i^{KS}\right|^2 \tag{A2}$$

Here, ρ^{KS} should be equal to the actual density ρ. This Ansatz solves the problem of inaccurate description of the kinetic energy term *T* of the electron to a large extend. The remaining correction, *i.e.* for an interacting system, is collected as the kinetic and potential energy difference between the real and the reference system, which is commonly referred to as the exchange correlation functional (A3). The energy differences are described in equation A4 and A5.

$$E_{xc}[\rho] = \Delta T_e[\rho] + \Delta V_{ee}[\rho] = E_x[\rho] + E_c[\rho] \tag{A3}$$

$$\Delta T_e[\rho] = T_e^{real}[\rho] - T_e^{KS}[\rho] = T_e^{real}[\rho] - \sum_i^N \left\langle \psi_i^{KS} \middle| -\frac{\nabla^2}{2} \middle| \psi_i^{KS} \right\rangle \tag{A4}$$

$$\Delta V_{ee}[\rho] = V_e^{real}[\rho] - J[\rho] = V_e^{real}[\rho] - \frac{1}{2}\sum_{i\neq j}^{N} \left\langle \psi_j^{KS} \middle| \frac{1}{r_{12}} \middle| \psi_i^{KS} \right\rangle \psi_j^{KS} \rangle \tag{A5}$$

This leads to the description of the ground state (A6):

$$E[\rho] = T_e^{KS}[\rho] + V_{en}[\rho] + V_{nn} + J[\rho] + E_{xc}[\rho] \tag{A6}$$

The analytical solution of the exchange-correlation functional is not known, but different approximations have been proposed. Often the generalised gradient approximation (GGA) is used in order to compute the exchange-correlation term.[237] The GGA method is based on the Local Density Approximation (LDA) and additionally includes local gradient information. This is especially desirable for the computation of transition metal complexes, since the electron density inhomogeneity is not well described in LDA. Typical functionals of this kind are the B88 exchange potential[238] as well as the LEE, YANG, PARR (LYP)[239] exchange correlation functional. To further improve the description of electron correlation, hybrid functionals were introduced. In these, the exchange energy is partially computed *via* HF methods. In this thesis, the B3LYP hybrid functional

was employed[239-241], which consists of an LDA-exchange functional E_x^{LDA}, an exact Hartree Fock exchange E_x^{HF}, BECKE's exchange functional E_x^{B88}, the LDA- correlation functional (VOSKO, WILK, NUSAIR) E_c^{VWN}, and the correlation functional from LEE, YANG and PARR E_C^{LYP},

$$E_{xc} = (1-a)E_x^{LDA} + aE_x^{HF} + 0.72\Delta E_x^{LDA} + 0.19E_c^{VWN} + 0.81E_C^{LYP} \quad \text{(A7)}$$

For the hybrid functional B3LYP the parameter 'a' is set to a value of 0.2. It is called B3LYP, since it uses the exchange functional from BECKE (E_x^{LDA}) and the LEE, YANG, PARR correlation functional, and the latter three (3) terms (equation A7) are parameterised to experimental electron affinities, proton affinities and ionisation potentials. Thus, B3LYP can be considered a semi-empirical method.

As basis sets for the orbitals, linear combinations of one-electron wave functions are employed. The minimum basis set would correspond to a description of a system with n electrons and n/2 spin orbitals with n/2 basis functions. To improve the accuracy, double zeta (DZ) and triple zeta (TZ) basis sets were introduced, including twice or three times the number of basis functions, each with different spatial extend, compared to the minimum basis set. The additional incorporation of polarisation functions (from the mixing of molecular orbitals with atomic orbitals of higher orbital angular momentum quantum number) further improves the accuracy of orbital description. An example is the Valence Triple Zeta plus Polarisation (TZVP) first introduced by AHLRICHS.[242] In this thesis the def2-TZVP[243] basis set has been used, which is derived from the TZVP basis set and parameterised against experimental data and contains additional *pseudo*-potentials for transition metals.

In this thesis fully optimised molecular structures were obtained through geometry optimisations employing the B3LYP [244] functional in conjunction with the def2-TZVP basis set.

All calculations on the structure optimisations of dinuclear complexes **1A, 1B, 2A, 2B, 3A-I, 3B-I, 3A-II, 3B-II, 4A, 4B** and **5A-5L** were performed with Gaussian 09.[245] Solvation was approximated by the polarisable continuum model[246] with the permittivity set to methanol. Frequency calculations were carried out on the optimised structures to validate the minimum structures. The coordinates of these species are given in the Appendix.

Calculations on the validation of the binding sites (see Chapter 3.2) were performed with ORCA 3.0.1.[247] Solvation was approximated by the conductor-like screening model COSMO[248] with the permittivity set to MeOH. Single point energy and frequency calculations were carried out on the

optimised structures. All plots of computed structures were produced with Avogadro 1.1.0.[249] The coordinates of all relevant species summarised in the Supporting Information of reference [115]. Broken-Symmetry DFT[212,219,220] calculations were carried out with ORCA 3.0.1 on geometry optimised structures using B3LYP as a functional and def2-TZVP as the basis set.

MM calculations

MM calculations were carried out with the MM programme MOMEC3.[128,250] The total strain energy E_{strain} is calculated from the sum of the bond deformation E_b, angle deformation E_θ and torsion angle deformation E_Φ as well as non-bonded interaction energies E_{nb}. Out-of-plane deformation, electrostatic interactions and hydrogen bonding were excluded.

$$E_{strain} = \sum E_b + \sum E_a + \sum E_t + \sum E_{nb} \quad \text{(A8)}$$

$$E_b = \frac{1}{2} k_s (r_c - r_0)^2 \quad \text{(A9)}$$

$$E_a = \frac{1}{2} k_B (\theta_c - \theta_0)^2 \quad \text{(A10)}$$

$$E_t = \frac{1}{2} k_T (1 - \cos(m\varphi_c - \varphi_0)) \quad \text{(A11)}$$

$$E_{nb} = Ae^{-Bd} + Cd^{-6} \quad \text{(A12)}$$

with k_s, k_B, k_T as potential constants and r_0, θ, and φ that are the strain-free (ideal) respective values. Out-of-plane deformation, electrostatic interactions and hydrogen bonding were excluded. The atom type labels were assigned according to the published atom types.[129,131,251-258] The MOMEC force field[130] was taken and supplemented with parameters for stretches, bends and torsions between not yet parameterised atom types. Details on the parameter optimisation programme are discussed in ref [130]. The force field and coordinates for all relevant species are summarised in the Supporting Information of reference [115].

A3) Hydrolysis measurements

In vitro hydrolase experiments

Preparation of the Multicomponent Buffer Solutions

The aqueous buffer consisted of CAPS, *N*-cyclohexyl-3-aminopropanesulfonic acid, pK_a = 10.40, CHES, 2-(*N*-cyclohexylamino)ethanesulfonic acid, pK_a = 9.30, HEPES, 4-(2-hydroxyethyl)-1-piperazinyl-ethanesulfonic acid, pK_a = 7.55 and MES, 2-(*N*-morpholino)ethanesulfonic acid, pK_a = 6.15. Lithium perchlorate was added to achieve a constant ionic strength of μ = 0.45. Each component was dissolved in Milli-Q water. A standard solution with 55.56 mM of the buffer components and 277.8 mM lithium perchlorate was prepared. Aliquots of 45 mL of the standard buffer were adjusted to the desired pH value by addition of 2M NaOH. A Metrohm 713 pH meter equipped with a KCl electrode was used to adjust pH values at 25°C. The pH-meter was calibrated with pH standard solutions at pH values of 4, 7 and 9. Subsequently the aliquots were filled up to 50 mL leading to a final buffer concentration of 50 mM and 250 mM lithium perchlorate. Metal ions were removed by stirring adjusted buffers over night with Chelex 100, which was afterwards filtered off by using 45 μm syringe filters. Finally, all buffers were degassed by flushing N_2 through the solution in an ultrasonic bath for 3 h in order to remove potentially dissolved CO_2.

Phosphatase-like activity

The phosphatase-like activity was determined by measuring the hydrolysis of BDNPP. The hydrolysis product 2,4-dinitrophenolate was detected by monitoring the increase of a strong absorbance at 400 nm (ε = 12,100 $M^{-1}cm^{-1}$, 25°C).[121,122] UV-vis data were recorded with a Jasco V-570 spectrophotometer equipped with a Jasco ETC-505T cryostat (set to 25°C) and in 45 : 50 : 5 MeCN : buffer : MeOH solutions. Initially, the optimum pH range for phosphatase activity was determined. The pH dependence of the catalysis rates was measured in steps of 0.5 pH units or smaller from pH = 4.5 to pH = 11.5, using time-course measurements at the fixed wavelength of λ_{max}=400 nm. The stock solution concentration of cyclic *pseudo*-peptides were 1 mM (dry MeOH), $Cu^{II}(CF_3SO_3)_2$ (25 mM, dry MeOH) and base (*n*-Bu_4N(OMe), 25 mM, (dry MeOH). The final concentrations of the dicopper(II) complexes of the ligands (ligand : metal : base ratio of 1 : 2 : 2) in the cuvette were 40 μM. All solutions were degassed and kept under argon at 4°C. For the determination of pH-dependent reaction velocities a substrate concentration of 5 mM (MeCN) was chosen. Rates were obtained by employing the initial rate method. The reported rates are

averages with standard deviations from triplicates. Blank tests, the autohydrolysis of BDNPP determined in duplicate, were subtracted from the measured kinetic rates. Tests with a ligand : Cu : base ratio of 1 : 1 : 1 were carried out and gave results in the range of the blank tests. Subsequently, MICHAELIS-MENTEN[99] measurements were carried out at the respective optimum pH.[121] For substrate dependence measurements at constant pH the substrate concentration was varied between 0.25 – 10 mM.

Glycosidase-like activity

The glycosidase-like activity was determined by measuring the hydrolysis of 4-nitrophenyl-α-*D*-glucopyranoside and 4-nitrophenyl-β-*D*-glucopyranoside. The hydrolysis product 4-nitrophenolate was detected by monitoring the increase of a strong absorbance at 410 nm (ε is pH-dependent).

Initially, the extinction coefficients of the product formation of 4-nitrophenolate in a multicomponent buffer were calculated by calibration curves for each pH value (pH = 5.5 – 11.5) using the LAMBERT BEER'S law (Table A1). The extinction coefficients at pH = 8.7 – 11.5 are similar to those determined for 4-nitrophenolate in CAPS buffer (ε = 16190 $M^{-1}cm^{-1}$).[159] The extinction coefficients obtained (see Table A1) were used to convert the absorbance of the reaction product into molar amounts.

UV-vis-spectra were recorded with a Jasco V-570 spectrophotometer equipped with a Jasco ETC-505T cryostat at 25°C and in a 0.3 : 1.3 : 1 MeCN:buffer:MeOH solution. Using time-course measurements at fixed wavelengths (λ_{max}=410 nm), spectrophotometric titrations were performed with a cyclic *pseudo*-peptide concentration of 1 mM ($MeOH_{dry}$). $Cu^{II}(CF_3SO_3)_2$ (25 mM, $MeOH_{dry}$) and base (*n*-Bu_4N)(OMe) (25 mM, $MeOH_{dry}$) were added to different pH samples (ligand : metal : base ratio of 1 : 2 : 2). The final concentrations of the dicopper(II) complexes of H_4pat^1 and H_4pat^2 in the cuvette were 40 µM. All solutions were degassed and kept under argon at 7°C. Blank tests, the autohydrolysis of 4-nitrophenyl-α-*D*-glucopyranoside or 4-nitrophenyl-β-*D*-glucopyranoside respectively, were subtracted from the reported kinetic rates. For the determination of pH dependent reaction velocities the substrate concentration of 30 mM ($MeOH_{dry}$) was chosen. For substrate dependency measurements at constant pH the substrate concentration was varied between 1 – 50 mM.

Table A1. Extinction coefficients of 4-nitrophenolate in a multicomponent buffer (λ_{max}=410 nm).

pH value	Extinction coefficient ε [$M^{-1}cm^{-1}$]
5.636	172 ± 2
5.981	306 ± 10
6.775	1160 ± 90
7.370	5352 ± 50
7.746	7853 ± 133
8.118	12423 ± 159
8.767	16867 ± 1021
9.210	18027 ± 201
9.840	18658 ± 206
10.190	20111 ± 61
10.708	19541 ± 1260
11.362	20495 ± 1191

β-*Lactamase-like activity*

The β-lactamase-like activity was determined by measuring the hydrolysis of nitrocefin. Reaction progress was monitored by observing a decrease of the strong absorbance of nitrocefin at 390 nm over a period of 420 s, whereas during the initial 120 s the equilibrium was reached, which is why these data have not been used for the analysis. As nitrocefin, as well as its hydrolysis product absorb at 390 nm, a corrected extinction coefficient (13415 $M^{-1}cm^{-1}$) was used. UV-Vis-spectra were recorded with a Jasco V-570 spectrophotometer equipped with a Jasco ETC-505T cryostat at 37°C and in a 1 : 1 MeCN:buffer solution. Using time-course measurements at fixed wavelengths (λ_{max}=390 nm), spectrophotometric titrations were performed with a cyclic *pseudo*-peptide concentration of 1 mM ($MeCN_{dry}$). $Cu^{II}(CF_3SO_3)_2$ (25 mM, $MeCN_{dry}$) and base (*n*-Bu_4N)(OMe) (25 mM, $MeCN_{dry}$) were added to different pH samples (ligand : metal : base ratio of 1 : 2 : 2). The final concentrations of dicopper(II) complexes of H_4pat^1 and H_4pat^2 in the cuvette were 5 µM. All solutions were degassed and kept under argon. Blank tests, the autohydrolysis of nitrocefin, were subtracted from the reported kinetic rates. For the determination of pH dependent reaction velocities the substrate concentration of 25 µM was chosen.

Analogous to glycosidase activity measurements, initially the optimum pH range for lactamase activity was determined. The pH-dependence of the catalysis rates were measured in steps of 0.5 pH units or smaller from pH = 9.0 to pH = 12.0. Subsequently MICHAELIS-MENTEN measurements

were carried out at the optimum pH value of 11.5. For substrate dependency measurements at constant pH the substrate concentration was varied between 10 - 50 µM.

Time dependent UV-vis spectra monitoring β-lactamase-like activity were recorded on a J&M Tidas II with the programme *Spectralysis 2.0* using an external cryostat *Q-Blue Wireless Temperature Control* in the range between 300 – 850 nm. These spectra were recorded at 37 °C at pH 11.5 with a nitrocefin concentration of 40 μM and a complex concentration of 5 μM for 20 min at time intervals of Δt=46.7 s (see Figure A1). The resulting spectra were corrected by subtraction the obtained spectrum of the complex.

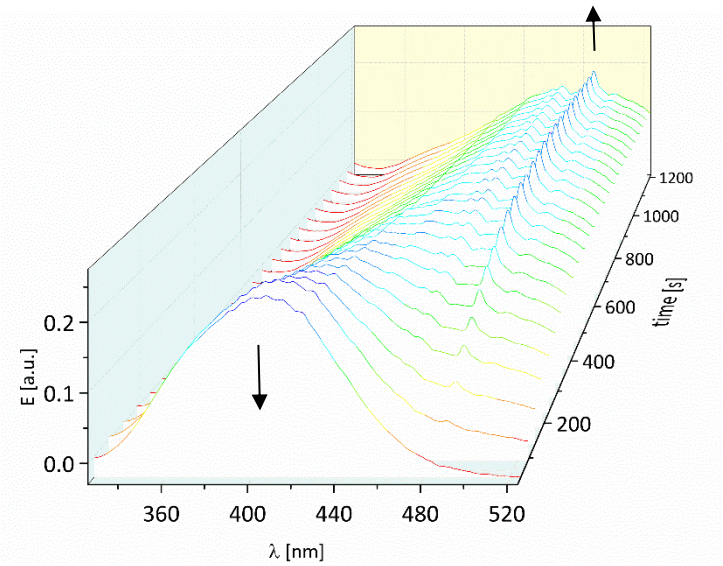

Figure A1. Time course measurement of nitrocefin hydrolysis by $[Cu_2(H_2pat^1)(OH)]^+$. Absorption of nitrocefin at λ_{max}=399 nm decreases upon addition of the catalyst while the absorption of the hydrolysis product at λ_{max}=486 nm increases (pH 10.0, concentrations as in the description).

In vivo hydrolase experiments

β-*Lactamase-like activity*

Three different *Prochloron* samples were prepared:

(I) 10 µL of *Prochloron* (in synthetic sea water, 35 ppt salinity, see Exp. Sec. D, OD_{750}=0.8)

(II) 10 µL of *Prochloron* incubated at room temperature for 15 min with H_4pat^1 (5 µL, 1 mM, final concentration of ligand H_4pat^2 in the cuvette: 5 µM) and

(III) *Prochloron* incubated at room temperature for 15 min with H_4pat^1 (like sample II), with additional 10 µL (1 mM) of cyclam.

Finally, nitrocefin (2.5 µL, 10 mM) was added. All samples were filled to 1 mL by the addition of respective amounts of BG 11 medium (pH 8.2). For the determination of the β-lactamase-like activity the hydrolysis of nitrocefin was measured, *i.e.* the increase of the strong absorbance of

the hydrolysis product of nitrocefin at 496 nm (20,500 $M^{-1}cm^{-1}$) was monitored over a period of 420 s, while the data of the initial 120 s were not used, as the equilibrium was reached during that time. Usually the decrease of the band of nitrocefin at 390 nm is monitored, but since the chlorophylls contained in *Prochloron*, show a strong absorption in that region, the increase of the hydrolysis product was chosen instead (λ_{max}=496 nm). UV-vis-spectra data were recorded with a Jasco V-570 spectrophotometer equipped with a Jasco ETC-505T cryostat at 25°C and in a MeCN/buffer solution (1 : 1 v/v). Using time-course measurements at fixed wavelengths (λ_{max}=496 nm), spectrophotometric titrations were performed. Hydrolysis measurements were recorded in triplicates. Blank tests (the autohydrolysis of nitrocefin) were measured in duplicates and subtracted from the reported kinetic rates. For the determination of pH-dependent reaction velocities the substrate concentration of 25 µM was chosen. Subsequently MICHAELIS-MENTEN measurements were carried out at pH 8.2. For substrate dependency measurements at constant pH the substrate concentration was varied between 10 – 50 µM.

Phosphatase-like activity

Three different *Prochloron* samples were prepared:

(I) 1 µL of *Prochloron* (in artificial sea water, 35 ppt salinity, see Exp. Sec. D, OD_{750}=0.06)

(II) 1 µL of *Prochloron* incubated at room temperature for 15 min with H_4pat^1 (2 µL, 100 µM, final concentration of ligand H_4pat^1 in the cuvette: 1 µM) and

(III) *Prochloron* incubated at room temperature for 15 min with H_4pat^1 (like sample II), with additional 4 µL (100 µM) of cyclam.

The phosphatase-like activity was determined using the Amplite Fluorimetric Alkaline Phosphatase Assay Kit (AAT Bioquest, Inc.) with SunRed substrate (added to 200 µL). All measurements were carried out in triplicates and blanks (duplicates) were subtracted from the data. The pH was kept at 8.7 using the prepared buffer from the Kit. The respective fluorescence emission measurements were performed on a Horiba Fluorolog-3 spectrometer with 3 mm x 3 mm quartz cuvettes.

Statistical analysis

A One-way ANOVA was used for statistical analysis. The required level of significance was defined to be 5 % ($p \geq 0.05$ – not significant (n.s.), $p \leq 05$ – Significant (*), $p \leq 01$ – highly significant (**), $p \leq 0.001$ extremely significant (***)).

B) Details of the syntheses

General procedure for the formation of the oxazole monomer (GP 1)

A flame-dried SCHLENK flask under an atmosphere of argon was charged with a solution of amide (1 eq.) in dry DCM before being cooled to 0°C. Then the required amount of triethylamine (4 eq.), triphenylphosphine (2 eq.) and carbon tetrachloride (2 eq.) were added. After 30 min the reaction mixture was allowed to warm to rt. Stirring was continued for additional five days. The solvent was removed under reduced pressure, the residue was dissolved in ethyl acetate, and then washed with saturated sodium hydrogen carbonate solution and brine. The combined organic layers were dried over Na_2SO_4. The solvent was concentrated under reduced pressure. The reaction mixture was purified by column chromatography over silica gel (PE:EE 3:1 v/v).

General procedure 2 (GP 2) - cleavage of the methyl group

The required amount of the protected compound (1 eq.) was dissolved in a mixture consisting of methanol/dioxane (10:7; resulting in a 0.08 M solution). Subsequently NaOH solution (2M, 10 eq.) was added dropwise at 0 °C and the reaction mixture was allowed to warm up to rt. Stirring was continued until TLC showed the consumption of all starting material. Then brine, HCl (1M) and DCM were added. The combined aqueous layers were repeatedly extracted with DCM. The combined organic layers were dried over Na_2SO_4. The solvent was concentrated under reduced pressure to yield the free acid. Remaining dioxane was removed through repetitive stripping with ethyl acetate.

General procedure 3 (GP 3) - cleavage of the Boc group

The required amount of the protected compound (1 eq.) was dissolved in ethyl acetate (resulting in a 0.1M solution). The solution was cooled to 0°C and TFA (3 mL/mmol starting material) was added dropwise. After 30 min the reaction mixture was allowed to warm to rt. Stirring was continued for additional three hours. The reaction mixture was concentrated under reduced pressure to provide a quantitative yield of the trifluoroacetate salt. Remaining solvent and TFA was removed through repetitive stripping with ethyl acetate.

General procedure 4 (GP 4) - peptide bond formation

The required amount of acid monomer building block (1 eq.) was dissolved in dry DMF at rt. Afterwards EDIPA (3 eq.) was added dropwise and the solution was cooled to 0°C and COMU (0.98 eq.) was added. The ice bath was removed, allowing the reaction solution to warm to rt again and stirring was continued for additional one hour. The required amount of basic monomer building block (1 eq.) was added and the reaction mixture was stirred for at least 4 days. Consumption of the starting material was monitored by TLC. After complete conversion, the reaction mixture was diluted with ethyl acetate and washed with HCl (1M), saturated $NaHCO_3$ solution and brine. The combined organic layers were dried over $MgSO_4$. The solvent was removed under reduced pressure.

Cyclic *pseudo*-octapeptide H_4pat[1]

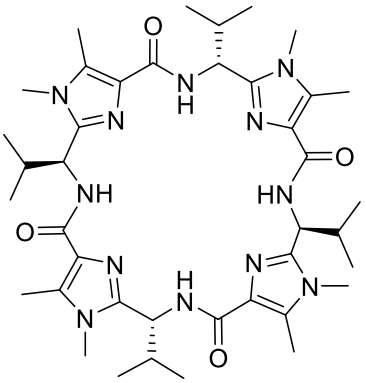

According to **GP 4** the dimeric building block 2-((*R*)-1-(2-((*S*)-1-amino-2-methylpropyl)-1,5-dimethyl-1H-imidazole-4-carboxamido)-2-methylpropyl)-1,5-dimethyl-1H-imidazole-4-carboxylic acid (336 mg, 0.670 mmol, 1 eq.) was dissolved in 50 mL of dry DMF, EDIPA (431 mg, 0.582 mL, 3.35 mmol, 5 eq.) and COMU (0.281 g, 0.657 mmol, 0.98 eq.) were added. The completion of the reaction was monitored by TLC, work up was carried out after seven days and delivered 186 mg (0.241 mmol, 36%) as a pale yellow powder.

^{1}H-NMR (600 MHz, MeOH-d_4) δ = 0.89 (d, 3H, *J* = 6.9 Hz, CHC**H**$_3$); 0.92 (d, 3H, *J* = 6.7 Hz, CHC**H**$_3$); 2.03-2.18 (m, 1H, C**H**$(CH_3)_2$); 2.54 (s, 3H, C_{het}C**H**$_3$); 3.56 (s, 3H, NC**H**$_3$); 5.16 (m, 1H, C_α**H**); 8.20 (d, 1H, *J* = 9.6 Hz, N**H**) ppm.

^{13}C-NMR (151 MHz, MeOH-d_4) δ = 10.10, 10.58 (Imi-C-**C**H_3); 18.41, 19.40, 20.01, 20.34 (CH(**C**$H_3)_2$); 30.11, 30.62 (**C**$H(CH_3)_2$); 32.12, 33.32 (Val-Imi-N-**C**H_3); 50.63, 50.97 **C**$_\alpha$H (Val-Imi); 132.18 (**C**$_{het}$CONH); 135.42, 135.67 (**C**$_{het}NCH_3$); 148.19, 148.74 (**C**$_{Azol}$); 164.31 (**C**ONH) ppm.

HR (+) ESI MS m/z calcd. for [MH^+] 773.4939, found 773.4925.

Cyclic *pseudo*-octapeptide H_4pat^2

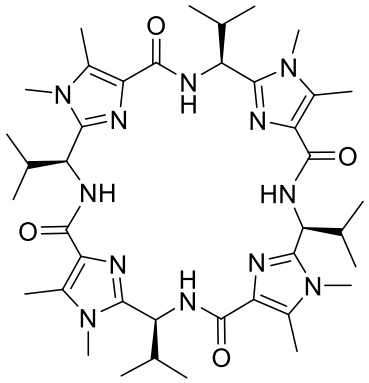

According to **GP 4** the dimeric building block 2-((*S*)-1-(2-((*S*)-1-amino-2-methylpropyl)-1,5-dimethyl-1H-imidazole-4-carboxamido)-2-methylpropyl)-1,5-dimethyl-1H-imidazole-4-carboxylic acid (1.52 g, 3.76 mmol, 1 eq.) was dissolved in 75 mL of dry DMF, EDIPA (1.458 g, 1.965 mL, 11.28 mmol, 3 eq.) and COMU (1.576 g, 3.68 mmol, 0.98 eq.) were added. The completion of the reaction was monitored by TLC, work up was carried out after five days and delivered 560 mg (0.725 mmol, 19%) as a pale yellow powder.

^{1}H-NMR (600 MHz, MeOH-d_4) δ = 0.87 (d, 3H, *J* = 6.7 Hz, CHC**H**$_3$); 1.11 (d, 3H, *J* = 6.7 Hz, CHC**H**$_3$); 2.21 – 2.35 (m, 1H, C**H**$(CH_3)_2$); 2.48 (s, 3H, C_{het}C**H**$_3$); 3.61 (s, 3H, NC**H**$_3$); 4.97 (m, 1H, C_α**H**); 7.81 (d, 1H, *J* = 9.6 Hz, N**H**) ppm.

^{13}C-NMR (151 MHz, MeOH-d_4) δ = 10.34 (Imi-C-**C**H_3); 19.58, 20.06 (CH(**C**$H_3)_2$); 30.13 (Val-Imi-N-**C**H_3); 33.07 (**C**$H(CH_3)_2$); 50.29 **C**$_\alpha$H (Val-Imi); 129.70 (**C**$_{het}$CONH); 132.10 (**C**$_{het}$NCH_3); 149.21 (**C**$_{Azol}$); 162.91 (**C**ONH) ppm.

HR (+) ESI MS m/z calcd. for [MH^+] 773.4339, found 773.4328.

Synthesis of H_4pat[4]

Methyl 2-((*S*)-1-(*tert*-butoxycarbonylamino)-2-methylpropyl)-5-methyl-oxazole-4-carboxylate **(1)**

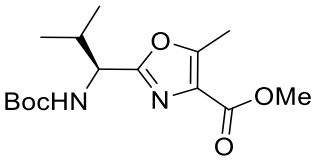

According to **GP 1** 2.0 g (6.05 mmol; 1 eq.) of Methyl-2-((*S*)-(*tert*-butoxycarbonylamino)-3-methylbutanamido)-3-oxobutanoate, 3.4 mL (24.22 mmol; 4 eq.) of triethylamine, 3.2 g (12.11 mmol; 2 eq.) of triphenylphosphine and 1.2 mL (12.11 mmol; 2 eq.) of carbon tetrachloride were dissolved in 125 mL dry DCM. Purification by column chromatography (petrol ether and ethyl acetate 3:1 v/v) afforded 1.27 g (4.07 mmol; 67 %) of **1** as a pale yellow oil.

^{1}H-NMR (200 MHz, $CDCl_3$) δ = 0.91 (d, 3H, *J* = 6.8 Hz, CHC**H**$_3$); 0.94 (d, 3H, *J* = 6.9 Hz, CHC**H**$_3$); 1.45 (s, 9H, C(C**H**$_3$)$_3$); 2.15 – 2.24 (m, 1H, C**H**(CH$_3$)$_2$); 2.63 (s, 3H, C_{het}C**H**$_3$); 3.88 (s, 1H, CO_2C**H**$_3$); 4.72 (m, 1H, C_α**H**); 5.25 (d, 1H, *J* = 9.1 Hz, N**H**) ppm.

(*S*)-2-(1-(*tert*-butoxycarbonylamino)-2-methylpropyl)-5-methyl-oxazole-4-carboxylic acid **(2)**

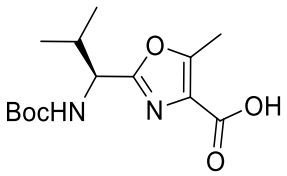

According to **GP 2** 1270 mg (4.07 mmol; 1 eq.) of **1** and 20 mL (10 eq.) of NaOH were dissolved in dioxane/MeOH mixture (51 mL). This gave 863 mg (2.89 mmol; 71%) of **2** as a pale yellow oil.

^{1}H-NMR (200 MHz, $CDCl_3$) δ = 0.92 (d, 3H, *J* = 6.9 Hz, CHC**H**$_3$); 0.94 (d, 3H, *J* = 6.9 Hz, CHC**H**$_3$); 1.41 (s, 9H, C(C**H**$_3$)$_3$); 2.11 – 2.26 (m, 1H, C**H**(CH$_3$)$_2$); 2.64 (s, 3H, C_{het}C**H**$_3$); 4.74 (m, 1H, C_α**H**); 5.94 (d, 1H, *J* = 9.1 Hz, N**H**) ppm.

Methyl 2-((*R*)-1-(*tert*-butoxycarbonylamino)-2-methylpropyl)-5-methyl-oxazole-4-carboxylate **(3)**

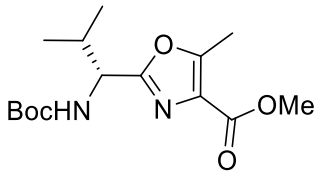

According to **GP 1** 2.0 g (6.05 mmol; 1 eq.) of Methyl-2-((*R*)-(*tert*-butoxycarbonylamino)-3-methylbutanamido)-3-oxobutanoate, 3.4 mL (24.22 mmol; 4 eq.) of triethylamine, 3.2 g (12.11 mmol; 2 eq.) of triphenylphosphine and 1.2 mL (12.11 mmol; 2 eq.) of carbon tetrachloride were dissolved in 125 mL dry DCM. This afforded 1.57 g (5.03 mmol; 83 %) of **3** as a pale yellow oil.

^{1}H-NMR (600 MHz, $CDCl_3$) δ = 0.88 (d, 3H, *J* = 6.8 Hz, CHC**H**$_3$); 0.91 (d, 3H, *J* = 6.9 Hz, CHC**H**$_3$); 1.42 (s, 9H, C(C**H**$_3$)$_3$); 2.10 – 2.20 (m, 1H, C**H**$(CH_3)_2$); 2.61 (s, 3H, C_{het}C**H**$_3$); 3.90 (s, 1H, CO_2C**H**$_3$); 4.72 (m, 1H, C_α**H**); 5.25 (d, 1H, *J* = 9.1 Hz, N**H**) ppm.

^{13}C NMR (151 MHz, MeOH-d_4) δ = 12.06 (Imi-C-**C**H_3); 17.95, 18.80 (CH(**C**$H_3)_2$); 28.31 (C(**C**$H_3)_3$); 30.97(CH(**C**$H_3)_2$); 52.06 (CO_2**C**H_3); 79.95 (**C**$(CH_3)_3$); 127.25 (**C**$_{het}$CONH); 155.42 (Imi-**C**-CH_3); 156.53 (**C**O_2-$C(CH_3)_3$); 162.17 (**C**O_2CH_3) ppm.

(+) ESI MS: m/z calcd. for [MH^+] 313.18, found 313.02, calcd. for [MNa^+] 335.16, found 335.09.

(*R*)-1-(4-carboxylate-5-methyl-oxazol-2-yl)-2-methylpropan-1-ammonium trifluoroacetate **(4)**

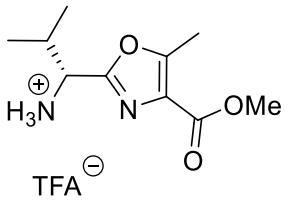

According to **GP 3** 1.57 g (5.03 mmol; 1 eq.) of **3** and 15.1 mL TFA were dissolved in 50 mL ethyl acetate. This yielded 1.64 g (5.04 mmol, quantitative) of **4** as a pale yellow oil.

^{1}H-NMR (600 MHz, MeOH-d_4) δ = 1.02 (d, 3H, *J* = 6.9 Hz, CHC**H**$_3$); 1.14 (d, 3H, *J* = 6.9 Hz, CHC**H**$_3$); 2.38 – 2.52 (m, 1H, C**H**$(CH_3)_2$); 2.59 (s, 3H, C_{het}C**H**$_3$); 3.90 (s, 1H, CO_2C**H**$_3$); 4.38-4.52 (m, 1H, C_α**H**); 8.97 (m, 3H, N**H**$_3$) ppm.

^{13}C-NMR (151 MHz, MeOH-d_4) δ = 11.92 (Imi-C-**C**H_3); 17.26, 19.47 (CH(**C**$H_3)_2$); 29.31(CH(**C**$H_3)_2$); 51.15 (CO_2**C**H_3); 127.40 (**C**$_{het}$CONH); 157.37 (Imi-**C**-CH_3); 162.25 (**C**O_2CH_3) ppm.

(+) ESI MS m/z calcd. for [MH^+] 213.12, found 213.01.

Methyl 2-((*R*)-1-((*S*)-1-(1-(*tert*-butoxycarbonylamino)-2-methylpropyl)-5-methyloxazole-4-carboxamido)-2-methylpropyl)-oxazole-4-carboxylate **(5)**

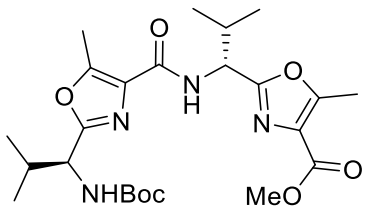

According to **GP 4** 0.75 g (2.51 mmol; 1 eq.) of **2**, 1.09 g (3.27 mmol; 1.3 eq.) of **4**, 1.06 g (2.46 mmol; 0.98 eq.) of COMU and 1.31 mL (7.54 mmol; 3 eq.) of EDIPA were dissolved in 150 mL dry DMF and stirred for 17 days. This yielded 1.08 g (2.19 mmol; 87%) of **5** as a pale yellow oil.

^{1}H-NMR (200 MHz, $CDCl_3$) δ = 0.94 (d, 3H, *J* = 6.9 Hz, CHC**H**$_3$); 0.95 (d, 3H, *J* = 6.9 Hz, CHC**H**$_3$); 0.96 (d, 3H, *J* = 6.8 Hz, CHC**H**$_3$); 1.00 (d, 3H, *J* = 6.9 Hz, CHC**H**$_3$); 1.46 (s, 9H, C(C**H**$_3$)$_3$); 2.08 – 2.21 (m, 1H, C**H**(CH$_3$)$_2$); 2.23 – 2.37 (m, 1H, C**H**(CH$_3$)$_2$); 2.59 (s, 3H, C_{het}C**H**$_3$); 2.61 (s, 3H, C_{het}C**H**$_3$); 3.90 (s, 1H, CO_2C**H**$_3$); 4.68 (m, 1H, C_α**H**); 5.13 (m, 1H, C_α**H**); 7.41 (d, 1H, *J* = 9.5 Hz, N**H**) ppm.
(+) ESI MS m/z calcd. for [MNa$^+$] 515.25, found 515.13.

Methyl 2-((*R*)-1-(1-((*S*)-1-(*tert*-butoxycarbonylamino)-2-methylpropyl)-5-methyloxazole-4-carboxamido)-2-methylpropyl)-oxazole-4-carboxylic acid **(6)**

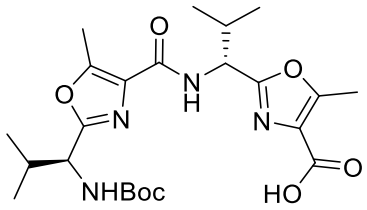

According to **GP 2** 1.08 g (2.19 mmol; 1 eq.) of **5** and 30 mL of NaOH (aqueous, 2M, 30 eq.) were dissolved in dioxane/MeOH mixture (51 mL). This afforded 0.66 g (1.37 mmol; 63 %) of **6** as a pale yellow oil.

^{1}H-NMR (200 MHz, $CDCl_3$) δ = 0.88 (d, 3H, *J* = 6.9 Hz, CHC**H**$_3$); 0.92 (d, 3H, *J* = 6.9 Hz, CHC**H**$_3$); 0.96 (d, 3H, *J* = 6.8 Hz, CHC**H**$_3$); 1.00 (d, 3H, *J* = 6.9 Hz, CHC**H**$_3$); 1.46 (s, 9H, C(C**H**$_3$)$_3$); 2.08 – 2.21 (m, 1H, C**H**(CH$_3$)$_2$); 2.23 – 2.37 (m, 1H, C**H**(CH$_3$)$_2$); 2.59 (s, 3H, C_{het}C**H**$_3$); 2.61 (s, 3H, C_{het}C**H**$_3$); 4.69 (m, 1H, C_α**H**); 5.14 (m, 1H, C_α**H**); 7.43 (d, 1H, *J* = 9.7 Hz, N**H**) ppm.

Methyl 2-((*R*)-1-(1-((*S*)-2-methylpropyl-1-ammonium fluoroacetate)-5-methyl-oxazol-2-yl-4-carboxamido)-2-methylpropyl)-oxazole-4-carboxylic acid **(7)**

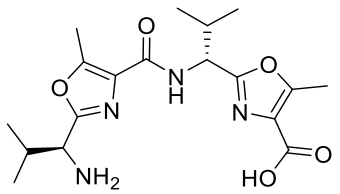

According to **GP 3** 0.66 g (1.37 mmol; 1 eq,) of **6** and 4.1 mL TFA were dissolved in ethyl acetate (20 mL). A quantitative yield was obtained 0.68 g (1.37 mmol; quantitative) of **7** as a pale yellow solid.

^{1}H-NMR (200 MHz, $CDCl_3$) δ = 0.89 (d, 3H, *J* = 6.9 Hz, CHC**H**$_3$); 0.92 (d, 3H, *J* = 6.9 Hz, CHC**H**$_3$); 0.95 (d, 3H, *J* = 6.8 Hz, CHC**H**$_3$); 1.01 (d, 3H, *J* = 6.9 Hz, CHC**H**$_3$); 2.09 – 2.20 (m, 1H, C**H**$(CH_3)_2$); 2.24 – 2.36 (m, 1H, C**H**$(CH_3)_2$); 2.59 (s, 3H, C_{het}C**H**$_3$); 2.61 (s, 3H, C_{het}C**H**$_3$); 4.67 (m, 1H, C_α**H**); 5.12 (m, 1H, C_α**H**); 7.46 (d, 1H, J = 9.7 Hz, N**H**) ppm.

(+) ESI MS m/z calcd. for [M^-] 377.18, found 377.49.

Cyclic *pseudo*-octapeptide H_4pat[4]

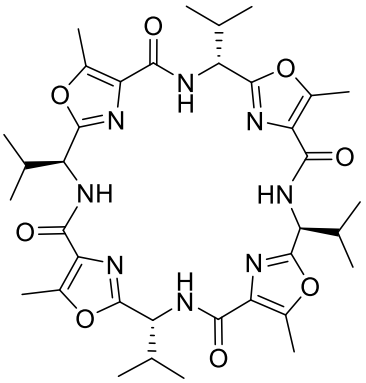

According to **GP 4** 0.68 g (2.26 mmol; 1 eq.) of **7**, 0.95 g (2.22 mmol; 0.98 eq.) of COMU and 1.18 mL (6.78 mmol; 3 eq.) of EDIPA were dissolved in 150 mL dry DMF. Work up and subsequent column chromatography (PE:EE 2:1) yielded 582 mg (37%) of the desired product as a white powder.

^{1}H-NMR (600 MHz, $CDCl_3$) δ = 0.91 (d, 3H, *J* = 6.9 Hz, CHC**H**$_3$); 0.95 (d, 3H, *J* = 6.9 Hz, CHC**H**$_3$), 2.25-2.32 (m, 1H, C**H**$(CH_3)_2$); 2.56-2.62 (m, 1H, C**H**$(CH_3)_2$); 2.65 (s, 3H, C_{het}C**H**$_3$); 5.28 (m, 1H, C_α**H**); 8.09 (d, 1H *J* = 9.6 Hz, N**H**) ppm.

^{13}C NMR (151 MHz, MeOH-d_4) δ = 14.17, 16.82 (Val-Imi-C-**C**H_3); 20.40, 21.53 CH(C**H**$_3)_2$; 36.96 (**C**$H(CH_3)_2$); 55.56 (**C**$_\alpha$H); 132.03 (**C**$_{het}$CONH) (**C**$_{het}$$NCH_3$); 158.29 (**C**$_{Azol}$); 165.01, 165.52 (**C**ONH) ppm.

HR (+) ESI MS m/z calcd. for [MNa^+] 743.35, found 743.35.

$[Cu_2pat^4(OH)]^-$

20 µL of a methanolic solution of H_4pat^4 were treated with 2 eq. of (*n*-Butyl)$_4$N(OMe) in MeOH and 2 eq. of Cu(OTf)$_2$, which gave a blue solution.

HR (-) FAB MS m/z calcd. for $[Cu_2pat^4(OH)]^-$ ($C_{36}H_{45}Cu_2N_8O_9^-$) 859.1907, found 859.1903 (Int.: 8x10^6, 47.4%)

Experimental:

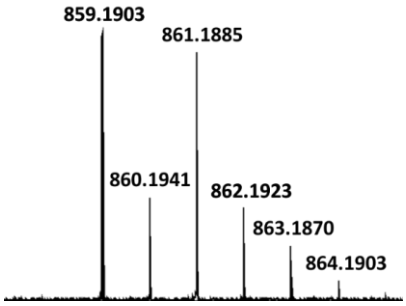

Simulated:

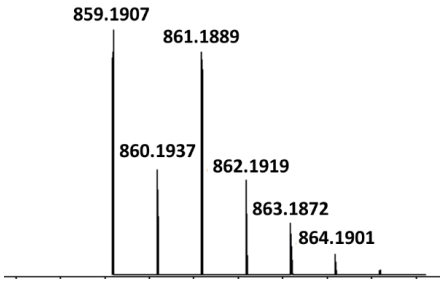

Cyclic *pseudo*-octapeptide H_4pat[5]

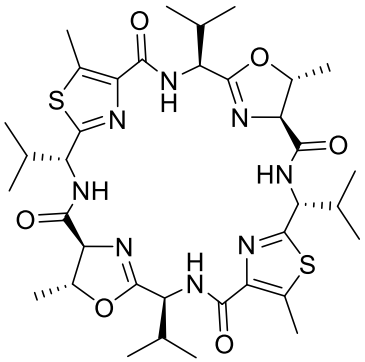

According to **GP 4** the dimeric building block (4*S*,5*R*)-2-((*S*)-1-(2-((*R*)-1-amino-2-methylpropyl)-5-methylthiazole-4-carboxamido)-2-methylpropyl)-5-methyl-4,5-dihydrooxazole-4-carboxylic acid (320 mg, 0.647 mmol, 1 eq.) was dissolved in 40 mL of dry DMF, EDIPA (251 mg, 0.337 mL, 1.941 mmol, 3 eq.) and COMU (0.271 g, 0.634 mmol, 0.98 eq.) were added. The completion of the reaction was monitored by TLC, work up was carried out after six days and delivered 142 mg (0.167mmol, 26%) as a pale yellow powder.

^{1}H-NMR (600 MHz, MeOH-d_4) δ = 0.78 (d, 3H, *J* = 6.9 Hz, CHC**H**$_3$); 0.92 (d, 3H, *J* = 6.6 Hz, CHC**H**$_3$); 0.97 (d, 3H, *J* = 6.8 Hz, CHC**H**$_3$); 0.99 (d, 6H, *J* = 6.9 Hz, C_{oxa}HC**H**$_3$); 1.04 (d, 3H, *J* = 6.9 Hz, CHC**H**$_3$); 2.17 – 2.29 (m, 2H, C**H**$(CH_3)_2$); 2.54 (s, 3H, $C_{thia}CH_3$); 4.02 (d, 1H, *J* = 6.3 Hz, C_{oxa}**H**CH_3); 4.78 – 4.82 (m, 1H, C_{oxa}**H**CH_3); 5.02 (d, 3H, *J* = 8.7 Hz); 5.24 (dd, 1H, *J* = 9.7, 8.2 Hz, C**H**C_{thia}); 7.61 (d, *J* = 9.7 Hz, N**H**); 8.63 (d, 1H, *J* = 8.2 Hz, N**H**) ppm.

^{13}C-NMR (151 MHz, MeOH-d_4) δ = 11.92 (C_{thia}**C**H_3); 18.42, 19,21, 19.47, 19.52 (CH(**C**$H_3)_2$); 21.87 (C_{oxa}H**C**H_3); 31.82, 33.21 (**C**H$(CH_3)_2$); 52.19 (**C**HC_{oxa}); 54.51 (**C**HC_{thia}); 74.21 (**C**$_{oxa}$HCO); 82.33 (**C**$_{oxa}$HCH_3); 140.85 (**C**$_{thia}CH_3$); 143.59 (**C**$_{thia}$CO); 161.42 (CH**C**$_{oxa}$); 164.02 (CH**C**$_{thia}$); 169.19 (C_{thia}**C**ONH), 171.21 (C_{oxa}H**C**ONH) ppm.

HR (+) ESI MS m/z calcd. for [MH^+] 757.9900, found 757.9972.

$[Cu_2pat^5(OH)]^-$

20 µL of a methanolic solution of H_4pat^5 were treated with 2 eq. of (*n*-Butyl)$_4$N(OMe) in MeOH and 2 eq. of $Cu(OTf)_2$, which gave a blue solution.

HR (-) FAB MS m/z calcd. for $[Cu_2pat^5(OH)]^-$ ($C_{36}H_{49}Cu_2N_8O_7S_2^-$) 895.1764, found 895.1763 (Int.: 2x10^6, 8.5%)
HR (-) FAB MS m/z calcd. for $[Cu_2pat^5(OMe)]^-$ ($C_{37}H_{51}Cu_2N_8O_7S_2^-$) 909.1921, found 909.1920 (Int.:3x10^6, 12.0%)

Experimental:

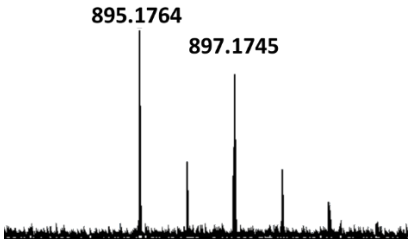

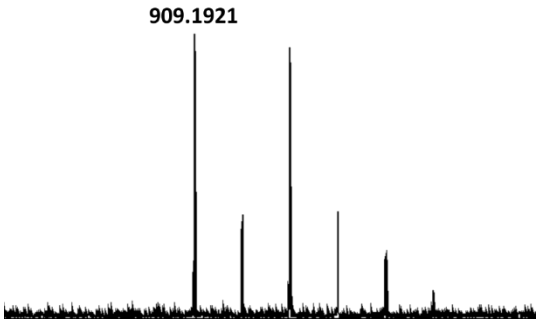

Simulated:

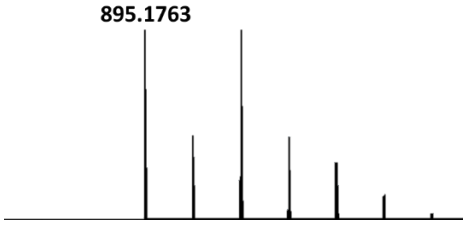

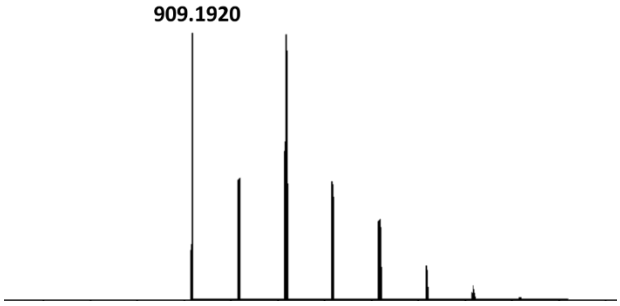

Synthesis of H_4pat-Atto550 and H_4pat-Reporter Group

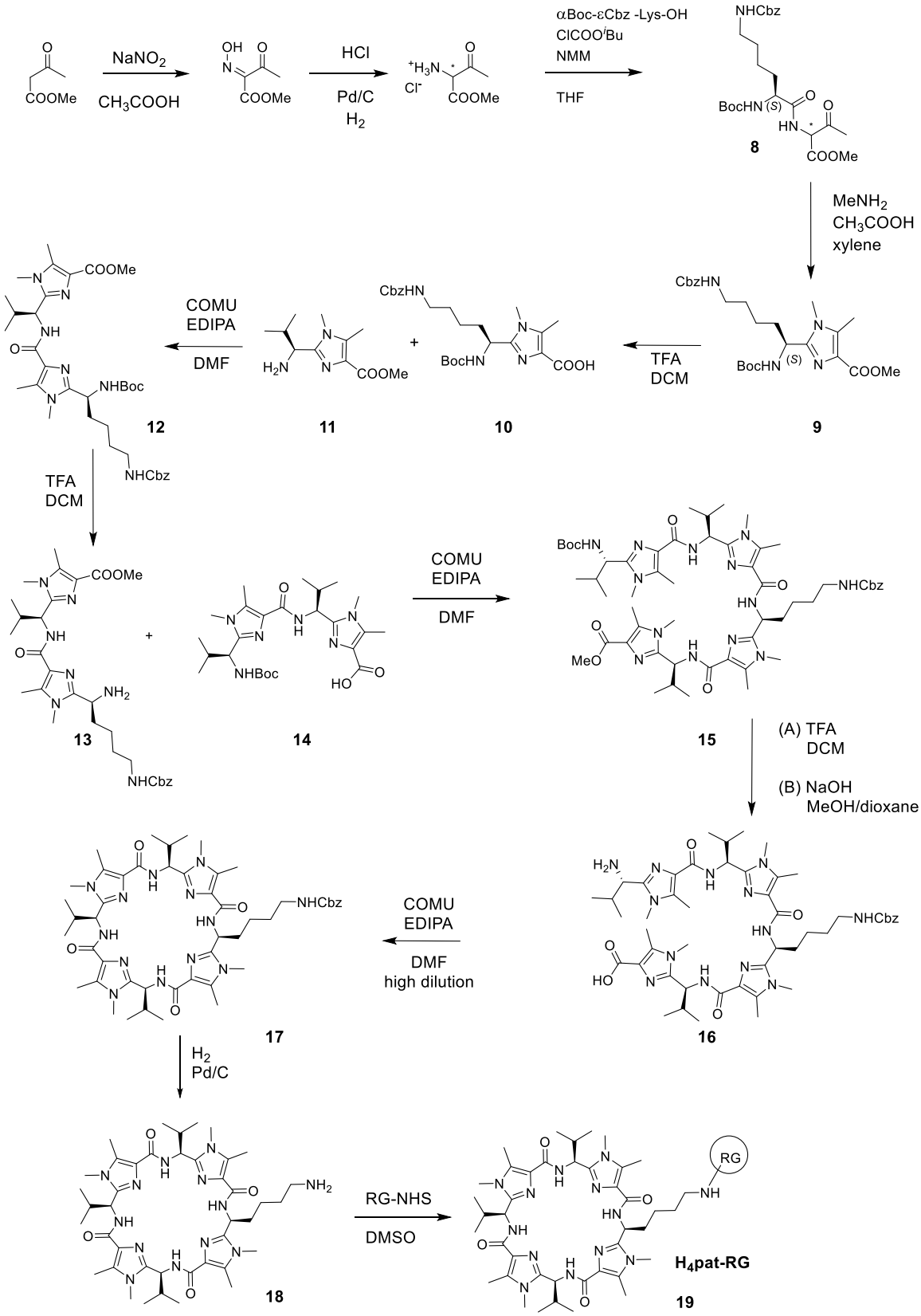

Scheme B1. Schematic synthesis of H_4pat-RG (**19**), the syntheses of **11** and **14** are omitted for clarity and were accomplished analogously as described by HABERHAUER *et al.*[62] RG: A: Atto550 or B: Proxyl.

Methyl2-((*S*)-6-(((benzyloxy)carbonyl)amino)-2-((*tert*-butoxycarbonyl)amino)hexanamido)-3-oxobutanoate **(8)**

The reaction was accomplished corresponding to literature procedures for similar compounds.[62]

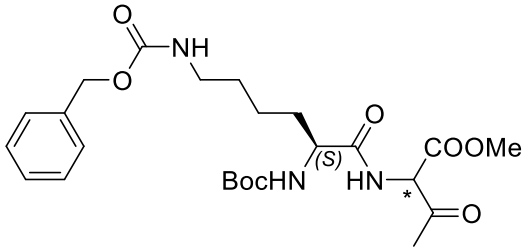

N-Boc-*N'*-Cbz-*S*-lysine (3.1 g, 12.4 mmol, 1 eq.) was dissolved in THF (90 mL) and N-methylmorpholine (2.7 mL, 2.5 g, 24.8 mmol, 2 eq.) was added. The reaction mixture was cooled to -30°C. *Iso*-butylchloroformate (4.9 mL, 5.1 g, 37.1 mmol, 1 eq.) was added to the reaction mixture, which was subsequently stirred for 1h at -30°C. 1-methoxy-1,3-dioxobutan-2-ammoniumchloride (3.0 g, 12.4 mmol, 1 eq.) was added and the reaction mixture was stirred for 6 h at -30°C, then allowed to warm to room temperature and stirred overnight. The solvent was evaporated and the residue was dissolved in EtOAc. The solution was washed with water and saturated NaCl solution, and finally dried over Na_2SO_4. Evaporation of the solvent delivered the crude product, which was purified by flash column chromatography with PE:EE (1:1 v/v) as eluent to yield a colourless oil (5.1 g, 85 %)

^{1}H-NMR (600 MHz, $CDCl_3$) δ = 1.35-1.41 (m, 2H, O-C**H$_2$** -Ph (Cbz)); 1.41 (s, 9H, C(C**H**$_3$)$_3$); 1.44-1.53 (m, 2H, Cbz-NH-CH$_2$-C**H$_2$**-(CH$_2$)$_2$-); 1.60-1.67 (m, 1H, Cbz-NH-(CH$_2$)$_3$-C**H**$_2$-); 1.76-1.84 (m, 1H, Cbz-NH-(CH$_2$)$_3$-C**H**$_2$-); 2.34 (s, 3H, COC**H$_3$**); 3.07-3.23 (m, 2H, Cbz-NH-C**H$_2$**-(CH$_2$)$_3$-); 3.68 (s, 3H, CO$_2$C**H$_3$**); 4.10-4.20 (m, 1H, Cbz-NH-(CH$_2$)$_4$-C**H**); 4.96-5.03 (bs, 1H, N**H**CH); 5.13-5.27 (m, 2H, Ph-C**H$_2$**); 5.20-5.28 (m, 1H, COCH$_3$-C**H**-CO$_2$Me); 7.26-7.30 (m, 1H, Cbz); 7.33-7.36 (m, 4H, Cbz) ppm.

^{13}C-NMR (151 MHz, $CDCl_3$) δ = 22.23 (Cbz-NH-(CH$_2$)$_2$-**C**H$_2$-); 27.95 (CO**C**H$_3$); 28.29 (C(**C**H$_3$)$_3$); 29.44 (Cbz-NH-(CH$_2$)$_3$-**C**H$_2$-); 31.74 (Cbz-NH-CH$_2$-**C**H$_2$-); 40.34 (Cbz-NH-**C**H$_2$-(CH$_2$)$_3$); 53.35 (Cbz-NH-(CH$_2$)$_4$-**C**H); 54.20 (CO$_2$**C**H$_3$); 62.88 (COCH$_3$-**C**H-CO$_2$Me); 66.62 (Ph-**C**H$_2$); 79.17 (**C**(CH$_3$)$_3$); 128.08 (*o*-**C**, Cbz); 128.14 (*o*-**C**, Cbz); 128.50 (*p*-**C**, Cbz); 128.53 (*m*-**C**, Cbz); 136.63 (*ipso*-**C**, Cbz); 155.73 (**C**O$_2$-C(CH$_3$)$_3$); 156.62 (**C**O$_2$-Bn); 166.41 (**C**O$_2$-CH$_3$); 171.08 (**C**O-NH); 198.23 (CH-**C**OCH$_3$) ppm.

(+) ESI MS m/z calcd. for [MNa$^+$] 516.24, found 516.23.

Microanalysis: calcd. C 58.41%, H 7.15%, N 8.51%, found: 58.04%, 7.02%, 8.63%

Methyl(*S*)-2-(13,13-dimethyl-3,11-dioxo-1-phenyl-2,12-dioxa-4,10-diazatetradecan-9-yl)-1,5-dimethyl-1H-imidazole-4-carboxylate **(9)**

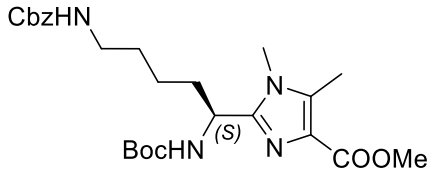

According to literature [62] the substrate **8** (13.0 g, 41.9 mmol, 1 eq.) was dissolved in 500 mL *o*-xylene and glacial acid (23.8 mL, 25.2 g, 419 mmol, 10 eq.) and $MeNH_2$ in EtOH (1.25 M, 18.1 mL, 6.5 g, 210 mmol, 5 eq.) was added. The reaction mixture was stirred for 8 h at 160 °C. The solvent was removed and the residue dissolved in EtOAc. The organic layer was washed with $NaHCO_3$ and brine, then dried over Na_2SO_4 and concentrated. Purification with flash column chromatography (SiO_2, ethyl acetate/petrol ether 2:1 v/v) delivered the desired product as a white solid (9.65 g, 72 %)

^{1}H-NMR (600 MHz, $CDCl_3$) δ = 1.28-1.35 (m, 2H, O-C**H$_2$**-Ph (Cbz)); 1.40 (s, 9H, C(C**H$_3$**)$_3$); 1.42-1.45 (m, 2H, Cbz-NH-CH$_2$-C**H$_2$**-(CH$_2$)$_2$-); 1.86-1.94 (m, 1H, Cbz-NH-(CH$_2$)$_3$-C**H$_2$**-); 1.94-2.00 (m, 1H, Cbz-NH-(CH$_2$)$_3$-C**H$_2$**-); 2.53 (s, 3H, Imi-C-C**H$_3$**); 3.15-3.22 (m, 2H, Cbz-NH-C**H$_2$**-(CH$_2$)$_3$-); 3.57 (s, 3H, Imi-N-C**H$_3$**); 3.86 (s, 3H, CO$_2$C**H$_3$**); 4.80-4.86 (m, 1H, Cbz-NH-(CH$_2$)$_4$-C**H**); 4.91-4.95 (bs, 1H, N**H**CH); 5.06-5.11 (m, 2H, Ph-C**H$_2$**); 7.29-7.33 (m, 1H, Cbz); 7.33-7.38 (m, 4H, Cbz) ppm.

^{13}C-NMR (151 MHz, $CDCl_3$) δ = 10.20 (Lys-Imi-C-**C**H$_3$); 22.71 (Cbz-NH-(CH$_2$)$_2$-**C**H$_2$-); 28.32 (C(**C**H$_3$)$_3$); 29.71 (Cbz-NH-(CH$_2$)$_3$-**C**H$_2$-); 30.30 (Cbz-NH-CH$_2$-**C**H$_2$-); 34.02 (Imi-N-CH$_3$); 40.55 (Cbz-NH-**C**H$_2$-(CH$_2$)$_3$); 53.41 (Cbz-NH-(CH$_2$)$_4$-**C**H); 56.06 (CO$_2$**C**H$_3$); 66.55 (Ph-**C**H$_2$); 79.95 (**C**(CH$_3$)$_3$); 128.07 (*o*-**C**, Cbz); 128.11 (*p*-**C**, Cbz); 128.51 (*m*-**C**, Cbz); 136.68 (*ipso*-**C**, Cbz); 148.12 (Lys-Imi-**C**-CH$_3$); 155.48 (**C**O$_2$-C(CH$_3$)$_3$); 156.46 (**C**O$_2$-Bn); 165.84 (**C**O$_2$CH$_3$) ppm.

(+) ESI MS m/z calcd. for [MH$^+$] 489.26, found 489.21.

(*S*)-2-(13,13-dimethyl-3,11-dioxo-1-phenyl-2,12-dioxa-4,10-diazatetradecan-9-yl)-1,5-dimethyl-1H-imidazole-4-carboxylic acid **(10)**

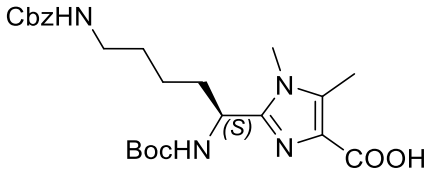

According to **GP 3** 1.27 g (4.07 mmol, 1 eq.) of **9** and 20 mL (10 eq.) of NaOH (2 M, aq) were dissolved in dioxane/MeOH mixture (51 mL). This gave 863 mg (2.89 mmol; 71%) of **10** as a pale yellow oil.

^{1}H-NMR (600 MHz, $CDCl_3$) δ = 1.28-1.35 (m, 2H, O-C**H$_2$** -Ph (Cbz)); 1.40 (s, 9H, C(C**H**$_3$)$_3$); 1.42-1.45 (m, 2H, Cbz-NH-CH$_2$-C**H$_2$**-(CH$_2$)$_2$-); 1.86-1.94 (m, 1H, Cbz-NH-(CH$_2$)$_3$-C**H**$_2$-); 1.94-2.00 (m, 1H, Cbz-NH-(CH$_2$)$_3$-C**H**$_2$-); 2.53 (s, 3H, Imi-C-C**H$_3$**); 3.15-3.22 (m, 2H, Cbz-NH-C**H$_2$**-(CH$_2$)$_3$-); 3.56 (s, 3H, Imi-N-C**H$_3$**); 4.80-4.86 (m, 1H, Cbz-NH-(CH$_2$)$_4$-C**H**); 4.91-4.95 (bs, 1H, N**H**CH); 5.06-5.11 (m, 2H, Ph-C**H$_2$**); 5.11-5.15 (m, 1H, COCH$_3$-C**H**-CO$_2$CH$_3$); 7.29-7.33 (m, 1H, Cbz); 7.33-7.38 (m, 4H, Cbz) ppm.
^{13}C-NMR (151 MHz, $CDCl_3$) δ = 10.21 (Lys-Imi-C-**C**H$_3$); 22.32 (Cbz-NH-(CH$_2$)$_2$-**C**H$_2$-); 28.32 (C(**C**H$_3$)$_3$); 29.18 (Cbz-NH-(CH$_2$)$_3$-**C**H$_2$-); 30.26 (Cbz-NH-CH$_2$-**C**H$_2$-); 33.92 (Lys-Imi-N-CH$_3$); 40.40 (Cbz-NH-**C**H$_2$-(CH$_2$)$_3$); 53.32 (Cbz-NH-(CH$_2$)$_4$-**C**H); 62.88 (COCH$_3$-**C**H-CO$_2$CH$_3$); 66.58 (Ph-**C**H$_2$); 79.80 (**C**(CH$_3$)$_3$); 127.27 (*o*-**C**, Cbz); 128.07 (*p*-**C**, Cbz); 128.50 (*m*-**C**, Cbz); 136.63 (*ipso*-**C**, Cbz); 148.29 (Imi-**C**-CH$_3$); 155.90 (**C**O$_2$-C(CH$_3$)$_3$); 156.70 (**C**O$_2$-Bn); 173.18 (**C**OOH) ppm.
(+) ESI MS m/z calcd. for [MH$^+$] 475.25, found 475.26.

Val-Imi-NH_3^+ TFA^- (11)

2,2,2-trifluoroacetic acid, (*S*)-1-(4-(methoxycarbonyl)-1,5-dimethyl-1H-imidazol-2-yl)-2-methylpropan-1-iminium salt

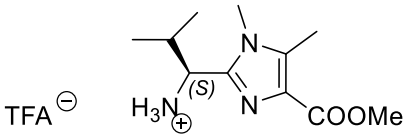

As described in **GP 3** 5.81 g of the monomer building block methyl (*S*)-2-(1-((*tert*-butoxycarbonyl) amino)-2-methylpropyl)-1,5-dimethyl-1H-imidazole-4-carboxylate (15.6 mmol, 1 eq.) and 46 mL TFA were dissolved in 150 mL ethyl acetate. This gave 5.29 g (14.8 mmol, 95%) as a colourless oil.

^{1}H-NMR (600 MHz, $CDCl_3$) δ = 0.84 (d, 3H, *J* = 6.3 Hz, CHC**H**$_3$); 1.08 (d, 3H, *J* = 6.9 Hz, CHC**H**$_3$); 2.32 – 2.43 (m, 1H, C**H**$(CH_3)_2$); 2.46 (s, 3H, C_{het}C**H**$_3$); 3.60 (s, 3H, N_{het}C**H**$_3$); 3.82 (s, 1H, CO_2C**H**$_3$); 4.45-4.58 (m, 1H, C_α**H**) ppm.

Lys(Imi)-Val(Imi) (12)

Methyl2-((*S*)-1-(1,5-dimethyl-2-((*S*)-2,2,14,14-tetramethyl-4,12-dioxo-3,13-dioxa-5,11-diazapentadecan-6-yl)-1H-imidazole-4-carboxamido)-2-methylpropyl)-1,5-dimethyl-1H-imidazole-4-carboxylate

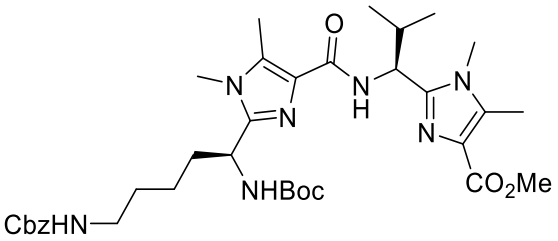

According to **GP 4**, **10** (2.14 g, 4.503 mmol, 1 eq.) was dissolved in 200 mL of dry DMF, EDIPA (2.91 g, 3.92 mL, 22.5 mmol, 5 eq.), COMU (1.89 g, 4.41 mmol, 0.98 eq.) and Val-Imi-NH_2 (**11**, synthesis reported in [62]) (1.53 g, 4.50 mmol, 1 eq.) were added. The completion of the reaction was monitored by TLC, work up was carried out after six days and delivered 1.60 g (2.47 mmol, 55%) as a white powder.

^{1}H-NMR (600 MHz, MeOH-d_4) δ = 0.82 (d, 3H, CH(C**H**$_3$)$_2$, *J* = 6.7 Hz); 1.05 (d, 3H, CH(C**H$_3$**)$_2$, *J* = 6.6 Hz); 1.29-1.35 (m, 2H, Cbz-NH-(CH$_2$)$_2$-C**H$_2$**-CH$_2$); 1.38 (s, 9H, C(C**H$_3$**)$_3$); 1.49-1.57 (m, 2H, Cbz-NH-CH$_2$-C**H$_2$**-(CH$_2$)$_2$-); 1.81-1.88 (m, 1H, Cbz-NH-(CH$_2$)$_3$-C**H$_2$**-); 1.89-1.96 (m, 1H, Cbz-NH-(CH$_2$)$_3$-C**H$_2$**-); 2.06-2.08 (m, 1H, C**H**(CH$_3$)$_2$); 2.46 (s, 3H, Val-Imi-C-C**H$_3$**); 2.49 (s, 3H, Lys-Imi-C-C**H$_3$**); 3.08-3.12 (m, 2H, Cbz-NH-C**H$_2$**-(CH$_2$)$_3$-); 3.51 (bs, 3H, Val-Imi-N-C**H$_3$**); 3.65 (s, 3H, Lys-Imi-N-C**H$_3$**); 3.81 (s, 3H, CO_2C**H$_3$**); 4.67-4.75 (m, 1H, C$_\alpha$**H** Lys-Imi); 5.03 (s, 2H, Ph-C**H$_2$**); 5.06-5.11 (m, 1H, C$_\alpha$**H** Val-Imi); 7.24-7.33 (m, 5H, Cbz) ppm.

^{13}C-NMR (151 MHz, MeOH-d_4) δ = 9.83 (Val-Imi-C-**C**H$_3$); 10.20 (Lys-Imi-C-**C**H$_3$); 19.62, 19.87 (CH(**C**H$_3$)$_2$); 24.67 (Cbz-NH-(CH$_2$)$_2$-**C**H$_2$-); 28.71 (C(**C**H$_3$)$_3$); 30.50 (Cbz-NH-(CH$_2$)$_3$-**C**H$_2$); 31.00 (Cbz-NH-CH$_2$-**C**H$_2$-); 32.92 (Lys-Imi-N-**C**H$_3$); 34.54 (Val-Imi-N-**C**H$_3$); 38.66 (**C**H(CH$_3$)$_2$); 40.48 (Cbz-NH-**C**H$_2$-(CH$_2$)$_3$); 52.15 **C$_\alpha$**H (Val-Imi); 52.22 **C$_\alpha$**H (Lys-Imi); 68.18 (Ph-**C**H$_2$);79.29 (**C**(CH$_3$)$_3$); 125.38 (**C$_{het}$**CO-NH); 126.52 (**C$_{het}$**CO_2CH_3); 128.74 (*o*-**C**, Cbz); 128.94 (*p*-**C**, Cbz); 129.47 (*m*-**C**, Cbz); 131.28 (**C$_{het}$**NCH_3); 132.01 (**C$_{het}$**NCH_3); 135.31 (*ipso*-**C**, Cbz); 152.23 (**C$_{Azol}$**); 152.26 (**C$_{Azol}$**); 153.42 (**C**O$_2$-C(CH$_3$)$_3$); 158.96 (**C**O$_2$-Bn); 161.20 (**C**O$_2$CH$_3$); 164.42 (**C**ONH) ppm.

HR (+) ESI MS m/z calcd. for [MNa$^+$] 704.3748, found 704.3776

NH_2-Lys(Imi)-Val(Imi) (13)

(*S*)-5-((*tert*-butoxycarbonyl)amino)-1-(4-(((*S*)-1-(4-(methoxycarbonyl)-1,5-dimethyl-1H-imidazol-2-yl)-2-methylpropyl)carbamoyl)-1,5-dimethyl-1H-imidazol-2-yl)pentan-1-aminium 2,2,2-trifluoroacetate **(13)**

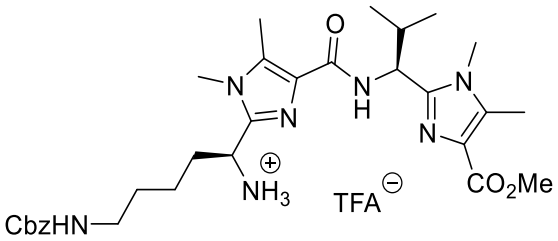

As described in **GP 3**, 1.60 g of **12** (2.47 mmol, 1 eq) and 10 mL TFA were dissolved in 50 mL ethyl acetate. This gave 1.63 g (2.464 mmol, quantitative) as a pale yellow oil.

^{1}H-NMR (600 MHz, MeOH-d_4) δ = 0.84 (d, 3H, CH(C**H**$_3$)$_2$, *J* = 6.7 Hz); 0.97 (d, 3H, CH(C**H**$_3$)$_2$, *J* = 6.5 Hz); 1.24-1.26 (m, 2H, Cbz-NH-(CH$_2$)$_2$-C**H**$_2$-CH$_2$); 1.50-1.59 (m, 2H, Cbz-NH-CH$_2$-C**H**$_2$-(CH$_2$)$_2$-); 1.81-1.88 (m, 1H, Cbz-NH-(CH$_2$)$_3$-C**H**$_2$-); 2.04-2.07 (m, 1H, C**H**(CH$_3$)$_2$); 2.16-2.24 (m, 1H, Cbz-NH-(CH$_2$)$_3$-C**H**$_2$-); 2.49 (s, 3H, Val-Imi-C-C**H**$_3$); 2.64 (s, 3H, Lys-Imi-C-C**H**$_3$); 3.15-3.20 (m, 2H, Cbz-NH-C**H**$_2$-(CH$_2$)$_3$-); 3.63 (bs, 3H, Val-Imi-N-C**H**$_3$); 3.73 (s, 3H, Lys-Imi-N-C**H**$_3$); 3.89 (s, 3H, CO$_2$C**H**$_3$); 4.87-4.94 (m, 1H, C$_\alpha$**H** (Lys-Imi)); 5.07 (s, 2H, Ph-C**H**$_2$); 5.13-5.18 (m, 1H, C$_\alpha$**H** (Val-Imi)); 7.28-7.39 (m, 5H, Cbz) ppm.

^{13}C-NMR (151 MHz, MeOH-d_4) δ = 9.70, 9.92 (Val-Imi-C-**C**H$_3$) / (Lys-Imi-C-**C**H$_3$); 19.42, 19.63 (CH(**C**H$_3$)$_2$);23.05 (Cbz-NH-(CH$_2$)$_2$-**C**H$_2$-); 30.72 (Cbz-NH-(CH$_2$)$_3$-**C**H$_2$-); 32.15 (Cbz-NH-CH$_2$-**C**H$_2$-); 33.37 (Val-Imi-N-**C**H$_3$); 35.34 (Lys-Imi-N-**C**H$_3$); 38.64 (**C**H(CH$_3$)$_2$); 43.99 (Cbz-NH-**C**H$_2$-(CH$_2$)$_3$); 50.98 (CO$_2$**C**H$_3$); 51.82 **C$_\alpha$**H (Val-Imi); 52.25 **C$_\alpha$**H (Lys-Imi); 67.34 (Ph-**C**H$_2$); 125.15 (**C**$_{het}$CO-NH); 125.96 (**C**$_{het}$CO$_2$Me); 128.74 (*o*-**C**, Cbz); 128.98 (*p*-**C**, Cbz); 129.47 (*m*-**C**, Cbz); 132.27 (**C**$_{het}$NCH$_3$); 132.42 (**C**$_{het}$NCH$_3$); 134.28 (*ipso*-**C**, Cbz); 155.88 (**C**$_{Azol}$); 156.19 (**C**$_{Azol}$); 158.78 (**C**O$_2$-Bn); 162.56 (**C**O$_2$CH$_3$); 169.81 (**C**ONH) ppm.

(+) ESI MS m/z calcd. for [MH$^+$] 582.3398, found 582.3402

Val-Imi-Val-Imi-OH (14)

2-((*S*)-1-(2-((*S*)-1-((*tert*-butoxycarbonyl)amino)-2-methylpropyl)-1,5-dimethyl-1H-imidazole-4-carboxamido)-2-methylpropyl)-1,5-dimethyl-1H-imidazole-4-carboxylic acid

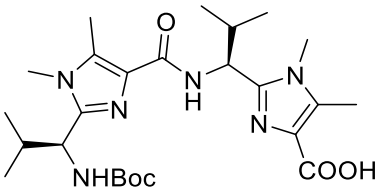

According to **GP 2** 1.2 g (2.41 mmol; 1 eq.) of the dimeric building block methyl 2-((*S*)-1-(2-((*S*)-1-((*tert*-butoxycarbonyl) amino) -2-methyl propyl) -1,5-dimethyl -1H-imidazole-4-carboxamido)-2-methyl propyl) -1,5-dimethyl-1H-imidazole-4-carboxylate and 40 mL of NaOH (aqueous, 2M, 10 eq.) were dissolved in dioxane/MeOH mixture (150 mL). This afforded 850 mg (1.69 mmol; 70 %) of **14** as a pale yellow oil.

^{1}H-NMR (200 MHz, $CDCl_3$) δ = 0.86 (d, 3H, *J* = 6.7 Hz, CHC**H**$_3$); 0.84 (d, 3H, *J* = 6.7 Hz, CHC**H**$_3$); 0.91 (d, 3H, *J* = 6.9 Hz, CHC**H**$_3$); 1.02 (d, 3H, *J* = 6.8 Hz, CHC**H**$_3$); 1.45 (s, 9H, C(C**H**$_3$)$_3$); 2.02 – 2.14 (m, 1H, C**H**$(CH_3)_2$); 2.14 – 2.23 (m, 1H, C**H**$(CH_3)_2$); 2.48 (s, 3H, C_{het}C**H**$_3$); 2.54 (s, 3H, C_{het}C**H**$_3$); 3.51 (s, 3H, C_{het}C**H**$_3$); 3.60 (s, 3H, C_{het}C**H**$_3$); 3.89 (s, 3H, CO_2C**H**$_3$); 4.92 (m, 1H, C_α**H**); 5.19 (m, 1H, C_α**H**) ppm.

Val(Imi)-Val(Imi)-Lys(Imi)-Val(Imi) (15)

Methyl 2-((*S*)-1-(2-((*S*)-5-(((benzyloxy)carbonyl)amino)-1-(2-((*S*)-1-(2-((*S*)-1-((*tert*-butoxycarbonyl)amino)-2-methylpropyl)-1,5-dimethyl-1H-imidazole-4-carboxamido)-2-methylpropyl)-1,5-dimethyl-1H-imidazole-4-carboxamido)pentyl)-1,5-dimethyl-1H-imidazole-4-carboxamido)-2-methylpropyl)-1,5-dimethyl-1H-imidazole-4-carboxylate

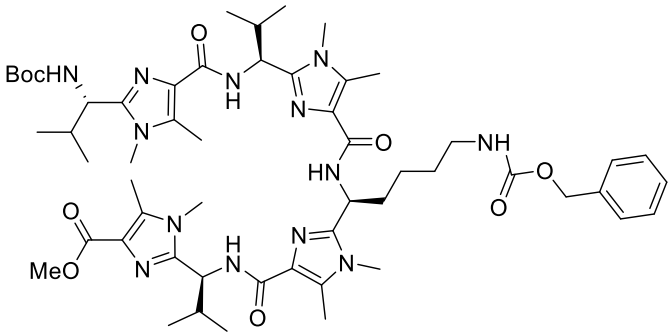

According to **GP 4**, **13** (1.14 g, 1.68 mmol, 1 eq.) was dissolved in 100 mL of dry DMF, EDIPA (1.08 g, 1.46 mL, 8.39 mmol, 5 eq.), COMU (0.70 g, 1.65 mmol, 0.98 eq.) and Val(Imi)-Val(imi)-OH (**14**, synthesis reported in [62]) (0.85 g, 1.68 mmol, 1 eq.) were added. The completion of the reaction was monitored by TLC, work up was carried out after 5 d and delivered 842 mg (0.79 mmol, 48%) as a pale yellow powder.

^{1}H-NMR (600 MHz, MeOH-d_4) δ = 0.78-1.18 (m, 18H, CH(C**H**$_3$)$_2$); 1.23-1.29 (m, 2H, Cbz-NH-(CH$_2$)$_2$-C**H$_2$**-CH$_2$); 1.51-1.60 (m, 2H, Cbz-NH-CH$_2$-C**H$_2$**-(CH$_2$)$_2$-); 1.82-1.96 (m, 1H, Cbz-NH-(CH$_2$)$_3$-C**H$_2$**-); 2.00-2.04 (m, 1H, Cbz-NH-(CH$_2$)$_3$-C**H$_2$**); 2.03-2.15 (m, 3H, C**H**(CH$_3$)$_2$); 2.45, 2.47, 2.52, 2.57 (s, á 3H, Val-Imi-C-C**H$_3$**) / (s, 3H, Lys-Imi-C-C**H$_3$**); 3.06-3.16 (m, 2H, Cbz-NH-C**H$_2$**-(CH$_2$)$_3$-); 3.61, 3.64, 3.66, 3.70 (bs, á 3H, (Val-Imi-N-C**H$_3$**) / (bs, 3H, Lys-Imi-N-C**H$_3$**); 4.65-4.75 (m, 1H, C$_\alpha$**H** (Val-Imi)); 4.94-5.13 (m, 2H, C$_\alpha$**H** (Val-Imi)); 5.13-5.28 (m, 1H, C$_\alpha$**H** (Lys-Imi)); 7.23-7.34 (m, 5H, Cbz) ppm.

(m, 2H, Ph-C**H$_2$**) overlaid by MeOH-d_4

^{13}C-NMR (151 MHz, MeOH-d_4) δ = 9.57, 9.64, 9.68, 10.28 (Val-Imi-C-**C**H$_3$), 18.51, 19.08, 19.18, 19.39, 19.43, 19.74 (CH(**C**H$_3$)$_2$); 23.90 (Cbz-NH-(CH$_2$)$_2$-**C**H$_2$-), 30.95 (Cbz-NH-CH$_2$-**C**H$_2$-), 31.35 (Val-Imi-N-CH$_3$), 32.04 (Lys-Imi-N-CH$_3$), 36.67 (**C**H(CH$_3$)$_2$), 38.35 (Cbz-NH-(CH$_2$)$_3$-**C**H$_2$-), 41.12 (Cbz-NH-**C**H$_2$-(CH$_2$)$_3$), 52.21, 52.30, 52.44, 53.80, **C$_\alpha$**H (Val-Imi), **C$_\alpha$**H (Lys-Imi), 54.29 (CO$_2$**C**H$_3$), 67.36 (Ph-**C**H$_2$), 125.46 (**C**$_{het}$CO-NH), 125.98 (**C**$_{het}$CO$_2$Me), 128.42 (*o*-**C**, Cbz), 128.67 (*p*-**C**, Cbz), 129.19, (*m*-**C**, Cbz), 132.18 (**C**$_{het}$NCH3); 133.18 (**C**$_{het}$NCH3), 135.81 (*ipso*-**C**, Cbz), 154.34 (**C**$_{Azol}$), 154.64 (**C**$_{Azol}$), 157.88 (**C**O$_2$-C(CH$_3$)$_3$), 158.17 (**C**O$_2$-Bn), 162.56 (**C**O$_2$CH$_3$), 169.81(**C**ONH) ppm.

HR (+) ESI MS m/z calcd. for [MNa$^+$] 1090.6178, found 1090.6195.

H_2N-Val(Imi)-Val(Imi)-Lys(Imi)-Val(Imi) (15A)

Methyl 2-((*S*)-1-(2-((*S*)-1-(2-((*S*)-1-(2-((*S*)-1-amino-2-methylpropyl)-1,5-dimethyl-1H-imidazole-4-carboxamido)-2-methylpropyl)-1,5-dimethyl-1H-imidazole-4-carboxamido)-5-(((benzyloxy)carbonyl)amino)pentyl)-1,5-dimethyl-1H-imidazole-4-carboxamido)-2-methylpropyl)-1,5-dimethyl-1H-imidazole-4-carboxylate

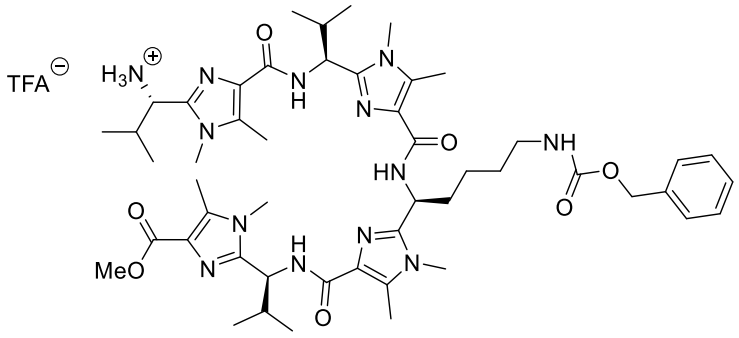

As described in **GP 3**, 1.60 g of **15** (2.47 mmol, 1 eq.) and 10 mL TFA were dissolved in 50 mL ethyl acetate. This gave quantitative yield (1.63 g, 2.464 mmol) as a pale yellow oil.

^{1}H-NMR (600 MHz, MeOH-d_4) δ = 0.80-1.13 (m, 18H, CH(C**H**$_3$)$_2$); 1.34-1.41 (m, 2H, Cbz-NH-(CH$_2$)$_2$-C**H$_2$**-CH$_2$); 1.53-1.64 (m, 2H, Cbz-NH-CH$_2$-C**H$_2$**-(CH$_2$)$_2$-); 1.73-1.95 (m, 1H, Cbz-NH-(CH$_2$)$_3$-C**H$_2$**-); 1.92-2.03 (m, 1H, Cbz-NH-(CH$_2$)$_3$-C**H$_2$**); 2.03-2.19 (m, 3H, C**H**(CH$_3$)$_2$); 2.49, 2.51, 2.55, 2.56 (s, á 3H, Val-Imi-C-C**H$_3$**) / (s, 3H, Lys-Imi-C-C**H$_3$**); 3.10-3.18 (m, 2H, Cbz-NH-C**H$_2$**-(CH$_2$)$_3$-); 3.62, 3.63, 3.68 (bs, á 3H, Val-Imi-N-C**H$_3$**); 3.70 (bs, 3H, Lys-Imi-N- C**H$_3$**); 4.86-4.90 (m, 1H, C$_\alpha$**H** (Val-Imi)); 4.96-5.05 (m, 1H, C$_\alpha$**H** (Lys-Imi)); 5.03-5.09 (m, 2H, C$_\alpha$**H** (Val-Imi); 5.22-5.33 (m, 1H, C$_\alpha$**H** (Lys-Imi)); 7.29.38 (m, 5H, Cbz) ppm. (m, 2H, Ph-C**H$_2$**) overlaid by MeOH-d_4

^{13}C-NMR (151 MHz, MeOH-d_4) δ = 9.43, 9.47, 9.53, 9.57 (Imi-C-**C**H$_3$); 17.35, 18.16, 18.30, 18.92, 19.37, 20.58 (CH(C**H**$_3$)$_2$); 24.16 (Cbz-NH-(CH$_2$)$_2$-**C**H$_2$); 30.70 (Cbz-NH-CH$_2$-**C**H$_2$-); 31.37 31.97, 32. 20, 32.79, (Val-Imi-N-**C**H$_3$) / (Lys-Imi-N-**C**H$_3$); 36.69 (**C**H(CH$_3$)$_2$); 38.36 (Cbz-NH-(CH$_2$)$_3$-**C**H$_2$-); 39.54 (Cbz-NH-(CH$_2$)$_3$-**C**H$_2$-); 51.29 (**C**O$_2$CH$_3$); 52.79, 52.87, 53.02, 53.22 **C$_\alpha$**H (Val-Imi) / (Lys-Imi); 67.03 (Ph-**C**H$_2$); 128.38 (*o*-**C**, Cbz); 128.41 (p-**C**, Cbz); 128.69 (*m*-**C**, Cbz); 129.02, 129.21, 129.24 (**C**$_{het}$CONH); 133.39, 134.74, 134.97, 135.22 (**C**$_{het}$NCH$_3$); 136.48 (*ipso*-**C**, Cbz); 157.51 **C**O$_2$Bn; 159.60, 159.89, 160.15, 160.42 (**C**$_{Azol}$); 164.87 (**C**ONH); 173.01 (**C**O$_2$CH$_3$) ppm.

APCI (+) MS m/z calcd. for [MH$^+$] 968.58, found 968.70.

NH_2-Val(Imi)-Val(Imi)-Lys(Imi)-Val(Imi)-OH (16)

2-((*S*)-1-(2-((*S*)-1-(2-((*S*)-1-(2-((*S*)-1-amino-2-methylpropyl)-1,5-dimethyl-1H-imidazole-4-carboxamido)-2-methylpropyl)-1,5-dimethyl-1H-imidazole-4-carboxamido)-5-(((benzyloxy)carbonyl)amino)pentyl)-1,5-dimethyl-1H-imidazole-4-carboxamido)-2-methylpropyl)-1,5-dimethyl-1H-imidazole-4-carboxylic acid

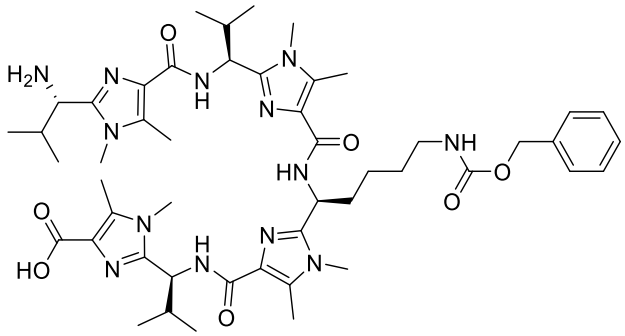

According to **GP 2**, **15B** (1.63 g, 2.464 mmol, 1 eq.) and 20 mL of NaOH (aqueous, 2M, 10 eq.) were stirred in a dioxane/MeOH mixture (100 mL). This yielded 1.60 g (1.676 mmol, 68%) as a white solid.

^{1}H-NMR (600 MHz, MeOH-d_4) δ = 0.80-1.13 (m, 18H, CH(C**H**$_3$)$_2$); 1.34-1.41 (m, 2H, Cbz-NH-(CH$_2$)$_2$-C**H$_2$**-CH$_2$); 1.53-1.64 (m, 2H, Cbz-NH-CH$_2$-C**H$_2$**-(CH$_2$)$_2$-); 1.73-1.95 (m, 1H, Cbz-NH-(CH$_2$)$_3$-C**H$_2$**-); 1.92-2.03 (m, 1H, Cbz-NH-(CH$_2$)$_3$-C**H$_2$**-); 2.01-2.19 (m, 3H, C**H**(CH$_3$)$_2$); 2.49 (s, 3H, Val-Imi-C-C**H$_3$**); 2.51 (s, 3H, Val-Imi-C-C**H$_3$**); 2.55 (s, 3H, Val-Imi-C-C**H$_3$**); 2.56 (s, 3H, Lys-Imi-C-C**H$_3$**); 3.10-3.18 (m, 2H, Cbz-NH-C**H$_2$**-(CH$_2$)$_3$); 3.62, 3.63, 3.68 (bs, 3H, Val-Imi-N-C**H$_3$**); 3.70 (bs, 3H, Lys-Imi-N- C**H$_3$**); 4.86-4.90 (m, 1H, C$_\alpha$**H** (Val-Imi)); 4.96-5.05 (m, 1H, C$_\alpha$**H** (Lys-Imi)); 5.03-5.09 (m, 2H, C$_\alpha$**H** (Val-Imi)); 5.22-5.33 (m, 1H, C$_\alpha$**H** (Lys-Imi)); 7.29.38 (m, 5H, Cbz) ppm.

(m, 2H, Ph-C**H$_2$**) overlaid by MeOH-d_4

^{13}C-NMR (151 MHz, MeOH-d_4) δ = 9.54, 9.59, 9.66, 9.71, (Val-Imi-C-**C**H$_3$) / (Lys-Imi- **C**H$_3$); 18.15, 18.37, 18.57, 18.62, 19.44, 19.49 CH(C**H**$_3$)$_2$; 23.76 (Cbz-NH-(CH$_2$)$_2$-**C**H$_2$); 30.75, 30.84, 31.64, (Val-Imi-N-CH$_3$) ; 33.01, 33.19 (Lys-Imi-N-**C**H$_3$); 36.96 (**C**H(CH$_3$)$_2$); 38.64 (Cbz-NH-(CH$_2$)$_3$-**C**H$_2$-); 39.99 (Cbz-NH-(CH$_2$)$_3$-**C**H$_2$); 50.38, 51.31, 53.56, 53.68 **C$_\alpha$**H (Val-Imi) / (Lys-Imi); 64.99 Bn (Ph-**C**H$_2$); 128.00 (*o*-**C**, Cbz); 128.28 (*p*-**C**, Cbz); 128.71 (*m*-**C**, Cbz); 128.97, 129.36, 129.47 (**C$_{het}$**CONH); 132.68, 132.89, 135.02, 135.63 (**C$_{het}$**NCH$_3$); 136.57 (*ipso*-**C**, Cbz); 153.49, 153.99, 154.58, 154.80 (**C$_{Azol}$**); 156.18 **C**O$_2$Bn, 164.63 (**C**ONH); 178.50 (**C**OOH) ppm.

APCI (+) MS m/z calcd. for [MH$^+$] 954.57, found 954.63.

H_4pat-Cbz (17)

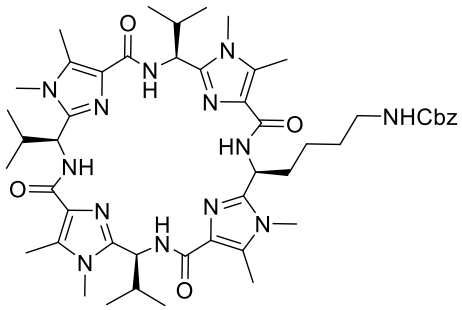

The cyclization of **16** was accomplished applying a high-dilution technique, similar, to the technique described in [259] using two syringe pumps. For that, the linear precursor **16** (551 mg, 0.578 mmol, 1 eq.) was dissolved in 2.5 mL dry DMF and transferred into a syringe (solution 1), similarly 257 mg of COMU (0.600 mmol, 1.04 eq.) were dissolved in 10 mL of dry DMF and transferred into a syringe (solution 2). The solutions were then added to a mixture of 1.5 L of dry DMF and 0.503 mL of EDIPA at a rate of: solution 1: 0.02 mL/h and solution 2: 0.1 mL/h. Upon completion of addition the mixture was stirred for additional 12 h at rt. The reaction mixture was diluted with ethyl acetate and washed with 1 M HCl, saturated $NaHCO_3$ solution and brine. The combined organic layers were dried over $MgSO_4$ and the solvent was removed under reduced pressure. Purification was accomplished by flash column chromatography on a silica column (DCM:EE:MeOH 75:25:2) and gave 147 mg (0.157 mmol, 27%) of **17** as a pale yellow oil.

^{1}H-NMR (600 MHz, MeOH-d_4) δ = 0.89-0.92 (m, 18H, CH(C**H**$_3$)$_2$); 1.31-1.39 (m, 2H, Cbz-NH-(CH$_2$)$_2$-C**H$_2$**-CH$_2$); 1.56-1.63 (m, 2H, Cbz-NH-CH$_2$-C**H$_2$**-(CH$_2$)$_2$-); 1.85-1.89 (m, 1H, Cbz-NH-(CH$_2$)$_3$-C**H$_2$**-); 1.93-1.97 (m, 1H, Cbz-NH-(CH$_2$)$_3$-C**H$_2$**); 2.02-2.09 (m, 3H, C**H**(CH$_3$)$_2$); 2.49-2.51 (m, 9H, Val-Imi-C-C**H$_3$**); 2.75 (s, 3H, Lys-Imi-C-C**H$_3$**); 3.17-3.21 (m, 2H, Cbz-NH-C**H$_2$**-(CH$_2$)$_3$-); 3.58 (bs, 3H, Lys-Imi-N-C**H$_3$**); 3.67 (bs, 9H, Val-Imi-N-C**H$_3$**); 4.93-4.96 (m, 3H, C$_α$**H** (Val-Imi)); 5.03 (s, 2H, Ph-C**H$_2$**); 5.11-5.17 (m, 1H, C$_α$**H** (Lys-Imi)); 7.24-7.33 (m, 5H, Cbz) ppm.

^{13}C-NMR (151 MHz, MeOH-d_4) δ = 9.61 11.15 (Val-Imi-C-**C**H$_3$) / (Lys-Imi-C-**C**H$_3$); 19.20, 19.23, 19.29, 19.57 (CH(C**H**$_3$)$_2$); 23.72 (Cbz-NH-(CH$_2$)$_2$-**C**H$_2$); 29.86, 30.42, 31.36, 31.42 (Val-Imi-N-**C**H$_3$) / (Lys-Imi-N-**C**H$_3$); 36.66 (**C**H(CH$_3$)$_2$); 38.35 (Cbz-NH-(CH$_2$)$_3$-**C**H$_2$-); 40.03 (Cbz-NH-**C**H$_2$-(CH$_2$)$_3$); 50.99, 51.06, 51.16 **C$_α$**H (Val-Imi) / (Lys-Imi); 67.35 (Ph-**C**H$_2$); 128.43 (*o*-**C**, Cbz); 128.63 (*p*-**C**, Cbz); 129.17 (*m*-**C**, Cbz); 130.29 (**C**$_{het}$CONH); 131.11 (**C**$_{het}$NCH$_3$); 132.39 (**C**$_{het}$NCH$_3$); 135.36 (*ipso*-**C**, Cbz); 154.72, 155.35 (**C**$_{Azol}$); 157.68 (**C**O$_2$-Bn); 164.88 (**C**ONH) ppm.

APCI (+) MS m/z calcd. for [MH$^+$] 936.56, found 936.68.

H_4pat-NH_2 (18)

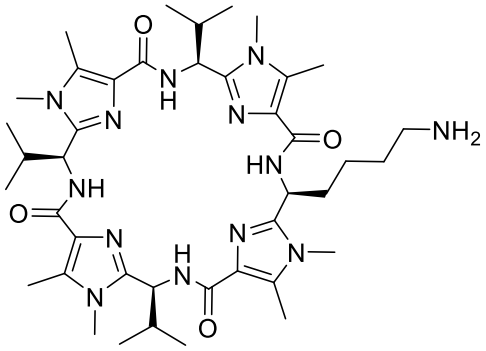

For the deprotection, **17** (100 mg., 0.107 mmol) was dissolved in 50 mL of ethyl acetate. 20 mg of Palladium on carbon (10 wt.% loading, dry basis, matrix activated carbon, wet support) was added and the reaction was refluxed under H_2 atmosphere for 2 h. After the mixture was cooled down, the hydrogen-atmosphere was removed and the reaction mixture was filtered over celite. Removal of the solvent under reduced pressure gave 72 mg (0.090 mmol, 84 %) of a white powder.

^{1}H-NMR (600 MHz, MeOH-d_4) δ = 0.89-0.92 (m, 18H, CH(C**H**$_3$)$_2$); 1.31-1.39 (m, 2H, Cbz-NH-(CH$_2$)$_2$-C**H$_2$**-CH$_2$); 1.56-1.63 (m, 2H, Cbz-NH-CH$_2$-C**H$_2$**-(CH$_2$)$_2$-); 1.85-1.89 (m, 1H, Cbz-NH-(CH$_2$)$_3$-C**H$_2$**-); 1.93-1.97 (m, 1H, Cbz-NH-(CH$_2$)$_3$-C**H$_2$**); 2.02-2.09(m, 3H, C**H**(CH$_3$)$_2$); 2.49-2.51 (m, 9H, Val-Imi-C-C**H$_3$**); 2.75 (s, 3H, Lys-Imi-C-C**H$_3$**); 3.17-3.21 (m, 2H, Cbz-NH-C**H$_2$**-(CH$_2$)$_3$-); 3.58 (bs, 3H, (Lys-Imi-N-C**H$_3$**); 3.67 (bs, 9H, Val-Imi-N-C**H$_3$**); 4.93-4.96 (m, 3H, C$_α$**H** (Val-Imi)); 5.11-5.17 (m, 1H, C$_α$**H** (Lys-Imi)) ppm.
^{13}C-NMR (151 MHz, MeOH-d_4) δ = 9.60, 11.13 (Val-Imi-C-**C**H$_3$) / (Lys-Imi-C-**C**H$_3$); 17.14, 18.06, 18.41, 19.78 (CH(C**H**$_3$)$_2$); 23.72 (Cbz-NH-(CH$_2$)$_2$-**C**H$_2$); 29.11, 29.38, 30.11 33.37 (Val-Imi-N-CH$_3$) / (Lys-Imi-N-CH$_3$); 35.34 (**C**H(CH$_3$)$_2$); 38.64 (Cbz-NH-(CH$_2$)$_3$-**C**H$_2$-); 40.14 (Cbz-NH-**C**H$_2$-(CH$_2$)$_3$); 50.63, 50.97, 51.12 **C$_α$**H (Val-Imi) / (Lys-Imi); 129.85 (**C**$_{het}$CONH); 132.41, 133.55 (**C**$_{het}$NCH$_3$); 154.83, 155.74 (**C**$_{Azol}$); 167.96, 168.01 (**C**ONH) ppm.
APCI (+) MS m/z calcd. for [MH$^+$] 802.52, found 802.30.

H_4pat-Atto550 (19A)

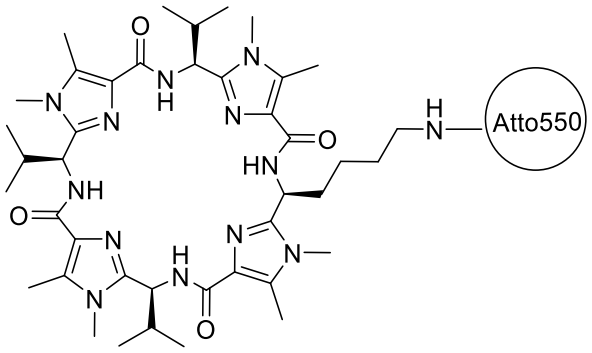

The labelling with the fluorescent tag was achieved by adding 10 µL of a 10 mg/mL solution of **18** in 100 µL DMF and 50 µL EDIPA (excess) to the 20 µL of the NHS-activated fluorescent tag in a 1.5 mL microtube. After shaking the samples mechanically for 30 s the reaction was left to react overnight at rt. After removal of the solvent under reduced pressure, the crude product was dissolved in 100 µL DMSO and purified by RP-HPLC (chromatogram below).

APCI (+) MS m/z calcd. for [MH^+] 1379.32, found 1379.29.

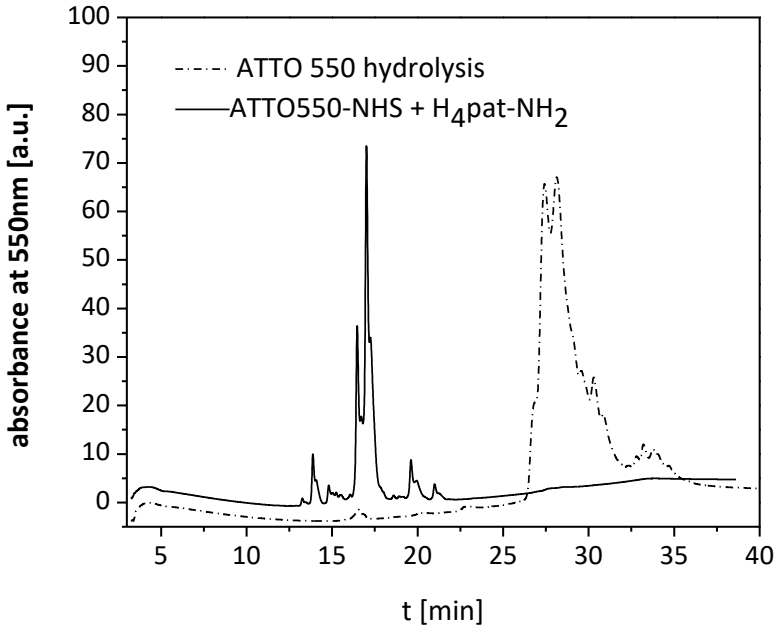

Figure B1. HPLC chromatogram of purification of H_4pat-Atto550.

Proxyl-CH_2-C(=O)-NHS (20)

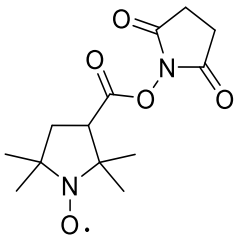

The synthesis of the NHS-activated Proxyl radical was accomplished according to a previously reported procedure [260]. Initially Proxyl-COOH (100 mg, 0.535 mmol, 1 eq.) was dissolved in dry THF (15 mL) and DCC (121.5 mg, 0.600 mmol, 1.12 eq.) as well as NHS (68 mg, 0.6 mmol, 1.12 eq.) were added at room temperature and stirred for 16 h. The solution was filtered to remove the urea by product and the solvent was removed under reduced pressure. Purification was accomplished by flash column chromatography on a silica column with DCM:acetone 5:1 as eluent and collecting the yellow band. Removal of the solvent under reduced pressure delivered the product as yellow crystals, 120 mg (79%).

FAB (+) MS m/z calcd. for $[M^+]$ 283.13, found 282.99.

ESI (+) MS m/z calcd. for $[M^-+M+MeOH+2H^+]$ 600.32, found 600.49.

Microanalysis: calcd. C 55.12, H 6.76, N 9.89, found: C 54.98, H 6.79, N 9.28.

H_4pat-Proxyl (19B)

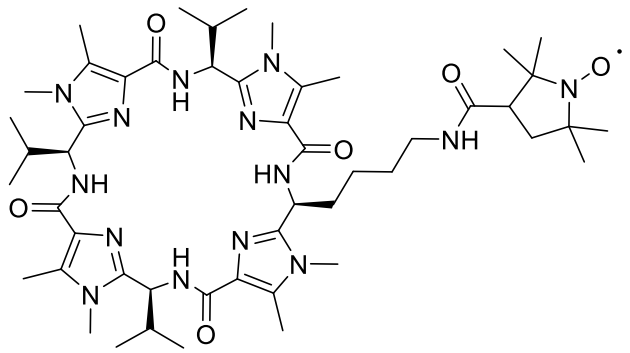

To a mixture of 20 mg of **18** (0.025 mmol, 1 eq.) in 3 mL of dry DMSO and 2 mL of EDIPA (excess), 14 mg of **20** (0.049 mmol, 2 eq.) were added and the reaction mixture was stirred overnight. Subsequently the mixture was diluted by the addition of brine/ice and extracted with diethylether and ethyl acetate. Evaporation of the solvent gave 13 mg (0.013 mmol, 52%) of a pale yellow oil.

FAB (+) MS m/z calcd. for [(M+MeOH)$^+$]: 1001.64, found: 1001.63.

Microanalysis: calcd. C 61.90, H 8.00, N 20.21, found: C 60.72,H 7.84, N 20.15.

C) Optical spectroscopy and photophysics of the H_4pat-Atto550 conjugate

As a copper(II) salt $CuSO_4x6H_2O$ (analytical grade, 0.16 M aq. solution) was used for all photophysical experiments and fluorescence titrations.

UV-Vis and fluorescence spectra

UV-Vis absorption spectra were recorded with the Cary 60 UV-Vis spectrometer (Agilent) at room temperature and fluorescence spectra (quenching experiments) of the H_4pat-Atto-550 - monitored with the 'Fluorolog 3' fluorescence spectrometer (Horiba). The measurements were carried out in quartz glass cuvettes. Fluorescence spectra (quenching experiments) of Atto550-NHS were recorded with 'Cary Eclipse 500' fluorescence spectrometer (Varian, Darmstadt) with temperature control. The measurements were carried out in dark quartz glass cuvettes (Suprasil©, Hellma, Müllheim).

Fluorescence lifetime measurements: Titration of H_4pat-Atto550 with Cu(II)

Fluorescence lifetimes were determined on a 'Fluotime 100' spectrometer with time-correlated single photon count card 'TCSPC TimeHarp 200' from PicoQuant. The excitation wavelength was generated by a pulsed diode 'PLS 500' (500 nm, 40 MHz) from PicoQuant with a pulse width of 300 ps tuneable fibre coupled diode. The instrument response function was measured with colloidal SiO_2 nano-particles (LUDOX®HS-40 (420816), Sigma-Aldrich). During the measurement, the excitation light was filtered with suited high-pass filters, data were analysed with the programme 'FluoFit' from PicoQuant.

Fluorescence quenching experiments

The metal salt used (analytical grade, $Cu(SO_4)x6H_2O$ hydrate 0.16 M aq. solution) was diluted in doubly distilled H_2O (0.01 M); a solution of H_4pat-Atto550 was adjusted to 1.8 µM and prepared from high concentration aqueous solutions (doubly distilled water) by dilution into 100 mM TRIS buffer, pH 8.2, doubly distilled H_2O.

To 200 µL of H_4pat-Atto550 in the required concentration, the metal salt in the required concentration was added in steps of 1 µL before measuring the fluorescence spectrum. The intensities were corrected by the corresponding dilution factor; the reported data are averages of triplicates.

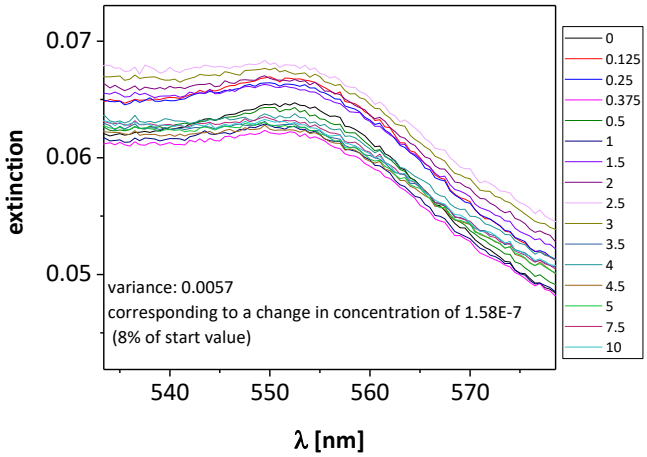

Figure C1. Copper(II) dependent absorbance measurements; 100 mM TRIS buffer, pH=8.2, rt. [H_4pat-Atto550]= 1.8 µM, 1-10 eq. of copper(II).

D) Cyanobacteria handling, field site and sample collection

For the experiments *Prochlorothrix hollandica* (SAG 10.89) and *Synechococcus leopolienses* (SAG 1402-1) were purchased from the Culture Collection of Algae at Göttingen University and stored on the bench at room temperature and without direct light irradiation for a maximum of two weeks.

Individual sponges and their coral rubble substrate were collected with a hammer and chisel.

Prochloron samples were collected together with its host *Lissoclinum patella* at Heron Reef on snorkel. Intact specimens (5-25 cm^2) of 5-20 mm thick *L. patella* were collected at low tide on snorkel on the outer reef flat and crest off Heron Island (First Point: S23°25'49.8, E151°57'15.8, Blue Pools: S23°26'03.2, E151°55'18.1,) in May 2016 covering coral patches on the outer reef flat and down to ~4 m depth on the reef crest. All samples were immediately transported in a bucket with sea water back to Heron Island Research Station and subsequently kept in an outdoor aquarium, which was continuously flushed with fresh aerated sea water (24–26°C) from the reef. As reported previously,[9] it is necessary to keep a continuous strong mixing of water in the aquarium to avoid the degradation of the ascidians. The aquaria were covered by a shading cloth, to prevent too high solar irradiance.

Samples were then transported to the University of Queensland, St Lucia Campus, in a plastic bag, filled with fresh aerated sea water and oxygen, and transported in a cold box at 25°C by plane and 6 h later put in an aquarium with synthetic sea water and constant water flow. The seawater is generated from Tropic Marine salt[261] mixed with water (that was purified *via* reverse osmosis) to a salinity of 35 ppt (23-25°C; the water is not sterilised but pumped through system of sediment and biological filters). Under these conditions we were able to keep the sampled ascidians healthy and with *Prochloron* actively photosynthesising for nine days.

Prochloron was collected using a pipette and by gently squeezing the middle section containing the cloacal cavity harbouring the deep green symbiont.

Prior to all measurements the viability of the cells was tested with a ToxyPAM.[206,207,262] Generally, specimens showed a high maximum PSII quantum yield of >0.6 for several hours after such handling indicative of fast recovery and minimal stress on *Prochloron* (Heinz Walz GmbH, Effeltrich).

1 cm x 1 cm patches were additionally cut from *L. patella* with a sterilised razor blade and stored in 20% glycerol solution at -80°C, transported back to St Lucia on dry ice and stored at -80°C. Healing was observed for the patches which had been cut.

E) Native PAGE experiment with *Prochloron*

Lysis buffer:

1% lysozyme, 50 mM TRIS HCl pH 7.5, 100 mM NaCl, 5% glycerol, 1 mM EDTA, 1 mM DTT

Sample buffer:

62.5 mM TRIS HCl pH 6.8, 25% glycerol, 1% bromophenole blue

Running buffer:

25 mM TRIS HCl pH 8.3, 192 mM glycine

separation gel:

6%: 2 mL Acrylamide/Bisacrylamide 30%/0.8% w/v ; 7.89 mL 0.375 M TRIS HCl pH 8.8; 100 µL 10% ammoniumpersulfate solution; 10 µL TMEDA

15%: 5 mL Acrylamide/Bisacrylamide 30%/0.8% w/v ; 4.89 mL 0.375 M TRIS HCl pH 8.8; 100 µL 10% ammoniumpersulfate solution; 10 µL TMEDA

3 mL of *Prochloron* extracted from the host were centrifuged down at 15.000 g for 5 min. The supernatant was discarded, and cells were resuspended to OD_{750}=0.8 in TRIS buffer, pH 8.2. Disintegration was accomplished by incubation of 1 mL of the sample with 1 mL of lysis buffer for 15 min at room temperature. Cell debris was spun down for 5 min at maximum speed. 1 mL of the supernatant was subsequently treated with 5 µL of a solution of H_4pat-Atto550 ($5x10^{-4}$M) and incubated for 15 min at room temperature. The electrophoresis was accomplished applying 200 V. To minimise the production of heat, and consequently to prevent the proteins from denaturation, the electrophoresis chamber was kept on ice. Staining was accomplished using COOMASSIE Blue.

F1) Protocol for the treatment of *Prochloron* (preparation of FCM and confocal microscopy experiments)

For the preparation of samples for FCM and confocal microscopy 40 µL of a 2.4 µM solution (100 mM TRIS buffer, pH 8.2) of H_4pat-Atto550 were added to 30 µL of the respective cyanobacteria at OD_{750}=0.8 in BG 11 medium (sample **a**). For samples **b** and **c** 40 µL of a 2.4 µM H_4pat-Atto550, with 5 eq. of copper(II) ($CuSO_4x6H_2O$) were used for the treatment of the cells. After heat shock treatment for 45 s at 40°C the samples were put on ice for 1 min. Washing with 50 µL buffer followed. The cells were then resuspended in 10 µL of buffer and 90 µL of a 4 % PFA solution was added and the cells were incubated for 15 min. Again the cells were washed with 50 µL buffer and either (samples **a** and **b**) resuspended in 50 µL of TRIS or (**c**) treated with 10 eq. of cyclam for 10 min. Sample c was afterwards washed with 50 µL of buffer and resuspended in 50 µL of TRIS. All experiments were carried out in triplicates. For FCM the final suspensions were analysed within 1 h after preparation.

For confocal microscopy the samples were placed in 8-well glass slides (ibidi GmbH, Lab-Tek) and the solvent was slowly evaporated under reduced pressure in a desiccator (1 h) and the cells were analysed immediately.

F2) Flow cytometry

The Flow cytometry (FCM) experiments were performed on a C6 cytometer (Accuri). Fluorescence excitation was at λ_{exc}=535 nm and λ_{exc}=640 nm, and the respective emission was detected using a 585/42 nm (FL1) and a 694/40 nm (FL2) filter. The mean ratio (and the respective SEM) of the fluorescence intensity observed at FL1 compared to FL2 is plotted. All flow cytometry measurements include minimum 4,000 events in the gated area and were carried out in triplicates.

F3) Confocal microscopy

All *Prochlorothrix hollandica* and *Synechococcus leopoliensis* samples were measured using a confocal laser scanning microscope (Leica SP5), applying a 63x water immersion objective. The image parameters were chosen 2048x2048 by 16 bit at 200 Hz. Each picture represented an area of 246x246 µm, representing a two-fold oversampling by a spatial resolution of 132 nm per pixel. Atto550 was excited *via* pulsed white light laser (80 MHz, SuperK Extreme, Koheras) at 561 nm, intensity 70 %. Emission detection was done using photomultiplier tubes (PMT) within 574 – 680 nm. At least ten measurements at random positions between one Lab-Tek chamber were conducted per condition.

Prochloron samples were measured using a confocal laser scanning microscope (ZEISS LSM 710) applying a 63x oil immersion objective (C-Apochromat 63x/1.2 W Korr). The image parameters were chosen 1024x1024 by 16 bit at 100 Hz. Each picture represented an area of 135x135 µm, representing a two-fold oversampling by a spatial resolution of 132 nm per pixel. Atto550 was excited *via* pulsed white light laser at 561 nm, intensity 70 % (561 nm continuous wave Diode-Pumped Solid State Laser DPSS on a ZEISS LSM 710 instrument). Emission detection was done using photomultiplier tubes (PMT) within 556-606 and 624-735 nm. At least ten measurements at random positions within three Lab-Tek chambers were conducted per condition.

For quantification, Fiji software was used.[263] Images were filtered by median, followed by background subtraction. Cells were selected using Otsu thresholding and subsequent particle analysis, followed by calculation of median intensity and standard error.

Like shown for FCM, for the establishment of a protocol to treat *Prochloron*, initially *Synechococcus leopoliensis* (SAG 1402-1) and *Prochlorothrix hollandica* (SAG 10.89) were studied. The results for the flow cytometry experiment are given in the Appendix I.

Measurement of the uptake of H_4pat-Atto550 in *Prochloron*

The uptake of Atto550 was verified by confocal microscopy (see Chapter 5.2.2, Figure 5.6B). The upper piture in Figure F1 shows *Prochloron* cells and their fluorescence intensity at 568, 573, 578, 57 588, 598, …, 708, 718 nm (λ_{exc}=556 nm). The lower picture shows *Prochloron* cells, that were treated with Atto550 (λ_{em}(Atto550)=574 nm; λ_{em}(Chl b)=670 nm). The upper series the cells do not show fluorescence between 568-618 nm, but show strong fluorescence between 628-718 nm originating from chlorophyll *b*. The lower series however shows cells treated with H_4pat-Atto550,

and these cells show two fluorescence ranges: between 568 nm and 598 nm and between 628-718 nm. This is a good validation for the uptake of the patellamide-fluorescent dye conjugate.

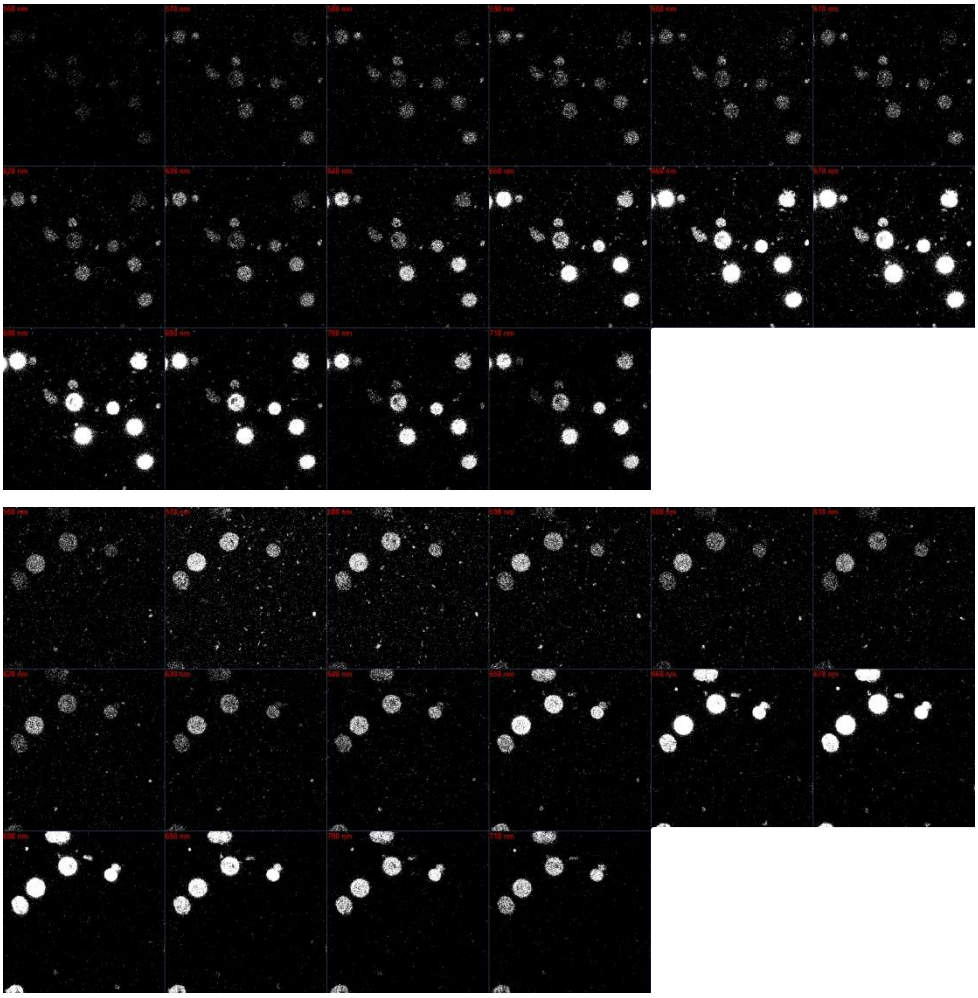

Figure F1. Raw data, microscopy picture series of *Prochloron* top: not treated, bottom: treated with H_4pat-Atto550 measured at emission wavelengths 568, 578, 588, 598,…, 708, 718 nm (left to right, top to bottom).

G) Absorption measurement of the *Prochlorothrix hollandica* lysate*

5 mL of *Prochlorothrix hollandica* (*P.H.*) from culture were centrifuged down at 18.000 g for 5 min. The supernatant was discarded, and cells were resuspended to OD_{600}=0.8 in TRIS buffer, pH 8.2. Disintegration was done using a sonicator (BW2070, Bandelin electronics Berlin GmbH) for 5x10 s at 75% of maximum power. In between repeats, lysate was chilled on ice for 1 min. Cell debris was spun down for 15 min at maximum speed. The supernatant was measured for absorbance properties (Cary 60 UV-Vis spectrometer (Agilent) at room temperature) with or without $CuSO_4$ (final concentration as described in E1: $2.9x10^{-7}$ M).As control the same volume of TRIS buffer was supplemented.

* The experiment discussed in this paragraph was carried out by Martin Seefeld.

Bibliography

[1] Mayer, H. In *Frankfurter Allgemeine Zeitung (Feuilleton)* 31.08.2016.

[2] Kaim, W.; Schwederski, B. *Bioanorganische Chemie - Zur Funktion chemischer Elemente in Lebensprozessen*; Teubner: Wiesbaden, 2005; Vol. 4th Edition.

[3] Mereschkowsky, K. *Biol. Centralbl.* **1910**, *30*, 353.

[4] Schwartz, W. *Z. allg. Mikrobiol.* **1973**, *13*, 186.

[5] Whatley, J. M.; John, P.; Whatley, F. R. *Proc. Roy. Soc. London. Series B. Biol. Sc.* **1979**, *204*, 165.

[6] Lewin, R. A.; Cheng, L. *Prochloron: A Microbial Enigma*; Chapman & Hall Inc.: London, 1989.

[7] Lewin, R. A.; Withers, N. W. *Nature* **1975**, *256*, 735.

[8] Newcomb, E. H.; Pugh, T. D. *Nature* **1975**, *253*, 533.

[9] Kühl, M.; Behrendt, L.; Trampe, E.; Qvortrup, K.; Schreiber, U.; Borisov, S. M.; Klimant, I.; Larkum, A. W. *Front. Microbiol.* **2012**, *3*, 402.

[10] Alberte, R. S.; Cheng, L.; Lewin, R. A. *Mar. Biol.* **1986**, *90*, 575.

[11] Patterson, G. M. L.; Withers, N. W. *Science* **1982**, *217*, 1034.

[12] Roche, J. L.; van der Staay, G. W. M.; Partensky, F.; Ducret, A.; Aebersold, R.; Li, R.; Golden, S. S.; Hiller, R. G.; Wrench, P. M.; Larkum, A. W. D.; Green, B. R. *Proc. Natl. Acad. Sci.* **1996**, *93*, 15244.

[13] Partensky, F.; Garczarek, L. In *Photosynthesis in Algae*; Larkum, A. W. D., Douglas, S. E., Raven, J. A., Eds.; Springer Netherlands: Dordrecht, 2003, p 29.

[14] Burger-Wiersma, T.; Veenhuis, M.; Korthals, H. J.; Van de Wiel, C. C. M.; Mur, L. R. *Nature* **1986**, *320*, 262.

[15] Chisholm, S. W.; Olson, R. J.; Zettler, E. R.; Goericke, R.; Waterbury, J. B.; Welschmeyer, N. A. *Nature* **1988**, *334*, 340.

[16] Tomitani, A.; Okada, K.; Miyashita, H.; Matthijs, H. C. P.; Ohno, T.; Tanaka, A. *Nature* **1999**, *400*, 159.

[17] Golden, S. S.; Morden, C. W.; Greer, K. L. *Comparison of sequences and organization of photosynthetic genes among the prochlorophyta Prochlorothrix hollandica, Cyanobacteria, and chloroplasts*; Chapman & Hall: New York / London, 1993.

[18] Palenik, B.; Haselkorn, R. *Nature* **1992**, *355*, 265.

[19] Lewin, R. A. *Photosynth. Res.* **2002**, *73*, 59.

[20] Hirose, E.; Neilan, B. A.; Schmidt, E. W.; Murakami, A. *Enigmatic life and evolution of prochloron and related cyanobacteria inhabiting colonial ascidians.*; Nova Science Publishers, Inc.. 2009.

[21] Donia, M. S.; Fricke, W. F.; Partensky, F.; Cox, J.; Elshahawi, S. I.; White, J. R.; Phillippy, A. M.; Schatz, M. C.; Piel, J.; Haygood, M. G.; Ravel, J.; Schmidt, E. W. *Proc. Natl. Acad. Sci.* **2011**, *108*, E1423.

[22] Griffiths, D. J. *Bot. Rev.* **2006**, *72*, 330.

[23] Swift, H.; Leser, G. P. *J. Phycol.* **1989**, *25*, 751.

[24] Kremer, B. P.; Pardy, R.; Lewin, R. A. *Phycologia* **1982**, *21*, 258.

[25] Olsen, R. R.; Porter, J. W. *Proceedings of the Fifth International Coral Reef Congress, Tahiti* **1985**, *5*, 257.

[26] Alberte, R. S.; Cheng, L.; Lewin, R. A. *Symbiosis* **1987**, 147.

[27] Bibby, T. S.; Nield, J.; Chen, M.; Larkum, A. W. D.; Barber, J. *Proc. Natl. Acad. Sci.* **2003**, *100*, 9050.

[28] Murray, J. W.; Duncan, J.; Barber, J. *TRPLS* **2006**, *11*, 152.

[29] Schreiber, U.; Gademann, R.; Ralph, P. J.; Larkum, A. W. D. *Plant Cell Physiol.* **1997**, *38*, 945.

[30] Schreiber, U.; Gademann, R.; Bird, P.; Ralph, P. J.; Larkum, A. W. D.; Kühl, M. *J. Phycol.* **2002**, *38*, 125.

[31] Odintsov, V. S. *Endocytobiosis & Cell Res.* **1990**, *7*, 253.

[32] Koike, I.; Yamamuro, M.; Pollard, P. *Mar. Freshwater Res.* **1993**, *44*, 173.

[33] Goodbody, I. In *Adv. Mar. Biol.*; Frederick, S. R., Maurice, Y., Eds.; Academic Press: 1975; Vol. Volume 12, p 1.

[34] Parry, D. L. *Mar. Biol.* **1985**, *87*, 219.

[35] Paerl, H. W. *Mar. Biol.* **1984**, *81*, 251.

[36] C., K. T.; A., L. R. *Natural [15]N/[14]N abundance as evidence for N[2] fixation by Prochloron (prochlorophyta) endosymbiotic with didemnid ascidians*; Balaban: Philadelphia, PA, ETATS-UNIS, 1999; Vol. 26.

[37] Donia, M. S.; Fricke, W. F.; Ravel, J.; Schmidt, E. W. *PLoS ONE* **2011**, *6*, 17897.

[38] Behrendt, L.; Larkum, A. W.; Trampe, E.; Norman, A.; Sorensen, S. J.; Kühl, M. *ISME J* **2012**, *6*, 1222.

[39] M., G.; J., B.; J.A., R. *Annu. Rev. Plant Biol.* **2005**, *56*, 99.

[40] Badger, M. R.; Hanson, D.; Price, G. D. *Funct. Plant Biol.* **2002**, *29*, 161.

[41] Critchley, C.; Andrews, T. J. *Arch. Microbiol.* **1984**, *138*, 247.

[42] Schmidt, E. W.; Donia, M. S. *Current Opinion in Biotechnology* **2010**, *21*, 827.

[43] Schmidt, E. W.; Donia, M. S.; McIntosh, J. A.; Fricke, W. F.; Ravel, J. *J. Nat. Prod.* **2012**, *75*, 295.

[44] Pettit, G. R.; Day, J. F.; Hartwell, J. L.; Wood, H. B. *Nature* **1970**, *227*, 962.

[45] Krebs, H. C. In *Progress in the Chemistry of Organic Natural Products*; Springer: Wien, 1986, p 151.

[46] Milne, B. F.; Long, P. F.; Starcevic, A.; Hranueli, D.; Jaspars, M. *Org. Biomol. Chem.* **2006**, *4*, 631.

[47] Mehrkens, N., Phosphatase Activity of Homo- and Heterodinuclear Transition Metal Complexes of Patellamide Derivatives (PhD), Heidelberg University, 2015.

[48] Banaigs, B.; Bonnard, I.; Witczak, A.; Inguimbert, N. In *Outstanding Marine Molecules*; Wiley-VCH Verlag GmbH & Co. KGaA: 2014, p 285.

[49] Schmidt, E. W.; Nelson, J. T.; Rasko, D. A.; Sudek, S.; Eisen, J. A.; Haygood, M. G.; Ravel, J. *Proc. Natl. Acad. Sci.* **2005**, *102*, 7315.

[50] Houssen, W. E.; Bent, A. F.; McEwan, A. R.; Pieiller, N.; Tabudravu, J.; Koehnke, J.; Mann, G.; Adaba, R. I.; Thomas, L.; Hawas, U. W.; Liu, H.; Schwarz-Linek, U.; Smith, M. C. M.; Naismith, J. H.; Jaspars, M. *Angew. Chem. Int. Ed.* **2014**, *53*, 14171.

[51] Schmidt, E. W.; Nelson, J. T.; Rasko, D. A.; Sudek, S.; Eisen, J. A.; Haygood, M. G.; Ravel, J. *Proc. Natl. Acad. Sci.* **2005**, *102*, 7315.

[52] Long, P. F.; Dunlap, W. C.; Battershill, C. N.; Jaspars, M. *ChemBioChem* **2005**, *6*, 1760.

[53] Houssen, W. E.; Jaspars, M. *ChemBioChem* **2010**, *11*, 1803.

[54] A. Shelnutt, J.; Song, X.-Z.; Ma, J.-G.; Jia, S.-L.; Jentzen, W.; J. Medforth, C.; J. Medforth, C. *Chem. Soc. Rev.* **1998**, *27*, 31.

[55] Hamamoto, Y.; Endo, M.; Nakagawa, M.; Nakanishi, T.; Mizukawab, K. *Chem. Commun.* **1983**, 323.

[56] Schmidt, U.; Utz, R.; Gleich, P. *Tetrahedron Lett.* **1985**, *26*, 4367.

[57] Ireland, C.; Scheuer, P. J. *J. Am. Chem. Soc.* **1980**, *102*, 5688.

[58] Prinsep, M. R.; Moore, R. E.; Levine, I. A.; Patterson, G. M. L. *J. Nat. Prod.* **1992**, *55*, 140.

[59] Hambley, T. W.; Hawkins, C. J.; Lavin, M. F.; van den Brenk, A.; Watters, D. J. *Tetrahedron* **1992**, *48*, 341.

[60] Haberhauer, G. *Tetrahedron Lett.* **2008**, *49*, 2421.

[61] Comba, P.; Dovalil, N.; Gahan, L. R.; Haberhauer, G.; Hanson, G. R.; Noble, C. J.; Seibold, B.; Vadivelu, P. *Chem. Eur. J.* **2012**, *18*, 2578.

[62] Haberhauer, G.; Rominger, F. *Eur. J. Org. Chem.* **2003**, *2003*, 3209.

[63] Wang, M.; Gould, S. J. *J. Org. Chem.* **1993**, *58*, 5176.

[64] Ikegami, F.; Murakoshi, I. *Phytochemistry* **1994**, *35*, 1089.

[65] Haberhauer, G.; Drosdow, E.; Oeser, T.; Rominger, F. *Tetrahedron* **2008**, *64*, 1853.

[66] Pintér, Á.; Haberhauer, G. *Tetrahedron* **2009**, *65*, 2217.

[67] Comba, P.; Dovalil, N.; Gahan, L. R.; Hanson, G. R.; Westphal, M. *Dalton Trans.* **2014**, *43*, 1935.

[68] Schmitz, F. J.; Ksebati, M. B.; Chang, J. S.; Wang, J. L.; Hossain, M. B.; Van der Helm, D.; Engel, M. H.; Serban, A.; Silfer, J. A. *J. Org. Chem.* **1989**, *54*, 3463.

[69] Wipf, P.; Fritch, P. C.; Geib, S. J.; Sefler, A. M. *J. Am. Chem. Soc.* **1998**, *120*, 4105.

[70] Degnan, B. M.; Hawkins, C. J.; Lavin, M. F.; McCaffrey, E. J.; Parry, D. L.; Watters, D. J. *J. Med. Chem.* **1989**, *32*, 1354.

[71] van den Brenk, A. L.; Byriel, K. A.; Fairlie, D. P.; Gahan, L. R.; Hanson, G. R.; Hawkins, C. J.; Jones, A.; Kennard, C. H. L.; Moubaraki, B.; Murray, K. S. *Inorg. Chem.* **1994**, *33*, 3549.

[72] Comba, P.; Dovalil, N.; Gahan, L. R.; Hanson, G. R.; Westphal, M. *Dalton Trans. (Dalton Perspective)* **2014**, *43*, 1935.

[73] Comba, P.; Dovalil, N.; Haberhauer, G.; Kowski, K.; Mehrkens, N.; Westphal, M. *Z. Allg. Anorg. Chem. (Special Issue Bioinorganic Chemistry)* **2013**, *639*, 1395.

[74] Comba, P.; Dovalil, N.; Gahan, L. R.; Haberhauer, G.; Hanson, G. R.; Noble, C. J.; Seibold, B.; Vadivelu, P. *Chem. Eur. J.* **2012**, *18*, 2578.

[75] Comba, P.; Dovalil, N.; Hanson, G. R.; Linti, G. *Inorg. Chem.* **2011**, *50*, 5165.

[76] Haberhauer, G.; Pinter, A.; Oeser, T.; Rominger, F. *Eur. J. Org. Chem.* **2007**, 1779.

[77] Comba, P.; Dovalil, N.; Gahan, L. R.; Haberhauer, G.; Hanson, G. R.; Noble, C. J.; Seibold, B.; Vadivelu, P. *Chemistry* **2012**, *18*, 2578.

[78] El-Faham, A.; Subiros Funosas, R.; Prohens, R.; Albericio, F. *Chemistry* **2009**, *15*, 9404.

[79] Westphal, M., Cu(II) Complexes of Cyclic Pseudo-Peptdies: Carbonic Anhydrase and Phosphatase Activity as Possible Metabolic Functions of Patellamides (PhD), Heidelberg University, 2013.

[80] Comba, P.; Gahan, L. R.; Haberhauer, G.; Hanson, G. A.; Noble, C. J.; Seibold, B.; van den Brenk, A. L. *Chem. Eur. J.* **2008**, *14*, 4393.

[81] Bernhardt, P. V.; Comba, P.; Hambley, T. W.; Massoud, S. S.; Stebler, S. *Inorg. Chem.* **1992**, *31*, 2644.

[82] Comba, P.; Cusack, R.; Fairlie, D. P.; Gahan, L. R.; Hanson, G. R.; Kazmaier, U.; Ramlow, A. *Inorg. Chem.* **1998**, *37*, 6721.

[83] Bernhardt, P. V.; Comba, P.; Fairlie, D. P.; Gahan, L. A.; Hanson, G. R.; Lötzbeyer, L. *Chem. Eur. J.* **2002**, *8*, 1527.

[84] Comba, P.; Dovalil, N.; Hanson, G.; Harmer, J.; Noble, C. J.; Riley, M. J.; Seibold, B. *Inorg. Chem.* **2014**, *53*, 12323.

[85] Dovalil, N., Copper(II) Coordination Chemistry of Cyclic Pseudo Hexa- and Octapeptides (PhD), Heidelberg University, 2010.

[86] Daumann, L. J.; Schenk, G.; Ollis, D. L.; Gahan, L. R. *Dalton Trans.* **2014**, *43*, 910.

[87] De la Cerda, B.; Castielli, O.; Durán, R. V.; Navarro, J. A.; Hervás, M.; De la Rosa, M. A. *Briefings in Functional Genomics & Proteomics* **2007**, *6*, 322.

[88] Dupont, C. L.; Grass, G.; Rensing, C. *Metallomics* **2011**, *3*, 1109.

[89] Porcheron, G.; Garénaux, A.; Proulx, J.; Sabri, M.; Dozois, C. M. *Front. Cell. Infect. Microbiol.* **2013**, *3*, 90.

[90] Ho, K. K.; Krogmann, D. W. *BBA Bioenergetics* **1984**, *766*, 310.

[91] Sandmann, G.; Reck, H.; Kessler, E.; Böger, P. *Arch. Microbiol.* **1983**, *134*, 23.

[92] Solomon, E. I.; Baldwin, M. J.; Lowery, M. D. *Chem. Rev.* **1992**, *92*, 521.

[93] Kenyon, G. D.; Harbach, R. H.; Guida, W. C.; Dou, Q. P. *Front Biosc* **2004**, *9*, 2652.

[94] Latifi, R.; Bagherzadeh, M.; Milne, B. F.; Jaspars, M.; de Visser, S. P. *J. Inorg. Biochem.* **2008**, *102*, 2171.

[95] Gerdemann, C.; Eicken, C.; Krebs, B. *Acc. Chem. Res.* **2002**, *35*, 183.

[96] Solomon, E. I.; Sundaram, U. M.; Machonkin, T. E. *Chem. Rev.* **1996**, *96*, 2563.

[97] Comba, P.; Gahan, L. R.; Hanson, G. R.; Maeder, M.; Westphal, M. *Dalton Trans.* **2014**, *43*, 3144.

[98] Garen, A.; Levinthal, C. *Biochim. Biophys. Acta* **1960**, *38*, 470.

[99] Segel, I. H. *Enzyme Kinetics - Behavior and Analysis of Rapid Equilibrium and Steady-State Enzyme Systems*; Wiley-VCH New York, 1975.

[100] Comba, P.; Gahan, L. R.; Hanson, G. R.; Westphal, M. *Chem. Comm.* **2012**, *48*, 9364.

[101] Gilson, R.; Durrant, M. C. *Dalton Trans.* **2009**, 10223.

[102] Pederson, K. J. *K. Dan. Vidensk. Selsk., Mat.-Fys. Medd.* **1943**, *7*, 20.

[103] Richens, D. T. *The chemistry of aqua ions : synthesis, structure and reactivity ; a tour through the periodic table of the elements*; Wiley: Chichester [u.a.], 1997.

[104] Crichton, R. R. *Biological Inorganic Chemistry*; Elsevier: Amsterdam, Oxford, 2012; Vol. 2.

[105] Bosch, S., The Impact of the Second Coordination Sphere in Phosphatase Model Complexes (PhD), Heidelberg University, 2015.

[106] Guddat, L. W.; McAlpine, A. S.; Hume, D.; Hamilton, S.; de Jersey, J.; Martin, J. L. *Structure* **1999**, *7*, 757.

[107] Duff, S. M. G.; Sarath, G.; Plaxton, W. C. *Physiol. Plant.* **1994**, *90*, 791.

[108] Raeisaenen, S. R.; Alatalo, S. L.; Ylipahkala, H.; Halleen, J. M.; Cassady, A. I.; Hume, D. A.; Vaeaenaenen, H. K. *Biochem. Biophys. Res. Commun.* **2005**, 120.

[109] Schenk, G.; Mitić, N.; Hanson, G. R.; Comba, P. *Coord. Chem. Rev.* **2013**, *257*, 473.

[110] Zajaczkowski-Fischer, M., Second Generation Model Complexes for the Enzyme Purple Acid Phosphatase (PhD), Heidelberg University, 2010.

[111] Desbouis, D.; Troitsky, I. P.; Belousoff, M. J.; Spiccia, L.; Graham, B. *Coord. Chem. Rev.* **2012**, *256*, 897.

[112] Jarenmark, M.; Csapo, E.; Singh, J.; Wockel, S.; Farkas, E.; Meyer, F.; Haukka, M.; Nordlander, E. *Dalton Trans.* **2010**, *39*, 8183.

[113] Jarenmark, M.; Kappen, S.; Haukka, M.; Nordlander, E. *Dalton Trans.* **2008**, 993.

[114] Jarenmark, M.; Carlsson, H.; Nordlander, E. *C. R. Chimie* **2007**, *10*, 433.

[115] Comba, P.; Eisenschmidt, A.; Gahan, L.; Hanson, G.; Mehrkens, N.; Westphal, M. *Dalton Trans.* **2016**.

[116] Comba, P.; Dovalil, N.; Hanson, G. R.; Linti, G. *Inorg Chem* **2011**, *50*, 5165.

[117] Bosch, S.; Comba, P.; Gahan, L. R.; Schenk, G. *Inorg. Chem.* **2014**, *53*, 9036.

[118] Comba, P.; Gahan, L. R.; Mereacre, V.; Hanson, G. R.; Powell, A. K.; Schenk, G.; Zajaczkowski-Fischer, M. *Inorg. Chem.* **2012**, *51*, 12195.

[119] Gahan, L. R.; Smith, S. J.; Neves, A.; Schenk, G. *Eur. J. Inorg. Chem.* **2009**, 2745.

[120] Neves, A.; Lanznaster, M.; Bortoluzzi, A. J.; Peralta, R. A.; Casellato, A.; Castellano, E. E.; Herrald, P.; Riley, M. J.; Schenk, G. *J. Am. Chem. Soc.* **2007**, *129*, 7486.

[121] Cox, R. S.; Schenk, G.; Mitić, N.; Gahan, L. R.; Hengge, A. C. *J. Am. Chem. Soc.* **2007**, *129*, 9550.

[122] Bunton, C. A.; Farber, S. J. *J. Org. Chem.* **1969**, *34*, 767.

[123] Brox, D., Synthese modularer chemischer Schalter für die optische Mikro- und Nanoskopie (PhD), Heidelberg University, 2016.

[124] Parkin, G. *Chem. Rev.* **2004**, *104*, 699.

[125] Vahrenkamp, H. *Dalton Trans.* **2007**, *42*, 4751.

[126] Kimura, E.; Koike, T.; Shionoya, M. In *Structure and Bonding*; Hill, H. A. O., Sadler, P. J., Thomson, A. J., Eds. Berlin, 1997.

[127] Wright, S. H.; Raab, A.; Feldmann, J.; Krupp, E.; Jaspers, M. In *Handbook of Marine Natural Products*; Fattorusso, E., Gerwick, W. H., Taglialatela-Scatati, O., Eds.; Springer: Heidelberg, New York, 2012, p 861.

[128] Comba, P.; Hambley, T. W.; Martin, B. *Molecular modeling of inorganic compounds. 3rd Edition with a Tutorial, based on MOMEC3 (ISBN 978-3-527-31799-8)*; Wiley-VCH: Weinheim, 2009.

[129] Comba, P.; Hambley, T. W.; Ströhle, M. *Helv. Chim. Acta.* **1995**, *78*, 2042.

[130] Comba, P.; Daubinet, A.; Martin, B.; Pietzsch, H. J.; Stephan, H. *J. Organomet. Chem.* **2006**, *691*, 2495.

[131] Bol, J. E.; Buning, C.; Comba, P.; Reedijk, J.; Ströhle, M. *J. Comput. Chem.* **1998**, *19*, 512.

[132] Wang, J.; Wolf, R. M.; Caldwell, J. W.; Kollman, P. A.; Case, D. A. *J. Comput. Chem.* **2004**, *25*, 1157.

[133] Bernhardt, P. V.; Comba, P. *Inorg. Chem.* **1992**, *31*, 2638.

[134] Comba, P.; Jakob, H.; Nuber, B.; Keppler, B. K. *Inorg. Chem.* **1994**, *33*, 3396.

[135] Comba, P. *Inorg. Chem.* **1994**, *33*, 4577.

[136] Comba, P.; Zimmer, M. *Inorg. Chem.* **1994**, *33*, 5368.

[137] Comba, P.; Hambley, T. W.; Hilfenhaus, P.; Richens, D. T. *J. Chem. Soc., Dalton Trans.* **1996**, 533.

[138] Comba, P.; Hilfenhaus, P.; Karlin, K. D. *Inorg. Chem.* **1997**, *36*, 2309.

[139] Comba, P.; Gloe, K.; Inoue, T.; Stephan, H.; Yoshizuka, K. *Inorg. Chem.* **1998**, *37*, 3310.

[140] Comba, P.; Gyr, T. *Eur. J. Inorg. Chem.* **1999**, 1787.

[141] Comba, P.; Remenyi, R. *J. Comput. Chem.* **2002**, *23*, 697.

[142] Martin, B.; Heidelberg University, bodo.martin@aci.uni-heidelberg.de, Momec-a molecular mechanics based program, work in progress: 2016.

[143] Metropolis, N.; Ulam, S. *J. Am. Stat. Assoc.* **1949**, *44*, 335.

[144] Bartol, J.; Comba, P.; Melter, M.; Zimmer, M. *J. Comput. Chem.* **1999**, *20*, 1549.

[145] Comba, P. *Coord. Chem. Rev.* **1993**, *123*, 1.

[146] Comba, P. *Coord. Chem. Rev.* **1999**, *182*, 343.

[147] Davies, G.; Henrissat, B. *Structure* **1995**, *3*, 853.

[148] Blake, C. C. F.; Koenig, D. F.; Mair, G. A.; North, A. C. T.; Phillips, D. C.; Sarma, V. R. *Nature* **1965**, *206*, 757.

[149] Matthews, B. W.; Remington, S. J. *Proc. Nat. Acad. Sc.* **1974**, *71*, 4178.

[150] Davies, G. J.; Gloster, T. M.; Henrissat, B. *Current Opinion in Structural Biology* **2005**, *15*, 637.

[151] Vocadlo, D. J.; Davies, G. J. *Current Opinion in Chemical Biology* **2008**, *12*, 539.

[152] Koshland, D. E. *Biol. Rev.* **1953**, *28*, 416.

[153] Sinnott, M. L. *Chem. Rev.* **1990**, *90*, 1171.

[154] McCarter, J. D.; Stephen Withers, G. *Current Opinion in Structural Biology* **1994**, *4*, 885.

[155] Varrot, A.; Yip, V. L. Y.; Li, Y.; Rajan, S. S.; Yang, X.; Anderson, W. F.; Thompson, J.; Withers, S. G.; Davies, G. J. *J. Mol. Biol.* **2005**, *346*, 423.

[156] Kempton, J. B.; Withers, S. G. *Biochem.* **1992**, *31*, 9961.

[157] Thompson, J.; Pikis, A.; Ruvinov, S. B.; Henrissat, B.; Yamamoto, H.; Sekiguchi, J. *J. Biol. Chem.* **1998**, *273*, 27347.

[158] Khan, S. H.; O`Neill, R. A. *Modern methods in carbohydrate synthesis*; Harwood Academic Publishers: Amsterdam, the Netherlands, 1996.

[159] Striegler, S.; Dunaway, N. A.; Gichinga, M. G.; Barnett, J. D.; Nelson, A. G. D. *Inorg. Chem.* **2010**, *49*, 2639.

[160] Striegler, S.; Dittel, M.; Kanso, R.; Alonso, N. A.; Duin, E. C. *Inorg. Chem.* **2011**, *50*, 8869.

[161] Striegler, S.; Barnett, J. D.; Dunaway, N. A. *ACS Catal.* **2012**, *2*, 50.

[162] Barnett, J. D.; Striegler, S. *Top. Catal.* **2012**, *55*, 460.

[163] Haldar, S.; Patra, A. K.; Bera, M. *RSC Adv.* **2014**, *4*, 62851.

[164] Striegler, S.; Dunaway, N. A.; Gichinga, M. G.; Barnett, J. D.; Nelson, A.-G. D. *Inorg. Chem.* **2010**, *49*, 2639.

[165] Comba, P.; Eisenschmidt, A.; Kipper, N.; Schiessl, J. *J. Inorg. Biochem.* **2016**, *159*, 70.

[166] Ortega-Caballero, F.; Rousseau, C.; Christensen, B.; Petersen, T. E.; Bols, M. *J. Am. Chem. Soc.* **2005**, *127*, 3238.

[167] Böttcher, S.; Thiem, J. *Eur. J. Org. Chem.* **2014**, *2014*, 564.

[168] Bebrone, C. *Biochem. Pharmacol.* **2007**, 1686.

[169] Crowder, M. W.; Spencer, J.; Vila, A. J. *Acc. Chem. Res.* **2006**, *39*, 721.

[170] Phelan, E. K.; Miraula, M.; Selleck, C.; Ollis, D. L.; Schenk, G.; Mitić, N. *AJMB* **2014**, *04*, 89.

[171] Daumann, L.; Schenk, G.; Gahan, L. R. *Eur. J. Inorg. Chem.* **2014**, 2869.

[172] Daumann, L. J.; Gahan, L. R.; Comba, P.; Schenk, G. *Inorg. Chem.* **2012**, *51*, 7669.

[173] Kaminskaia, N. V.; Spingler, B.; Lippard, S. J. *J. Am. Chem. Soc.* **2000**, *122*, 6411.

[174] Song, W. J.; Tezcan, F. A. *Science* **2014**, *346*, 1525.

[175] Felici, A.; Amicosante, G.; Oratore, A.; Strom, R.; Ledent, P.; Joris, B.; Fanuel, L.; Frere, J. M. *Biochem. J.* **1993**, *291*, 151.

[176] Garribba, E.; Micera, G. *J. Chem. Educ.* **2006**, *83*, 1229.

[177] Lötzbeyer, L., Synthese neuer Patellamid-Derivate und Eigenschaften ihrer Kupfer(II)-Komplexe (PhD), Heidelberg University, 2001.

[178] Corvaja, C. In *Electron Paramagnetic Resonance*; John Wiley & Sons, Inc.: 2008, p 1.

[179] Jeschke, G. 01.05.2016 Introduction to EPR Spectroscopy https://www.ethz.ch/content/dam/ethz/special-interest/chab/physical-chemistry/epr-dam/documents/basicEducation/skripts/epr_skript_mainz_1998.pdf, 2006.

[180] Abragam, A.; Pryce, M. H. L. *Proc. R. Soc. London A* **1951**, *205*, 135.

[181] Hanson, G. R.; Noble, C. J.; Benson, S. In *High Resolution EPR: Applications to Metalloenzymes and Metals in Medicine*; Berliner, L., Hanson, G., Eds.; Springer New York: New York, NY, 2009, p 105.

[182] Hanson, G. R.; Gates, K. E.; Noble, C. J.; Griffin, M.; Mitchell, A.; Benson, S. *J. Inorg. Biochem.* **2004**, *98*, 903.

[183] Foster, A. W.; Osman, D.; Robinson, N. J. *J. Biol. Chem.* **2014**, *289*, 28095.

[184] Porcheron, G.; Garenaux, A.; Proulx, J.; Sabri, M.; Dozois, C. *FCIMB* **2013**, *3*.

[185] Morris, L. A.; Jaspars, M.; Kettenes-van den Bosch, J. J.; Versluis, K.; Heck, A. J. R.; Kelly, S. M.; Price, N. C. *Tetrahedron* **2001**, *57*, 3185.

[186] Quigley, M. N.; Vernon, F. *J. Chem. Educ.* **1996**, *73*, 671.

[187] M.G. van den Berg, C. *Marine Chemistry* **1984**, *15*, 1.

[188] Bennett, B. D.; Kimball, E. H.; Gao, M.; Osterhout, R.; Van Dien, S. J.; Rabinowitz, J. D. *Nat. Chem. Biol.* **2009**, *5*, 593.

[189] Sarma, T. A. *Handbook of cyanobacteria*; CRC Press, 2012.

[190] Hallman, P. S.; Perrin, D. D.; Watt, A. E. *Biochem. J.* **1971**, *121*, 549.

[191] Ermler, U.; Grabarse, W.; Shima, S.; Goubeaud, M.; Thauer, R. K. *Current Opinion in Structural Biology* **1998**, *8*, 749.

[192] Krämer, R. *Coord. Chem. Rev.* **1999**, *182*, 243.

[193] Solomon, E. I.; Heppner, D. E.; Johnston, E. M.; Ginsbach, J. W.; Cirera, J.; Qayyum, M.; Kieber-Emmons, M. T.; Kjaergaard, C. H.; Hadt, R. G.; Tian, L. *Chem. Rev.* **2014**, *114*, 3659.

[194] Hiller, R. G.; Larkum, A. W. D. *Biochimica et Biophysica Acta* **1985**, *806*, 107.

[195] Reddy, T. J.; Iwama, T.; Halpern, H. J.; Rawal, V. H. *J. Org. Chem.* **2002**, *67*, 4635.

[196] Sano, T.; Umeda, F.; Hashimoto, T.; Nawata, H.; Utsumi, H. *Diabetologia* **1998**, *41*, 1355.

[197] Lakowicz, J. R. In *Principles of Fluorescence Spectroscopy*; Lakowicz, J. R., Ed.; Springer US: Boston, MA, 2006, p 1.

[198] Raven, J. In *The Royal Society Policy Document* Ocean acidification due to increasing atmospheric carbon dioxide

https://royalsociety.org/~/media/Royal_Society_Content/policy/publications/2005/9634.pdf 01.11.2016.

[199] Valeur, B.; Berberan-Santos, M. N. *Molecular Fluorescence - Principles and Applications*; 2nd Edition, pp. 512 ed.; Wiley-VCH, 2012.

[200] Minsky, M. Microscopy Apparatus, US Patent 3.013.467, 1961.

[201] Eisenstein, M. *Nat. Meth.* **2012**, *9*, 1049.

[202] Park, Y. I.; Lee, K. T.; Suh, Y. D.; Hyeon, T. *Chem. Soc. Rev.* **2015**, *44*, 1302.

[203] Ormeod, M. G. *Flow Cytometry A Practical Approach*; Third Edition Reprinted 2003 ed.; Oxford University Press: Great Clarendon Street, Oxford OX1 6DP, 2003.

[204] Introduction to Flow Cytometry www.abcam.com/protocols/introduction-to-flow-cytometry 29.10.2016.

[205] EMBL; https://www.embl.de/pepcore/pepcore_services/cloning/transformation/transformation_heatshock/: 04.10.2016.

[206] Campbell, D.; Hurry, V.; Clarke, A. K.; Gustafsson, P.; Öquist, G. *Microbiol. Mol. Biol. Rev.* **1998**, *62*, 667.

[207] Murchie, E. H.; Lawson, T. *J. Exp. Bot.* **2013**.

[208] Puranik, D. B.; Singh, A.; Chang, E. L. *J. Coord. Chem.* **1996**, *39*, 321.

[209] Bianchi, A.; Micheloni, M.; Paoletti, P. *Coord. Chem. Rev.* **1991**, *110*, 17.

[210] Bowman, M. K.; Carbonera, D. In *Electron Paramagnetic Resonance*; John Wiley & Sons, Inc.: 2008, p 383.

[211] Höfer, P. In *Electron Paramagnetic Resonance*; John Wiley & Sons, Inc.: 2008, p 37.

[212] Comba, P.; Hausberg, S.; Martin, B. *J. Phys. Chem. A* **2009**, *113*, 6751.

[213] van Vleck, J. H. *The theory of electric and magnetic susceptibilities*; Oxford University Press: Oxford, 1932.

[214] Heisenberg, W. *Zts. f. Phys* **1926**, *38*, 411.

[215] Heisenberg, W. *Zts. f. Phys* **1928**, *49*, 619.

[216] Dirac, P. A. In *Proc. R. Soc. London* The Royal Society: 1929; Vol. 123, p 714.

[217] Ciofini, I.; Daul, C. A.; Adamo, C. *J. Phys. Chem. A* **2003**, *107*, 11182.

[218] Noodleman, L. *J. Chem. Phys.* **1981**, *74*, 5737.

[219] Yamaguchi, K.; Takahara, Y.; Fueno, T. *Applied Quantum Chemistry*; 1986: Reidel, Dordrecht.

[220] Soda, T.; Kitagawa, Y.; Onishi, T.; Takano, Y.; Shigeta, Y.; Nagao, H.; Yoshioka, Y.; Yamaguchi, K. *Chem. Phys. Lett.* **2000**, *319*, 223.

[221] Noodleman, L.; Li, J.; Zhao, X.-G.; Richardson, W. H. *Density-functional methods in chemistry and materials science*; Wiley: Chichester, 1997.

[222] Ruiz, E.; Cano, J.; Alvarez, S.; Alemany, P. *J. Comput. Chem.* **1999**, *20*, 1391.

[223] Fagaly, R. L. *Rev. Sci. Instrum.* **2006**, *77*, 101101.

[224] Evans, D. F. *J. Chem. Soc.* **1959**, 2003.

[225] Piguet, C. *J. Chem. Educ.* **1997**, *74*, 815.

[226] Bowman, M. K. In *Electron Paramagnetic Resonance*; John Wiley & Sons, Inc.: 2008, p 159.

[227] DEER www.chem.ucsb.edu/hangroup/sites/secure.lsit.ucsb.edu.chem.d7_han/files/sitefiles/Links/DEER%20ppt.pdf 30.10.2016.

[228] Rowan, L. G.; Hahn, E. L.; Mims, W. B. *Phys. Rev. A* **1965**, *137*, 61.

[229] Mims, W. B. *Phys. Rev. B* **1972**, *5*, 2409.

[230] Comba, P.; Dovalil, N.; Haberhauer, G.; Hanson, G. R.; Kato, Y.; Taura, T. *JBIC Journal of Biological Inorganic Chemistry* **2010**, *15*, 1129.

[231] Schafer, F. Q.; Buettner, G. R. *Free Radical Biology and Medicine* **2001**, *30*, 1191.

[232] Reinhold, J. *Quantentheorie der Moleküle*; Springer Spektrum: Wiesbaden, 2013; Vol. 4.

[233] Møller, C.; Plesset, M. S. *Phys. Rev.* **1934**, *46*, 618.

[234] Pople, J. A.; Head-Gordon, M.; Raghavachari, K. *J. Chem. Phys.* **1987**, *87*, 5968.

[235] Hohenberg, P.; Kohn, W. *Phys. Rev. B* **1964**, *136*, 864.

[236] Kohn, W.; Sham, L. J. *Phys. Rev. A* **1965**, *140*, 1133.

[237] Perdew, J. P.; Chevary, J. A.; Vosko, S. H.; Jackson, K. A.; Pederson, M. R.; Singh, D. J.; Fiolhais, C. *Phys. Rev. B* **1992**, *46*, 6671.

[238] Becke, A. D. *J. Chem. Phys.* **1988**, *88*, 1053.

[239] Lee, C.; Yang, W.; Parr, R. G. *Phys. Rev. B* **1988**, *37*, 785.

[240] Becke, A. D. *Phys. Rev. A* **1988**, *38*, 3098.

[241] Becke, A. D. *J. Chem. Phys.* **1993**, *98*, 5648.

[242] Schäfer, A.; Horn, H.; Ahlrichs, R. *J. Chem. Phys.* **1992**, *97*, 2571.

[243] Weigend, F.; Ahlrichs, R. *Phys. Chem. Chem. Phys.* **2005**, *7*, 3297.

[244] Becke, A. D. *J. Chem. Phys.* **1993**, *98*, 5648.

[245] Frisch, M. J.; Trucks, G. W.; Schlegel, H. B.; Scuseria, G. E.; Robb, M. A.; Cheeseman, J. R.; Scalmani, G.; Barone, V.; Mennucci, B.; Petersson, G. A.; Nakatsuji, H.; Caricato, M.; Li, X.; Hratchian, H. P.; Izmaylov, A. F.; Bloino, J.; Zheng, G.; Sonnenberg, J. L.; Hada, M.; Ehara, M.; Toyota, K.; Fukuda, R.; Hasegawa, J.; Ishida, M.; Nakajima, T.; Honda, Y.; Kitao, O.;

Nakai, H.; Vreven, T.; Montgomery Jr., J. A.; Peralta, J. E.; Ogliaro, F.; Bearpark, M.; Heyd, J. J.; Brothers, E.; Kudin, K. N.; Staroverov, V. N.; Keith, T.; Kobayashi, R.; Normand, J.; Raghavachari, K.; Rendell, A.; Burant, J. C.; Iyengar, S.; Tomasi, J.; Cossi, M.; Rega, N.; Millam, N. J.; Klene, M.; Knox, J. E.; Cross, J. B.; Bakken, V.; Adamo, C.; Jaramillo, J.; Gomperts, R.; Stratmann, R. E.; Yazyev, O.; Austin, A. J.; Cammi, R.; Pomelli, C.; Ochterski, J. W.; Martin, R. L.; Morokuma, K.; Zakrzewski, V. G.; Voth, G. A.; Salvador, P.; Dannenberg, J. J.; Dapprich, S.; Daniels, A. D.; Farkas, O.; Foresman, J. B.; Ortiz, J. V.; Cioslowski, J.; Fox, D. J.; Gaussian, Inc.: Wallingford CT, 2013.

[246] Scalmani, G.; Frisch, M. J. *J. Chem. Phys.* **2010**, *132*, 114110.

[247] Neese, F. *Wiley Interdiscip. Rev. Comput. Mol. Sci.* **2012**, *2*, 73.

[248] Sinnecker, S.; Rajendran, A.; Klamt, A.; Diedenhofen, M.; Neese, F. *J. Phys. Chem. A* **2006**, *110 (6)*, 2235.

[249] Hanwell, M. D.; Curtis, D. E.; Lonie, D. C.; Vandermeersch, T.; Zurek, E.; Hutchinson, G. R. *J. Chem. Inf.* **2012**, *4*, 17.

[250] Comba, P. *Modeling of Molecular Properties*; Wiley VCH, Weinheim, 2011.

[251] Comba, P. *Inorg. Chem.* **1994**, *33*, 4577.

[252] Comba, P.; Zimmer, M. *Inorg. Chem* **1994**, *33*, 5368.

[253] Comba, P.; Hambley, T. W.; Hilfenhaus, P.; Richens, D. T. *J. Chem. Soc., Dalton Trans.* **1996**, 533.

[254] Comba, P.; Hilfenhaus, P.; Karlin, K. D. *Inorg. Chem.* **1997**, *36*, 2309.

[255] Comba, P.; Gloe, K.; Inoue, T.; Stephan, H.; Yoshizuka, K. *Inorg. Chem.* **1998**, *37*, 3310.

[256] Comba, P.; Gyr, T. *Eur. J. Inorg. Chem.* **1999**, 1787.

[257] Comba, P.; Remenyi, R. *J. Comput. Chem.* **2002**, *23*, 697.

[258] Bernhardt, P. V.; Comba, P. *Inorg. Chem.* **1992**, *31*, 2638.

[259] Malesevic, M.; Strijowski, U.; Bachle, D.; Sewald, N. *J. Biotechnol.* **2004**, *112*, 73.

[260] Degrand, C.; Limoges, B.; Blankespoor, R. L. *J. Org. Chem.* **1993**, *58*, 2573

[261] Tropic-Marine-Salt http://www.aquabluedistribution.com.au/productdetails/brandname/Tropic%20Marin/category/Salt/prdname/TM+Pro+Reef+750ltr%0Abucket+25kg 08.11.2016.

[2612] ToxyPAM user manual http://www.lombardemarozzini.com/sites/default/files/toxyp_2e.pdf 01.11.2016.

[263] FIJI http://fiji.sc/ 03.11.2016.

Appendix

Appendix I

Flow cytometry results for *Synechococcus leopoliensis*

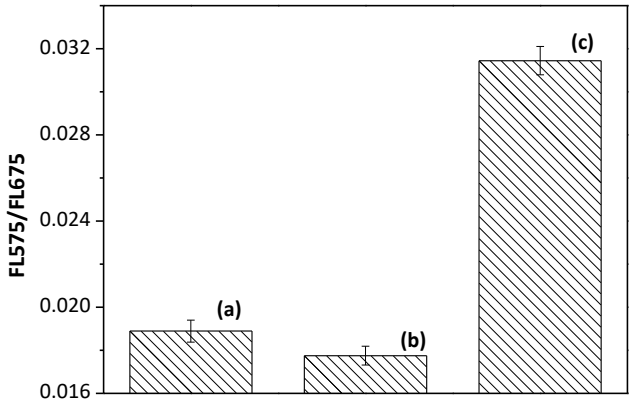

Figure AI-1. Mean and SEM of FL575/FL675 for *Synechococcus leopoliensis* (n=12,000) and treated with **(a)** with H_4pat-Atto550 **(b)** with H_4pat-Atto550 and Cu(II) and **(c)** with H_4pat-Atto550 and Cu(II) and subsequently cyclam.

Confocal microscopy results for *Synechococcus leopoliensis* and *Prochlorothrix hollandica*

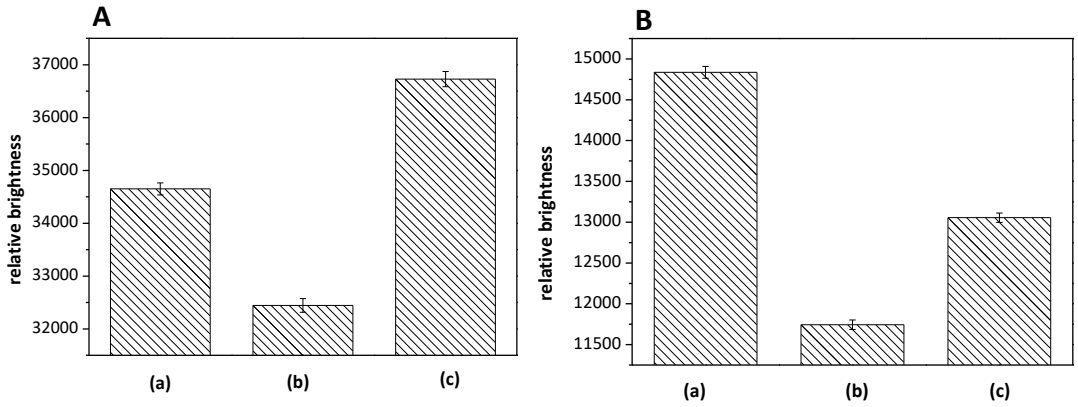

Figure AI-2. Mean and SEM -of FL574 for **A** *Synechococcus leopoliensis* and **B** *Prochlorothrix hollandica;* treated with **(a)** with H_4pat-Atto550 **(b)** with H_4pat-Atto550 and Cu(II) and **(c)** with H_4pat-Atto550 and Cu(II) and subsequently cyclam.

Appendix II

Cartesian Coordinates of Structures discussed in this thesis:

Chapter 3

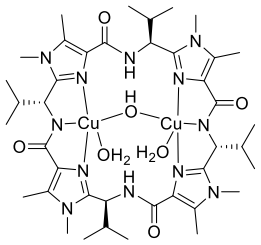

1A $[Cu_2(H_2pat^1)(\mu\text{–}OH)(H_2O)_2]^+$

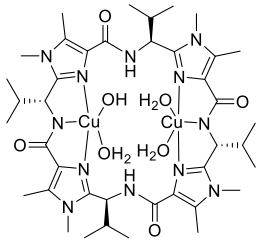

1B $[Cu_2(H_2pat^1)(OH)(H_2O)_3]^+$

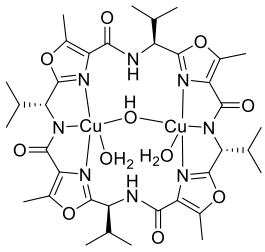

2A $[Cu_2(H_2pat^4)(\mu\text{-}OH)(H_2O)_2]^+$

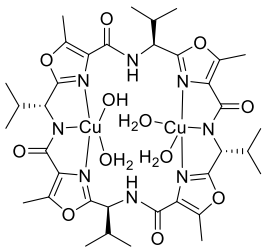

2B $[Cu_2(H_2pat^4)(OH)(H_2O)_3]^+$

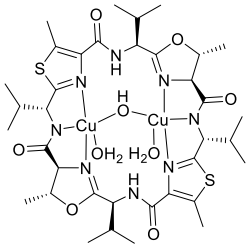

3A-I $[Cu_2(H_2pat^5)(\mu\text{–}OH)(H_2O)_2]^+$

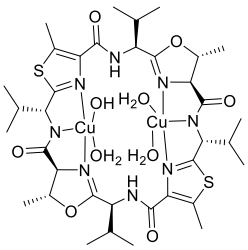

3B-I $[Cu_2(H_2pat^5)(OH)(H_2O)_3]^+$

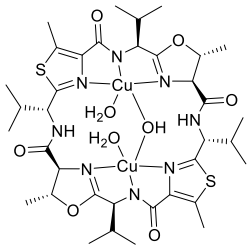

3A-II $[Cu_2(H_2pat^5)(\mu\text{–}OH)(H_2O)_2]^+$

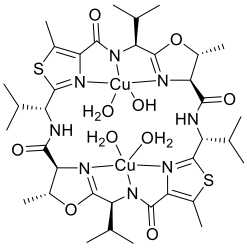

3B-II $[Cu_2(H_2pat^5)(OH)(H_2O)_3]^+$

1A

124

Cu	-0.526502	1.548025	-0.023527
N	1.402306	0.923817	0.515869
N	0.499747	2.603469	-1.301258
N	-2.021195	2.994809	-0.546076
N	-3.831876	1.771377	1.334286
H	-3.048883	1.270793	0.924712
N	3.421349	0.366641	1.170841
N	-2.329109	4.870060	-1.661606
O	2.563998	3.595771	-1.596953
O	-5.193332	3.580628	1.179330
O	-1.626602	0.006729	0.690337
O	-0.537567	2.710562	2.225313
C	2.089617	0.106288	1.294323
C	3.581329	1.413747	0.280602
C	2.314541	1.741078	-0.120453
C	1.816571	2.748851	-1.082160
C	-0.196871	3.567341	-2.130750
H	0.375249	4.500753	-2.154845
C	-1.508612	3.811710	-1.450672
C	-3.432921	4.728497	-0.850081
C	-3.234741	3.558385	-0.151648
C	-4.170104	2.981719	0.836323
C	-4.751889	0.994911	2.152315
H	-5.545762	1.682119	2.437261
C	4.520990	-0.306638	1.854383
H	5.390449	-0.316224	1.203173
H	4.774408	0.208561	2.780463
H	4.249523	-1.334270	2.075036
C	4.905817	1.974774	-0.094357
H	5.530256	1.231708	-0.596963
H	4.750803	2.810600	-0.771040
H	5.453849	2.328785	0.781894
C	-0.400351	3.115629	-3.613481
H	-1.001818	3.899746	-4.084860
C	-1.169752	1.800796	-3.734003
H	-1.331409	1.557879	-4.785693
H	-2.147588	1.848446	-3.251894
H	-0.611103	0.978144	-3.285097
C	0.928454	3.045569	-4.366878
H	0.747024	2.807775	-5.417213
H	1.575392	2.270230	-3.953420
H	1.468036	3.992028	-4.318067
C	-2.099204	5.990295	-2.567221
H	-2.380196	6.917645	-2.074141
H	-1.045913	6.039994	-2.823681
H	-2.686293	5.875737	-3.477945
C	-4.533381	5.728793	-0.849324
H	-5.352332	5.365529	-0.238981
H	-4.892669	5.915102	-1.863778
H	-4.195314	6.684921	-0.440077
C	-4.096037	0.464462	3.454140
H	-3.277529	-0.203112	3.168244
C	-3.526602	1.615576	4.285177
H	-3.058274	1.226712	5.191082
H	-4.320483	2.303256	4.588926
H	-2.775446	2.181068	3.735750
C	-5.091516	-0.352565	4.282982
H	-4.601525	-0.739998	5.177200
H	-5.493044	-1.205615	3.733392
H	-5.931155	0.266639	4.609250
H	0.360768	2.990672	2.439432
H	-1.055719	3.524809	2.207503
Cu	-2.726787	-1.534823	-0.023612
C	1.499057	-0.982056	2.151554
C	-5.342533	-0.093274	1.294933
N	-4.655415	-0.910645	0.516134
N	-3.753262	-2.589885	-1.301509
N	-1.232268	-2.981425	-0.546690
O	-2.714678	-2.697042	2.224940
C	-5.567836	-1.727575	-0.120339
C	-5.070099	-2.735116	-1.082394
C	-1.744996	-3.798178	-1.451348
H	-3.612739	-2.976889	2.440548
C	-3.056795	-3.553654	-2.131250
C	-0.018678	-3.545092	-0.152520
H	-2.196554	-3.511317	2.207462
C	-6.834536	-1.400230	0.280983
O	-5.817684	-3.581752	-1.597424
N	-0.924572	-4.856531	-1.662526
N	-6.674322	-0.353443	1.171549
H	-3.628970	-4.487029	-2.155446
C	-2.853424	-3.101721	-3.613934
C	0.179363	-4.715111	-0.851139
C	0.916859	-2.968631	0.835402
C	-8.159097	-1.961012	-0.094107
C	-1.154652	-5.976646	-2.568246
C	-7.773684	0.319814	1.855559
H	-2.252061	-3.885812	-4.085488
C	-4.182283	-3.031423	-4.367218
C	-2.083928	-1.786931	-3.734311
C	1.279795	-5.715440	-0.850697
N	0.578856	-1.758276	1.333504
O	1.940048	-3.567698	1.178238
H	-8.004157	-2.796626	-0.771067

H	-8.783468	-1.217727	-0.596473
H	-8.707166	-2.315281	0.782014
H	-0.873511	-6.904053	-2.075362
H	-2.208001	-6.026344	-2.824467
H	-0.567772	-5.861941	-3.479087
H	-8.643908	0.327841	1.205367
H	-8.025663	-0.194443	2.782558
H	-7.502788	1.347952	2.074605
H	-4.000896	-2.793500	-5.417532
H	-4.829113	-2.256078	-3.953605
H	-4.721955	-3.977832	-4.318494
H	-2.642482	-0.964314	-3.285220
H	-1.922347	-1.543862	-4.785978
H	-1.106052	-1.834720	-3.252298
H	2.098895	-5.352258	-0.240506
H	1.638851	-5.901677	-1.865245
H	0.941791	-6.671588	-0.441446
H	-0.204076	-1.257526	0.924032
H	2.292896	-1.669402	2.436245
C	0.843487	-0.451813	3.453617
H	0.024878	0.215762	3.168013
C	0.274332	-1.603079	4.284632
C	1.839122	0.365151	4.282341
H	-0.193837	-1.214357	5.190681
H	1.068337	-2.290726	4.588125
H	-0.476914	-2.168563	3.735317
H	1.349363	0.752241	5.176837
H	2.240307	1.218437	3.732877
H	2.678982	-0.253998	4.608142
H	-1.626406	0.006356	1.654304

1B

127

C	2.781258	-4.575026	-0.728404
C	3.080984	-3.249402	-0.556598
N	2.138056	-2.663191	0.268265
C	1.271923	-3.610101	0.599331
N	1.627248	-4.783981	-0.000607
C	4.144938	-2.415368	-1.171036
O	5.052097	-2.911379	-1.864371
Cu	2.646925	-0.586172	0.381898
O	1.260001	0.082157	1.525977
C	0.086712	-3.513791	1.528562
C	0.494079	-2.999808	2.936724
C	-0.716445	-2.749369	3.835539
N	3.276584	1.391409	-0.278510
C	3.246506	2.734326	0.092466
C	4.454077	3.310742	-0.235530
N	5.203202	2.311893	-0.822350
C	4.447523	1.184184	-0.859946
C	2.064947	3.480309	0.604886
O	2.042487	4.716814	0.553994
C	4.777494	-0.107247	-1.557512
C	4.480523	-0.052314	-3.099966
C	3.050675	0.384120	-3.423117
N	1.033534	2.758684	1.089291
C	-0.124617	3.405030	1.697963
C	-0.534282	2.714566	3.025047
C	0.638211	2.684541	4.010169
C	-1.295312	3.557615	0.747029
N	-2.110757	2.623635	0.271534
C	-3.116326	3.277544	-0.421297
C	-2.897122	4.627494	-0.380955
N	-1.738392	4.786760	0.351636
C	-4.199592	2.490862	-1.062482
O	-5.150328	3.028788	-1.657753
Cu	-2.448099	0.569011	0.048895
O	-0.579298	-0.136844	-0.067172
N	-3.344962	-1.314626	-0.297761
C	-3.361749	-2.625075	0.176794
C	-4.582394	-3.187231	-0.134920
N	-5.294051	-2.207862	-0.793375
C	-4.513341	-1.103097	-0.886058
C	-2.269213	-3.355766	0.872504
N	-1.030044	-2.805988	0.894036
C	-4.850524	0.200294	-1.558098
N	-3.999302	1.179729	-0.911746
O	-2.506478	-4.447284	1.398597
C	-4.629823	0.190639	-3.112459
C	-3.223470	-0.247650	-3.522095
C	-5.690996	-0.604111	-3.874432
O	-2.935968	0.249332	2.377608
O	4.279896	-0.712138	2.249806
N	3.967111	-1.118570	-0.905190
C	-1.733315	3.421103	3.665526
C	5.495750	0.775449	-3.888714
C	1.458515	-3.994058	3.592360
H	0.194305	4.414258	1.952333
H	-0.825005	1.686725	2.796701
H	0.333245	2.196588	4.937714
H	0.961402	3.699239	4.258483
H	1.497534	2.143784	3.615675
H	-2.025198	2.903910	4.580838
H	-2.603030	3.450851	3.007554
H	-1.483404	4.450767	3.934630
H	5.841711	-0.339710	-1.443515
H	4.597303	-1.090354	-3.414229
H	2.887922	1.439423	-3.191713
H	2.315955	-0.201273	-2.869283
H	2.854704	0.245800	-4.488414
H	5.405905	1.843971	-3.682297
H	6.522531	0.468109	-3.680019
H	-0.289431	-4.522531	1.683165
H	1.032707	-2.061735	2.808435
H	-0.383461	-2.398254	4.813923
H	-1.290897	-3.665822	3.984559
H	-1.382041	-1.993900	3.419280
H	1.777369	-3.622041	4.567187
H	2.355046	-4.156499	2.991736
H	0.973893	-4.961684	3.747177
H	-5.904483	0.443780	-1.385998
H	-4.751953	1.239835	-3.387694
H	-3.049393	-1.304260	-3.304596
H	-2.453807	0.336120	-3.016676
H	-3.091854	-0.106824	-4.596768
H	-6.703381	-0.298400	-3.602827
H	-5.597822	-1.679341	-3.708393
H	1.166139	1.757257	1.267449
H	-0.861318	-1.928964	0.411081
H	-5.574875	-0.435388	-4.946765
H	5.325273	0.641683	-4.958885
H	-3.406452	1.008370	2.744735
H	-3.531381	-0.500092	2.505477
H	4.979489	-1.308962	1.956064
H	3.992158	-1.059914	3.102988
H	1.182514	-0.305094	2.401181
H	0.161721	-0.026122	0.687317

H	-0.186716	0.129219	-0.907574
C	3.461712	-5.641049	-1.511081
H	2.815552	-6.036729	-2.298860
H	4.350479	-5.219708	-1.972008
H	3.758468	-6.478482	-0.875176
C	0.934056	-6.065063	0.104116
H	1.202543	-6.678383	-0.750386
H	1.218154	-6.587702	1.017375
H	-0.141503	-5.913003	0.091173
C	6.602732	2.459560	-1.206430
H	7.006097	1.493371	-1.486204
H	6.703742	3.145834	-2.045429
H	7.170939	2.842977	-0.360921
C	5.002633	4.680485	-0.047955
H	5.243177	5.145229	-1.007828
H	4.271903	5.298951	0.460368
H	5.922724	4.655391	0.541343
C	-5.168794	-4.534919	0.096151
H	-4.391313	-5.227155	0.397196
H	-5.919902	-4.505626	0.890852
H	-5.659608	-4.905297	-0.805649
C	-6.691661	-2.346991	-1.190729
H	-7.091144	-1.375093	-1.455944
H	-6.787550	-3.017726	-2.042672
H	-7.264076	-2.744653	-0.355335
C	-3.662127	5.760726	-0.965691
H	-4.545189	5.365182	-1.459494
H	-3.974959	6.472449	-0.198267
H	-3.068347	6.308057	-1.702179
C	-1.121007	6.078918	0.646589
H	-1.406372	6.784842	-0.127775
H	-1.459181	6.458196	1.611080
H	-0.039189	5.976975	0.644155

2A

110

Cu	-0.584883	1.475461	-0.069626
N	1.372700	0.810696	0.290734
N	0.375338	2.599392	-1.356491
N	-2.131920	2.909824	-0.501194
N	-3.821937	1.856373	1.608462
H	-2.987829	1.381340	1.278947
O	2.400771	3.681774	-1.635305
O	-5.404960	3.399715	1.077837
O	-1.648184	-0.020356	0.737717
O	-0.481391	2.566248	2.144787
C	2.107965	-0.035483	0.941434
C	3.514223	1.385405	0.050282
C	2.250312	1.723797	-0.293113
C	1.692215	2.784224	-1.164094
C	-0.370792	3.575767	-2.127627
H	0.122945	4.552613	-2.080965
C	-1.687237	3.685778	-1.442662
C	-3.650455	4.489258	-0.967320
C	-3.402421	3.417083	-0.168623
C	-4.302197	2.893835	0.882841
C	-4.681448	1.124150	2.524646
H	-5.516382	1.781116	2.768962
C	4.860227	1.920162	-0.232331
H	5.483879	1.164032	-0.713760
H	4.768081	2.780680	-0.890198
H	5.357666	2.228184	0.689969
C	-0.567928	3.227752	-3.638627
H	-1.233569	4.006785	-4.024670
C	-1.243722	1.872558	-3.848678
H	-1.402140	1.697762	-4.913963
H	-2.217371	1.814390	-3.358118
H	-0.622679	1.060873	-3.465518
C	0.746736	3.315774	-4.413391
H	0.557687	3.157006	-5.477020
H	1.454822	2.554927	-4.081427
H	1.220463	4.290421	-4.292533
C	-4.751669	5.456843	-1.141585
H	-5.536937	5.248306	-0.422792
H	-5.159033	5.389078	-2.153055
H	-4.385484	6.475734	-0.997939
C	-3.961704	0.736112	3.841551
H	-3.097012	0.117142	3.581353
C	-3.462977	1.988233	4.564968
H	-2.933005	1.704885	5.475629
H	-4.300475	2.629866	4.850808
H	-2.781518	2.569575	3.945372
C	-4.874745	-0.090065	4.751263
H	-4.344650	-0.347367	5.668959
H	-5.196942	-1.022484	4.285809
H	-5.767976	0.475011	5.028817
H	0.382246	2.641188	2.569158
H	-0.858584	3.454155	2.178824
Cu	-2.882339	-1.445507	0.068722
C	1.697475	-1.270653	1.689624
C	-5.261128	-0.047990	1.787036
N	-4.700468	-0.830165	0.918383
N	-4.118778	-2.478123	-1.046153
N	-1.487129	-2.842407	-0.802920
O	-2.508557	-2.670298	2.192183
C	-5.695078	-1.704512	0.480767
C	-5.359148	-2.688476	-0.574121
C	-2.141697	-3.544005	-1.677849
H	-3.294835	-2.807460	2.734860
C	-3.577517	-3.389388	-2.036933
C	-0.182670	-3.372435	-0.800581
H	-2.131793	-3.550283	2.067631
C	-6.844014	-1.409918	1.131075
O	-6.164286	-3.553229	-0.939712
H	-4.058573	-4.369963	-1.950726
C	-3.727574	-2.931518	-3.523650
C	-0.134630	-4.378595	-1.713833
C	0.934365	-2.931759	0.063831
C	-8.221823	-1.938003	1.123800
H	-3.183499	-3.681231	-4.107606
C	-5.187323	-2.960299	-3.975964
C	-3.094613	-1.565561	-3.790751
C	0.886635	-5.325918	-2.202418
N	0.647811	-1.931236	0.929936
O	2.037176	-3.469041	-0.006753
H	-8.285339	-2.749947	0.403724
H	-8.934684	-1.157400	0.849902
H	-8.498812	-2.314089	2.111094
H	-5.247232	-2.720808	-5.039591
H	-5.784877	-2.226471	-3.432887
H	-5.637815	-3.940851	-3.820383
H	-3.600246	-0.780424	-3.225898
H	-3.177450	-1.319238	-4.850460
H	-2.034331	-1.540471	-3.531477
H	1.822741	-5.151057	-1.682819
H	1.037298	-5.199118	-3.276888
H	0.561747	-6.354659	-2.031158
H	-0.223394	-1.423811	0.810319
H	2.559158	-1.938111	1.684828
C	1.293360	-1.003305	3.162550

H 0.389239 -0.385902 3.154736
C 0.978385 -2.319707 3.874857
C 2.385508 -0.230752 3.907199
H 0.657095 -2.121471 4.898497
H 1.865394 -2.956838 3.919444
H 0.184361 -2.872176 3.374234
H 2.079815 -0.064510 4.940770
H 2.585295 0.745282 3.462856
H 3.322513 -0.793038 3.922426
H -1.535015 -0.072504 1.693632
O 81.443281 -0.335386 0.209826
H 80.582413 -0.763025 0.284697
H 82.078981 -1.032240 0.409473
O -2.553061 4.649081 -1.776849
O -6.560950 -0.345569 1.961119
O -1.386475 -4.476807 -2.269000
O 3.416436 0.256006 0.836096

2B

110

C 3.810780 -3.936005 -0.269569
C 3.787855 -2.583012 -0.261604
N 2.627022 -2.161596 0.395040
C 1.994298 -3.241990 0.743565
C 4.701538 -1.582010 -0.874553
O 5.775878 -1.922710 -1.391965
Cu 2.728288 -0.024662 0.420253
O 1.229053 0.392466 1.544486
C 0.707892 -3.487668 1.489429
C 0.741001 -2.956416 2.947424
C -0.511961 -3.390646 3.709065
N 2.920715 1.954952 -0.383212
C 2.480513 3.292455 -0.348510
C 3.407393 4.049743 -0.996018
C 4.035892 1.967488 -1.049839
C 1.203631 3.813246 0.213909
O 0.864273 4.974825 -0.016495
C 4.837740 0.771324 -1.455992
C 4.920777 0.622017 -3.013478
C 3.551068 0.696638 -3.689750
N 0.462397 2.965846 0.957403
C -0.724325 3.426261 1.659599
C -0.816877 2.813813 3.082799
C 0.434752 3.149487 3.89456
C -2.001443 3.218098 0.879407
N -2.585730 2.167307 0.381308
C -3.819648 2.604803 -0.115538
C -3.924285 3.935220 0.102208
C -4.752780 1.632644 -0.740088
O -5.881746 1.967990 -1.125722
Cu -2.503404 0.094046 0.040914
O -0.556178 -0.255423 0.022089
N -2.996313 -1.916880 -0.417929
C -2.652504 -3.276404 -0.273863
C -3.648051 -4.013684 -0.838123
C -4.141778 -1.904069 -1.032490
C -1.461853 -3.858990 0.406928
N -0.450266 -3.021479 0.731653
C -4.922155 -0.688778 -1.417247
N -4.201641 0.417494 -0.817024
O -1.441951 -5.063580 0.655797
C -5.098096 -0.540875 -2.965428
C -3.776121 -0.650618 -3.725954
C -6.156044 -1.497023 -3.520121
O -2.843135 -0.360087 2.348417
O 4.246256 0.235344 2.304826
N 4.184466 -0.351430 -0.806744
C -2.070065 3.302090 3.815765
C 5.921686 1.595022 -3.640157
C 2.004498 -3.422036 3.676572
H -0.638253 4.509467 1.757825
H -0.883215 1.727838 2.969601
H 0.356789 2.707944 4.893308
H 0.538724 4.230865 4.019932
H 1.345714 2.771314 3.436242
H -2.117204 2.850129 4.807159
H -2.993076 3.043860 3.294453
H -2.050099 4.387130 3.944195
H 5.863888 0.894963 -1.087369
H 5.315331 -0.384293 -3.152713
H 3.130228 1.704964 -3.648828
H 2.838644 0.010640 -3.229278
H 3.640818 0.425613 -4.743215
H 5.590081 2.631695 -3.569035
H 6.901295 1.519045 -3.163012
H 0.608903 -4.571761 1.536696
H 0.747908 -1.865122 2.901750
H -0.505381 -2.960243 4.711522
H -0.549824 -4.477734 3.809668
H -1.424135 -3.063249 3.211586
H 1.998149 -3.052969 4.702982
H 2.916876 -3.058002 3.201666
H 2.053099 -4.513154 3.716014
H -5.926818 -0.776197 -0.985482
H -5.478868 0.474470 -3.083187
H -3.370953 -1.665688 -3.690414
H -3.023760 0.031188 -3.326814
H -3.928689 -0.398121 -4.776746
H -7.102715 -1.396468 -2.984794
H -5.840693 -2.539609 -3.457802
H 0.833380 2.045215 1.212311
H -0.500950 -2.045159 0.451353
H -6.342121 -1.270511 -4.571675
H 6.048643 1.360364 -4.698863
H -3.409555 0.284498 2.790715
H -3.268041 -1.213524 2.501571
H 5.119405 -0.137554 2.129520
H 3.992322 -0.106558 3.171095
H 1.264473 0.024888 2.432054
H 0.163886 0.040351 0.759991
H -0.192829 -0.056675 -0.850128
C 4.727870 -4.970565 -0.787578
H 4.216722 -5.616962 -1.504255
H 5.568455 -4.485953 -1.277020

H	5.099991	-5.599343	0.024342
C	3.589392	5.481102	-1.311719
H	3.539070	5.643731	-2.391180
H	2.811611	6.063724	-0.830373
H	4.570395	5.817925	-0.970244
C	-3.933146	-5.448341	-1.042858
H	-3.054040	-6.036572	-0.803409
H	-4.754993	-5.769373	-0.397669
H	-4.232097	-5.625905	-2.077373
C	-4.939092	4.969808	-0.178092
H	-5.789773	4.506468	-0.670798
H	-5.273915	5.444557	0.746713
H	-4.528821	5.748394	-0.824952
O	-2.764590	4.320112	0.729168
O	-4.586412	-3.132665	-1.315835
O	2.665870	-4.350571	0.366326
O	4.393896	3.199433	-1.431632

3A-I

115

Cu	1.671776	-1.898371	-0.027856
N	-0.219789	-2.351297	0.677803
N	1.262096	-3.356618	-1.237853
N	3.746046	-2.310362	-0.815881
N	4.617669	-0.143413	0.855625
H	3.658795	-0.209519	0.531643
O	0.116434	-5.364079	-1.287707
O	6.742790	-0.897866	0.713067
O	1.729097	0.007940	0.626944
O	2.599959	-2.883043	1.941450
C	-0.959370	-2.201374	1.717105
C	0.268267	-4.192569	-0.912116
C	2.278905	-3.803036	-2.168085
H	2.329982	-4.896426	-2.157785
C	3.598509	-3.267397	-1.696534
C	5.974656	-2.799352	-1.308177
C	5.098712	-2.037743	-0.574733
C	5.561751	-0.986258	0.383787
C	4.967097	1.056290	1.600624
H	6.051827	1.058542	1.703855
C	-2.707641	-5.088665	0.666264
H	-3.540830	-4.415683	0.463156
H	-2.499244	-5.669709	-0.231174
H	-3.000590	-5.778313	1.457748
C	2.007147	-3.378634	-3.649403
H	2.873073	-3.736938	-4.216703
C	1.914209	-1.863334	-3.831910
H	1.770092	-1.624375	-4.887032
H	2.818013	-1.350066	-3.498394
H	1.066766	-1.452406	-3.280461
C	0.768638	-4.076939	-4.211795
H	0.669573	-3.851401	-5.275638
H	-0.140290	-3.734869	-3.713130
H	0.829842	-5.159294	-4.095238
C	7.467476	-2.821177	-1.394177
H	7.893065	-2.028465	-0.791513
H	7.788101	-2.704912	-2.431377
H	7.855464	-3.778637	-1.038753
C	4.351661	1.117641	3.025976
H	3.262127	1.149434	2.927436
C	4.728968	-0.133073	3.820289
H	4.312059	-0.072008	4.826860
H	5.814111	-0.222874	3.911414
H	4.347866	-1.039589	3.351519
C	4.796347	2.383218	3.767665
H	4.327792	2.419857	4.751650
H	4.527785	3.300186	3.241251
H	5.879519	2.388276	3.911525
H	2.080836	-3.516963	2.451282
H	3.494468	-3.245486	1.932477
Cu	1.554047	1.917456	-0.026210
C	-0.990838	-1.012746	2.643401
C	4.612820	2.239736	0.737935
N	3.566688	2.380638	0.005439
N	1.537175	3.349760	-1.334287
N	-0.656362	2.311885	-0.096466
O	1.342418	2.913863	2.132585
C	2.576129	4.191419	-1.380711
C	-0.817953	3.242758	-1.002508
H	2.007837	3.547687	2.428353
C	0.267755	3.765501	-1.896709
C	-1.852252	2.037359	0.579628
H	0.501337	3.281596	2.430778
O	2.592615	5.345036	-1.827665
H	0.209532	4.858616	-1.901974
C	0.044586	3.291688	-3.371741
C	-2.930186	2.773692	0.154207
C	-1.962805	1.005182	1.657601
C	5.847125	5.190449	-0.789855
H	-0.966715	3.623035	-3.631399
C	1.013079	3.978097	-4.335690
C	0.099108	1.771529	-3.525109
C	-4.369964	2.783435	0.558726
N	-0.903746	0.180840	1.815393
O	-2.968021	0.922846	2.360111
H	5.330775	5.793218	-1.536909
H	6.571884	4.551572	-1.295396
H	6.377005	5.860798	-0.113823
H	0.759697	3.710899	-5.363610
H	2.042935	3.664760	-4.154822
H	0.970217	5.063811	-4.243337
H	1.090252	1.387379	-3.277433
H	-0.115498	1.494015	-4.558593
H	-0.630506	1.265965	-2.889918
H	-4.565203	2.003026	1.283784
H	-5.009441	2.639509	-0.314511
H	-4.634562	3.746806	1.001044
H	-0.111054	0.241151	1.183310
H	-1.976248	-1.003436	3.107718
C	0.067457	-1.082394	3.776604
H	1.058722	-1.134069	3.316017
C	0.000736	0.169288	4.653147
C	-0.125661	-2.343462	4.625516
H	0.728942	0.092099	5.462126

H	-0.989321	0.276383	5.103107
H	0.221084	1.073180	4.087373
H	0.652608	-2.401500	5.387273
H	-0.082702	-3.262098	4.038555
H	-1.092603	-2.322475	5.134137
H	1.896900	0.009721	1.576683
O	-79.277579	-0.094408	-0.434727
H	-78.416651	-0.033785	-0.005313
H	-79.914796	0.021061	0.279321
S	5.080162	-3.888718	-2.301857
S	-2.423940	3.840684	-1.102857
O	5.527516	3.215907	0.650826
O	-1.854318	-3.169870	1.951138
C	3.855609	3.541337	-0.888352
H	4.389694	3.140060	-1.757967
C	4.840765	4.337621	-0.059127
H	4.318251	4.874014	0.738714
C	-1.479149	-4.292156	1.045044
H	-0.750048	-4.868823	1.618927
C	-0.793810	-3.512071	-0.064816
H	-1.553967	-3.111242	-0.741910

3B-I

115

N	1.239978	-2.793367	-0.035337
C	0.396413	-3.636875	0.443156
C	3.345284	-2.999101	-1.416686
O	4.139620	-3.717531	-2.040796
Cu	2.374270	-0.953333	0.281460
O	1.277380	0.023389	1.480567
C	-0.743139	-3.458721	1.434554
C	-0.308968	-2.857500	2.791752
C	-1.481839	-2.835399	3.774017
N	3.622487	0.865247	-0.256380
C	3.853469	2.162481	0.196577
C	5.171537	2.547478	0.170754
C	4.717070	0.297698	-0.699616
C	2.780264	3.158433	0.540332
O	3.041107	4.358058	0.436114
C	4.737822	-1.027821	-1.414005
C	4.841626	-0.847560	-2.971360
C	3.810274	0.128367	-3.538894
N	1.573182	2.704961	0.945138
C	0.574079	3.638867	1.465287
C	0.059157	3.216722	2.863982
C	1.220874	3.079804	3.851590
C	-0.560234	3.848666	0.488745
N	-1.530551	3.033371	0.202215
C	-3.416966	2.946652	-1.314803
O	-4.232123	3.558007	-2.211984
Cu	-2.432886	0.981241	0.465380
O	-0.776489	-0.203211	0.024863
N	-3.725433	-1.109258	-0.452056
C	-4.111307	-2.301469	0.119243
C	-5.460811	-2.565062	0.072631
C	-4.722624	-0.446678	-0.954086
C	-3.099266	-3.212879	0.736679
N	-1.830930	-2.732897	0.789275
C	-4.594561	0.869628	-1.698076
N	-3.600797	1.692512	-1.009106
O	-3.424452	-4.317406	1.172546
C	-4.243954	0.658070	-3.214832
C	-2.901880	-0.036686	-3.446012
C	-5.373865	-0.052235	-3.963441
O	-2.926497	0.658376	2.541666
O	3.893046	-1.613746	2.075127
N	3.529607	-1.739972	-1.025047
C	-0.972688	4.217664	3.393307
C	6.258406	-0.504756	-3.433402
C	0.869419	-3.634534	3.385836
H	1.071703	4.604582	1.551662
H	-0.426191	2.242266	2.757640
H	0.843545	2.766596	4.826479
H	1.733966	4.036008	3.983871
H	1.954675	2.343442	3.525804
H	-1.312356	3.912990	4.384306
H	-1.852575	4.285597	2.752205
H	-0.538925	5.216966	3.483286
H	5.626215	-1.587721	-1.101414
H	4.615403	-1.842268	-3.354566
H	4.032346	1.162339	-3.263812
H	2.802843	-0.105688	-3.191900
H	3.809075	0.072789	-4.629320
H	6.561253	0.501910	-3.137733
H	6.990919	-1.210922	-3.035805
H	-1.121705	-4.463045	1.621099
H	0.003028	-1.828422	2.608687
H	-1.176128	-2.359450	4.707251
H	-1.815293	-3.849394	4.007075
H	-2.332917	-2.280750	3.380505
H	1.150749	-3.208342	4.350030
H	1.749083	-3.604867	2.742436
H	0.603232	-4.681753	3.551151
H	-5.568382	1.369895	-1.676537
H	-4.173522	1.667037	-3.621796
H	-2.911236	-1.066029	-3.084628
H	-2.084964	0.489860	-2.951712
H	-2.683716	-0.059492	-4.515586
H	-6.337136	0.436188	-3.799995
H	-5.468428	-1.097970	-3.665120
H	1.458400	1.702058	1.155032
H	-1.627511	-1.810505	0.407775
H	-5.170765	-0.034603	-5.035838
H	6.311846	-0.549334	-4.523131
H	-3.256086	1.454867	2.977070
H	-3.616838	-0.005046	2.667089
H	4.348940	-2.446069	1.899581
H	3.641395	-1.649101	3.006075
H	1.314505	-0.277510	2.392643
H	0.007584	-0.097523	0.660727
H	-0.455878	-0.057982	-0.871354
C	5.838421	3.824063	0.573051
H	5.760019	4.568602	-0.220703
H	5.368177	4.245096	1.458657
H	6.895837	3.656184	0.778796
C	-6.250430	-3.731556	0.574305
H	-6.012516	-4.631767	0.005653
H	-6.009506	-3.939243	1.615924

H	-7.320455	-3.545374	0.490312
S	6.121984	1.264151	-0.474953
S	-6.244068	-1.250123	-0.722974
O	-0.606216	5.032025	-0.142808
O	0.474357	-4.889409	-0.032572
C	-1.820321	5.048618	-0.962856
C	-2.343771	3.656225	-0.709294
H	-3.971744	4.471814	-2.379925
C	1.930804	-3.498242	-1.146092
H	1.376084	-3.256656	-2.061511
C	1.712347	-4.981186	-0.829272
C	-2.695298	6.217141	-0.525357
H	-2.134743	7.147301	-0.614271
H	-3.576611	6.299157	-1.163411
H	-3.026110	6.091456	0.505115
H	-1.492214	5.189729	-1.997608
H	1.457196	-5.553325	-1.716807
C	2.770403	-5.689787	-0.009664
H	2.396707	-6.662473	0.311036
H	3.661385	-5.837265	-0.617135
H	3.046396	-5.112418	0.874130

3A-II

112

Cu	0.816328	-1.617483	-0.128173
Cu	-0.802165	1.643723	-0.162971
N	1.199566	-2.529643	1.537972
C	2.467478	-2.628059	1.954343
O	2.877564	-3.323080	2.894182
C	3.396147	-1.809340	1.121066
N	2.871970	-1.176803	0.004644
C	4.739615	-1.643710	1.305720
S	5.347530	-0.663433	0.022889
C	3.784932	-0.539252	-0.682446
C	3.552587	0.297244	-1.918937
C	3.144752	-0.521797	-3.169018
C	4.194822	-1.587997	-3.493902
C	2.923508	0.398697	-4.371334
N	2.584364	1.328189	-1.579454
C	2.880895	2.636854	-1.569461
O	3.949319	3.114717	-1.935427
C	1.748322	3.561626	-1.118015
C	2.288238	4.818096	-0.388550
C	2.038952	6.134892	-1.083062
N	0.798084	2.972994	-0.162034
O	1.553010	4.793255	0.887587
C	0.759122	3.735634	0.873508
C	-0.190145	3.511368	2.009298
C	0.500376	3.038296	3.327011
C	1.403633	1.821793	3.129416
C	1.238515	4.182727	4.025159
N	-1.176297	2.578371	1.494519
C	-2.438946	2.676603	1.925498
O	-2.839146	3.382077	2.862439
C	-3.375049	1.840588	1.120554
N	-2.864907	1.176859	0.015347
C	-4.717815	1.690190	1.323253
S	-5.344813	0.680504	0.074446
C	-3.789873	0.529534	-0.646111
C	-3.593141	-0.346314	-1.862113
C	-3.260213	0.424805	-3.164282
C	-4.322685	1.484036	-3.465780
C	-3.115823	-0.544984	-4.339701
N	-2.598699	-1.354419	-1.527588
C	-2.875712	-2.667267	-1.498577
O	-3.944775	-3.163024	-1.838567
C	-1.727656	-3.575713	-1.053761
C	-2.246561	-4.828982	-0.302930
C	-1.954868	-6.154558	-0.963858
N	-0.770943	-2.967545	-0.115054
O	-1.528409	-4.758640	0.981637
C	-0.734590	-3.702221	0.941460
C	0.214339	-3.451921	2.072678
C	-0.474164	-2.952209	3.380803
C	-1.368049	-1.732449	3.161596
C	-1.222825	-4.078925	4.096544
H	4.483199	0.817174	-2.147887
H	2.199746	-1.022889	-2.941072
H	5.165538	-1.128876	-3.698532
H	3.901208	-2.144950	-4.385228
H	4.331958	-2.302474	-2.680281
H	3.848067	0.913762	-4.643964
H	2.160583	1.151818	-4.174234
H	2.600890	-0.187255	-5.233377
H	1.206374	3.843338	-2.025139
H	3.340170	4.699462	-0.139301
H	0.978772	6.267103	-1.305802
H	2.596744	6.154264	-2.020599
H	2.378163	6.966478	-0.465318
H	-0.667825	4.471715	2.230073
H	-0.337260	2.743178	3.963519
H	0.879364	1.004787	2.632689
H	1.749671	1.453836	4.096787
H	2.288695	2.068478	2.536972
H	2.087021	4.535514	3.436248
H	0.576170	5.031953	4.206031
H	-4.524867	-0.888133	-2.028870
H	-2.305460	0.933375	-3.013927
H	-4.391207	2.233977	-2.677746
H	-5.307459	1.025529	-3.590698
H	-4.078533	2.002254	-4.394381
H	-4.055935	-1.067125	-4.533815
H	-2.342567	-1.292321	-4.161130
H	-2.846530	0.004443	-5.243266
H	-1.191917	-3.858353	-1.963778
H	-3.304013	-4.731003	-0.069937
H	-0.889988	-6.262150	-1.177306
H	-2.505846	-6.213453	-1.903743
H	-2.274215	-6.979861	-0.327260
H	0.692314	-4.407712	2.312241
H	0.364397	-2.652634	4.013993
H	-1.714307	-1.347255	4.122153
H	-2.253090	-1.982052	2.570388
H	-0.836773	-0.926595	2.654414
H	-2.079149	-4.427724	3.516649
H	-0.570568	-4.934495	4.284030
H	1.676342	1.018928	-1.242609
H	-1.693676	-1.028451	-1.203307

O	0.003205	-0.005419	-1.059566
H	-0.017108	-0.026796	-2.022897
O	-1.545889	3.191900	-2.111208
H	-1.412606	3.221177	-3.066232
O	1.441921	-3.404877	-2.081101
H	1.488255	-4.244095	-1.606299
H	-1.624247	4.113567	-1.836827
H	2.170788	-3.443329	-2.712161
H	-1.595358	-3.724291	5.059363
H	1.620945	3.844665	4.990056
C	-5.607642	2.259639	2.380177
H	-5.873063	3.292767	2.145412
H	-6.529961	1.685927	2.466090
H	-5.097306	2.265168	3.340336
C	5.643689	-2.178757	2.368320
H	5.128198	-2.199026	3.325382
H	5.946457	-3.202506	2.137304
H	6.545254	-1.573237	2.456916

3B-II

115

Cu	2.497601	0.266638	-0.288960
Cu	-2.657617	-0.215243	-0.389841
N	3.898789	0.420694	1.024595
C	4.290868	1.635735	1.407834
O	5.255265	1.916300	2.134034
C	3.402462	2.705371	0.844545
N	2.439084	2.338448	-0.085170
C	3.445324	4.038687	1.140497
S	2.243201	4.840072	0.203903
C	1.753499	3.363127	-0.533059
C	0.702655	3.416975	-1.627690
C	1.184776	2.792559	-2.962789
C	2.480552	3.463765	-3.431913
C	0.111673	2.922653	-4.048023
N	-0.599352	2.906360	-1.196644
C	-1.664835	3.727039	-1.074220
O	-1.594916	4.950283	-1.127328
C	-3.048228	3.059538	-0.940731
C	-4.065147	3.977485	-0.217174
C	-5.305478	4.322688	-1.005478
N	-3.087995	1.811707	-0.165748
O	-4.447044	3.176955	0.960609
C	-3.858154	1.998019	0.847596
C	-4.098458	0.944084	1.882995
C	-3.496529	1.333642	3.274916
C	-2.034499	1.773125	3.186058
C	-4.356748	2.359929	4.014015
N	-3.531409	-0.274251	1.333983
C	-3.851736	-1.446491	1.881660
O	-4.617055	-1.631210	2.841870
C	-3.156793	-2.594304	1.225212
N	-2.382773	-2.359854	0.096459
C	-3.187437	-3.891262	1.660583
S	-2.192408	-4.831622	0.625105
C	-1.807635	-3.456781	-0.337201
C	-0.920372	-3.685885	-1.550169
C	-1.588856	-3.313346	-2.894904
C	-2.980657	-3.942070	-3.014442
C	-0.718409	-3.749899	-4.079110
N	0.393312	-3.041654	-1.425659
C	1.418516	-3.609976	-0.742814
O	1.271923	-4.586179	-0.023988
C	2.806466	-2.952710	-0.954071
C	3.958936	-3.874061	-0.486178
C	4.899528	-4.346553	-1.567856
N	3.011396	-1.721856	-0.170227
O	4.697736	-3.028000	0.472502
C	4.067141	-1.871278	0.552277
C	4.603460	-0.779666	1.435809
C	4.444085	-1.105469	2.957917
C	3.010622	-1.479113	3.337134
C	5.449010	-2.155739	3.435385
H	0.528092	4.477154	-1.816267
H	1.391660	1.733826	-2.794979
H	2.319533	4.529172	-3.615689
H	2.815643	3.010914	-4.365518
H	3.289420	3.362997	-2.709521
H	-0.120664	3.973086	-4.242320
H	-0.815762	2.416292	-3.783440
H	0.474985	2.483878	-4.978389
H	-3.371186	2.861192	-1.967028
H	-3.576867	4.870126	0.163734
H	-5.797089	3.423334	-1.379666
H	-5.028196	4.946608	-1.856996
H	-6.009282	4.881045	-0.388239
H	-5.181343	0.841416	2.018776
H	-3.538896	0.401241	3.839174
H	-1.429430	1.042051	2.648346
H	-1.617044	1.881243	4.188807
H	-1.930559	2.738302	2.682790
H	-4.371827	3.323567	3.503612
H	-5.387929	2.014211	4.114608
H	-0.724841	-4.760938	-1.564244
H	-1.694604	-2.226167	-2.907733
H	-3.659074	-3.603486	-2.231278
H	-2.927739	-5.032552	-2.966255
H	-3.421920	-3.674818	-3.975662
H	-0.589896	-4.835414	-4.087503
H	0.272719	-3.296197	-4.071520
H	-1.199887	-3.464436	-5.015569
H	2.898799	-2.714393	-2.016460
H	3.562619	-4.704326	0.092834
H	5.312389	-3.506905	-2.129082
H	4.356190	-4.993307	-2.259224
H	5.718968	-4.921872	-1.137905
H	5.677631	-0.690749	1.235083
H	4.693357	-0.162478	3.446326
H	2.918554	-1.547592	4.422503
H	2.723313	-2.449080	2.922951
H	2.295478	-0.733350	2.987530
H	5.249426	-3.137741	3.004269
H	6.472581	-1.875070	3.178409
H	-0.777822	1.909237	-1.227617
H	0.601890	-2.291994	-2.067511

H	5.393181	-2.252108	4.521381
H	-3.959655	2.520726	5.018394
O	0.638261	-0.150572	-0.798182
H	-0.191265	-0.018207	-1.447794
O	3.591692	0.398285	-2.452834
H	4.462567	0.808176	-2.376881
O	-1.497978	-0.041093	-1.915305
H	-1.852460	0.283729	-2.746424
O	-4.666675	-0.591550	-1.786329
H	-5.400913	-0.957886	-1.277464
H	-4.592918	-1.154689	-2.566821
H	3.732546	-0.392624	-2.987428
H	0.422245	-0.962666	-0.323959
C	4.334501	4.792558	2.076593
H	4.443707	4.252660	3.014839
H	5.332336	4.909184	1.649977
H	3.935363	5.785251	2.281262
C	-3.901638	-4.509260	2.820674
H	-4.981449	-4.432165	2.693419
H	-3.639804	-5.561802	2.923987
H	-3.648902	-3.992882	3.745682

Chapter 4

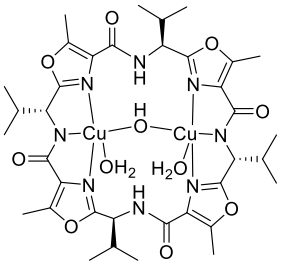

4A $[Cu_2(H_2pat^2)(\mu\text{-}OH)(H_2O)_2]^+$

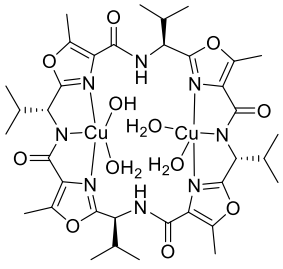

4B $[Cu_2(H_2pat^2)(OH)(H_2O)_3]^+$

4A

124

N	-2.968972	-1.155707	0.458711
N	-4.147120	-2.940851	0.959423
N	-3.492249	0.945974	-1.041551
N	-1.410520	2.551935	-0.713514
N	-1.819248	3.887773	-2.419178
N	0.708539	2.803663	1.236792
C	-4.098769	-1.181278	-0.332283
C	-4.850156	-2.285858	-0.034162
C	-3.015236	-2.235091	1.221900
C	-4.523939	-4.211423	1.571544
H	-3.733640	-4.942343	1.411637
H	-5.435162	-4.568934	1.103797
H	-4.706939	-4.086131	2.637028
C	-6.148243	-2.760811	-0.582699
H	-6.494125	-2.046137	-1.324631
H	-6.906685	-2.851520	0.198440
H	-6.049880	-3.736062	-1.065879
C	-4.320324	-0.078620	-1.287120
C	-3.577117	2.149179	-1.843232
H	-3.770023	1.891323	-2.890503
C	-4.691940	3.171789	-1.402548
H	-4.464191	4.099382	-1.935421
C	-6.099872	2.758536	-1.835018
H	-6.142332	2.537294	-2.902235
H	-6.794528	3.576555	-1.629146
H	-6.443293	1.874795	-1.299942
C	-4.651496	3.484826	0.093957
H	-5.394506	4.248520	0.331178
H	-4.882445	2.597677	0.685415
H	-3.678136	3.862406	0.410964
C	-2.246538	2.817918	-1.702748
C	-0.431667	3.543445	-0.755038
C	-0.674370	4.371746	-1.828455
C	-2.428221	4.436434	-3.625905
H	-1.664374	4.567453	-4.389414
H	-2.895669	5.398317	-3.418416
H	-3.177067	3.746340	-3.999898
C	0.040625	5.555840	-2.372983
H	0.355406	5.378771	-3.404592
H	0.915082	5.765152	-1.767874
H	-0.605071	6.437721	-2.375795
C	0.609818	3.751029	0.263981
C	1.941547	2.764005	2.026797
H	2.166523	3.789845	2.311441
C	1.792553	1.939502	3.323304
H	1.519186	0.916274	3.049322
C	0.697538	2.520286	4.219905
H	-0.272469	2.524864	3.726447
H	0.939672	3.546333	4.509906
H	0.607193	1.928557	5.132485
C	3.124369	1.875804	4.077160
H	3.016541	1.267216	4.975950
H	3.444995	2.873179	4.389766
H	3.920990	1.437116	3.473853
O	-5.179609	-0.143187	-2.181255
O	1.336426	4.747050	0.246700
C	-1.895559	-2.731788	2.097935
C	3.032604	2.284804	1.106614
N	-0.693450	-2.790768	1.265268
H	-2.128923	-3.754235	2.389943
C	-1.680314	-1.914642	3.389886
H	-0.270456	-1.888429	1.060841
C	-0.666161	-3.690881	0.243583
H	-1.402620	-0.894833	3.107686
C	-0.557116	-2.514472	4.238353
C	-2.977240	-1.831178	4.200392
C	0.378736	-3.487869	-0.773651
H	0.393457	-2.525064	3.708144
H	-0.798855	-3.540513	4.528845
H	-0.425796	-1.931732	5.151736
H	-2.822525	-1.219072	5.089884
H	-3.295335	-2.822575	4.533596
H	-3.794819	-1.386307	3.630477
N	1.431309	-2.588910	-0.646307
C	0.565342	-4.245336	-1.908035
C	2.264281	-2.849686	-1.640872
N	1.758517	-3.814674	-2.448886
C	-0.240397	-5.318729	-2.546623
C	3.638082	-2.251872	-1.667134
C	2.308338	-4.286345	-3.715272
H	-1.156470	-5.470078	-1.986670
H	-0.491036	-5.056785	-3.577503
H	0.310854	-6.262420	-2.574363
N	3.489965	-0.958485	-1.033182
H	4.012255	-2.138686	-2.688571
C	4.622415	-3.180688	-0.862999
H	3.205598	-3.725501	-3.951339
H	2.555032	-5.344751	-3.655060
H	1.578891	-4.131526	-4.508379
C	4.312996	0.050514	-1.346277
H	4.184336	-3.267655	0.136689
C	4.748356	-4.589934	-1.449698
C	6.015692	-2.566742	-0.711134
C	4.080201	1.206189	-0.456929
H	3.801963	-5.129662	-1.464728
H	5.440939	-5.175606	-0.842795

H	5.149752	-4.563801	-2.465855
H	5.987971	-1.598062	-0.216459
H	6.499581	-2.436818	-1.680601
H	6.637495	-3.232141	-0.108051
N	2.980550	1.184669	0.376130
C	4.817166	2.335111	-0.220305
N	4.136119	3.007937	0.777847
C	6.086043	2.815724	-0.828538
C	4.521291	4.293442	1.353042
H	6.424278	2.078142	-1.551520
H	6.866350	2.954355	-0.076687
H	5.950310	3.768188	-1.346926
H	3.687593	4.988714	1.282543
H	5.359035	4.691705	0.790250
H	4.823160	4.174918	2.392518
Cu	1.905855	-0.590709	0.066220
Cu	-1.887403	0.603142	0.053114
H	0.322137	1.890776	1.003998
O	-1.447471	-4.642516	0.186372
O	5.183653	0.054286	-2.232289
O	0.016402	0.005993	0.676710
O	2.421564	-1.486578	2.253856
O	-2.280077	1.481143	2.272614
H	2.408318	-2.449417	2.178843
H	3.332830	-1.262898	2.481897
H	-3.173410	1.265651	2.568813
H	-2.248943	2.445554	2.237821
H	0.005798	0.021351	1.641708

4B

127

N	2.836831	-2.007203	-0.392240
N	4.009502	-3.020828	-1.957275
N	4.414245	0.151937	-0.311941
N	2.775991	2.104698	0.398856
N	2.939105	4.292029	0.271580
N	-0.271957	2.903754	0.711569
O	5.882671	1.579456	-1.374476
O	-0.222351	4.533952	-0.844591
C	2.081466	-3.061963	-0.898450
C	2.808432	-3.694800	-1.885197
C	3.993223	-2.028659	-1.034048
C	5.097798	-1.069052	-0.694000
H	5.736449	-0.885557	-1.562136
C	4.857332	1.348873	-0.710222
C	3.956710	2.430274	-0.246790
C	4.074900	3.791035	-0.331689
C	2.175723	3.245795	0.700342
C	0.871692	3.456403	1.433796
H	0.717958	4.535101	1.472917
C	-0.786511	3.547220	-0.357371
C	2.525286	-4.856766	-2.769895
H	1.565959	-5.287105	-2.508002
H	3.298832	-5.622457	-2.672150
H	2.500598	-4.550811	-3.819439
C	5.981275	-1.619769	0.472031
H	5.304984	-1.732021	1.326327
C	6.594899	-2.988921	0.167372
H	5.840608	-3.751973	-0.029394
H	7.182445	-3.328150	1.022328
H	7.268764	-2.940764	-0.691888
C	7.077279	-0.625812	0.858760
H	6.668289	0.349854	1.117087
H	7.788914	-0.489167	0.041120
H	7.628211	-1.000789	1.723875
C	5.143477	4.642539	-0.919197
H	5.933723	3.997056	-1.292325
H	5.566177	5.325447	-0.178590
H	4.767621	5.244879	-1.750136
C	2.618802	5.711422	0.401210
H	1.605230	5.886089	0.049384
H	3.308933	6.280521	-0.212860
H	2.721144	6.039310	1.434855
C	0.903535	2.953939	2.898333
H	0.961253	1.864190	2.871395
C	-0.369853	3.364865	3.644395
H	-1.275130	2.989681	3.167685
H	-0.448696	4.453780	3.702677
H	-0.346062	2.978043	4.664598
C	2.138841	3.476046	3.637669
H	3.068640	3.150531	3.170049
H	2.138545	3.107863	4.664668
H	2.141132	4.568420	3.680529
C	0.786130	-3.542487	-0.361475
N	0.249408	-2.884017	0.686672
O	0.245101	-4.551064	-0.832633
C	-0.889106	-3.458357	1.399952
C	-2.197770	-3.249170	0.672243
H	-0.725651	-4.535881	1.416862
C	-0.920122	-2.990318	2.876339
N	-2.800148	-2.108809	0.371830
N	-2.966112	-4.295023	0.250570
H	-0.970412	-1.900273	2.879618
C	0.354273	-3.420858	3.609091
C	-2.156400	-3.522462	3.606319
C	-3.986742	-2.433128	-0.263295
C	-4.106726	-3.793893	-0.344190
C	-2.646829	-5.714776	0.378878
H	1.256763	-3.037505	3.133838
H	0.429463	-4.510972	3.644321
H	0.336242	-3.055175	4.637184
H	-3.085509	-3.184523	3.146109
H	-2.153759	-3.175051	4.640530
H	-2.162085	-4.615352	3.627664
C	-4.886638	-1.348264	-0.722686
C	-5.179633	-4.644971	-0.924244
H	-1.628660	-5.887750	0.039689
H	-3.327855	-6.281625	-0.247418
H	-2.762749	-6.047672	1.409516
N	-4.421800	-0.151292	-0.349061
O	-5.931040	-1.575316	-1.356959
H	-5.972187	-3.999124	-1.291999
H	-5.597782	-5.327650	-0.180868
H	-4.809699	-5.247394	-1.757766
C	-5.103028	1.078192	-0.704651
C	-3.997364	2.041525	-1.032822
H	-5.747343	0.914357	-1.572732
C	-5.975644	1.616483	0.475976
C	-2.084722	3.072707	-0.892534
N	-2.839346	2.013734	-0.392663
N	-4.015722	3.043086	-1.945334
H	-5.290476	1.721693	1.323957
C	-6.591622	2.988445	0.188264
C	-7.068816	0.621300	0.867245
C	-2.814599	3.716273	-1.869380
H	-5.839248	3.753102	-0.009474
H	-7.170936	3.320798	1.051473

H	-7.273569	2.947182	-0.664958
H	-6.659019	-0.355648	1.118766
H	-7.787452	0.488159	0.055334
H	-7.611798	0.993787	1.738510
C	-2.535971	4.892048	-2.736900
H	-1.588965	5.335934	-2.453397
H	-3.325222	5.642263	-2.647094
H	-2.484624	4.596889	-3.788678
Cu	2.631323	-0.001105	0.408538
Cu	-2.595849	-0.022663	0.271882
O	1.152832	-0.371941	1.606069
H	-0.161937	0.028660	1.629845
H	0.679304	-2.027665	1.046526
O	-1.185928	0.361043	1.648807
H	-1.523576	0.275855	2.547884
H	-0.732320	2.079678	1.083933
H	1.493138	-0.378370	2.508311
O	1.338622	0.495399	-1.971987
H	1.795153	0.050767	-2.697605
O	-1.272709	-0.385988	-1.651928
H	-1.209236	-1.338212	-1.788134
H	-0.362425	-0.041561	-1.763558
C	5.075121	-3.334199	-2.902402
H	5.540892	-4.286428	-2.652999
H	4.665147	-3.388301	-3.908898
H	5.826339	-2.553029	-2.872760
C	-5.082992	3.366902	-2.885125
H	-5.549653	4.315366	-2.623339
H	-4.673771	3.433615	-3.891150
H	-5.833213	2.584564	-2.864375
H	1.487210	1.439031	-2.113689

Chapter 5

Table AII-1. Expected minimum and maximum distances from Cu_1 and Cu_2 to C_1 of Rhodamine and O_1 of Proxyl [Å].

	$[Cu_2(H_2pat\text{-}FT)(OH)(H_2O)_3]^{2+}$		$Cu_2(H_2pat\text{-}FT)(\mu\text{-}OH)(H_2O)_2]^{2+}$	
	$d_{C1\text{-}Cu1}$ / $d_{C1\text{-}Cu2}$ min.	$d_{C1\text{-}Cu1}$ / $d_{C1\text{-}Cu2}$ max.	$d_{C1\text{-}Cu1}$ /$d_{C1\text{-}Cu2}$ min.	$d_{C1\text{-}Cu1}$ / $d_{C1\text{-}Cu2}$ max.
⊥	**5A** 18.32 / 20.88	**5B** 20.97 / 24.37	**5E** 18.36 / 23.96	**5F** 21.35 / 25.34
‖	**5C** 13.65 / 16.65	**5D** 21.48 / 21.78	**5G** 18.52 / 19.32	**5H** 18.16 / 20.47
	$[Cu_2(H_2pat\text{-}Proxyl)(OH)(H_2O)_3]^{2+}$		$Cu_2(H_2pat\text{-}Proxyl)(\mu\text{-}OH)(H_2O)_2]^{2+}$	
	$d_{C1\text{-}Cu1}$ / $d_{C1\text{-}Cu2}$		$d_{C1\text{-}Cu1}$ /$d_{C1\text{-}Cu2}$ min.	$d_{C1\text{-}Cu1}$ / $d_{C1\text{-}Cu2}$ max.
⊥	**5I** 12.75 / 16.47		**5K** 13.71 / 12.38	
‖	**5J** 11.17 / 13.07		**5L** 12.62 / 17.66	

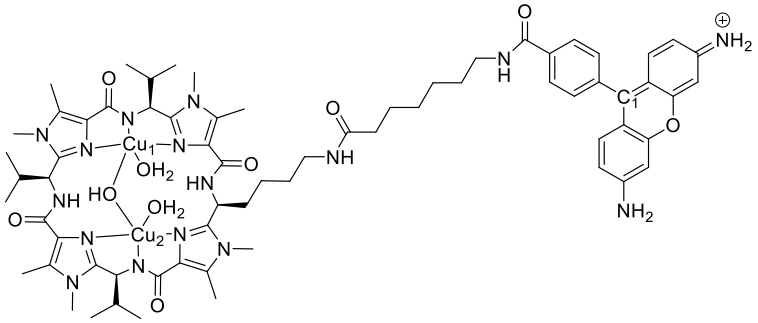

5A+B: $[Cu_2(H_2pat\text{-}‖\text{-}FT)(OH)(H_2O)]^{2+}$

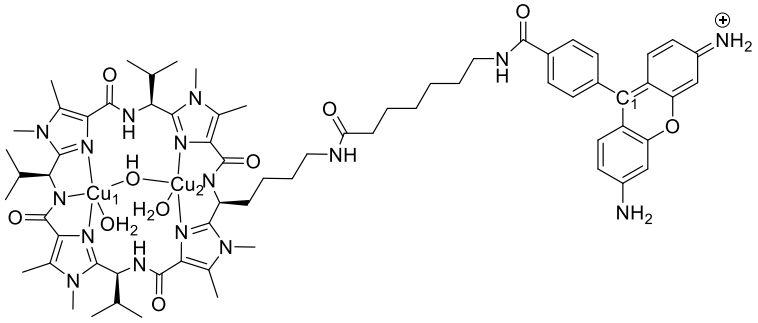

5C+D: $[Cu_2(H_2pat\text{-}⊥\text{-}FT)(OH)(H_2O)]^{2+}$

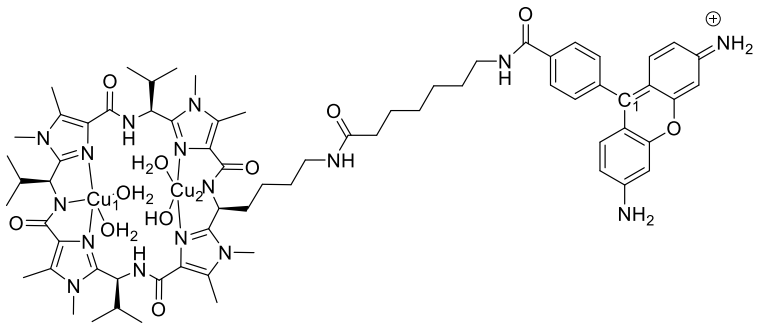

5E+F: $[Cu_2(H_2pat\text{-}\perp\text{-}FT)(OH)(H_2O)_3]^{2+}$

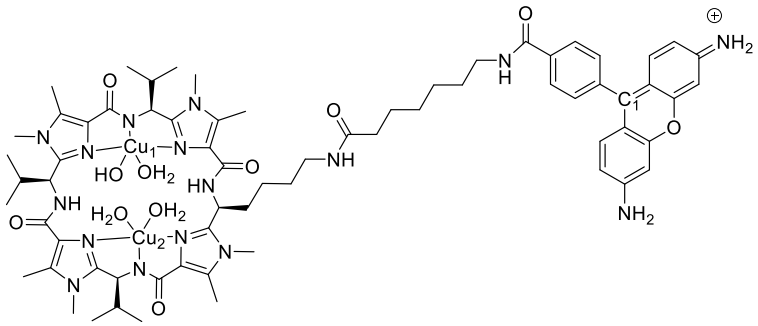

5G+H: $[Cu_2(H_2pat\text{-}\parallel\text{-}FT)(OH)(H_2O)_3]^{2+}$

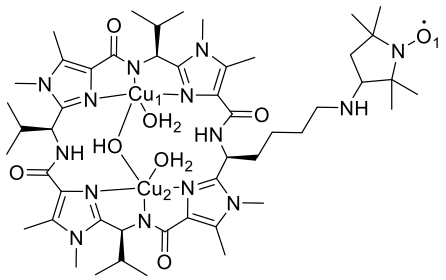

5I: $[Cu_2(H_2pat\text{-}\perp\text{-}FT)(OH)(H_2O)_3]^{2+}$

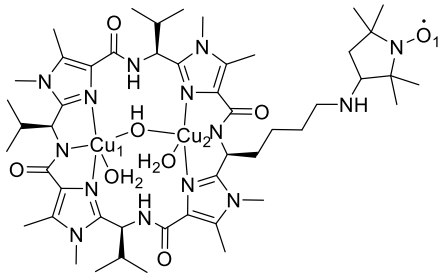

5J: $[Cu_2(H_2pat\text{-}\parallel\text{-}FT)(OH)(H_2O)_3]^{2+}$

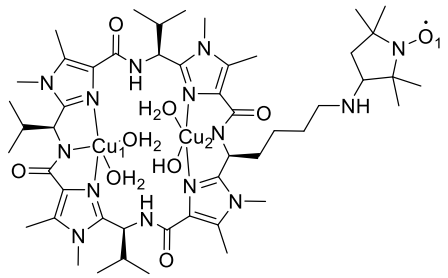

5K: $[Cu_2(H_2pat\text{-}\perp\text{-}FT)(\mu\text{-}OH)(H_2O)_3]^{2+}$

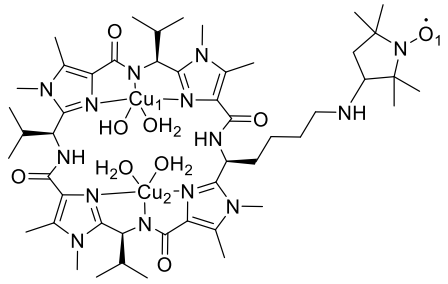

5L: $[Cu_2(H_2pat\text{-}\parallel\text{-}FT)(\mu\text{-}OH)(H_2O)_3]^{2+}$

5A

184

N	4.961193	2.816602	-0.504434
N	5.458350	4.902274	-0.982230
N	3.102130	1.746833	1.025649
N	3.328766	-0.865715	0.646750
N	2.114656	-1.502742	2.373291
N	4.532980	-2.557718	-1.364336
C	4.233086	3.649177	0.319851
C	4.525803	4.955939	0.036575
C	5.702285	3.596974	-1.273503
C	6.119155	6.052430	-1.591751
H	7.196117	5.966514	-1.460761
H	5.774752	6.955734	-1.099454
H	5.875766	6.119862	-2.650362
C	4.006976	6.221438	0.620384
H	3.266700	5.976880	1.377377
H	3.538645	6.852864	-0.138305
H	4.801684	6.803553	1.093496
C	3.297976	3.046165	1.288665
C	2.182136	0.977865	1.837989
H	2.267113	1.276570	2.888724
C	2.591253	-0.450135	1.662442
C	3.266898	-2.258113	0.665937
C	2.521766	-2.661254	1.751969
C	1.329436	-1.449502	3.601567
H	1.771409	-2.111976	4.342757
H	0.300989	-1.756519	3.414978
H	1.336915	-0.437750	3.992940
C	2.152290	-3.999575	2.283188
H	2.522277	-4.127919	3.303626
H	2.576964	-4.772863	1.653648
H	1.066894	-4.125094	2.311574
C	3.795671	-3.145644	-0.382333
C	5.379048	-3.421707	-2.191185
H	4.771820	-4.278797	-2.475185
C	5.849755	-2.729973	-3.488441
H	6.421940	-1.838976	-3.213631
C	4.657256	-2.305865	-4.347709
H	4.007918	-1.605879	-3.825393
H	4.061389	-3.175590	-4.637575
H	5.006791	-1.821895	-5.261332
C	6.781471	-3.650734	-4.282289
H	7.131858	-3.142723	-5.181724
H	6.259356	-4.558172	-4.597304
H	7.659625	-3.947446	-3.706233
O	2.784779	3.705019	2.207663
O	3.558613	-4.355649	-0.379789
C	6.804561	3.128107	-2.186177
C	6.494926	-3.912331	-1.307511
N	7.685267	2.272029	-1.390334
H	7.388879	3.998954	-2.478281
C	6.318131	2.437249	-3.478189
H	7.315590	1.345178	-1.192299
C	8.390340	2.845980	-0.376312
H	5.765596	1.535844	-3.197235
C	7.499175	2.035392	-4.364142
C	5.355650	3.345868	-4.248868
C	8.976785	1.924063	0.610572
H	8.165873	1.336158	-3.862736
H	8.080482	2.914798	-4.654505
H	7.137425	1.558848	-5.276908
H	4.988848	2.831800	-5.138248
H	5.858605	4.258485	-4.579391
H	4.488692	3.633593	-3.651586
N	9.028565	0.543365	0.458108
C	9.688237	2.282294	1.733475
C	9.810848	0.092393	1.425405
N	10.196153	1.105127	2.241368
C	9.945090	3.591644	2.388313
C	10.305610	-1.321996	1.414723
C	10.947877	1.000477	3.487349
H	9.419879	4.376101	1.854999
H	9.609046	3.579831	3.428064
H	11.012496	3.827914	2.392856
N	9.239841	-2.081159	0.794649
H	10.502688	-1.690931	2.425266
C	11.634897	-1.399237	0.574916
H	11.151579	-0.042820	3.700388
H	11.890431	1.539611	3.412295
H	10.359279	1.416773	4.303027
C	9.066281	-3.375798	1.090070
H	11.375748	-1.001610	-0.411789
C	12.769414	-0.544282	1.147605
C	12.126496	-2.835813	0.385722
C	8.037543	-3.974895	0.216285
H	12.523272	0.516398	1.187166
H	13.653875	-0.644018	0.516102
H	13.048715	-0.873953	2.151440
H	11.384278	-3.465087	-0.101042
H	12.384457	-3.295711	1.341152
H	13.021498	-2.829527	-0.240406
N	7.285457	-3.139280	-0.583588
C	7.703518	-5.278426	-0.034327
N	6.721952	-5.218783	-1.006848
C	8.227900	-6.546220	0.539001

C	6.025540	-6.364809	-1.584225
H	9.017203	-6.305661	1.246295
H	8.636765	-7.199901	-0.234890
H	7.450117	-7.102650	1.067941
H	4.951153	-6.226798	-1.483870
H	6.316470	-7.259606	-1.043982
H	6.290913	-6.487868	-2.633090
Cu	7.866389	-1.150062	-0.254176
Cu	4.415329	0.821276	-0.119001
H	4.946406	-1.658058	-1.126528
O	8.559592	4.064678	-0.302447
O	9.677267	-4.032281	1.949606
O	6.130137	-0.158902	-0.803556
O	8.818000	-0.882141	-2.462556
O	3.447816	0.550968	-2.319481
H	9.517401	-0.219572	-2.393987
H	9.266751	-1.698673	-2.716208
H	2.991844	1.357790	-2.590300
H	2.762211	-0.127678	-2.278821
H	6.087025	-0.144976	-1.767670
C	0.012972	2.434790	1.622628
H	0.102600	2.706636	2.678018
H	0.521166	3.220134	1.061424
C	-1.464859	2.395617	1.230079
H	-1.984670	1.625058	1.807284
H	-1.563322	2.119262	0.174961
C	-2.162555	3.737285	1.462785
H	-1.680731	4.518925	0.871600
H	-2.088573	4.020763	2.512190
N	-3.576476	3.716492	1.116908
H	-3.827008	3.813177	0.146643
C	0.698420	1.091051	1.384101
H	0.122762	0.317894	1.900432
H	0.665280	0.840716	0.319340
O	-4.350566	3.318551	3.209757
C	-4.565458	3.488046	2.009025
C	-5.975742	3.450508	1.445824
H	-6.543624	4.234392	1.955200
H	-5.978012	3.689333	0.379808
C	-6.649872	2.094225	1.685677
H	-6.592647	1.857635	2.750988
H	-6.086879	1.315464	1.160380
C	-8.108805	2.061829	1.230956
H	-8.670097	2.834564	1.768122
H	-8.167429	2.322586	0.168335
C	-8.774551	0.703792	1.455067
H	-8.694386	0.432605	2.513671
H	-8.224457	-0.064222	0.899816
C	-10.244668	0.672138	1.038257
H	-10.802510	1.424089	1.605757
H	-10.334193	0.951547	-0.016581
C	-10.897696	-0.703991	1.250384
H	-10.802009	-0.984867	2.302511
H	-10.347573	-1.450462	0.670764
C	-12.351810	-0.732915	0.854638
C	-13.358533	-0.484857	1.789894
C	-12.733718	-0.975722	-0.466901
C	-14.698102	-0.484209	1.424689
H	-13.093026	-0.294813	2.823112
C	-14.068656	-0.956970	-0.846454
H	-11.975870	-1.185419	-1.212540
C	-15.070550	-0.714143	0.097650
H	-15.457563	-0.290924	2.171575
H	-14.336087	-1.152931	-1.877034
C	-16.499229	-0.706916	-0.300250
C	-16.996025	0.281780	-1.171786
C	-17.384486	-1.689065	0.185515
C	-16.220242	1.351434	-1.701260
C	-18.369304	0.259974	-1.540840
C	-18.749813	-1.654234	-0.210903
C	-17.005572	-2.764530	1.037509
C	-16.758285	2.280632	-2.537918
H	-15.179467	1.426507	-1.422991
C	-18.931737	1.188186	-2.386264
C	-19.676936	-2.576065	0.216878
H	-15.972295	-2.848399	1.340010
C	-17.907375	-3.687540	1.470820
C	-18.133531	2.216190	-2.911237
H	-16.147823	3.086045	-2.924802
H	-19.982283	1.118203	-2.633102
C	-19.276112	-3.611062	1.075956
H	-20.702055	-2.496129	-0.118000
H	-17.592692	-4.496832	2.116533
O	-19.198417	-0.694008	-1.054251
N	-20.155249	-4.526347	1.518261
H	-19.865960	-5.272399	2.126921
H	-21.122889	-4.497198	1.246002
N	-18.646612	3.136880	-3.745025
H	-19.614781	3.115841	-4.015882
H	-18.075194	3.875352	-4.117643

5B

184

N	-4.357042	-2.235752	1.913240
N	-4.771151	-3.343353	3.764514
N	-2.117240	-1.710833	0.628944
N	-2.878681	-0.495625	-1.599011
N	-0.901921	0.293334	-2.174139
N	-5.347475	-0.283511	-3.088151
C	-3.161476	-2.523685	2.538126
C	-3.396479	-3.217463	3.694414
C	-5.314880	-2.730882	2.679438
C	-5.513456	-3.967578	4.855552
H	-6.194317	-3.241807	5.296089
H	-4.810836	-4.297584	5.613411
H	-6.069349	-4.832117	4.497784
C	-2.460136	-3.769436	4.709347
H	-1.442019	-3.556352	4.394880
H	-2.575520	-4.850395	4.818222
H	-2.617187	-3.317378	5.691809
C	-1.904655	-2.095551	1.894885
C	-1.001411	-1.292080	-0.193971
H	-0.291757	-0.707961	0.402411
C	-1.597196	-0.449356	-1.276671
C	-3.001597	0.196256	-2.802822
C	-1.771606	0.704050	-3.158461
C	0.514354	0.638527	-2.118703
H	0.632172	1.709322	-2.270656
H	1.071464	0.104418	-2.887557
H	0.912158	0.381294	-1.142766
C	-1.313935	1.534405	-4.303387
H	-0.881920	2.475109	-3.952536
H	-2.151954	1.752039	-4.955309
H	-0.543553	1.017002	-4.880838
C	-4.219279	0.254965	-3.627434
C	-6.632228	0.084083	-3.688378
H	-6.511596	0.000852	-4.766573
C	-7.777996	-0.862130	-3.270250
H	-7.875880	-0.821693	-2.181409
C	-7.478519	-2.303482	-3.686278
H	-6.565849	-2.678255	-3.226915
H	-7.371629	-2.377809	-4.771889
H	-8.298603	-2.958263	-3.386560
C	-9.107637	-0.396392	-3.871277
H	-9.915344	-1.053702	-3.546651
H	-9.075227	-0.427118	-4.963654
H	-9.365611	0.619774	-3.568147
O	-0.817482	-2.113379	2.494680
O	-4.206424	0.745548	-4.758575
C	-6.789293	-2.480416	2.502814
C	-6.869186	1.533170	-3.355552
N	-6.968446	-1.031835	2.396054
H	-7.292805	-2.795325	3.415191
C	-7.433883	-3.244134	1.326195
H	-6.689273	-0.631294	1.503553
C	-6.686864	-0.269873	3.489175
H	-6.964534	-2.903310	0.398665
C	-8.936693	-2.966885	1.248994
C	-7.172654	-4.748341	1.448771
C	-6.533703	1.175167	3.252129
H	-9.149239	-1.910454	1.095369
H	-9.435761	-3.286702	2.167815
H	-9.377798	-3.522346	0.419543
H	-7.598766	-5.272008	0.592028
H	-7.640014	-5.154894	2.349529
H	-6.107357	-4.982992	1.483859
N	-6.854833	1.811165	2.058548
C	-6.208754	2.122718	4.196566
C	-6.792791	3.110339	2.302070
N	-6.366377	3.340487	3.568992
C	-5.765355	2.023985	5.611780
C	-7.332603	4.101760	1.316632
C	-6.044076	4.628350	4.174003
H	-5.663959	0.981186	5.890944
H	-4.806014	2.527131	5.755501
H	-6.485800	2.496316	6.284880
N	-7.109180	3.493960	0.021509
H	-6.816406	5.063606	1.384031
C	-8.866083	4.324977	1.593862
H	-6.174619	5.415572	3.440117
H	-6.692545	4.824143	5.025977
H	-5.006871	4.625243	4.504575
C	-6.948347	4.255413	-1.068358
H	-9.318130	3.329753	1.530347
C	-9.158665	4.890592	2.986890
C	-9.530734	5.208761	0.536327
C	-6.906928	3.419422	-2.284960
H	-8.820135	4.236910	3.790189
H	-10.235839	5.016116	3.109178
H	-8.700153	5.873393	3.121968
H	-9.426364	4.800935	-0.466966
H	-9.107658	6.214693	0.537365
H	-10.597912	5.289317	0.754838
N	-6.824096	2.049824	-2.139966
C	-7.013794	3.738007	-3.611857
N	-6.989255	2.525697	-4.277088
C	-7.149237	5.054305	-4.290089

C	-7.047088	2.348486	-5.725183
H	-7.183677	5.832219	-3.531935
H	-8.061066	5.107087	-4.889389
H	-6.303609	5.256655	-4.952135
H	-6.200346	1.749405	-6.053141
H	-6.992401	3.322789	-6.199427
H	-7.980273	1.869374	-6.017248
Cu	-6.748216	1.568209	-0.099067
Cu	-3.961107	-1.262057	0.090329
H	-5.357818	-0.359633	-2.072788
O	-6.597526	-0.752226	4.619963
O	-6.866822	5.494362	-1.106230
O	-5.775655	-0.260929	-0.183696
O	-8.922482	0.506692	-0.093164
O	-4.843543	-3.104115	-1.205584
H	-9.283272	0.599078	0.797991
H	-9.521564	1.006709	-0.661956
H	-4.605535	-3.947653	-0.800603
H	-4.418578	-3.108883	-2.072561
H	-6.414214	-0.925200	-0.471021
C	0.557675	-3.392773	0.016801
H	1.275967	-2.801049	0.591159
H	-0.093083	-3.875637	0.746802
C	1.303342	-4.456312	-0.791249
H	1.978600	-3.976177	-1.506337
H	0.592001	-5.044525	-1.380036
C	2.110265	-5.403573	0.100139
H	1.440264	-5.910153	0.798599
H	2.817893	-4.839109	0.705814
N	2.831949	-6.429085	-0.641976
H	2.295661	-7.218062	-0.974047
C	-0.257988	-2.470025	-0.886505
H	0.412446	-2.054185	-1.643847
H	-1.009739	-3.052951	-1.427394
O	4.561084	-7.349343	-1.742266
C	4.121501	-6.425390	-1.056416
C	4.991871	-5.254199	-0.625480
H	4.500490	-4.322590	-0.921728
H	5.025869	-5.236217	0.468753
C	6.408338	-5.297158	-1.189499
H	6.892582	-6.228418	-0.885501
H	6.363199	-5.319112	-2.281526
C	7.252889	-4.105759	-0.736026
H	6.761006	-3.174462	-1.039366
H	7.296537	-4.085461	0.358846
C	8.675061	-4.128461	-1.296803
H	8.631000	-4.153975	-2.391395
H	9.170188	-5.056203	-0.988843
C	9.521421	-2.934878	-0.855333
H	9.576092	-2.906949	0.237850
H	9.033484	-2.004731	-1.164450
C	10.947738	-2.969025	-1.429859
H	10.889108	-2.999311	-2.521296
H	11.436156	-3.894143	-1.112145
C	11.785959	-1.790180	-1.007093
C	11.782212	-0.603590	-1.743933
C	12.570568	-1.839037	0.146993
C	12.524940	0.497879	-1.341466
H	11.192969	-0.539594	-2.651180
C	13.332087	-0.749518	0.547859
H	12.594046	-2.746114	0.739419
C	13.315655	0.436743	-0.190641
H	12.508333	1.402464	-1.936059
H	13.934592	-0.816960	1.444788
C	14.128298	1.603267	0.232334
C	13.508008	2.795512	0.654055
C	15.535280	1.539314	0.217790
C	12.099960	2.979647	0.752777
C	14.314087	3.899048	1.047570
C	16.288976	2.672288	0.631757
C	16.285982	0.412804	-0.222990
C	11.558943	4.156372	1.172228
H	11.448762	2.158361	0.492392
C	13.787224	5.096924	1.471739
C	17.664418	2.692118	0.645106
H	15.756024	-0.459987	-0.574490
C	17.647095	0.412982	-0.218999
C	12.394097	5.253958	1.536728
H	10.484898	4.269614	1.240606
H	14.451552	5.901584	1.755753
C	18.374753	1.556788	0.225238
H	18.182279	3.583361	0.972479
H	18.194441	-0.455794	-0.560790
O	15.665245	3.807225	1.028181
N	19.718370	1.537426	0.228980
H	20.226377	0.729781	-0.087747
H	20.252035	2.338181	0.520493
N	11.844506	6.411074	1.943738
H	12.414453	7.194223	2.214276
H	10.846718	6.523130	1.993339

5C

184

N	-3.414428	-2.883216	-1.772807
N	-4.348199	-4.315091	-3.152405
N	-1.249404	-3.021317	-0.277725
N	-1.000161	-0.606656	0.784161
N	0.469439	-1.137940	2.339417
N	-2.035627	2.024392	0.181777
C	-2.787884	-4.104896	-1.639734
C	-3.353101	-5.012797	-2.494018
C	-4.360801	-3.039030	-2.683722
C	-5.272921	-4.874948	-4.133469
H	-6.295943	-4.749523	-3.784067
H	-5.065681	-5.933907	-4.245659
H	-5.146668	-4.392308	-5.100714
C	-3.037125	-6.443823	-2.746655
H	-2.196409	-6.729715	-2.120302
H	-2.772494	-6.619509	-3.792000
H	-3.882014	-7.092948	-2.503646
C	-1.667792	-4.226737	-0.687261
C	-0.126491	-2.918781	0.631202
H	-0.169642	-3.721707	1.375464
C	1.294110	-2.988328	-0.046900
H	2.000147	-2.657659	0.720185
C	1.711726	-4.407333	-0.436903
H	1.622262	-5.096528	0.403758
H-	2.755298	-4.399420	-0.760908
H	1.103349	-4.797666	-1.251004
C	1.431941	-2.034075	-1.234149
H	2.452497	-2.070237	-1.619796
H	0.757732	-2.317234	-2.043752
H	1.219931	-0.999591	-0.959588
C	-0.265907	-1.583074	1.289865
C	-0.668374	0.540857	1.502562
C	0.238372	0.210839	2.485472
C	1.340201	-1.930564	3.200572
H	1.105697	-1.722558	4.242357
H	2.386747	-1.691905	3.014663
H	1.173393	-2.985775	3.011955
C	0.907714	1.003522	3.550104
H	0.666062	0.606831	4.539497
H	0.584147	2.036439	3.495043
H	1.994723	0.968652	3.441289
C	-1.110416	1.905586	1.173482
C	-2.771536	3.287277	0.084055
H	-2.038937	4.086692	0.174705
C	-2.612350	3.504343	-2.485799
H	-1.974072	2.617910	-2.519868
H	-3.256265	3.449491	-3.368532
O	-1.208706	-5.329124	-0.346672
O	-0.644387	2.889298	1.752657
C	-5.431416	-2.031310	-3.009463
C	-3.684246	3.352605	1.279659
N	-6.051851	-1.640209	-1.742980
H	-6.197853	-2.536295	-3.594860
C	-4.942677	-0.817180	-3.828131
H	-5.492947	-1.013330	-1.168890
C	-6.757336	-2.582521	-1.058053
H	-4.202400	-0.277007	-3.230666
C	-6.100711	0.129213	-4.151490
C	-4.250208	-1.275110	-5.115257
C	-7.059873	-2.272464	0.349116
H	-6.569868	0.522221	-3.251346
H	-6.865704	-0.384210	-4.740358
H	-5.739985	0.975237	-4.739044
H	-3.875108	-0.410800	-5.664870
H	-4.948840	-1.803808	-5.769068
H	-3.403666	-1.935324	-4.918706
N	-6.857302	-1.029747	0.938074
C	-7.719703	-3.091889	1.237132
C	-7.444107	-1.080701	2.123009
N	-7.940647	-2.320752	2.358821
C	-8.163193	-4.508545	1.162400
C	-7.654480	0.165147	2.928618
C	-8.538752	-2.814222	3.594649
H	-7.851688	-4.939509	0.217478
H	-7.736055	-5.094173	1.980166
H	-9.251013	-4.586035	1.238836
N	-6.524238	1.009971	2.603799
H	-7.681597	-0.044826	4.001617
C	-9.015857	0.832275	2.504546
H	-8.515907	-2.032096	4.345053
H	-9.570669	-3.116798	3.426420
H	-7.968667	-3.667002	3.959133
C	-6.076615	1.914912	3.483688
H	-8.931456	0.998344	1.425588
C	-10.236193	-0.059414	2.752980
C	-9.235439	2.191935	3.171120
C	-5.037114	2.765970	2.870616
H	-10.197474	-0.996254	2.197981
H	-11.139406	0.463867	2.434550
H	-10.351840	-0.289198	3.815149
H	-8.433954	2.893856	2.950345
H	-9.309530	2.094577	4.255522
H	-10.168974	2.624848	2.804784
N	-4.538710	2.408921	1.634577

C	-4.481804	3.952382	3.267641
N	-3.625088	4.310635	2.242692
C	-4.695202	4.766183	4.493682
C	-2.776716	5.498672	2.218981
H	-5.446916	4.276754	5.107292
H	-5.039905	5.774536	4.253301
H	-3.778673	4.859047	5.081633
H	-1.744791	5.206045	2.037525
H	-2.837401	5.991323	3.183748
H	-3.109567	6.193898	1.449856
Cu	-5.460593	0.635010	0.997122
Cu	-2.459163	-1.483051	-0.525867
H	-2.591482	1.191841	-0.004626
O	-7.151723	-3.622220	-1.589855
O	-6.466348	2.073932	4.652403
O	-4.007819	-0.099387	-0.286970
O	-6.647147	1.703022	-0.821045
O	-1.666435	-0.189428	-2.409847
H	-7.452132	1.192320	-0.976104
H	-6.950917	2.573549	-0.534084
H	-1.402483	-0.771745	-3.133346
H	-0.861657	0.277804	-2.152367
H	-4.058027	0.400407	-1.111139
C	-1.753315	4.766389	-2.582586
H	-1.066957	4.837686	-1.734474
H	-2.396027	5.651617	-2.542228
C	-3.514036	3.441456	-1.249274
H	-4.107678	4.357874	-1.185444
H	-4.236041	2.630104	-1.359726
C	-0.938045	4.805317	-3.878036
H	-1.609534	4.711039	-4.735032
H	-0.258896	3.955360	-3.921622
N	-0.175392	6.034446	-4.046962
H	-0.690886	6.856573	-4.328310
O	1.606887	7.395902	-3.940673
C	1.134431	6.268423	-3.791835
C	1.984355	5.090426	-3.338667
H	1.506562	4.620025	-2.474278
H	1.973470	4.335395	-4.131624
C	3.422836	5.467988	-2.999490
H	3.891657	5.928188	-3.872663
H	3.422007	6.231411	-2.217022
C	4.254273	4.268638	-2.542857
H	3.785771	3.813927	-1.662508
H	4.247154	3.500276	-3.324326
C	5.700719	4.636423	-2.210998
H	5.706957	5.414836	-1.439846
H	6.172062	5.079202	-3.095594
C	6.538526	3.450515	-1.733967
H	6.081145	3.013914	-0.840010
H	6.535096	2.666103	-2.497804
C	7.992769	3.837540	-1.416498
H	8.452707	4.255672	-2.316052
H	7.991860	4.630027	-0.663301
C	8.820888	2.679724	-0.921543
C	8.921354	2.398221	0.442620
C	9.490319	1.837980	-1.812728
C	9.669379	1.323762	0.904256
H	8.413619	3.034114	1.158251
C	10.224857	0.749401	-1.362780
H	9.441875	2.038602	-2.876506
C	10.328386	0.480752	0.005112
H	9.732360	1.131698	1.967784
H	10.738784	0.117646	-2.076143
C	11.126723	-0.670038	0.492513
C	10.737004	-1.990728	0.195445
C	12.289138	-0.462888	1.260376
C	9.567266	-2.339832	-0.536524
C	11.524173	-3.074248	0.673316
C	13.031626	-1.586217	1.718453
C	12.815881	0.816553	1.595103
C	9.239595	-3.637027	-0.787236
H	8.923547	-1.550510	-0.895393
C	11.211116	-4.391705	0.429919
C	14.177476	-1.469947	2.470741
H	12.302461	1.698791	1.242625
C	13.948856	0.952780	2.336858
C	10.061937	-4.701991	-0.313610
H	8.343927	-3.876024	-1.345401
H	11.850414	-5.172066	0.819561
C	14.658379	-0.193815	2.802762
H	14.697400	-2.362267	2.791375
H	14.330322	1.936862	2.575553
O	12.634144	-2.845016	1.414935
N	9.723892	-5.976781	-0.572960
H	8.897815	-6.196746	-1.102145
H	10.284209	-6.744715	-0.244963
N	15.772496	-0.039360	3.538327
H	16.299817	-0.831328	3.863917
H	16.121902	0.876160	3.763264

5D

184

N	-2.96952889	-1.15189307	0.45377586
N	-4.14894450	-2.93643911	0.95363442
N	-3.49070204	0.95011355	-1.04676225
N	-1.40835511	2.55497564	-0.71727241
N	-1.81524150	3.89108676	-2.42316279
N	0.70952666	2.80552852	1.23446312
C	-4.09880838	-1.17684629	-0.33797652
C	-4.85097187	-2.28104419	-0.04039861
C	-3.01686837	-2.23127954	1.21689541
C	-4.52683739	-4.20683562	1.56545757
H	-3.73681314	-4.93816264	1.40605468
H	-5.43793308	-4.56385428	1.09708693
H	-4.71048643	-4.08148544	2.63082305
C	-6.14893857	-2.75529995	-0.58982282
H	-6.49394967	-2.04041939	-1.33196128
H	-6.90795152	-2.84564025	0.19080418
H	-6.05076087	-3.73058524	-1.07297130
C	-4.31914713	-0.07403924	-1.29292281
C	-3.57440404	2.15339083	-1.84845735
H	-3.76674231	1.89567235	-2.89586662
C	-4.68898814	3.17656744	-1.40848483
H	-4.46039746	4.10406007	-1.94117211
C	-6.09684542	2.76406496	-1.84191354
H	-6.13870524	2.54288261	-2.90916661
H	-6.79121204	3.58243941	-1.63647844
H	-6.44108664	1.88048466	-1.30709927
C	-4.64938427	3.48953078	0.08805805
H	-5.39215427	4.25360439	0.32480779
H	-4.88119313	2.60248176	0.67932961
H	-3.67604004	3.86659127	0.40573110
C	-2.24357051	2.82142992	-1.70705740
C	-0.42895683	3.54597576	-0.75810484
C	-0.67050733	4.37444106	-1.83165501
C	-2.42311850	4.44010805	-3.63027845
H	-1.65869133	4.57075490	-4.39327040
H	-2.89020316	5.40222776	-3.42306889
H	-3.17207380	3.75041835	-4.00479800
C	0.04547095	5.55818059	-2.37566145
H	0.36085119	5.38098341	-3.40706540
H	0.91963114	5.76701465	-1.76995876
H	-0.59976239	6.44039878	-2.37887521
C	0.61195282	3.75298007	0.26161971
C	1.94198371	2.76519887	2.02529340
H	2.16730445	3.79091125	2.31012456
C	0.69637713	2.52205265	4.21755803
H	-0.27329620	2.52715454	3.72344982
H	0.60511115	1.93033890	5.13005628
O	-5.17786591	-0.13812610	-2.18763614
O	1.33909229	4.74862207	0.24486127
C	-1.89803865	-2.72859195	2.09366348
C	3.03340716	2.28546042	1.10582530
N	-0.69540248	-2.78817053	1.26180072
H	-2.13213234	-3.75092718	2.38547869
C	-1.68323340	-1.91160380	3.38578748
H	-0.27180031	-1.88604539	1.05768940
C	-0.66789838	-3.68826182	0.24010236
H	-1.40481769	-0.89193006	3.10380990
C	-0.56091806	-2.51205007	4.23498626
C	-2.98065889	-1.82749093	4.19542653
C	0.37778644	-3.48575985	-0.77642351
H	0.39000464	-2.52311990	3.70541447
H	-0.80338760	-3.53797487	4.52527973
H	-0.42990632	-1.92941077	5.14847777
H	-2.82622081	-1.21549701	5.08504377
H	-3.29949496	-2.81873336	4.52838202
H	-3.79762308	-1.38217302	3.62497915
N	1.43074312	-2.58735515	-0.64834183
C	0.56475755	-4.24328441	-1.91070895
C	2.26424561	-2.84853124	-1.64235725
N	1.75851973	-3.81322662	-2.45074442
C	-0.24111346	-5.31623406	-2.54987517
C	3.63837592	-2.25143386	-1.66767678
C	2.30894348	-4.28514028	-3.71677814
H	-1.15764068	-5.46712427	-1.99054199
H	-0.49092424	-5.05412304	-3.58091374
H	0.30966313	-6.26021185	-2.57727893
N	3.49050927	-0.95799192	-1.03377842
H	4.01329289	-2.13840745	-2.68885862
C	4.62168424	-3.18079201	-0.86291477
H	3.20665436	-3.72475666	-3.95222350
H	2.55504429	-5.34367708	-3.65643822
H	1.58010947	-4.12991252	-4.51036864
C	4.31427686	0.05058810	-1.34628567
H	4.18288957	-3.26756528	0.13647614
C	4.74728271	-4.59008301	-1.44957912
C	6.01517951	-2.56757906	-0.71009372
C	4.08148905	1.20635331	-0.45705304
H	3.80061827	-5.12931615	-1.46526289
H	5.43915261	-5.17613792	-0.84223255
H	5.14937367	-4.56412399	-2.46546578
H	5.98763265	-1.59890207	-0.21540309
H	6.49978634	-2.43787377	-1.67923140
H	6.63623036	-3.23332386	-0.10661744
N	2.98126854	1.18537838	0.37526758

C	4.81888465	2.33488198	-0.21989488
N	4.13751988	3.00802855	0.77782402
C	6.08842007	2.81485358	-0.82725980
C	4.52297732	4.29331204	1.35332273
H	6.42675462	2.07712041	-1.55004095
H	6.86829498	2.95305068	-0.07488078
H	5.95353216	3.76740653	-1.34570496
H	3.68968999	4.98902181	1.28228930
H	5.36130642	4.69115722	0.79110677
H	4.82408722	4.17459394	2.39299673
Cu	1.90585462	-0.58942725	0.06457405
Cu	-1.88676977	0.60640507	0.04896657
H	0.32280418	1.89285161	1.00137771
O	-1.44966670	-4.63948664	0.18233370
O	5.18552970	0.05393648	-2.23171347
O	0.01640200	0.00599300	0.67671000
O	2.42156400	-1.48657800	2.25385600
O	-2.28007700	1.48114300	2.27261400
H	2.40831800	-2.44941700	2.17884300
H	3.33283000	-1.26289800	2.48189700
H	-3.17341000	1.26565100	2.56881300
H	-2.24894300	2.44555400	2.23782100
H	0.00579800	0.02135100	1.64170800
C	1.03789467	3.96700973	4.62629366
H	0.50186951	4.65055610	4.00152060
H	2.08934374	4.13043605	4.51383619
C	1.79168972	1.94072832	3.32167098
H	2.85839196	1.91573240	3.40180543
H	1.39578707	0.96785322	3.52581587
C	0.63758706	4.19295874	6.09608986
H	1.16355466	3.50041902	6.71950531
H	-0.41609365	4.04264743	6.20592362
N	0.98046441	5.56657277	6.49171546
H	1.71492568	5.54460054	7.17001029
O	-1.34353695	5.71032524	6.92223601
C	-0.20234347	6.21929964	7.07120934
C	-0.27485634	7.36027798	7.88166123
H	-0.99438827	8.04058721	7.47625630
H	-0.56934408	7.07716986	8.87061359
C	1.10488947	8.04242721	7.93239533
H	1.81627557	7.37593461	8.37354999
H	1.41676963	8.29065571	6.93941327
C	1.01189629	9.32656377	8.77734833
H	0.68634622	9.07996938	9.76634194
H	0.31100141	9.99894302	8.32840234
C	2.39621641	9.99788795	8.84503613
H	2.69589324	10.29718880	7.86243102
H	3.10964213	9.30511373	9.23998883
C	2.32242578	11.23551929	9.75850405
H	2.03737586	10.93431249	10.74487163
H	1.59808891	11.92157615	9.37177148
C	3.70139743	11.91925378	9.80894544
H	4.43096669	11.22457024	10.16956087
H	3.97403354	12.24517485	8.82693474
C	3.63794209	13.13373022	10.75373133
C	3.90669111	12.97446632	12.11346675
C	3.31191080	14.39294320	10.25011004
C	3.84873809	14.07409810	12.96943002
H	4.16294525	11.98145419	12.51033259
C	3.25486186	15.49319461	11.10603184
H	3.10023974	14.51867971	9.17842225
C	3.52307013	15.33395732	12.46553352
H	4.05994231	13.94852651	14.04130738
H	2.99817587	16.48598396	10.70859526
C	3.45924639	16.54794790	13.41091884
C	4.60732278	17.31993223	13.61932392
C	2.25396458	16.86346461	14.04755886
C	5.84926197	17.01153294	12.97472225
C	4.54834575	18.44634656	14.49631608
C	2.19547457	17.98872960	14.92598705
C	1.06847273	16.08499347	13.84379395
C	6.95624365	17.78046457	13.18810370
H	5.88182636	16.14078409	12.30260569
C	5.73232829	19.22831221	14.69568924
C	0.95361845	18.29723544	15.57059884
H	1.12642329	15.22141585	13.16414338
C	-0.09719826	16.41019487	14.47443928
C	6.89687498	18.90574331	14.06168439
H	7.91067173	17.54805849	12.69308376
H	5.67381059	20.09303195	15.37380179
C	-0.15534047	17.53266825	15.35161950
H	0.92210159	19.16619405	16.24511998
H	-1.00949153	15.81533023	14.31991532
O	3.34376729	18.76031481	15.13496394
N	8.11459554	19.70417380	14.26309294
H	7.93444887	20.65560380	14.01343692
H	8.38853241	19.65776085	15.22372004
N	-1.43213809	17.84573101	16.00940331
H	-1.32393946	17.76954294	17.00060886
H	-1.70818391	18.77782646	15.77488940

5E

187

N	-9.339038	-1.002190	0.838996
N	-11.123456	-1.370584	2.079790
N	-9.925789	1.528333	0.283916
N	-7.795660	2.704811	-0.728177
N	-7.200960	4.819693	-0.859278
N	-4.612081	2.721918	-1.535816
O	-10.749454	3.475821	1.211547
O	-3.488839	4.673634	-1.756700
C	-9.150073	-2.186187	1.545992
C	-10.264930	-2.420585	2.326170
C	-10.533624	-0.548169	1.175631
C	-11.087840	0.712244	0.573186
H	-11.724489	1.223208	1.300998
C	-9.886818	2.825882	0.595449
C	-8.681254	3.469903	0.013156
C	-8.321279	4.790214	-0.057149
C	-6.918663	3.541406	-1.257462
C	-5.800850	3.225158	-2.224526
H	-5.495108	4.169600	-2.669400
C	-3.506407	3.486969	-1.408029
C	-10.634426	-3.501967	3.279065
H	-9.852941	-4.251537	3.300005
H	-11.574885	-3.974926	2.985650
H	-10.771809	-3.105230	4.288545
C	-11.932968	0.436035	-0.714764
H	-11.260638	-0.083716	-1.406079
C	-13.143110	-0.467027	-0.463894
H	-12.858952	-1.453368	-0.095501
H	-13.689332	-0.616630	-1.396692
H	-13.836501	-0.017471	0.251015
C	-12.378587	1.744477	-1.371220
H	-11.529761	2.360164	-1.664658
H	-13.004802	2.329760	-0.693740
H	-12.964714	1.529669	-2.266857
C	-8.938391	6.009919	0.528404
H	-9.798912	5.715991	1.122290
H	-9.269133	6.702295	-0.249758
H	-8.235947	6.547844	1.169598
C	-6.503872	6.046481	-1.240277
H	-5.465220	5.827037	-1.468189
H	-6.536940	6.742054	-0.405817
H	-6.985704	6.507028	-2.103440
C	-6.250520	2.301006	-3.383284
H	-6.521754	1.332693	-2.957395
C	-5.112524	2.100006	-4.388878
H	-4.213406	1.690853	-3.928068
H	-4.841661	3.047751	-4.861793
H	-5.426374	1.412979	-5.176446
C	-7.479557	2.872809	-4.097892
H	-8.336979	2.974542	-3.433211
H	-7.771373	2.214992	-4.918080
H	-7.260063	3.855414	-4.524499
C	-7.951698	-3.059563	1.488880
N	-6.900674	-2.634992	0.753659
O	-7.931344	-4.131403	2.106635
C	-5.745962	-3.501697	0.520658
C	-4.543595	-3.099181	1.342929
H	-6.048099	-4.485619	0.873997
C	-5.418921	-3.652780	-0.986690
N	-3.658972	-2.140788	1.101438
N	-4.163568	-3.803338	2.449783
H	-5.169504	-2.666722	-1.381763
C	-6.630834	-4.194514	-1.751439
C	-4.214045	-4.575249	-1.201343
C	-2.664235	-2.264764	2.057590
C	-2.967741	-3.292920	2.907740
C	-4.833170	-4.962936	3.036214
H	-7.514207	-3.567226	-1.633145
H	-6.887272	-5.200233	-1.408112
H	-6.404362	-4.254181	-2.817150
H	-3.307956	-4.191677	-0.733093
H	-4.015341	-4.684263	-2.268700
H	-4.410248	-5.572658	-0.798451
C	-1.426810	-1.458367	1.933095
C	-2.233387	-3.848147	4.075327
H	-5.901650	-4.905748	2.850307
H	-4.665496	-4.956215	4.109700
H	-4.429666	-5.886881	2.620923
N	-1.471277	-0.659630	0.861292
O	-0.463118	-1.601273	2.703229
H	-1.326908	-3.269162	4.226023
H	-1.959575	-4.893762	3.914235
H	-2.834074	-3.802102	4.986832
C	-0.329000	0.109687	0.432997
C	-0.903950	1.420008	0.001379
H	0.373408	0.239732	1.260238
C	-2.297686	2.864504	-0.819863
N	-2.134933	1.523852	-0.469174
N	-0.266276	2.612966	-0.018019
C	1.151564	-1.844528	-0.367339
C	-1.133609	3.549464	-0.533271
H	0.442759	-2.538200	0.091956
H	1.910941	-1.629177	0.391317
C	-0.717839	4.969517	-0.688703

H	-1.519249	5.536910	-1.145430
H	0.174628	5.046938	-1.314858
H	-0.474613	5.414599	0.279802
Cu	-8.288696	0.638538	-0.243033
Cu	-3.170882	-0.217962	0.081200
O	-6.911798	-0.364643	-1.174223
H	-5.608452	-0.195014	-1.276756
H	-6.988406	-1.792055	0.180058
O	-4.527173	-0.215513	-1.510091
H	-4.433615	-0.421862	-2.448094
H	-4.561686	1.727805	-1.331131
H	-7.270638	-0.773805	-1.969696
O	-7.091603	0.850695	1.736171
H	-7.503083	0.320365	2.432925
O	-4.118517	0.577519	1.938288
H	-3.830064	0.085049	2.716155
H	-5.084319	0.606111	1.998444
C	-12.393687	-1.170985	2.769559
H	-13.127137	-1.908455	2.447367
H	-12.242122	-1.262860	3.843049
H	-12.771497	-0.177907	2.555092
C	1.081965	2.896664	0.460121
H	1.741435	3.131827	-0.374612
H	1.059023	3.739690	1.147268
H	1.469564	2.029608	0.984386
H	-7.191312	1.769531	2.023204
C	0.431835	-0.551185	-0.743435
H	1.158664	0.166765	-1.136471
H	-0.286926	-0.742461	-1.545706
C	1.807440	-2.517033	-1.573540
H	2.500826	-1.823862	-2.059809
H	1.042077	-2.765407	-2.315710
C	2.559617	-3.794604	-1.192683
H	1.883597	-4.476656	-0.671189
H	3.365791	-3.565528	-0.497539
N	3.107984	-4.506436	-2.339440
H	2.455332	-5.030212	-2.905560
O	4.645048	-5.097681	-3.866116
C	4.368254	-4.482593	-2.835416
C	5.413386	-3.690432	-2.063506
H	5.050301	-2.667764	-1.924443
H	5.492957	-4.116281	-1.057914
C	6.784269	-3.673599	-2.731728
H	6.692722	-3.252037	-3.736206
H	7.134916	-4.700066	-2.863903
C	7.818964	-2.877921	-1.935098
H	7.467772	-1.847761	-1.806219
H	7.905862	-3.299599	-0.927230
C	9.197148	-2.863719	-2.596713
H	9.110185	-2.439015	-3.603135
H	9.543380	-3.894865	-2.729560
C	10.247490	-2.080550	-1.809688
H	9.915994	-1.044927	-1.681641
H	10.342153	-2.501846	-0.803587
C	11.626118	-2.088574	-2.490999
H	11.530446	-1.657432	-3.491122
H	11.948698	-3.125140	-2.622485
C	12.678455	-1.333709	-1.719987
C	12.919873	0.019958	-1.963018
C	13.428111	-1.961816	-0.722730
C	13.869634	0.725409	-1.236199
H	12.361367	0.531362	-2.738079
C	14.392653	-1.270427	-0.002725
H	13.263078	-3.011639	-0.510771
C	14.624566	0.085839	-0.249331
H	14.041804	1.772038	-1.453060
H	14.962099	-1.783904	0.761619
C	15.659983	0.828031	0.510148
C	17.022952	0.502190	0.368235
C	15.299968	1.872967	1.383190
C	17.523975	-0.501473	-0.508107
C	17.994689	1.229660	1.109185
C	16.316799	2.571076	2.091268
C	13.960728	2.276599	1.647072
C	18.855361	-0.766375	-0.607156
H	16.825125	-1.059970	-1.112956
C	19.344342	0.976884	1.024477
C	16.049509	3.602735	2.961134
H	13.153892	1.754015	1.154896
C	13.675212	3.293764	2.505443
C	19.804292	-0.034040	0.166264
H	19.210715	-1.533836	-1.282240
H	20.034986	1.563769	1.614562
C	14.719359	3.992265	3.181592
H	16.866313	4.098154	3.467967
H	12.648156	3.579973	2.690909
O	17.619284	2.232350	1.938875
N	14.419980	4.998468	4.020777
H	15.138383	5.500439	4.513759
H	13.466607	5.275527	4.178740
N	21.114655	-0.312145	0.058526
H	21.443227	-1.023624	-0.571177
H	21.804137	0.203393	0.578014

5F

187

N	8.606080	-3.039685	0.019806
N	10.249024	-4.323822	-0.695147
N	10.152721	-1.389653	1.413090
N	8.767715	0.761408	2.046002
N	9.381310	2.804107	2.588649
N	6.066135	2.619699	1.856349
O	12.167358	-0.262852	1.356651
O	6.161766	4.840259	2.280174
C	8.126648	-3.836799	-1.015641
C	9.152886	-4.642207	-1.468056
C	9.875420	-3.365586	0.190276
C	10.710803	-2.718098	1.258747
H	11.749549	-2.644382	0.924549
C	10.931198	-0.307416	1.483382
C	10.132051	0.891943	1.844095
C	10.528225	2.161145	2.175632
C	8.337352	1.923173	2.508873
C	6.944123	2.277741	2.975699
H	7.032479	3.191574	3.559191
C	5.691394	3.897703	1.631797
C	9.244862	-5.674556	-2.535632
H	8.273635	-5.810608	-2.995219
H	9.582697	-6.629577	-2.125697
H	9.962881	-5.379724	-3.305596
C	10.680193	-3.515852	2.604851
H	9.624788	-3.573324	2.892778
C	11.213117	-4.944859	2.475118
H	10.629939	-5.546314	1.776917
H	11.168120	-5.443038	3.444987
H	12.256896	-4.954866	2.151989
C	11.437711	-2.768427	3.704420
H	11.007273	-1.787081	3.897723
H	12.487449	-2.631776	3.434127
H	11.403294	-3.340491	4.633619
C	11.867696	2.806977	2.165750
H	12.597055	2.094156	1.792235
H	12.166215	3.121300	3.168945
H	11.882396	3.692761	1.526148
C	9.350616	4.180631	3.078893
H	8.365229	4.608390	2.920987
H	10.077125	4.767141	2.522629
H	9.606222	4.214295	4.138538
C	6.328549	1.202409	3.905059
H	6.194142	0.288826	3.322067
C	4.965278	1.659223	4.433708
H	4.262020	1.891510	3.633937
H	5.070214	2.553376	5.053964
H	4.522081	0.876200	5.051140
C	7.262330	0.890056	5.079216
H	8.225906	0.500630	4.751816
H	6.804846	0.141682	5.728241
H	7.442730	1.784332	5.682051
C	6.746533	-3.829053	-1.560960
N	5.886215	-2.906379	-1.077237
O	6.416471	-4.641462	-2.433845
C	4.471498	-2.929339	-1.447204
C	4.113337	-1.844834	-2.436853
H	4.322826	-3.877978	-1.959277
C	3.540061	-2.943051	-0.208611
N	3.857184	-0.564246	-2.204741
N	3.904049	-2.120420	-3.758077
H	3.712553	-2.026415	0.357629
C	3.855337	-4.141626	0.691983
C	2.065825	-2.979903	-0.625772
C	3.431680	-0.017828	-3.404522
C	3.460825	-0.974184	-4.382536
C	4.032197	-3.414882	-4.425072
H	4.894677	-4.156202	1.019692
H	3.656932	-5.081186	0.169521
H	3.225151	-4.116309	1.582384
H	1.777144	-2.106961	-1.210594
H	1.429836	-3.010770	0.260333
H	1.850641	-3.873588	-1.217943
C	2.878374	1.357093	-3.425515
C	3.088810	-0.916304	-5.820961
H	4.787990	-4.014369	-3.926198
H	4.342354	-3.248114	-5.452945
H	3.076842	-3.940478	-4.424683
N	2.900082	1.909911	-2.207874
O	2.391277	1.859176	-4.451614
H	2.774714	0.095397	-6.060635
H	2.269014	-1.601936	-6.049161
H	3.930130	-1.183708	-6.464748
C	2.276240	3.181084	-1.933946
C	3.222187	3.866123	-1.001365
H	2.151421	3.750259	-2.858642
C	4.695284	4.150060	0.564797
N	4.009651	3.191170	-0.181700
N	3.363825	5.201024	-0.833610
C	-0.175909	2.421366	-2.177377
C	4.298618	5.407629	0.155459
H	0.167477	1.443381	-2.524575
H	-0.296887	3.042357	-3.070392
C	4.671151	6.785108	0.576580

H	5.386044	6.738067	1.388680
H	3.791026	7.341321	0.909099
H	5.112911	7.342456	-0.253764
Cu	8.246066	-1.161523	1.163875
Cu	4.091653	1.209851	-0.872834
O	6.311976	-1.202193	1.328135
H	5.383319	-0.297796	1.088013
H	6.164186	-2.315124	-0.289577
O	4.468413	0.314606	0.978740
H	3.912115	0.150623	1.749990
H	5.588104	1.863731	1.373963
H	6.045404	-1.789435	2.044405
O	8.257624	-0.166316	-0.934868
H	8.567654	-0.796178	-1.600592
O	5.967729	1.392127	-2.067276
H	5.805885	1.213071	-3.001382
H	6.730633	0.844846	-1.831330
C	11.583465	-4.878484	-0.896951
H	11.615531	-5.924443	-0.596020
H	11.853853	-4.800398	-1.947944
H	12.302336	-4.318394	-0.310040
C	2.695321	6.257034	-1.585144
H	1.988726	6.789417	-0.949319
H	3.432455	6.959399	-1.968171
H	2.160122	5.821708	-2.422356
H	8.931024	0.528253	-0.908495
C	0.884343	3.040260	-1.269500
H	0.553153	4.032981	-0.948313
H	0.999620	2.437863	-0.363562
C	-1.525786	2.265612	-1.476652
H	-1.882853	3.239880	-1.129695
H	-1.408395	1.637961	-0.587256
C	-2.585966	1.646356	-2.389548
H	-2.243287	0.675190	-2.754624
H	-2.758343	2.284685	-3.255047
N	-3.869283	1.457677	-1.730070
H	-3.958891	0.686536	-1.088989
O	-4.907477	3.269974	-2.615527
C	-4.928284	2.284592	-1.877251
C	-6.169513	1.915714	-1.083506
H	-6.414472	2.776874	-0.455481
H	-5.968677	1.074711	-0.415811
C	-7.362063	1.591340	-1.991815
H	-7.532875	2.434440	-2.665777
H	-7.111410	0.731274	-2.621419
C	-8.638875	1.291565	-1.206641
H	-8.890553	2.157439	-0.584113
H	-8.454277	0.460968	-0.516184
C	-9.830088	0.947143	-2.101109
H	-10.015486	1.776220	-2.793062
H	-9.577306	0.080512	-2.722134
C	-11.107666	0.649140	-1.316726
H	-11.372109	1.516164	-0.702703
H	-10.926435	-0.177403	-0.621904
C	-12.298861	0.292082	-2.221640
H	-12.483649	1.120200	-2.911018
H	-12.033417	-0.576013	-2.831383
C	-13.556807	-0.005232	-1.446575
C	-14.488484	0.997486	-1.170576
C	-13.810403	-1.286571	-0.951784
C	-15.634896	0.733260	-0.433189
H	-14.319126	2.001108	-1.542279
C	-14.943022	-1.556733	-0.196437
H	-13.111985	-2.088115	-1.161493
C	-15.873941	-0.548412	0.069821
H	-16.340980	1.529815	-0.235918
H	-15.115728	-2.560051	0.171717
C	-17.091894	-0.833936	0.866434
C	-16.992148	-1.183725	2.227220
C	-18.369106	-0.758703	0.277907
C	-15.769620	-1.254305	2.952677
C	-18.176602	-1.455708	2.965707
C	-19.518835	-1.031790	1.069098
C	-18.607375	-0.453258	-1.091809
C	-15.737390	-1.590729	4.271273
H	-14.847133	-1.026773	2.439351
C	-18.165510	-1.799402	4.297752
C	-20.800142	-0.977136	0.571216
H	-17.762005	-0.268758	-1.738050
C	-19.867133	-0.395186	-1.604069
C	-16.941465	-1.879258	4.979822
H	-14.794537	-1.634857	4.800551
H	-19.100031	-1.996378	4.805033
C	-21.002674	-0.647477	-0.778049
H	-21.635170	-1.191634	1.224125
H	-20.020718	-0.162038	-2.649654
O	-19.392003	-1.373111	2.373761
N	-22.240033	-0.576868	-1.297881
H	-23.054881	-0.758892	-0.737517
H	-22.384467	-0.343945	-2.265109
N	-16.891165	-2.211624	6.281145
H	-16.015036	-2.251671	6.772524
H	-17.727863	-2.398279	6.806803

5G

187

N	7.084296	-2.533497	-0.427199
N	8.939155	-3.702922	-0.201147
N	5.741921	-3.808010	1.437164
N	3.716148	-2.177738	2.086522
N	2.541021	-1.972848	3.930364
N	2.109247	0.710906	1.874818
O	5.865949	-4.696888	3.554549
O	0.872686	1.414030	3.637779
C	8.107122	-1.880461	-1.114004
C	9.270941	-2.609269	-0.969672
C	7.618471	-3.629440	0.088440
C	6.798254	-4.616841	0.868413
H	7.401009	-5.073133	1.658633
C	5.374122	-3.921783	2.718295
C	4.261475	-3.001117	3.058591
C	3.536669	-2.883662	4.211922
C	2.666876	-1.575492	2.630400
C	1.651967	-0.674688	1.969800
H	0.790957	-0.647362	2.634463
C	1.618737	1.673128	2.685916
C	10.663640	-2.421373	-1.459044
H	10.716033	-1.537541	-2.082057
H	10.990521	-3.287590	-2.039575
H	11.359861	-2.308371	-0.623538
C	6.203691	-5.743842	-0.034264
H	5.614194	-5.232750	-0.803490
C	7.273773	-6.581315	-0.739016
H	7.901462	-5.985174	-1.402603
H	6.795920	-7.348743	-1.350292
H	7.919141	-7.092753	-0.020640
C	5.264814	-6.647621	0.767103
H	4.431762	-6.089425	1.192197
H	5.797715	-7.139253	1.584367
H	4.855034	-7.424867	0.119357
C	3.681246	-3.553755	5.530846
H	4.543592	-4.213363	5.495085
H	2.796070	-4.145430	5.776994
H	3.826794	-2.829247	6.335585
C	1.502728	-1.583351	4.882800
H	1.128393	-0.593768	4.639285
H	1.935869	-1.556827	5.879290
H	0.685734	-2.305667	4.871387
C	0.460956	-2.536426	0.672656
H	1.092097	-3.290450	1.152516
H	-0.422328	-2.419530	1.309502
C	8.005568	-0.626697	-1.901240
N	6.848021	0.070619	-1.875194
O	8.976189	-0.241697	-2.565032
C	6.651743	1.193019	-2.794705
C	6.842631	2.535988	-2.127715
H	7.455137	1.104671	-3.523334
C	5.325500	1.090466	-3.592722
N	5.980170	3.215244	-1.390888
N	7.962669	3.294062	-2.333579
H	4.498447	1.130303	-2.881155
C	5.253224	-0.235045	-4.357020
C	5.176636	2.262543	-4.568719
C	6.549380	4.453029	-1.141088
C	7.788693	4.515954	-1.718412
C	9.137334	2.939890	-3.127522
H	5.349320	-1.099665	-3.700205
H	6.046510	-0.294178	-5.106743
H	4.297504	-0.314667	-4.877592
H	5.150414	3.226501	-4.061329
H	4.248433	2.159720	-5.133078
H	6.000369	2.277341	-5.287839
C	5.740298	5.482179	-0.445810
C	8.800372	5.604944	-1.757530
H	9.280799	1.863725	-3.110009
H	10.011163	3.415368	-2.690013
H	9.024206	3.286261	-4.155410
N	4.538184	4.977490	-0.162505
O	6.163607	6.622143	-0.189198
H	8.421646	6.454245	-1.195927
H	9.003577	5.924985	-2.782425
H	9.749091	5.287891	-1.317615
C	3.496364	5.762577	0.471517
C	2.827900	4.858850	1.472761
H	3.934937	6.622290	0.986287
C	2.478249	6.280053	-0.597131
C	2.013287	3.073706	2.415414
N	2.726432	3.548547	1.315310
N	2.235396	5.246382	2.628726
H	2.045715	5.384847	-1.057223
C	1.336634	7.097087	0.013541
C	3.182365	7.086879	-1.689473
C	1.703953	4.133548	3.239010
H	0.742036	6.519412	0.721976
H	0.661439	7.433610	-0.775037
H	1.711997	7.987440	0.524099
H	3.925537	6.490492	-2.216724
H	3.683744	7.961991	-1.270329
H	2.451185	7.437209	-2.420643
C	0.972912	4.241000	4.530317

H	0.606718	3.264666	4.824058
H	0.126800	4.927282	4.443091
H	1.624793	4.626874	5.318519
Cu	5.208743	-2.285335	0.410098
Cu	4.337502	3.068398	-0.343459
O	4.680913	-0.885336	-0.803385
H	4.118146	0.333323	-0.650598
H	6.034173	-0.300522	-1.379738
O	3.641299	1.278350	-0.415242
H	2.947853	1.444224	-1.064689
H	2.647029	0.972004	1.053492
H	4.389403	-1.280877	-1.633230
O	7.374931	-0.139255	1.379096
H	8.321561	0.009428	1.270721
O	5.768109	2.278950	1.236563
H	6.473895	2.928352	1.347894
H	6.228309	1.420765	1.171629
C	9.897216	-4.697577	0.269250
H	10.243453	-5.318224	-0.555592
H	10.749068	-4.194551	0.721805
H	9.427810	-5.328869	1.014625
C	2.209089	6.586570	3.203193
H	1.199069	6.993319	3.185081
H	2.561235	6.546565	4.231799
H	2.864484	7.236897	2.634853
H	7.278930	-0.546300	2.247918
C	1.207212	-1.203817	0.597904
H	2.077736	-1.300274	-0.054327
H	0.554436	-0.447411	0.155000
C	0.031887	-3.044152	-0.703923
H	-0.586791	-2.291865	-1.202632
H	0.914709	-3.191957	-1.333642
C	-0.745326	-4.360339	-0.623881
H	-1.646653	-4.230226	-0.026999
H	-0.140193	-5.113209	-0.113063
N	-1.110750	-4.896799	-1.927932
H	-0.379510	-5.351039	-2.456744
C	-2.284204	-4.785403	-2.595834
O	-2.402484	-5.248463	-3.730939
C	-3.435327	-4.090403	-1.883575
H	-3.662960	-4.651864	-0.971444
H	-3.101257	-3.103839	-1.548742
C	-4.690663	-3.955695	-2.739317
H	-5.010958	-4.946892	-3.069262
H	-4.451046	-3.395943	-3.647368
C	-5.837944	-3.266387	-2.000167
H	-6.075886	-3.829540	-1.090524
H	-5.515399	-2.272711	-1.668929
C	-7.099531	-3.129965	-2.853048
H	-7.414675	-4.123515	-3.191141
H	-6.862854	-2.560125	-3.758653
C	-8.261540	-2.456799	-2.123627
H	-7.958027	-1.460009	-1.787410
H	-8.507586	-3.025992	-1.221225
C	-9.520587	-2.331589	-2.997898
H	-9.814602	-3.327765	-3.339548
H	-9.276272	-1.749219	-3.890440
C	-10.679880	-1.688400	-2.281314
C	-11.585638	-2.456325	-1.546085
C	-10.868039	-0.304864	-2.308095
C	-12.634747	-1.867590	-0.853572
H	-11.472766	-3.533684	-1.517261
C	-11.925482	0.292162	-1.634930
H	-10.181892	0.317297	-2.870595
C	-12.821555	-0.483003	-0.893819
H	-13.325524	-2.488055	-0.296859
H	-12.048803	1.366942	-1.675893
C	-13.953023	0.147749	-0.171710
C	-14.011794	0.117285	1.235337
C	-14.990524	0.785155	-0.879732
C	-13.012556	-0.456402	2.070851
C	-15.114006	0.721516	1.900456
C	-16.062800	1.380441	-0.159603
C	-15.073941	0.852642	-2.299133
C	-13.123622	-0.451526	3.427491
H	-12.142111	-0.899852	1.610544
C	-15.246100	0.735282	3.269775
C	-17.114773	2.018698	-0.774882
H	-14.297367	0.387871	-2.888309
C	-16.106993	1.478203	-2.926976
C	-14.254218	0.140537	4.064967
H	-12.348079	-0.892542	4.039791
H	-16.109502	1.208762	3.716795
C	-17.155572	2.087840	-2.176061
H	-17.900570	2.453636	-0.172399
H	-16.148350	1.513078	-4.007778
O	-16.095656	1.330511	1.193550
N	-18.164655	2.706114	-2.812910
H	-18.197168	2.745699	-3.816965
H	-18.919833	3.134788	-2.305903
N	-14.350616	0.130851	5.405561
H	-15.133256	0.550503	5.877340
H	-13.635956	-0.289370	5.974343

5H

187

N	-3.406634	3.459937	-1.582015
N	-3.472743	5.461456	-2.503268
N	-3.428875	4.313935	0.902416
N	-4.200983	2.205473	2.365782
N	-5.199754	2.070040	4.316878
N	-5.314875	-0.900821	2.651052
O	-4.380733	5.823536	2.352889
O	-6.550171	-1.464723	4.464224
C	-3.698226	3.315007	-2.937854
C	-3.744552	4.568181	-3.515676
C	-3.259719	4.757696	-1.366250
C	-2.892613	5.297366	-0.013451
H	-3.363262	6.271044	0.149039
C	-4.117757	4.664095	1.994362
C	-4.546397	3.481528	2.781262
C	-5.167953	3.410495	3.996966
C	-4.592240	1.367312	3.316517
C	-4.348072	-0.118493	3.419945
H	-4.526332	-0.384547	4.459800
C	-6.313129	-1.580580	3.255856
C	-4.008824	5.048254	-4.899182
H	-4.151964	4.201751	-5.558722
H	-3.174016	5.650218	-5.266518
H	-4.902292	5.677764	-4.930738
C	-1.348839	5.439884	0.173396
H	-0.931916	4.441735	-0.000686
C	-0.704967	6.401282	-0.828728
H	-0.839106	6.079574	-1.862282
H	0.369339	6.457688	-0.645330
H	-1.105866	7.412775	-0.727258
C	-1.007932	5.858482	1.604848
H	-1.364365	5.132211	2.334059
H	-1.450724	6.827895	1.845221
H	0.074140	5.947509	1.717989
C	-5.710954	4.474295	4.881819
H	-5.570901	5.436676	4.397869
H	-5.200307	4.488988	5.847857
H	-6.776616	4.330592	5.075253
C	-5.744168	1.545769	5.568136
H	-6.068526	0.518915	5.430068
H	-6.603128	2.147336	5.853809
H	-4.996258	1.598599	6.360090
C	-1.863451	0.060245	4.018817
H	-1.943772	1.150800	4.063194
H	-2.076028	-0.308232	5.027885
C	-3.906962	2.049258	-3.683701
N	-3.961170	0.886262	-2.997155
O	-4.027382	2.078220	-4.914802
C	-3.962333	-0.387578	-3.719054
C	-5.338055	-1.007264	-3.809920
H	-3.681140	-0.134005	-4.739240
C	-2.881905	-1.372478	-3.200481
N	-5.976805	-1.722195	-2.899417
N	-6.063376	-0.993276	-4.969771
H	-3.112439	-1.610667	-2.160264
C	-1.491015	-0.733742	-3.262093
C	-2.891717	-2.676380	-4.005614
C	-7.128648	-2.203817	-3.499257
C	-7.199681	-1.753624	-4.789776
C	-5.698703	-0.357237	-6.233926
H	-1.435181	0.196657	-2.696894
H	-1.210081	-0.515136	-4.295616
H	-0.746637	-1.418962	-2.853303
H	-3.842164	-3.204220	-3.932270
H	-2.111926	-3.345249	-3.637951
H	-2.689222	-2.482722	-5.062677
C	-7.977719	-3.158525	-2.747732
C	-8.211499	-1.980669	-5.855422
H	-5.082531	0.515715	-6.040780
H	-6.606433	-0.038461	-6.739376
H	-5.164519	-1.058437	-6.876023
N	-7.437230	-3.375323	-1.547349
O	-9.021786	-3.650117	-3.209054
H	-9.004445	-2.607149	-5.456798
H	-7.773031	-2.479921	-6.722961
H	-8.647456	-1.040598	-6.202303
C	-8.008863	-4.308744	-0.595669
C	-7.900885	-3.660253	0.758531
H	-9.060699	-4.490981	-0.834151
C	-7.238878	-5.669497	-0.638327
C	-7.145764	-2.475421	2.421327
N	-6.930399	-2.822715	1.088179
N	-8.740606	-3.851093	1.805405
H	-6.204708	-5.437513	-0.361128
C	-7.779673	-6.692219	0.364336
C	-7.235005	-6.260942	-2.049049
C	-8.277352	-3.117592	2.873417
H	-7.699817	-6.348212	1.396041
H	-7.209427	-7.619625	0.288644
H	-8.825871	-6.934649	0.161869
H	-6.752307	-5.596614	-2.764343
H	-8.252094	-6.454047	-2.397077
H	-6.693778	-7.209115	-2.051614
C	-8.986150	-3.133388	4.181392

H	-8.446923	-2.522663	4.895438
H	-9.063351	-4.151814	4.570423
H	-10.003343	-2.745805	4.080365
Cu	-3.490315	2.514849	0.256505
Cu	-6.038441	-2.167292	-0.998071
O	-3.346972	0.738587	-0.475265
H	-4.024983	-0.415352	-0.291127
H	-3.787338	0.874357	-1.989579
O	-4.617744	-1.289762	-0.046399
H	-4.030097	-2.051362	0.022883
H	-5.097077	-1.088978	1.676833
H	-2.420379	0.549431	-0.664261
O	-6.270120	2.557140	-1.327125
H	-6.618538	2.951928	-2.135027
O	-7.135506	-0.180543	-0.873130
H	-7.868020	-0.206793	-1.501609
H	-6.709909	0.684689	-1.023867
C	-3.506003	6.911935	-2.656555
H	-2.663239	7.254862	-3.254550
H	-4.433875	7.203641	-3.143848
H	-3.461606	7.380690	-1.680464
C	-9.974700	-4.628029	1.819210
H	-9.866537	-5.511113	2.447204
H	-10.785782	-4.012508	2.202507
H	-10.218724	-4.937732	0.809252
H	-6.582833	3.123047	-0.611785
C	-2.905678	-0.497876	3.048816
H	-2.690065	-0.155579	2.034564
H	-2.847613	-1.589274	3.041408
C	-0.435745	-0.323154	3.629661
H	-0.345958	-1.411554	3.571440
H	-0.207905	0.067729	2.632988
C	0.599406	0.205138	4.625069
H	0.405530	-0.202528	5.616626
H	0.534143	1.293087	4.692041
N	1.968717	-0.139341	4.270325
H	2.448029	0.454536	3.615057
O	2.076886	-2.028799	5.511623
C	2.605199	-1.237320	4.729180
C	4.030036	-1.476842	4.247685
H	4.623053	-1.642024	5.151514
H	4.011159	-2.440140	3.728717
C	4.700235	-0.423464	3.366732
H	4.123332	-0.279844	2.446693
H	4.716624	0.540363	3.885764
C	6.132280	-0.808150	2.989062
H	6.717962	-0.954868	3.903020
H	6.120833	-1.774832	2.473868
C	6.824950	0.227978	2.104166
H	6.239441	0.371923	1.189130
H	6.833556	1.195715	2.617838
C	8.255382	-0.158474	1.730166
H	8.848396	-0.296591	2.639964
H	8.250582	-1.124610	1.215111
C	8.944200	0.884937	0.834638
H	8.953083	1.848016	1.351775
H	8.350890	1.018351	-0.074353
C	10.353502	0.503512	0.460578
C	11.442939	0.920326	1.228379
C	10.608491	-0.305059	-0.649254
C	12.740624	0.553085	0.898173
H	11.276448	1.548220	2.095764
C	11.900155	-0.694454	-0.976569
H	9.784598	-0.634567	-1.271363
C	12.985310	-0.265398	-0.207797
H	13.566817	0.893804	1.509332
H	12.068380	-1.318126	-1.845432
C	14.369372	-0.665728	-0.561478
C	14.775636	-2.009444	-0.455871
C	15.300480	0.291465	-1.008498
C	13.946703	-3.066128	0.015393
C	16.108533	-2.364471	-0.803315
C	16.621879	-0.120399	-1.335172
C	15.007206	1.671228	-1.198232
C	14.397750	-4.347642	0.099195
H	12.935354	-2.838135	0.318376
C	16.583230	-3.653191	-0.727229
C	17.587939	0.751270	-1.781859
H	14.007982	2.024344	-0.989999
C	15.948299	2.549165	-1.641655
C	15.732918	-4.677596	-0.280895
H	13.746850	-5.131674	0.463579
H	17.606253	-3.862287	-1.009130
C	17.272124	2.109858	-1.940271
H	18.576887	0.379069	-2.012263
H	15.698658	3.592967	-1.780330
O	16.984985	-1.421028	-1.224509
N	18.190933	2.991018	-2.371893
H	17.959299	3.960635	-2.502238
H	19.125146	2.700973	-2.605345
N	16.160578	-5.949019	-0.201385
H	17.100295	-6.201554	-0.454994
H	15.554823	-6.681773	0.125697

5l

158

N	5.106039	-2.495618	0.173610
N	6.656656	-3.872968	-0.573334
N	6.627718	-0.320003	0.089154
N	5.097302	1.811935	0.331116
N	5.394604	3.914489	-0.247210
N	2.149518	3.248325	0.518491
O	8.211736	0.773222	-1.186534
O	1.893225	5.430057	-0.023741
C	4.496304	-3.691880	-0.193238
C	5.463655	-4.557739	-0.663395
C	6.398608	-2.644294	-0.058027
C	7.378614	-1.548421	0.254041
H	8.204772	-1.573732	-0.462156
C	7.129170	0.722637	-0.576918
C	6.253760	1.913333	-0.424887
C	6.450312	3.218048	-0.794794
C	4.602436	3.033782	0.437687
C	3.401521	3.482249	1.238569
H	3.476838	4.562960	1.337325
C	1.452075	4.274476	-0.015111
C	5.418964	-5.948221	-1.191111
H	4.404815	-6.324848	-1.139478
H	6.073582	-6.605258	-0.613164
H	5.757845	-5.984617	-2.229936
C	7.971628	-1.671908	1.697104
H	7.111273	-1.653321	2.374990
C	8.729563	-2.980951	1.931283
H	8.093886	-3.858884	1.810960
H	9.119053	-3.002511	2.950442
H	9.582292	-3.076139	1.254689
C	8.868690	-0.476967	2.027149
H	8.323638	0.464440	1.978629
H	9.712413	-0.417136	1.335605
H	9.270514	-0.582085	3.036772
C	7.535216	3.864470	-1.579968
H	8.236117	3.100374	-1.903212
H	8.073624	4.604159	-0.982232
H	7.142963	4.377241	-2.461516
C	5.228703	5.362339	-0.358153
H	4.178640	5.623097	-0.267194
H	5.582652	5.681923	-1.334792
H	5.807745	5.873087	0.412016
C	3.379965	2.894962	2.671611
H	3.262500	1.812219	2.591305
C	2.204747	3.463902	3.472752
H	1.243139	3.281889	2.992811
H	2.311782	4.544064	3.603249
H	2.173991	3.010404	4.464804
C	4.694901	3.182563	3.403994
H	5.555445	2.741178	2.902032
H	4.653960	2.773265	4.414631
H	4.865375	4.259220	3.490202
C	3.047077	-3.999408	-0.107692
N	2.216779	-3.005750	0.277938
O	2.631727	-5.129725	-0.391851
C	0.800725	-3.265402	0.535227
C	-0.093296	-2.748824	-0.568272
H	0.701369	-4.349082	0.533236
C	0.360225	-2.782111	1.940313
N	-0.530855	-1.512792	-0.768675
N	-0.663872	-3.589111	-1.481367
H	0.506411	-1.701965	1.990472
C	1.210226	-3.442448	3.030498
C	-1.123084	-3.078204	2.187041
C	-1.438973	-1.574597	-1.812994
C	-1.528174	-2.860903	-2.270637
C	-0.485142	-5.036052	-1.587926
H	2.275976	-3.255238	2.900260
H	1.059801	-4.525245	3.035915
H	0.922042	-3.061380	4.011481
H	-1.772746	-2.569124	1.475592
H	-1.405754	-2.749689	3.188435
H	-1.322066	-4.151504	2.123194
C	-2.253848	-0.381520	-2.143964
C	-2.359791	-3.462752	-3.346277
H	0.504932	-5.312828	-1.237741
H	-0.578215	-5.322766	-2.631796
H	-1.246960	-5.558254	-1.008362
N	-1.950320	0.651477	-1.350539
O	-3.151142	-0.409850	-3.002038
H	-2.948468	-2.678638	-3.813464
H	-3.038173	-4.221781	-2.948901
H	-1.743125	-3.940755	-4.111146
C	-2.709357	1.877717	-1.367668
C	-1.681204	2.953319	-1.226978
H	-3.255180	1.973671	-2.309721
C	0.128618	3.976969	-0.610395
N	-0.539081	2.751948	-0.592541
N	-1.786954	4.231064	-1.658664
C	-4.890497	0.986758	-0.309402
C	-0.645838	4.902221	-1.281593
H	-4.503521	-0.031907	-0.390431
H	-5.451133	1.181697	-1.228833
C	-0.464874	6.342161	-1.609313

H	0.471064	6.696231	-1.195253
H	-1.283550	6.939749	-1.200388
H	-0.456862	6.499550	-2.691174
Cu	4.745510	-0.327909	0.543813
Cu	-0.260765	0.676390	-0.435646
O	3.034094	-0.396005	1.458009
H	1.904736	0.258703	1.273876
H	2.604310	-2.113960	0.596983
O	0.895190	0.710138	1.306298
H	0.676574	0.873053	2.231960
H	1.715719	2.332665	0.596482
H	3.155495	-0.621018	2.387303
O	3.842009	-0.360089	-1.595800
H	4.042977	-1.201131	-2.029726
O	1.024450	0.414406	-2.240961
H	0.604873	-0.166280	-2.887156
H	1.922354	0.068959	-2.133050
C	7.935302	-4.387145	-1.052704
H	8.292988	-5.190140	-0.410148
H	7.817418	-4.765653	-2.065931
H	8.667577	-3.588012	-1.062644
C	-2.880482	4.810320	-2.430361
H	-3.434007	5.529511	-1.827571
H	-2.484554	5.310616	-3.311461
H	-3.554554	4.022596	-2.749715
H	4.317085	0.310159	-2.107328
C	-3.727604	1.971244	-0.205366
H	-4.120632	2.992195	-0.170133
H	-3.184460	1.810487	0.730669
C	-5.828674	1.081578	0.893487
H	-6.204275	2.104169	0.995700
H	-5.268472	0.857893	1.807725
C	-7.013820	0.126555	0.785180
H	-6.651508	-0.898110	0.648694
H	-7.604247	0.385505	-0.091587
N	-7.848478	0.214166	1.982903
H	-7.368664	0.457548	2.839259
C	-9.124217	-0.189041	2.187127
O	-9.611248	-0.170843	3.317518
C	-9.939349	-0.651210	0.984404
H	-9.265179	-0.930883	0.176385
C	-10.830622	-1.859282	1.318694
H	-10.254396	-2.782711	1.371502
H	-11.302546	-1.702894	2.288007
C	-11.887877	-1.910438	0.206067
C	-10.925253	0.411375	0.411434
N	-11.950798	-0.480407	-0.202880
O	-12.848331	-0.033426	-0.982667
C	-13.255687	-2.374275	0.705511
H	-13.602778	-1.751534	1.530992
H	-13.992808	-2.331871	-0.096405
H	-13.188062	-3.405126	1.056781
C	-11.441978	-2.755964	-0.995329
H	-10.443368	-2.476089	-1.333778
H	-11.428802	-3.812119	-0.721715
H	-12.135982	-2.623978	-1.826184
C	-11.610582	1.289141	1.468189
H	-10.902445	1.998933	1.896556
H	-12.414580	1.849937	0.990452
H	-12.029825	0.696820	2.279525
C	-10.298193	1.289456	-0.670746
H	-11.057975	1.927582	-1.121151
H	-9.530887	1.931345	-0.236384
H	-9.846416	0.685032	-1.458534

5J

158

N	-1.420162	3.998059	-0.147959
N	-1.993560	6.092834	0.229249
N	0.416116	3.887017	1.727663
N	0.796125	1.274265	2.188448
N	1.507126	0.193401	3.962955
N	0.022116	-1.914108	1.734191
O	0.910743	4.466203	3.897615
O	0.441327	-3.395769	3.395667
C	-2.609492	4.261682	-0.826431
C	-2.972635	5.572230	-0.587558
C	-1.074387	5.124561	0.455158
C	0.191788	5.236161	1.255420
H	0.051566	5.919900	2.097324
C	0.753720	3.627175	2.995742
C	0.945458	2.174833	3.231007
C	1.389915	1.513521	4.342059
C	1.155436	0.083159	2.648501
C	1.296531	-1.214701	1.891137
H	1.906047	-1.865945	2.514204
C	-0.275473	-3.010978	2.464055
C	-4.120323	6.412347	-1.025069
H	-4.752891	5.845883	-1.696653
H	-3.769243	7.311172	-1.537958
H	-4.715385	6.738643	-0.167750
C	1.399700	5.726842	0.395976
H	1.492876	5.010349	-0.427666
C	1.185727	7.116312	-0.209579
H	0.325347	7.152738	-0.879015
H	2.061899	7.400835	-0.794658
H	1.052094	7.874591	0.565851
C	2.696308	5.695328	1.207340
H	2.927386	4.691487	1.561131
H	2.631193	6.355742	2.075222
H	3.529356	6.035770	0.589490
C	1.727392	2.005148	5.703638
H	1.540461	3.074405	5.745440
H	2.777345	1.822141	5.945114
H	1.123171	1.513107	6.469481
C	1.999344	-0.864477	4.843584
H	1.605978	-1.825013	4.525254
H	1.655094	-0.664563	5.854936
H	3.089683	-0.886611	4.839006
C	3.440562	-0.550381	0.654786
H	3.475571	0.400253	1.194502
H	4.009675	-1.269919	1.252534
C	-3.378239	3.332072	-1.690625
N	-2.999696	2.036277	-1.757437
O	-4.347737	3.755172	-2.332506
C	-3.608743	1.148668	-2.749919
C	-4.664303	0.244108	-2.156250
H	-4.134018	1.810446	-3.435690
C	-2.557741	0.385928	-3.598383
N	-4.496053	-0.891362	-1.500094
N	-6.000037	0.460982	-2.357053
H	-1.982063	-0.255030	-2.927788
C	-1.600479	1.365076	-4.284877
C	-3.234877	-0.501866	-4.648052
C	-5.755310	-1.432216	-1.299445
C	-6.704836	-0.597722	-1.824022
C	-6.617711	1.573486	-3.075689
H	-1.090388	2.015371	-3.574149
H	-2.137953	2.000161	-4.993870
H	-0.839652	0.815601	-4.841612
H	-3.872718	-1.263636	-4.200601
H	-2.478224	-1.012497	-5.245854
H	-3.845075	0.097356	-5.329579
C	-5.863081	-2.785004	-0.703185
C	-8.186410	-0.708991	-1.883036
H	-5.994140	2.458051	-2.987811
H	-7.585902	1.783547	-2.628978
H	-6.761224	1.318942	-4.126372
N	-4.639285	-3.248827	-0.443873
O	-6.948813	-3.353313	-0.496384
H	-8.487753	-1.629078	-1.390313
H	-8.544733	-0.730552	-2.915155
H	-8.672674	0.132472	-1.383433
C	-4.410049	-4.575569	0.095517
C	-3.313889	-4.439017	1.118182
H	-5.319116	-4.947178	0.577123
C	-4.003669	-5.564476	-1.046090
C	-1.512549	-3.750872	2.128409
N	-2.350184	-3.535535	1.034665
N	-3.149751	-5.209033	2.221645
H	-3.075417	-5.166801	-1.470788
C	-3.722509	-6.980394	-0.536308
C	-5.059678	-5.599168	-2.152254
C	-2.009623	-4.797698	2.872944
H	-2.899326	-7.011288	0.178220
H	-3.447873	-7.625444	-1.372655
H	-4.605822	-7.416893	-0.063526
H	-5.197985	-4.620570	-2.609630
H	-6.024622	-5.932540	-1.764145
H	-4.753673	-6.296433	-2.934653
C	-1.554876	-5.466077	4.121912

H	-0.626301	-5.019701	4.456736
H	-1.397001	-6.534834	3.956592
H	-2.301861	-5.366292	4.913849
Cu	-0.215567	2.486126	0.589172
Cu	-3.196697	-1.971777	-0.519581
O	-0.766609	1.192530	-0.727683
H	-1.179709	-0.092583	-0.672787
H	-2.153569	1.721450	-1.277309
O	-1.471222	-1.125113	-0.515456
H	-1.068614	-1.667684	-1.203706
H	-0.543890	-1.681256	0.923419
H	-0.277763	1.346586	-1.544609
O	-3.270280	2.306276	1.523716
H	-4.066326	2.845392	1.448726
O	-3.726109	-0.542320	1.166453
H	-4.686037	-0.549308	1.270088
H	-3.482523	0.402721	1.173167
C	-2.027788	7.435059	0.799998
H	-1.855441	8.184994	0.029712
H	-2.998601	7.608956	1.259100
H	-1.260625	7.525395	1.560101
C	-4.042985	-6.251593	2.713589
H	-3.575700	-7.231382	2.626572
H	-4.282842	-6.060051	3.757341
H	-4.961196	-6.243180	2.137140
H	-2.930625	2.475620	2.410120
C	1.993074	-1.027702	0.534439
H	1.420063	-0.326049	-0.075542
H	1.970816	-1.993278	0.022904
C	4.111977	-0.378272	-0.708083
H	4.073089	-1.317884	-1.266638
H	3.557323	0.360971	-1.295410
C	5.566936	0.068714	-0.584841
H	6.135236	-0.689405	-0.052941
H	5.620725	0.989263	0.006437
N	6.161431	0.290783	-1.899493
H	5.597727	0.824903	-2.548013
C	7.412007	0.060311	-2.364467
O	7.733620	0.445120	-3.489014
C	8.401677	-0.691585	-1.480904
H	8.098593	-0.604688	-0.439103
C	9.831451	-0.142073	-1.617162
H	10.046764	0.050980	-2.667084
H	9.956168	0.793263	-1.072168
C	8.537534	-2.212178	-1.795515
C	10.750702	-1.244483	-1.071320
C	8.463336	-2.565962	-3.287583
H	8.765986	-3.605404	-3.418182
H	7.443923	-2.455429	-3.657905
H	9.113970	-1.933068	-3.888624
C	7.561726	-3.080141	-1.002413
H	7.622611	-2.870062	0.066262
H	6.539613	-2.901714	-1.338372
H	7.789183	-4.134331	-1.157775
C	12.074290	-1.344554	-1.829227
H	12.668479	-2.179640	-1.458029
H	11.904381	-1.485522	-2.897413
H	12.646757	-0.426223	-1.689800
C	11.007915	-1.108441	0.436239
H	11.641267	-0.240791	0.627532
H	10.077625	-0.983974	0.992425
H	11.517347	-1.996417	0.812315
N	9.927951	-2.460481	-1.316481
O	10.392290	-3.635301	-1.184267

5K

155

N	-0.004124	2.196137	-0.815501
N	-0.414682	4.291589	-1.331755
N	-1.420204	0.367990	0.424898
N	-0.003812	-1.869692	0.261496
N	-1.141940	-3.022649	1.757519
N	2.171696	-2.803919	-1.382814
C	-1.166917	2.591568	-0.186450
C	-1.442256	3.896042	-0.496316
C	0.435719	3.243104	-1.492930
C	-0.235532	5.630201	-1.886031
H	0.701517	6.052076	-1.527230
H	-1.057077	6.257685	-1.557169
H	-0.237217	5.597711	-2.973647
C	-2.569546	4.778167	-0.093333
H	-3.247925	4.207966	0.535633
H	-3.121295	5.147783	-0.960841
H	-2.221040	5.645058	0.473353
C	-1.903687	1.601528	0.621357
C	-2.064350	-0.763510	1.055202
H	-2.399068	-0.500832	2.063947
C	-1.036520	-1.849872	1.085731
C	0.546598	-3.146229	0.362523
C	-0.151555	-3.865630	1.307325
C	-2.122052	-3.361283	2.783102
H	-1.612523	-3.778962	3.648848
H	-2.838276	-4.089563	2.403922
H	-2.649873	-2.464583	3.090568
C	-0.000412	-5.243620	1.843460
H	0.169799	-5.223392	2.922948
H	0.838996	-5.731952	1.362314
H	-0.902216	-5.835235	1.666120
C	1.608820	-3.678881	-0.505035
C	3.456859	-3.169234	-1.983871
H	3.367590	-4.200473	-2.319876
C	3.803380	-2.302818	-3.211686
H	3.851071	-1.258385	-2.891111
C	2.734645	-2.437755	-4.298637
H	1.752920	-2.124361	-3.947372
H	2.661597	-3.473816	-4.640431
H	2.996339	-1.820646	-5.159984
C	5.181056	-2.677380	-3.766589
H	5.433001	-2.032667	-4.609632
H	5.190480	-3.709751	-4.125708
H	5.970665	-2.571779	-3.020655
O	-2.850013	1.917493	1.361634
O	1.948198	-4.863280	-0.455331
C	1.772869	3.339165	-2.178509
C	4.481228	-3.121686	-0.880955
N	2.787702	2.955909	-1.195818
H	1.947685	4.385845	-2.421996
C	1.885674	2.527860	-3.486761
H	2.835685	1.959218	-0.996893
C	2.982832	3.774204	-0.124655
H	1.772325	1.467501	-3.242356
C	3.250383	2.738935	-4.145788
C	0.761220	2.898986	-4.458751
C	3.743601	3.203091	0.998956
H	4.069236	2.438841	-3.494600
H	3.391800	3.790424	-4.409774
H	3.318503	2.152349	-5.063492
H	0.835134	2.293124	-5.362752
H	0.832692	3.947681	-4.758932
H	-0.229126	2.735349	-4.030526
N	4.420903	1.989853	0.951345
C	4.029233	3.834794	2.188545
C	5.148793	1.928556	2.054674
N	4.909684	3.003357	2.847340
C	3.574949	5.120621	2.779413
C	6.206045	0.879853	2.220369
C	5.411966	3.237529	4.197168
H	2.860654	5.593637	2.114979
H	3.105319	4.958758	3.752733
H	4.415320	5.803136	2.931207
N	5.701445	-0.271158	1.501783
H	6.371889	0.631298	3.272361
C	7.555315	1.398922	1.599051
H	5.999071	2.384578	4.518052
H	6.033890	4.130431	4.226009
H	4.573064	3.362039	4.879659
C	6.059546	-1.508871	1.867188
H	7.318011	1.643847	0.558838
C	8.089440	2.666728	2.273225
C	8.647282	0.327503	1.588278
C	5.574889	-2.501025	0.886707
H	7.403860	3.509897	2.192637
H	9.023712	2.966410	1.795491
H	8.305563	2.495328	3.330733
H	8.341485	-0.566533	1.048745
H	8.925237	0.033063	2.601696
H	9.536745	0.726887	1.096039
N	4.698431	-2.082692	-0.093180
C	5.899987	-3.815265	0.685515
N	5.196014	-4.192640	-0.443504
C	6.808569	-4.720884	1.437396

C	5.200576	-5.525360	-1.039724
H	7.259313	-4.160073	2.251926
H	7.603055	-5.114931	0.799363
H	6.269940	-5.571768	1.861819
H	4.176660	-5.862633	-1.183104
H	5.702322	-6.208806	-0.362529
H	5.731418	-5.520997	-1.990589
Cu	4.270687	-0.045696	0.178612
Cu	0.348700	0.158937	-0.407042
H	2.074638	-1.818395	-1.149360
O	2.578228	4.938355	-0.106422
O	6.730053	-1.825666	2.863699
O	2.403624	0.068858	-0.721274
O	5.350595	0.652926	-1.858100
O	-0.059556	-0.527401	-2.682332
H	5.626246	1.571510	-1.745059
H	6.166451	0.158813	-2.008666
H	-0.770342	-0.005152	-3.075159
H	-0.391275	-1.434261	-2.661423
H	2.543795	0.074727	-1.675999
C	-4.521085	-0.438032	0.184014
H	-4.855279	-0.203518	1.198272
H	-4.287088	0.515652	-0.290513
C	-5.648369	-1.131318	-0.582874
H	-5.895810	-2.084609	-0.106135
H	-5.308140	-1.366360	-1.597421
C	-6.912026	-0.278831	-0.666834
H	-6.676767	0.688285	-1.124145
H	-7.283521	-0.082769	0.335702
N	-7.941332	-0.964008	-1.444920
H	-7.612517	-1.461214	-2.262180
C	-3.273668	-1.317365	0.245676
H	-3.556831	-2.283156	0.673354
H	-2.916964	-1.520944	-0.768628
C	-9.291357	-0.921228	-1.365399
O	-9.980691	-1.498210	-2.207120
C	-9.935813	-0.158056	-0.212335
H	-9.235865	0.585691	0.165656
C	-11.224408	0.559984	-0.647366
H	-11.008708	1.467025	-1.211438
H	-11.807473	-0.101196	-1.286837
C	-11.986760	0.865352	0.649965
C	-10.371188	-1.040089	0.997787
N	-11.486076	-0.213704	1.544183
O	-12.002761	-0.451523	2.680002
C	-11.611911	2.228127	1.249857
H	-10.530245	2.349940	1.322984
H	-12.005944	3.030223	0.623832
H	-12.037433	2.330312	2.248828
C	-13.502798	0.753202	0.489788
H	-14.003640	0.905507	1.445905
H	-13.855394	1.513926	-0.208481
H	-13.783889	-0.226772	0.102019
C	-9.282227	-1.190281	2.059091
H	-9.685085	-1.695867	2.936202
H	-8.458016	-1.790148	1.671853
H	-8.895164	-0.218979	2.370206
C	-10.925200	-2.419736	0.615200
H	-10.123203	-3.072591	0.269472
H	-11.381620	-2.872649	1.495859
H	-11.673444	-2.354518	-0.172922

5L

155

N	2.054820	3.119290	-0.637798
N	3.135438	4.534667	-1.924056
N	0.947797	3.378504	1.738959
N	-0.259934	1.062499	2.183729
N	-0.595273	1.335228	4.345668
N	-1.131919	-1.153145	0.544210
C	2.301756	4.273034	0.076810
C	2.972855	5.171432	-0.708086
C	2.578415	3.297449	-1.839370
C	3.846640	5.075098	-3.078683
H	4.670045	4.414184	-3.342469
H	4.245804	6.049952	-2.819347
H	3.173593	5.190013	-3.926177
C	3.452807	6.549751	-0.422804
H	3.167547	6.813798	0.591969
H	3.017962	7.278310	-1.111101
H	4.540147	6.623530	-0.503441
C	1.813884	4.364045	1.466181
C	0.318277	3.312455	3.041625
H	1.036614	3.588190	3.821652
C	-0.944773	4.236675	3.224068
H	-1.427854	3.892624	4.143043
C	-0.592820	5.708888	3.444971
H	0.127745	5.831354	4.254596
H	-1.498629	6.260003	3.709299
H	-0.165946	6.160295	2.550962
C	-1.960512	4.083368	2.090963
H	-2.843508	4.689192	2.302770
H	-1.541867	4.421810	1.142076
H	-2.290947	3.050669	1.969165
C	-0.114983	1.890102	3.204670
C	-0.929573	-0.054276	2.681088
C	-1.127861	0.104926	4.034804
C	-0.545347	1.904771	5.687754
H	-0.152800	1.163916	6.381018
H	-1.539024	2.209424	6.014205
H	0.113880	2.766324	5.691556
C	-1.747574	-0.759008	5.073737
H	-1.027335	-0.997539	5.860513
H	-2.096007	-1.680800	4.622584
H	-2.594587	-0.256929	5.548215
C	-1.459896	-1.158750	1.865568
C	-1.307061	-2.398649	-0.206709
H	-2.287064	-2.790807	0.057474
C	-2.378440	-1.342566	-2.309787
H	-2.393122	-0.361695	-1.827472
H	-2.143681	-1.160782	-3.362830
O	2.187823	5.261238	2.238988
O	-2.184577	-2.028266	2.354547
C	2.730349	2.230204	-2.890905
C	-0.266722	-3.362020	0.299773
N	3.386836	1.088911	-2.251878
H	3.414808	2.604877	-3.650023
C	1.416983	1.835834	-3.599945
H	2.789377	0.541667	-1.636656
C	4.671525	1.244808	-1.827546
H	0.736654	1.417377	-2.852412
C	1.670951	0.782157	-4.680006
C	0.736265	3.067934	-4.203648
C	5.174568	0.226523	-0.890619
H	2.094672	-0.131457	-4.266977
H	2.357934	1.165716	-5.439295
H	0.734934	0.523159	-5.177892
H	-0.208999	2.782373	-4.667046
H	1.360460	3.519684	-4.979134
H	0.520297	3.831560	-3.454394
N	4.509557	-0.956180	-0.588578
C	6.419704	0.208155	-0.303505
C	5.362171	-1.695012	0.102929
N	6.511644	-1.012260	0.331941
C	7.529271	1.196291	-0.263146
C	5.080062	-3.141863	0.372069
C	7.636937	-1.427320	1.162574
H	7.233336	2.099424	-0.785083
H	7.789100	1.448463	0.767895
H	8.429615	0.798272	-0.738712
N	3.638753	-3.221970	0.485627
H	5.557907	-3.484050	1.294415
C	5.614295	-4.005992	-0.830479
H	7.418639	-2.388911	1.613171
H	8.543194	-1.510908	0.565568
H	7.793617	-0.696405	1.953962
C	3.067432	-4.175759	1.232197
H	5.115311	-3.603797	-1.718233
C	7.126665	-3.888259	-1.042438
C	5.231486	-5.482319	-0.707489
C	1.600906	-4.162267	1.059460
H	7.446332	-2.870452	-1.263963
H	7.424178	-4.508481	-1.889684
H	7.679954	-4.244179	-0.169759
H	4.154826	-5.625326	-0.642946
H	5.685803	-5.937653	0.174079
H	5.587686	-6.020256	-1.588879
N	1.028388	-3.109767	0.375248

C	0.636695	-5.073501	1.396390
N	-0.544100	-4.548093	0.903946
C	0.731968	-6.373378	2.112090
C	-1.866667	-5.150870	1.042527
H	1.775748	-6.562435	2.348549
H	0.354850	-7.197774	1.502556
H	0.164317	-6.363063	3.045901
H	-2.550080	-4.431584	1.488622
H	-1.791023	-6.014480	1.694922
H	-2.244690	-5.476018	0.074509
Cu	2.526317	-1.762647	-0.211661
Cu	0.933548	1.799144	0.557111
H	-0.298927	-0.621316	0.298966
O	5.387711	2.164759	-2.227667
O	3.646411	-4.997164	1.962371
O	1.419425	-0.015727	-0.359464
O	2.261093	-2.229594	-2.570878
O	-0.994076	1.955089	-0.895877
H	3.114403	-2.065355	-2.992481
H	2.096686	-3.173475	-2.691292
H	-1.098768	2.857112	-1.223873
H	-1.790461	1.777687	-0.379591
H	0.917114	-0.049726	-1.182930
C	-3.763435	-1.986207	-2.216169
H	-4.071614	-2.096074	-1.172846
H	-3.733131	-2.993691	-2.642971
C	-1.244578	-2.189902	-1.724711
H	-1.258675	-3.180310	-2.188268
H	-0.280826	-1.753103	-1.992939
C	-4.824371	-1.169641	-2.957722
H	-4.531511	-1.053276	-4.003409
H	-4.887581	-0.164092	-2.545309
N	-6.144697	-1.789513	-2.947990
H	-6.290238	-2.533597	-3.616613
C	-7.201705	-1.606756	-2.123190
O	-8.216951	-2.291815	-2.255534
C	-7.107219	-0.529370	-1.048453
H	-6.064019	-0.268603	-0.896254
C	-7.708891	-1.006143	0.300348
H	-7.733818	-2.092027	0.355079
H	-7.075637	-0.651459	1.112759
C	-7.891341	0.771074	-1.404421
C	-9.126070	-0.411774	0.443601
C	-10.242738	-1.440206	0.231882
H	-10.237604	-2.161235	1.051112
H	-11.212522	-0.941159	0.220758
H	-10.099473	-1.972407	-0.706359
C	-9.324037	0.302392	1.786554
H	-8.560355	1.063505	1.951754
H	-10.303203	0.780068	1.822430
H	-9.264800	-0.423566	2.599070
C	-7.167180	2.005961	-0.839226
H	-6.262909	2.208545	-1.414746
H	-7.819544	2.877038	-0.907202
H	-6.884463	1.865489	0.204560
C	-8.191418	0.983753	-2.887314
H	-8.785703	1.887984	-3.012337
H	-7.263894	1.105867	-3.447265
H	-8.747622	0.146562	-3.306723
N	-9.165722	0.580069	-0.663991
O	-10.143577	1.378542	-0.811152

Acknowledgements - Danksagung

Danke Peter! Für den Raum und das Vertrauen und gleichzeitig für den Boden unter den Füßen. Obwohl ich mich eigentlich für ein ganz anderes Thema beworben hatte, bin ich sehr froh darüber, dass ich das spannendste Thema von allen bearbeiten durfte! Vielen Dank für die herausragende, bereichernde Möglichkeit auch im Ausland forschen (und schnorcheln) zu dürfen, das hätte ich mir alles niemals träumen lassen!

Für die Übernahme der Zweitkorrektur sowie für die Möglichkeit in seinem Arbeitskreis Flow Cytometry durchzuführen, möchte ich Prof. Dr. Krämer danken.

Ein großer Dank gebührt auch den Festangestellten im AK Comba und Linti. Danke Bodo, für MOMEC und für Deine Zeit. Danke Marion, nicht zuletzt für all die Stunden am ESR! Bedanken möchte ich mich auch bei Maik für Hilfe bei großen und kleinen Problemen und für die Bestellungen. Vielen Dank auch Dir, Philipp, für Deine unkomplizierte, schnelle Hilfe bei jedem Problem und natürlich für das Trockeneis! Nicht weniger dankbar bin ich Marlies und Karin für das 'Endnoten' und die Hilfe beim ganz normalen Bürokratiewahnsinn.

Für die finanzielle Unterstützung und die Gelegenheit mit anderen Doktoranden in Kontakt zu kommen, danke ich der Graduiertenschule HGS MathComp.

Dankbar ich Prof. Dr. Herten für die gute Kooperation! Ein großes Dankeschön gebührt auch an den gesamten AK Herten für die offene Aufnahme und die tolle Arbeitsatmosphäre!

Allen Festangestellten des Chemischen Instituts, den Schlossern, den Elektrikern, den Feinmechanikern, den Reinigungskräften sei herzlich gedankt, nicht zuletzt dafür, dass sie unseren Umzug nach Möglichkeit unterstützt haben.

Beate Termin und Prof. Dr. Enders möchte ich für das Messen der NMR Spektren danken! Ein herzlicher Dank gebührt auch Dr. Gross und seinen Mitarbeitern in der Massenspektrometrie-Abteilung des OCI, auch dafür, dass eine Lösung gefunden werden konnte, die uns Combas erlaubt die UPLC-MS mitzubenutzen!

Ich danke Lars Behrendt, ohne dessen Ergebnisse meine Arbeit vermutlich nur Rätsel aufgeben würde. Vor allem danke ich ihm aber für seine schnelle Hilfe bei meinen Bioproblemen und die wunderbare Schatzkarte von Heron Island!

Thanks a lot Prof. Sastry for hosting me in Hyderabad. Thank you my lovely lab partners, Anamika, Aparna and Preethi for the shared teas and the cake! Thanks Nandan for your help and your passionate problem solving attitude! And thank you Naveen, for organising WiFi and virtually everything else for me!

Lawrie, thank you so much for the time under your supervision, I would come back at once, if only it was possible! Thanks also for proof-reading, you made this a better thesis.
Thanks Gary for funding my stay at UQ and welcoming me in your group! I also owe my gratitude to Jeff Harmer for the shared hours at the EPR machine. Thank you very much Steven Mason for the help with the confocal microscopy setup at UQ. And of course, Geoff, thank you so much for making me enjoy and not only work on Heron Island, thanks for taking care of all the organisation, thanks for cooking, the sunset pistacchios and the shared pizzas back at UQ, I miss that! I am also grateful to Prof. Dr. Peter Vize and Daniel Wuitchik for help with the collection of *L. patella* on SCUBA. The excellent facillities at Heron Island Research Station are gratefully acknowledged. Without the help of Prof. Dr. Bernhard Degnan and Jabin Watson however, we would not have been able to keep *L. patella* alive-thanks for your great setup and help throughout my stay! Thank you Evan Moore, and thank you Josh and Jane for helping out with the fluorescence spectroscopy and your interest in my vegan cakes! And thank you Liam for making my time in the Schenk labs fun :) Thank you so much for the quick, uncomplicated, funny cooperation, Prof. Thomas Müller and Jake O'Brien!

Liebe Kathi, Dir gebührt ein ganz besonderer Dank. Dafür, dass Du Dir drei Jahre lang angehört hast, warum in Leipzig alles besser ist und für Deine stete Unterstützung! Danke für den schnellen, organisierten Umzug und für Deine Fähigkeit beruhigend auf mich einzuwirken. Schade, dass wir erst so spät Laborkollegen geworden sind.

Danke lieber AK Comba! Dafür, dass ich es nie bereut habe nach Heidelberg gegangen zu sein dafür, dass ihr immer eine klasse Gruppe wart und seid, mit einem familiären, kollegialen, offenen Arbeitsklima. Und natürlich danke ich auch euch Lintis für die Möglichkeit jederzeit bei euch vorbei

kommen zu können mit möglichen Kristallen ;) Ein Dank gebührt auch meinen Labornachbarn Michael für das beherzte Löschen und Julian für die Starthilfe in Heidelberg und in der 503!

Martin, Danke, dass Du auch nicht hierher passt :) Für die schnelle, verlässliche, engagierte, witzige Zusammenarbeit im BZH/Bioquant bin ich Dir sehr dankbar! An dieser Stelle sei auch Prof. Söllner gedankt, in dessen Labors ich die Probenvorbereitung für alle Bakterien- uns Algenexperimente durchführen durfte.

Vielen Dank, Sandra, für Deine Hilfe bei der Flow Cytometry!

Bei meinen Forschungsstudenten Max M., Jasmin S., Christina S., Michael Z., Nora K., Brenna C., Benedikt B., Alex K. und Hendrik H. möchte ich mich für die tatkräftige Unterstützung und für alle kritischen Gegenfragen bedanken!

Ein großer Dank gilt natürlich auch den fleißigen Korrekturlesern Asha, Bianca, Bodo, Kathi, Katrin, Lawrie, Markus, Marion und Martin.

Vielen Dank Maria, Conrad, Kathi und Sonja, dafür, dass ihr uns 'adoptiert' habt!

Meiner Familie und im Speziellen Mama, Papa und Oma, danke ich für die stete Ermunterung und dafür, dass ich immer heimkommen kann. Ich bin sehr dankbar für eure Unterstützung all meiner Ideen und Entscheidungen! Ebenfalls möchte ich meinem Bruder Johannes danken für die Freundschaft und die sportliche Bereitschaft im Notfall auch mal schnell nach der Arbeit 800 km zu fahren, um einen Beutel in Heidelberg vorbei zu bringen.

Und zu guter Letzt: Danke Markus für die gemeinsame Zeit und die allabendliche Spektren- und Synthesediskussion, ich fände es schön, wenn das so bliebe.

Eidesstattliche Versicherung

gemäß § 8 der Promotionsordnung der Naturwissenschaftlich-Mathematischen Gesamtfakultät der Universität Heidelberg

1. Bei der eingereichten Dissertation zu dem Thema

Dinuclear copper(II) patellamide complexes: Studies on their potential hydrolase-like activities and *in vivo* stabilities

handelt es sich um meine eigenständig erbrachte Leistung.

2. Ich habe nur die angegebenen Quellen und Hilfsmittel benutzt und mich keiner unzulässigen Hilfe Dritter bedient. Insbesondere habe ich wörtlich oder sinngemäß aus anderen Werken übernommene Inhalte als solche kenntlich gemacht.

3. Die Arbeit oder Teile davon habe ich bislang nicht an einer Hochschule des In- oder Auslands als Bestandteil einer Prüfungs- oder Qualifikationsleistung vorgelegt.

4. Die Richtigkeit der vorstehenden Erklärungen bestätige ich.

5. Die Bedeutung der eidesstattlichen Versicherung und die strafrechtlichen Folgen einer unrichtigen oder unvollständigen eidesstattlichen Versicherung sind mir bekannt. Ich versichere an Eides statt, dass ich nach bestem Wissen die reine Wahrheit erklärt und nichts verschwiegen habe.

_____ _____

Ort und Datum Unterschrift

Epilogue

From [6]

"The Emerald Crystal Ball

When the tides are warm and low
Where the tropic sun has shone,
That is where we look for Pro-
chloron.

On the shores of Mexico,
Eniwetok and Ceylon
Lurk didemnids bearing Pro-
chloron.

There are things we ought to know –
Mysteries to think upon –
Problems that relate to Pro-
chloron.

How to get the cells to grow:
Media to grow them on –
These are what we need for Pro-
chloron.

Progress has been somewhat slow
Towards our chosen Rubicon:
How to tame the tiny Pro-
chloron.

***

Prince, if you desire to know
Where the last year's snows have gone
Peer into the heart of Pro-
chloron."